Royal Institution of Great Britain
Davy-Faraday Research Laboratories

Department of Chemistry
University College London

Multifunctional Microporous Metallosilicate Catalysts

A dissertation submitted to the University of London
for the degree of doctor of philosophy

By
Amber Elizabeth Welch

2007

Supervisors: Prof. G. Sankar and Dr. G. Hogarth

I, Amber Elizabeth Welch, confirm that the work presented in this thesis is my own. Where information has been derived from other sources, I confirm that this has been indicated in the thesis.

ProQuest LLC
789 East Eisenhower Parkway
P.O. Box 1346
Ann Arbor, MI 48106-1346

Abstract

The work reported in this thesis is concerned with the synthesis and characterisation of a range of metallosilicate materials. A range of heteroatom containing materials with 3D framework structures were synthesised from amorphous cogel precursors, via a facile hydrothermal process. Titanosilicate, aluminosilicate and ferrisilicate materials were synthesised and characterisation of these materials demonstrated that the heteroatoms encompassed within them were in the ideal coordination geometry for active catalysis. These materials were compared to those synthesised from conventional means using a variety of techniques including, XRD, NMR, FTIR, TPD-MS and catalysis. Both the framework materials and their amorphous precursors were employed as catalysts for a range of oxidative and acidic reactions. The catalysis results demonstrated that although the amorphous cogel precursors were catalytically active and to some degree selective, the framework materials were more effective catalysts (regardless of the nature of the incorporated heteroatom).

A range of bimetallosilicate materials were also synthesised from cogel precursors, these framework materials contained two of the heteroatoms previously employed (titanium, iron or aluminium). These materials were similarly characterised and their catalytic properties also evaluated. The differing chemical nature of the inserted heteroatoms allowed one catalyst to behave as both an active oxidative and an acidic catalyst.

Acknowledgments

The Royal Institution of Great Britain is the world's oldest independent research facility and I feel immensely proud to say that I have been a part of that institution. Working in such a historic building has been a privilege, but is the people (past and present) who make the Ri such a pleasurable place to work.

I would like to thank my supervisor Prof. G. Sankar whose instruction and guidance were invaluable. I am also indebted to my other supervisor Dr. Graeme Hogarth, for his never failing enthusiasm and for the many useful discussions throughout my three years.

Further to this I would like to thank Mike Shehee for building a lot of the equipment I used throughout my work, but also for being one of life's true gentlemen. I am also grateful to Dr. Kevin Reeves for his SEM help, Dr. Jill Maxwell for her help with chemical analysis and to Dr. Abil Aliev for help with NMR work.

I would also like to express gratitude to Sami Barri and to Sankar's Group, for continued help and support throughout this work. A special mention should also be given to T.C. whose proof-reading in the final stages proved to be invaluable.

Finally, I would like to thank my family for their continued love and support, especially my parents, and it is to them that I dedicate this thesis. To my Father, for helping to keep my feet on the ground and to my Mother, for lifting them up.

Contents

Section		*Page*
Title Page		1
Abstract		2
Acknowledgements		3
Contents		4
List of Figures		9
List of Tables		15

Section	*Title*	*Page*
	Chapter 1: Introduction	
1.0	**Summary**	**17**
1.1	**Zeolite Introduction**	**18**
1.1.1	Structure and Composition	19
1.1.2	Applications	27
1.2	**Synthesis**	**29**
1.2.1	Conventional Synthesis Methods	29
1.2.2	Cogel Synthesis Methods	32
1.2.2.1	Cogel Formation	33
1.2.2.2	Framework Synthesis	35
1.3	**Zeolite Activity**	**36**
1.3.1	Hydrophilic / Hydrophobic Activity	36
1.3.2	Catalytic Activity	37
1.3.2.1	Shape Selective Catalysis	40
1.3.2.2	Oxidative Catalysis Activity	41
1.3.2.3	Acidic Catalysis Activity	44
1.4	**Research Hypothesis**	**46**
1.5	**Research Aims**	**47**
1.6	**References**	**48**

Chapter 2: Experimental

2.0	**Summary**	**50**
2.1	**Synthesis**	**51**
2.1.1	Cogel Precursors	52
2.1.2	MFI Framework Materials	52
2.1.3	AFI Framework Materials	52
2.1.4	Blank Materials	53
2.1.5	Silylation	53
2.2	**Characterisation**	**54**
2.2.1	X-Ray Diffraction (XRD)	54
2.2.1.1	Principles of XRD	54
2.2.1.2	XRD Data Collection	56
2.2.2	Infrared (IR) Spectroscopy	57
2.2.2.1	Principles of IR	57
2.2.2.2	IR Data Collection	58
2.2.3	Solid State Nuclear Magnetic Resonance (NMR) Spectroscopy	59
2.2.3.1	Principles of NMR	59
2.2.3.2	NMR Data Collection	60
2.2.4	Diffuse Reflectance Ultra Violet – Visible (UV-vis) Spectroscopy	61
2.2.4.1	Principles of UV-vis	61
2.2.4.2	UV-vis Data Collection	61
2.2.5	Temperature Programmed Desorption – Mass Spectroscopy (TPD-MS)	62
2.2.5.1	Principles of TPD-MS	62
2.2.5.2	TPD-MS Data Collection	63
2.2.6	Scanning Electron Microscopy (SEM)	64
2.2.6.1	Principles of SEM	64
2.2.6.2	SEM Data Collection	65
2.2.7	Energy Dispersive X-ray Analysis (EDX)	65
2.2.7.1	Principles of EDX	65

2.2.7.2	EDX Data Collection	65
2.3	**Catalysis Experiments**	**66**
2.3.1	Epoxidation of Cyclohexene	66
2.3.1.1	Experimental	67
2.3.2	Phenol Hydroxylation	67
2.3.2.1	Experimental	68
2.3.3	Adipic Acid (AA) Formation	69
2.3.3.1	Experimental	69
2.3.4	Ethylation of Benzene	70
2.3.4.1	Experimental	71
2.4	**Gas Chromatography (GC)**	**72**
2.4.1	Principles of GC	72
2.4.2	GC Data Collection	73
2.5	**References**	**73**

Chapter 3: Titanosilicates

3.0	**Summary**	**76**
3.1	**Introduction**	**77**
3.2	**Aims**	**80**
3.3	**Experimental**	**81**
3.3.1	Cogel Synthesis	81
3.3.2	TS-1 Synthesis	82
3.3.3	Blank Material Synthesis	83
3.4	**Results and Discussion**	**83**
3.4.1	Titanosilicate Materials	83
3.4.2	Silicalite Materials	97
3.4.3	Epoxidation of Cyclohexene	97
3.4.4	Urea-H_2O_2 Adduct Alteration	102
3.4.5	Silylation Alteration	106
3.4.6	Phenol Hydroxylation	117
3.4.7	Adipic Acid	121

3.5	**Conclusions**	**125**
3.6	**References**	**128**

Chapter 4: Aluminosilicates

4.0	**Summary**	**130**
4.1	**Introduction**	**131**
4.2	**Aims**	**135**
4.3	**Experimental**	**136**
4.3.1	Cogel Synthesis	136
4.3.2	ZSM-5 Synthesis	136
4.3.3	Al SAPO-5 Synthesis	137
4.3.4	Standard Materials	137
4.4	**Results and Discussion**	**138**
4.4.1	Aluminosilicate Materials	138
4.4.2	Ammonia Absorption	151
4.4.3	Acid Catalysis	154
4.5	**Conclusions**	**159**
4.6	**References**	**160**

Chapter 5: Ferrisilicates

5.0	**Summary**	**161**
5.1	**Introduction**	**162**
5.2	**Aims**	**164**
5.3	**Experimental**	**165**
5.3.1	Cogel Synthesis	165
5.3.2	Fe-MFI Synthesis	165
5.3.3	Standard Materials	166
5.4	**Results and Discussion**	**166**
5.4.1	Ferrisilicate Materials	166
5.4.2	Ammonia Absorption	175

5.4.3	Acid Catalysis	178
5.5	**Conclusions**	**185**
5.6	**References**	**186**

Chapter 6: Bimetallosilicate Materials

6.0	**Summary**	**187**
6.1	**Introduction**	**188**
6.2	**Aims**	**190**
6.3	**Experimental**	**192**
6.3.1	Cogel Synthesis	192
6.3.1.1	Mixing of Powder Cogel Materials	193
6.3.1.2	One Solution	193
6.3.1.3	Two Solution	193
6.3.2	MM'-S1 Synthesis	194
6.4	**Results and Discussion**	**195**
6.4.1	Mixed Metallosilicate Materials	195
6.4.2	Ammonia Absorption	208
6.4.3	Acid Catalysis	210
6.4.4	Oxidative Catalysis	216
6.4.5	Acidic and Oxidative Catalysis	218
6.5	**Conclusions**	**223**
6.6	**References**	**226**

Chapter 7: Conclusions and Further Work

7.0	**Summary**	**227**
7.1	**Titanosilicates (Chapter 3)**	**228**
7.2	**Aluminosilicates (Chapter 4)**	**229**
7.3	**Ferrisilicates (Chapter 5)**	**230**
7.4	**Bimetallosilicates (Chapter 6)**	**230**
7.5	**Overall Conclusions and Further Work**	**231**

7.6 References 232

List of Figures

Figure	*Caption*	*Page*
	Chapter 1: Introduction	
1.1	Comparison of naturally grown and laboratory synthesised zeolite materials.	18
1.2	Zeolite framework component, containing aluminium (III) and silicon (IV) atoms bound through an oxygen bridge.	19
1.3	General zeolite formula, where A is a cation with charge m, and (x+y) is the number of tetrahedra per crystallographic unit cell.	20
1.4	The prism secondary building units, join together to form the ordered macromolecular zeolite framework.	20
1.5	Examples of different zeolite framework types **i)** CHA, **ii)** BEA, **iii)** MFI.	21
1.6	Charge neutral silicate framework containing silicon (IV) bridged by oxygen atoms.	22
1.7	Charge neutral AlPO framework containing phosphorus (V) and aluminium (III) centres bridged by oxygen atoms.	23
1.8	SAPO framework.	23
1.9	Demonstrating the different properties introduced when a heteroatom is inserted in an **i)** AlPO and **ii)** silicate framework.	24
1.10	Titanium silicalite-1 framework.	25
1.11	Equilibrium of silica species during gel formation.	30
1.12	Hydrolysis and condensation process utilised to form amorphous cogel precursors.	34
1.13	Energy pathways for an uncatalysed and catalysed reaction.	38
1.14	Shape selective catalysis.	40
1.15	Interconversion of tetrapodal and tripodal tetrahedral titanium sites in TS-1.	41
1.16	Proposed models of the titanium (IV) catalytically active sites.	42
1.17	Proposed mechanism of alkene epoxidation.	43
1.18	Catalytically reactive acid site in zeotype framework.	44
1.19	Friedel-Crafts alkylation type, acid catalysed reaction.	45

Chapter 2: Experimental

2.1	XRD patterns of standard materials.	51
2.2	Bragg's Law and Bragg reflection from a set of crystal planes.	55
2.3	Laboratory based angular-dispersive XRD machine using Bragg-Brentano Geometry.	56
2.4	Schematic of an IR spectrometer.	58
2.5	Schematic demonstrating magic angle spinning.	59
2.6	Demonstrating four different silicon Q^n environments within silica framework, which can be differentiated by ^{29}Si NMR.	60
2.7	Example TPD profile indicating the two predominate acid sites in the silicate based materials synthesised.	63
2.8	TPD-MS apparatus.	64
2.9	Epoxidation of cyclohexene to form products **i)** epoxide and **ii)** diol as well as side products **iii)** mono-alcohol and **iv)** ketone.	67
2.10	Hydroxylation of phenol to form products **i)** catechol, **ii)** hydroquinone and **iii)** p-benzoquinone.	68
2.11	Reaction pathway for the oxidation of cyclohexene (**i**) to adipic acid (**ii**).	69
2.12	Possible products for the ethylation of benzene reaction.	71
2.13	Schematic of gas chromatograph.	73

Chapter 3: Titanosilicates

3.1	Titanium silicalite-1 (MFI) framework.	77
3.2	Common catalytic applications of TS-1.	78
3.3	Schematic representation of conventional TS-1 synthesis.	78
3.4	Transformation of amorphous cogel into TS-1 via a wetness impregnated, hydrothermal synthesis route.	79
3.5	Titanium composition (%) of TS-1 and cogel materials of both Si:Ti 10 and Si:Ti 80.	84
3.6	XRD patterns of calcined cogel and TS-1materials.	85
3.7	^{29}Si NMR spectra of Cogel 8 and TS-1 8-2.	85
3.8	IR spectra of titanosilicate materials.	87
3.9	I_{960}/I_{550} values for different TS-1 materials.	88
3.10	UV-vis spectra of cogel 8, TS-1 8-2 and standard TS-1.	90
3.11	UV-vis spectra of cogel and TS-1 materials with varying titanium	92

	concentrations.	
3.12	UV-vis spectra of cogel and TS-1 materials with different preparation methods.	93
3.13	Typical SEM images of Cogel 8, and TS-1 8-2.	94
3.14	Packed bulk density of all titanosilicate materials.	96
3.15	Typical cyclohexene conversion of titanosilicate materials.	98
3.16	Cyclohexene conversion for TS-1 and cogel materials.	98
3.17	The typical catalytic selectivity of cogel 8, TS-1 8-2, standard TS-1, for the epoxidation of cyclohexene.	100
3.18	Epoxide selectivity for TS-1 and cogel materials for the epoxidation of cyclohexene.	101
3.19	Cyclohexene conversion of titanosilicate materials using urea-H_2O_2 oxidant.	103
3.20	Cyclohexene conversion for TS-1 and cogel materials using urea-H_2O_2 oxidant.	104
3.21	Catalytic selectivity of cogel 8, TS-1 8-2, TS-1 standard, for the epoxidation of cyclohexene using urea-H_2O_2 oxidant.	105
3.22	Epoxide selectivity for TS-1 and cogel materials for the epoxidation of cyclohexene using urea-H_2O_2 oxidant.	106
3.23	Premise of silylation.	107
3.24	XRD patterns of cogel 8 and TS-1 8-2 after silylation.	108
3.25	Packed bulk density of silylated cogel and TS-1 materials.	109
3.26	I_{960}/I_{550} ratios for different TS-1 materials.	110
3.27	UV-vis spectra of cogel 8 and TS-1 8-2 materials before and after silylation with TMCS.	111
3.28	Ratio of Q_4/Q_n for cogel and TS-1 materials.	112
3.29	Cyclohexene conversion for silylated and cogel TS-1 materials.	113
3.30	Cyclohexene conversion of silylated titanosilicate materials.	114
3.31	Schematic diagram of a typical material surface after silylation with TMCS and TCMS.	114
3.32	Epoxide selectivity for cogel and TS-1 silylated materials.	115
3.33	Catalytic selectivity of silylated materials Cogel 8-TMCS, TS-1 8-2-TMCS, for the epoxidation of cyclohexene reaction.	116
3.34	Phenol conversion after six hours for cogel and TS-1 materials.	118
3.35	Product selectivity for phenol hydroxylation reaction using different catalysts.	120
3.36	CA:HQ ratio for titanosilicate catalysts during the hydroxylation of phenol reaction.	121
3.37	Formation of AA from cyclohexene.	122

3.38	Cyclohexene conversion for adipic acid formation utilising titanosilicate catalysts.	122
3.39	Selectivity of adipic acid for titanosilicate materials.	124

Chapter 4: Aluminosilicates

4.1	Conversion of Brønsted and Lewis acid sites by dehydration.	131
4.2	MFI and AFI framework types synthesised from identical aluminosilicate cogel precursors.	132
4.3	Schematic representation of standard ZSM-5 synthesis	132
4.4	Substitution of phosphorous atom (V) by a silicon atom (IV) in an AlPO framework to form a SAPO material.	133
4.5	Schematic representation of standard SAPO-5 synthesis.	133
4.6	Schematic representation of aluminosilicate cogel conversion into Al SAPO-5 via hydrothermal synthesis	134
4.7	Schematic showing the same cogel precursor forming different framework types.	135
4.8	XRD patterns of **i)** cogel , **ii)** ZSM-5 and **iii)** Al SAPO-5 materials.	139
4.9	Packed bulk density for aluminium materials synthesised.	140
4.10	Typical SEM images of Cogel 15, and ZSM-5 15-2.	141
4.11	Typical SEM images of Al SAPO-5 15-4.	142
4.12	^{27}Al NMR spectra of cogel materials	143
4.13	^{27}Al NMR spectra of ZSM-5 15-1 as-prepared and calcined.	144
4.14	^{27}Al NMR spectra of calcined ZSM-5 materials:	145
4.15	^{27}Al NMR spectra of Al SAPO-5 materials	148
4.16	^{27}Al NMR spectra of AlPO-5 and SAPO-5 materials.	150
4.17	TPD profiles of aluminium containing materials	152
4.18	Benzene and ethanol conversion for all aluminium materials.	155
4.19	Product selectivity for aluminium containing catalysts.	157

Chapter 5: Ferrisilicates

5.1	Fe-MFI framework.	162
5.2	Schematic representation of standard Fe-MFI synthesis.	163
5.3	XRD patterns of cogel and calcined Fe-MFI materials.	167
5.4	Packed bulk density measurements for all ferrisilicate materials	168

5.5	Typical SEM images of Cogel 20, Fe-MFI 20-2.	169
5.6	UV-vis spectra of Cogel 20.	170
5.7	UV-vis spectra of calcined cogel materials.	171
5.8	UV-vis spectra of cogel 20 and calcined Fe-MFI 20.	172
5.9	UV-vis spectra of Fe-MFI materials prepared from cogel materials with different Si:Fe ratios.	173
5.10	UV-vis spectra of calcined Fe-MFI materials prepared from cogel precursors condensed under stirred or sonocation conditions.	174
5.11	TPD of ammonia for ferrisilicate materials.	175
5.12	Benzene and ethanol conversion for ferrisilicate materials.	179
5.13	Benzene and ethanol conversion for iron and aluminium cogel materials.	180
5.14	Benzene and ethanol conversion for Fe-MFI and ZSM-5 materials.	181
5.15	Product selectivity for ferrisilicate catalysts.	182
5.16	Product selectivity for iron and aluminium cogel catalysts.	183
5.17	Product selectivity for Fe-MFI and ZSM-5 catalysts.	184

Chapter 6: Bimetallosilicate Materials

6.1	A typical example of how insertion of different heteroatoms can introduce catalytically sites into the framework.	188
6.2	Schematic representation of standard synthesis of MFI framework materials containing aluminium and one other heteroatom.	189
6.3	Schematic of cogel precursor method employed by Ovejero *et al.*, to synthesise a silica based MFI framework material containing both titanium and aluminium heteroatoms. (See chapter for reference).	190
6.4	Schematic representation of the three synthesis pathways employed to produce bimetallosilicate materials.	191
6.5	Packed bulk density for all bimetallosilicate materials synthesised.	195
6.6	XRD patterns of calcined cogel materials and MM'-S1 materials.	196
6.7	Typical SEM images of bimetallosilicate cogel and MM'-S1 materials.	198
6.8	UV-vis spectra of cogel and TiAl-S1 materials.	203
6.9	UV-vis spectra of cogel and FeAl-S1 materials.	204
6.10	I_{960}/I_{550} values for different titanium containing MM'-S1 materials synthesised from cogel precursors prepared various methods.	205
6.11	^{27}Al NMR spectra of MAl-S1 materials.	206

6.12	TPD of ammonia for bimetallosilicate materials.	209
6.13	Benzene and ethanol conversions for cogel and framework bimetallosilicate materials.	211
6.14	Benzene and ethanol conversions for mono- and bimetallosilicate cogel materials.	212
6.15	Benzene and ethanol conversions for mono- and bimetallosilicate MFI framework materials.	213
6.16	Product selectivity for bimetallosilicate catalysts.	214
6.17	Product selectivity for cogel catalysts.	214
6.18	Product selectivity for MFI framework catalysts.	215
6.19	Phenol conversion for mono- and bimetallosilicate MFI framework materials.	216
6.20	CA:HQ ratio for titanium containing catalysts for the hydroxylation of phenol reaction.	218
6.21	Reaction pathway for the oxidation of cyclohexene to AA.	219
6.22	Cyclohexene conversion for adipic acid formation utilising titanium containing catalysts.	219

Chapter 7: Conclusions and Further Work

7.1	MFI framework with one inserted heteroatom.	227
7.2	Further areas of possible research, demonstrating versatility of cogel precursors.	231

List of Tables

Table	*Caption*	*Page*
	Chapter 1: Introduction	
1.1	The chemical composition and properties of some zeotype materials.	22
1.2	The catalytic nature of the inserted heteroatom active sites.	38
	Chapter 2: Experimental	
	(None)	
	Chapter 3: Titanosilicates	
3.1	Specific synthesis details of titanium cogel materials produced.	81
3.2	Details of TS-1 materials produced.	82
3.3	Silylated titanosilicate materials synthesised.	107
3.4	Summary of adipic acid selectivity for all titanosilicate materials.	124
	Chapter 4: Aluminosilicates	
4.1	Specific synthesis details of aluminosilicate cogels synthesised.	136
4.2	Details of ZSM-5 materials produced.	136
4.3	Details of Al SAPO-5 materials produced.	137
	Chapter 5: Ferrisilicates	
5.1	Synthesis details of iron cogel materials.	165
5.2	Fe-MFI materials synthesised.	165
	Chapter 6: Bimetallosilicate Materials	
6.1	Details of the bimetallosilicate cogel materials synthesised.	192
6.2	Specific synthesis details of bimetallosilicate cogel materials synthesised.	192
6.3	Details of MM'-S1 materials produced.	194

Chapter 7: Conclusions and Further Work

(None)

Chapter 1: Introduction

1.0 Summary

Due to the unique properties of zeolite materials, they are commonly employed as catalysts for a range of different reactions. By insertion of specific heteroatoms onto the lattice sites within the zeolite framework, a wider range of catalytic applications can be achieved which are dependant upon the nature of the heteroatoms inserted.[1]

The conventional synthesis of such heteroatom inserted materials can lead to the formation of non-ideal materials. A common problem being the formation of materials which contain clusters of heteroatoms that reduce catalytic ability. Additionally, coordination geometry of the heteroatom can vary from the catalytically ideal tetrahedral. Whilst the concentration of the inserted heteroatom has some limitations based on framework stability, further limitations are imposed to ensure that the heteroatoms are isolated.

The employment of a co-precipitated gel (cogel) precursor to form such framework materials has the potential to overcome such problems.[2] A cogel is an amorphous silica matrix which contains the desired heteroatom in isolated tetrahedral coordination geometry. Via a solid-solid transfer mechanism the cogel is crystallised into an ordered framework structure. Theoretically, the framework structure contains the isolated heteroatom in the maintained tetrahedral coordination geometry which existed in the precursor.

The cogel precursors themselves contained the heteroatoms in the desired coordination geometry for active catalysis and hence they exhibited catalytic potential. Therefore, all of the materials synthesised (both precursor and framework) were characterised and their catalytic activity ascertained.

1.1 Zeolite Introduction

The word zeolite is Greek in origin [coming from the words *zeo* (to boil) and *lithos* (stone)] and is commonly applied to a range of aluminosilicate materials. It was first used by the Swedish mineralogist Axel Cronstedt, who in 1756 found that when heated a zeolite evolved steam.[3] For the next 200 years further research efforts were sparse, in part due to the limited availability of zeolitic material.[1] In the late 1930's the founders of modern zeolite chemistry, Barrer and Sameshima, began attempts to synthesise zeolite materials. In 1948, Barrer succeeded and was accredited with being the first to synthesise a naturally occurring zeolite.[4] This was shortly followed by Milton who reported the synthesis of zeolite A, a zeolite with no naturally occurring counterpart.[5] Research activities intensified when Mobil incorporated organic cations into zeolite syntheses in the 1960's, and then further escalated when the catalytic appeal of zeolites became more apparent in the 1970's.[1] From these beginnings zeolite research continued to grow, and is now undertaken both industrially and academically the world over (Figure 1.1).

Figure 1.1: Comparison of naturally grown (left) and laboratory synthesised (right) zeolite materials.

Zeolites can be synthetically produced as naturally occurring zeolites have several drawbacks, **i)** they almost always contain undesired impurity phases, **ii)** their chemical composition varies greatly, **iii)** their properties are not optimised for research applications. Approximately 40 naturally occurring zeolites have been characterised and in the quest

for new materials and more than 140 entirely synthetic zeolite structures have been developed.[6]

1.1.1 Structure and Composition

Zeolites are crystalline microporous materials, which have complex pores and inner cavities. They are aluminosilicate materials containing frameworks made of silicon and aluminium atoms bound through bridging oxygen atoms (Figure 1.2). Lowenstein's rule states that in zeolites the Si:Al ratio can range from 1 to ∞, provided that two tetrahedral aluminium atoms are not separated by an oxygen atom alone. However if two aluminium atoms are separated by an oxygen atom alone, one of the aluminium atoms must have a coordination number greater than four.[7]

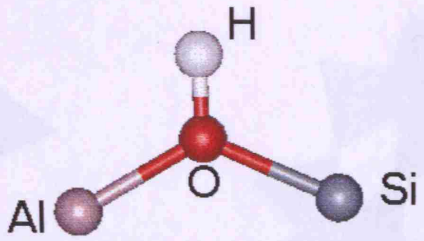

Figure 1.2: Zeolite framework component, containing aluminium (III) and silicon (IV) atoms bound through an oxygen bridge.

A charge imbalance is created throughout a zeolite framework, which can be considered as being made up of tetrahedra with differing charges ($[SiO_4]^{4-}$ and $[AlO_4]^{5-}$). To preserve the overall charge neutrality of the material, each $[AlO_4]^{5-}$ tetrahedra delocalises negativity across neighbouring atoms. This delocalisation allows exchangeable cations (usually protons) to bond to the zeolite framework, in the case of protons giving the material acidic properties (Figure 1.3). The nature of the charge balancing cation can influence the catalytic, optical, magnetic or electronic properties of a zeolite. For example a large cation could block or reduce the effective size of a pore opening whilst a small cation may only distort a pore opening.

$$A^{m+}\,[(SiO_2)_x \cdot (AlO_2)^-_y]\cdot zH_2O$$

Figure 1.3: General zeolite formula, where A is a cation with charge m, and (x+y) is the number of tetrahedra per crystallographic unit cell.

These inorganic macromolecules (as previously described) are made up of $[SiO_4]^{4-}$ and $[AlO_4]^{5-}$ tetrahedra, linked together by corner sharing. Many diverse three-dimensional frameworks can be formed from these tetrahedra due to the flexibility of the bent oxygen bridges. A common abbreviation is to represent these tetrahedra as prisms (known as secondary building units) which are joined together to form cages that represent the zeolite framework (Figure 1.4).

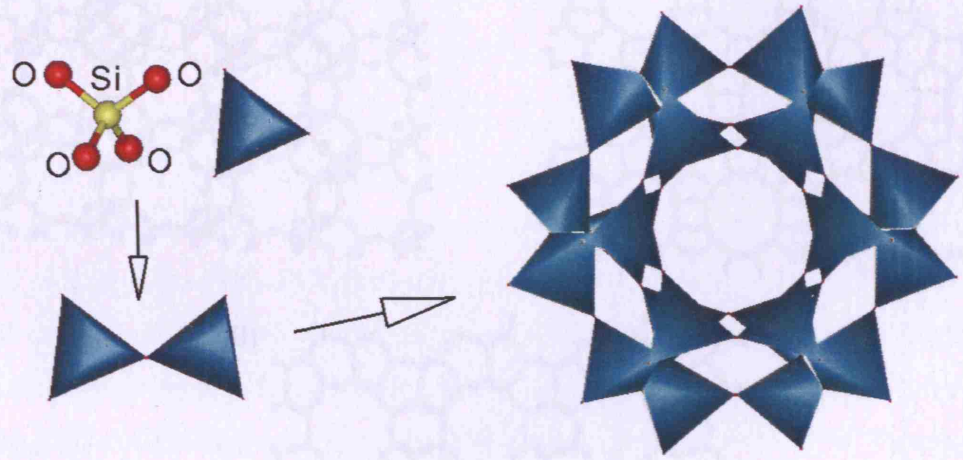

Figure 1.4: The prism secondary building units, join together to form the ordered macromolecular zeolite framework.

Every known zeolite framework has been designated an arbitrary three letter code, (by the international zeolite association structure commission) known as a framework type code (FTC) as a means of identification and classification.[8] The framework type describes the connectivity (topology) of the tetrahedral atoms (T-atoms), without reference to either chemical composition or unit cell dimensions of the framework. The FTC defines the size and shape of the pore openings, the dimensionality of the channel system, the volume and

arrangement of the cages as well as the types of cations available (Figure 1.5).[9] The nomenclature of the FTC was obscure and originally related to the name given to the materials by those first to discover them (**MFI**: Zeolite Socony **M**obil-**Fi**ve), more recently discovered materials are named in relation to their composition (**AFI**: **A**luminophosphate five $AlPO_4$-5 (**Fi**ve)). It is still common to use one code to describe the topology of the framework and different codes to indicate the difference in composition e.g. ZSM-5 (**MFI**) is used for aluminosilicate composition and -S1 (**MFI**) for the silicate polymorph.

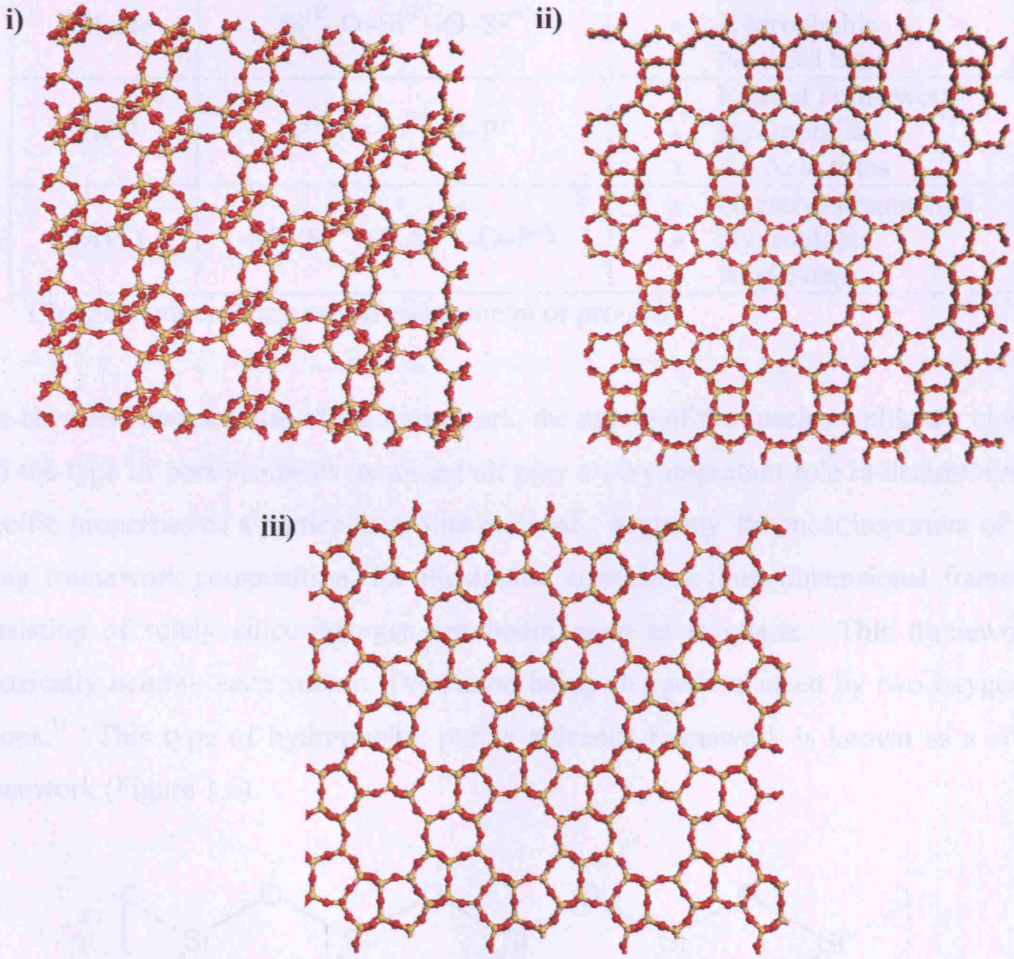

*Figure 1.5: Examples of different zeolite framework types **i)** CHA, **ii)** BEA, **iii)** MFI.*

Today a wide variety of zeolite-like microporous materials are known with T-atoms other than silicon and aluminium. Dyer proposed the term zeotypes, which refers to a range of materials such as silicates, aluminophosphates (AlPOs) and silicoaluminophosphates (SAPOs) (Table 1.1).[10]

Table 1.1: The chemical composition and properties of some zeotype materials.

Material	Composition	Properties
Zeolite	$M^+ (Si^{IV}–O–Al^{III}–O–Si^{IV})^-$	• Negative Framework • Hydrophilic • Acid Sites
Silicate	$Si^{IV}–O–Si^{IV}–O–Si^{IV}$	• Neutral Framework • Hydrophobic • No Acid Sites
AlPO	$P^{V}–O–Al^{III}–O–P^{V}$	• Neutral Framework • Hydrophilic • No Acid Sites
SAPO	$M^+ (Si^{IV}–O–Al^{III}–O–P^{V})$	• Negative Framework • Hydrophilic • Acid Sites

(M^+: Charge compensating cation either metal or proton)

The chemical composition of the framework, the nature of the species within the channels and the type of post synthesis treatment all play a very important role in determining the specific properties of a particular zeolite material. Arguably, the most important of these being framework composition, for illustration consider a three-dimensional framework consisting of solely silicon-oxygen tetrahedra, such as in quartz. This framework is electrically neutral, each silicon (IV) cation being charged balanced by two oxygen (II) anions.[11] This type of hydrophobic purely siliceous framework is known as a silicate framework (Figure 1.6).

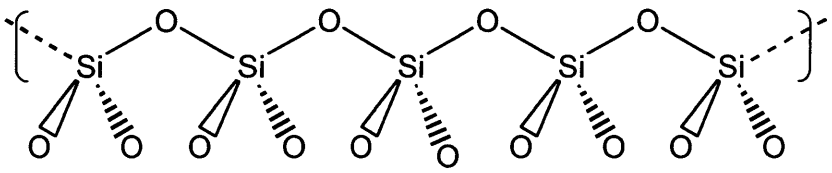

Figure 1.6: Charge neutral silicate framework containing silicon (IV) bridged by oxygen atoms.

In 1982 Union Carbide discovered a new class of zeotype materials known as aluminophosphates (AlPOs).[7] AlPOs are hydrophilic, microporous crystalline materials which have the same range of three-dimensional structures as zeolites but are built of $[PO_4]^{3-}$ and $[AlO_4]^{5-}$ tetrahedra (Figure 1.7). AlPOs can be thought of as zeolites having had the $[SiO_4]^{4-}$ tetrahedra substituted by $[PO_4]^{3-}$ tetrahedra. Individually the constituent AlPO tetrahedra have different charges ($[PO_4]^{3-}$ and $[AlO_4]^{5-}$), but overall the charge neutrality of the AlPO framework is maintained, as it is with silicate frameworks (but unlike aluminosilicate materials).

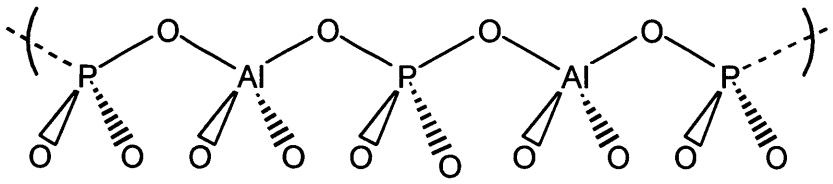

Figure 1.7: Charge neutral AlPO framework containing phosphorus (V) and aluminium (III) centres bridged by oxygen atoms.

Consequently AlPO materials do not possess the same acidic properties exhibited by zeolites (as no charge compensating proton is required) and are thus less reactive. It has been shown that some phosphorous atoms within an AlPO framework can be substituted by silicon atoms to form silicoaluminophosphates, SAPOs (Figure 1.8). By alteration of the phosphorous (V) for silicon (IV) atoms a charge deficiency is created within the framework, which is commonly compensated by addition of a proton that results in the hydrophilic material possessing acidic properties.

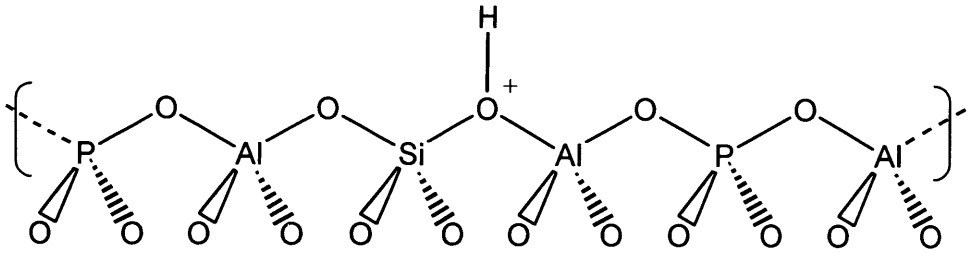

Figure 1.8: SAPO framework, containing phosphorus (V), silicon (IV) and aluminium (III) centres. The framework charge neutrality is maintained by the addition of a proton.

The number of potential applications for zeolite based materials already seems immense, but another branch of research is increasing their potential further. By inserting a heteroatom (usually a metal) onto the lattice site within the three-dimensional framework, further reactivity is introduced (Figure 1.9).

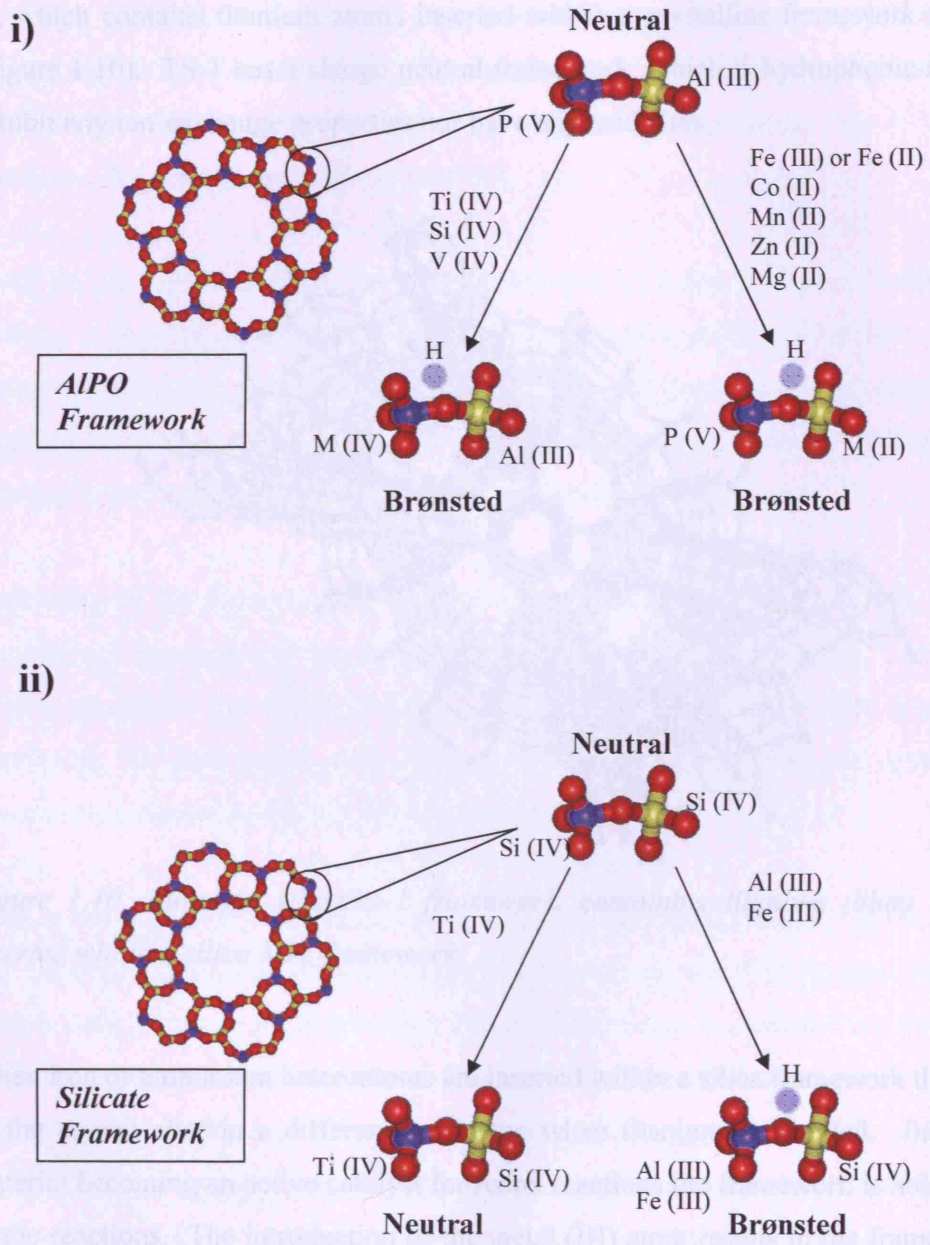

Figure 1.9: Demonstrating the different properties introduced when a heteroatom is inserted in an ***i)*** *AlPO and* ***ii)*** *silicate framework.*

The inserted heteroatoms can help in fine-tuning the strength of any existing acid sites, whilst also introducing further catalytic abilities. The type of catalytic reaction these inserted active sites are used for, depends upon the identity of the heteroatom inserted. For example titanium atoms will introduce reduction and oxidation (redox) possibilities. The most well known illustration of a titanium inserted silicate is titanium silicalite-1 (TS-1), which contains titanium atoms inserted within a crystalline framework of type MFI (Figure 1.10). TS-1 has a charge neutral framework, which is hydrophobic and does not exhibit any ion-exchange properties nor have any acid sites.

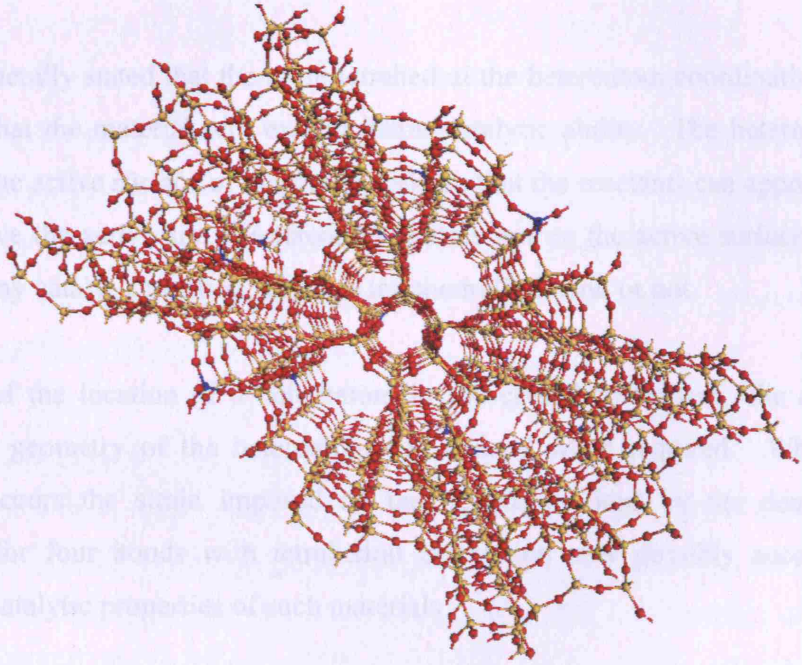

Figure 1.10: Titanium silicalite-1 framework, containing titanium (blue) heteroatoms inserted within a silica MFI framework.

When iron or aluminium heteroatoms are inserted within a silica framework the properties of the crystal alter in a different way from when titanium is inserted. Instead of the material becoming an active catalyst for redox reactions the framework is able to catalyse acidic reactions. The introduction of the metal (III) atom results in the framework being negatively charged, and hence charge compensating acidic protons become attached to the framework.

According to Pauling's principle heteroatoms such as titanium (IV) and iron (III) cannot normally be included within framework positions in the silicalite structure, as their ionic radius is too large compared to the framework silicon (IV) atoms. The more stable coordination geometry of the inserted heteroatoms is commonly octahedral rather than tetrahedral, making formation of these materials yet more problematic. However, the flexibility of the MFI framework (reversible orthorhombic–monoclinic transformation) allows for such a substitution. But because of the differences in ionic radii, the coordination about the heteroatom whilst being four-coordinate, cannot be perfectly tetrahedral but instead is pseudo-tetrahedral.

It can be generally stated that the more tetrahedral the heteroatom coordination, the more likely it is that the material will exhibit better catalytic ability. The heteroatom centre must be on the active surface of the framework, so that the reactants can approach and the products leave the active site. Heteroatom centres not on the active surface will not be engaged in any catalytic reaction, whether tetrahedrally bound or not.

Depending of the location of a heteroatom in the crystal framework, the coordination number and geometry of the heteroatom can expand when required. When such an expansion occurs the strain imposed on the heteroatom ions by the demand of the framework for four bonds with tetrahedral orientation may possibly account for the remarkable catalytic properties of such materials.

When a heteroatom is incorporated in a silicate framework, the volume of the average unit cell expands (consistent with the flexible geometry of the MFI lattice), but beyond a certain limit it cannot expand further, and the heteroatom is ejected from the framework forming extra-framework species. The maximum heteroatom concentration that be accommodated within a silicate framework has been evaluated by many authors and the subject is still actively debated.[12] Although a relationship between heteroatom content and catalytic activity certainly exists, a direct proportionality is limited to very low heteroatom concentrations because other factors (such as diffusion) limit high catalytic activity.

1.1.2 Applications

Zeolite and zeotype materials have many applications in a wide range of fields, as well as a vast range of potential applications currently being investigated globally. One of their first applications was as dehydrating agents, zeolitic materials can contain absorbed water molecules which are coordinated to the exchangeable cations on the framework surface. Heating the material under vacuum, will dehydrate the sample causing the extra framework cations to move position and to settle on sites with a lower coordination number. The dehydrated zeolites will then readily adsorb water to recover the preferred coordination.

Another common use of these framework macromolecules is as ion exchange materials, during which charge stabilising cations are simply exchanged for another cation. Zeolite-A is commonly exploited for ion exchange as a water softener.[10] Additionally zeolite-A has also been used in 'clean-up operations' to remove radioactive strontium after the Chernobyl and Three Mile Island disasters.

Adsorption and separation are further common applications of zeolite and zeotype materials (which have open porous structures with large internal surface areas and hence are capable of adsorbing large quantities of substances). The micropore diameter leading into the cavities determines the size of molecules which can be adsorbed. Each specific framework material has a precise sieving ability that can be exploited for purification or separation. This was first noted for the chabazite framework in 1932, chabazite can adsorb and retain small molecules such as methanol or formic acid but will not adsorb larger molecules such as benzene.[10]

The use of zeolite-based materials as heterogeneous catalysts is an area of common research and is relevant to the investigations reported herein. Zeolite materials are exceptional catalysts, which exhibit several properties that their amorphous counterparts do not. Traditionally amorphous catalysts are prepared in a highly divided state, to achieve the highest surface area (and thus highest concentration of catalytically active

sites) possible.[13] The inner pores and cavities within a zeolite framework provide a high surface area, which can accommodate as many as one hundred times more molecules than the equivalent amount of amorphous catalyst. Also, due to their ordered crystalline structure, zeolites do not have varying catalytic ability, as is typical of amorphous catalytic materials.[14,15]

Insertion of heteroatoms within the framework of a zeolite increases the reactivity of the material, many different heteroatom inserted materials are currently utilised and researched within industry today. One such example is titanium silicalite-1 (TS-1) (described above section 1.1.1) which was one of the earliest classes of molecular sieves containing a transition metal cation within framework positions. TS-1 has remarkable activity and selectivity for the partial oxidation of organic reactants by aqueous H_2O_2.[16,17] Since 1986, TS-1 has been used in the production of two industrial chemicals, catechol (CA) and hydroquinone (HQ), which are produced by the catalysed hydroxylation of phenol.[18]

Fe-MFI is a material with the same MFI framework as TS-1 but instead of containing titanium centres, it contains iron centres on the lattice positions. Fe-MFI has also attracted great interest from the catalysis industry due to its remarkable catalytic activity in partial oxidation reactions, for example catalysing the oxidation of benzene to phenol. This is a promising process for the phenol industry as it is a one-step process with no side products or dangerous reaction intermediates (such as form during the cumene process conventionally used).[19] A similar silicate material with MFI framework is ZSM-5, which has aluminium centres as the inserted heteroatoms. ZSM-5 has many reported applications, especially within the petrochemical industry. One such application is as a catalyst for the formation of methyl-*tert*-butyl ether (MTBE) (from methanol and isobutene) which is commonly used as an antiknock agent in gasoline.[20]

The concentration of the inserted heteroatoms within the silicate framework is limited, if the concentration is too high the framework can become unstable and degrade. Additionally, for optimum catalysis the inserted heteroatoms should be completely

enclosed in a silica environment (surrounded by solely –OSi- groups). The distribution of heteroatoms within the framework is random, but their low concentration makes it improbable that non-isolated species will occur.

1.2 Synthesis

The synthesis of heteroatom inserted zeotype materials has been widely reported employing a variety of techniques, discussed below.

1.2.1 Conventional Synthesis Methods

Grafting is a common method to produce heteroatom inserted zeolite based materials, wherein the heteroatom is first grafted onto a silica support which is then used as a starting material to produce the desired framework. This method has the advantage that no heteroatom oxide can form, but grafted materials are often unstable. Thus the components of the grafted material have to be carefully chosen to be stable towards solvents and reagents. Therefore the versatility of the materials produced can be limited regardless of them often being well defined, catalytically enhanced materials.

Another procedure for the formation of heteroatom containing microporous framework materials is ion exchange. In this process the ions of an existing zeolite are exchanged for ions of the desired heteroatom. For example, Zn/HZSM-5 can be prepared from HZSM-5 by mixing HZSM-5 with $Zn(NO_3)_2$ at 60 °C for 6 hours. The materials prepared by ion exchange are not the same as those produced by grafting procedures, as the inserted heteroatom is located within the pores of the framework rather than on lattice sites.

Heteroatom inserted zeotype materials can also be prepared via a hydrothermal synthesis procedure.[21] During this process the heteroatom source is added to a homogenous gel before crystallisation. Although this method is widespread, it offers little control over the coordination environment of the heteroatom, and formation of insoluble heteroatom oxides is common. The number of preparative variants of this basic synthetic premise is

immense. Including both reaction (crystallisation temperature, degree of agitation) and reagent parameters (identity and concentration).

When employing the hydrothermal synthesis procedure, firstly a homogenous gel is formed. The homogeneity of the gel being important as it directly relates to the homogeneity of the zeolitic product material. The gel contains a source of all elements required, distilled water (to minimise the introduction of ion contaminants), an organic structure directing reagent and possibly a mineralising agent to encourage crystallisation. The gel is then crystallised under hydrothermal conditions (100-200 °C) and the product recovered by filtration and repeated washing with distilled water.[6]

The chemical composition of the synthesis gel greatly influences the product formed, the ratio of all the materials added gives rise to different properties within the material once crystallised. The effect of the organic structure directing reagent is also evident as it has been reported that the framework takes the shape and size of the organic molecules.[22] One theory of how the structure directing reagent directs crystal growth is that the tetrahedral building blocks of the framework align into a particular geometry around the organic molecules, resulting in a foundation for further nucleation and crystal growth. Various computational reports have demonstrated that the organic molecules fit exactly into the pores formed during the crystal growth and thus agree with the template hypothesis.[23] However, some structure directing reagents allow growth of more than one framework type and some structures are made by more than one 'template'. Thus the exact method of interaction of the structure directing reagent with the framework species during crystal growth is still debated. Whilst the homogenous gel is formed it contains a range of silicate species such as monomeric and polymeric silica units and colloidal material. These species equilibrate within the solution by a series of polymerisation and de-polymerisation reactions (Figure 1.11).

$$(SiO)_xSi\text{-}OH + HO\text{-}Si(OSi)_y \leftrightarrow (SiO)_xSi\text{-}O\text{-}Si(OSi)_y + H_2O$$

Figure 1.11: Equilibrium of silica species during gel formation.

As all of the components (including the structure directing reagent) are added to the gel they become encompassed within this equilibrium. Commonly the gel is left to equilibrate (known as ageing) usually for 1 hour. It is worth reiterating that at this stage the gel is still amorphous and hence exhibits no long range order.

The gel is then heated under hydrothermal conditions, mimicking how zeolites are formed in nature. The crystals then grow via a solution-mediated crystallisation process, with two main steps: nucleation and growth.[24] Nucleation is defined as the formation of the first, very small, crystalline nuclei. However, the method of this nucleation is not clear with several methods having been proposed.[25-27]

The main types of nucleation proposed are **i)** homogeneous nucleation (the formation of nuclei directly from the solution) **ii)** heterogeneous nucleation (the formation of nuclei at the solid-liquid interface) **iii)** autocatalytic nucleation (the nuclei are formed within the gel particles prior to hydrothermal treatment and are released as the gel dissolves) **iv)** secondary nucleation (the nuclei appear associated with seed crystals). The crystal growth mechanism has however been considered to occur via the progressive incorporation of soluble species around the nuclei previously formed.[28]

There are however problems associated with the synthesis of these heteroatom inserted zeotype materials. For the inserted heteroatoms to be catalytically active they must exhibit tetrahedral coordination geometry, but commonly the most stable geometry of the heteroatoms is octahedral. This leads to the formation of heteroatom centres which are either only partially inserted within the framework, or are a completely extra framework species. Additionally most of the heteroatoms which are conventionally inserted are metals, thus clustering can occur during incorporation within the framework. This clustering reduces the catalytic reactivity of the heteroatoms and can lead to instability within the framework.

1.2.2 Cogel Synthesis Method

To overcome the problems of heteroatom insertion outlined above, co-precipitated gels can be employed as precursors to form zeotype framework materials. This work was first outlined by Padovan and co-workers, who reported the conversion of commercial SiO_2-TiO_2 co-precipitate into TS-1.[29] Their method involved wetness impregnation of the co-precipitate with tetra-*n*-propylammonium hydroxide solution, followed by crystallisation under autogenous pressure for 10 days. Uguina and co-workers further altered this procedure by replacing the co-precipitate with a SiO_2-TiO_2 co-precipitated gel (cogel) prepared by a sol-gel process.[30] This cogel was then subjected to hydrothermal conditions for only 1 day. It was demonstrated that utilisation of the cogel precursor (which was prepared 'in-house') enabled control over the properties and chemical composition of the raw material, which was carried through to the crystalline product. The reported cogel materials contain titanium and silicon atoms bound through oxygen bridges (analogous to those present in TS-1), which stabilise the titanium centres and prevent precipitation of anatase. Additionally, the clustering of titanium heteroatoms was negated and the coordination geometry of the titanium species in both the cogel precursor and the final TS-1 product was predominantly tetrahedral.

The work reported within this thesis utilises cogel precursors to produce a range of silicate framework materials which contain different heteroatoms. However, principally the same cogel and framework synthesis procedures were employed throughout the work and are discussed below.

1.2.2.1 Cogel Formation

The preparation of titanium cogel precursors as reported by Uguina and co-workers follows a two-step (acid-base) sol-gel process (Figure 1.12).[30] Wherein the silicon and titanium alkoxides are first hydrolysed in an acidic medium. The acid catalysed hydrolysis of the alkoxides is fast but the subsequent condensation reactions proceeds slowly, which avoids the formation of TiO_2. The second step involves the conversion of the liquid obtained into a solid gel, by increasing the rate of the condensation reactions via increasing the pH of the solution (by addition of an ammonium base) (Figure 1.12**iv**). The sequence of hydrolysis and mixing of the silicon and titanium alkoxides must be carefully performed due to the difference in their hydrolysis rates.[31] Commonly, the titanium containing sources are hydrolysed faster than the silicon alkoxide which may lead to the homo-condensation of the titanium species and hence TiO_2 formation. Thus to overcome this, the titanium alkoxide is added to a pre-hydrolysed and partially condensed solution of the silicon alkoxide. This silicon alkoxide solution contains a high concentration of Si-OH groups which favours the formation of hetero-condensation reactions to form Si-O-Ti bonds (Figure 1.12**iii**).

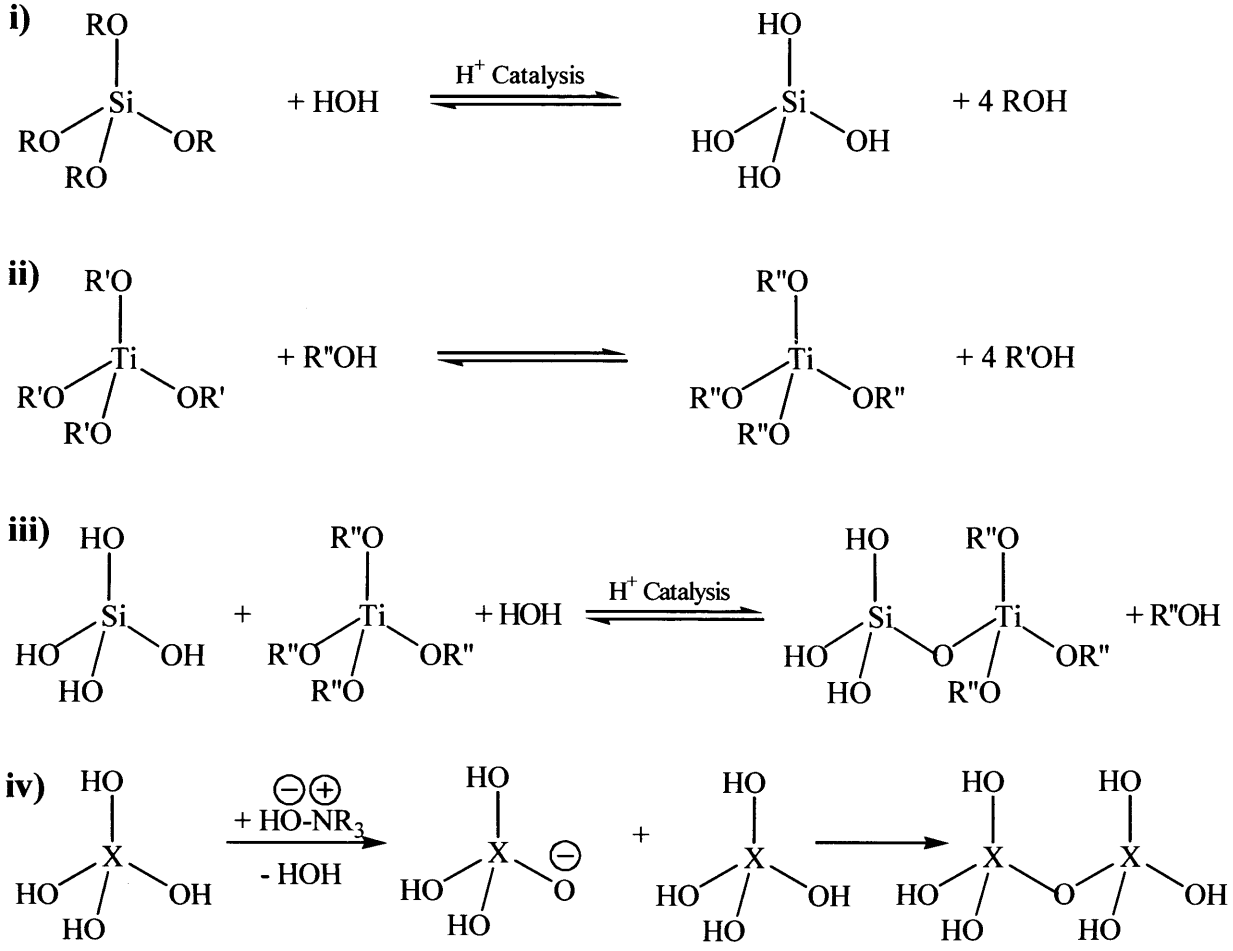

Figure 1.12: Hydrolysis and condensation process utilised to form amorphous cogel precursors, detailed description below:

i) ***Acid catalysed hydrolysis of silica source.*** *This reaction produces a range of hydroxyl-silicon materials due to the reversible nature of the hydrolysis. Additionally some condensation reactions occur to form oligomeric silicon products, which further undergo hydrolysis themselves.*

ii) ***Hydrolysis of titanium source.*** *This reaction is slower than the silicon hydrolysis, but similarly condensation reactions of the titanium centres are possible.*

iii) ***Mixing of i) and ii).*** *This mixing leads to further hydrolysis and some condensation of the titanium and silicon units to form oligomeric units.*

iv) ***Condensation of silicon and titanium species (X = silicon or titanium).*** *Addition of the ammonium base increases the condensation rate to form a polymeric co-precipitated gel.*

Once the gel is formed it is carefully dried to remove any alcohol or water within the material. The condensation reaction is still ongoing at this point and results in a denser product, which can be considered as an amorphous polymeric matrix. It was demonstrated (by Serrano and co-workers) that the weight loss produced after drying matches the theoretical content of alcohol and water.[32] Once dried the cogel precursor can be utilised to produce framework materials, TS-1 has been reported to have been synthesised from a cogel-type precursor by both microwave and hydrothermal means.[30,33] The scope of the work reported herein utilises solely hydrothermal techniques to synthesise framework products.

1.2.2.2 Framework Synthesis

The amorphous cogel is transformed into the desired framework structure by means of a solid-solid transfer mechanism. At this stage complete dissolution of the cogel must be avoided in order to prevent breaking of the Si-O-Ti linkages. Therefore, the framework synthesis takes place in a supersaturated system obtained by incipient wetness impregnation of the cogel with a structure directing reagent. The proposed stepwise method of crystal growth was reported by Serrano and co-workers for the synthesis of TS-1 from a titanium containing cogel.[34]

In the first step of crystal growth the cogel is converted into a particulate material, made up from amorphous particles with approximate sizes of 50 nm. During this step the cogel loses most of its porosity due to the tight packing of these primary particles. In the second step the primary particles undergo an aggregation process within the cogel, which leads to the formation of larger units, known as secondary particles. These secondary particles become separated from the cogel once they reach a critical size. It is these separated particles which first exhibit signs of long range order and hence crystallinity. It is reported that any titanium centres incorporated within these particles have maintained their tetrahedral coordination geometry. In the next step, the conversion of the pseudo-crystalline secondary particles is completed. As the concentration of secondary particles separated from the cogel increases, the amount of crystallinity in the system also

increases. This is due to the easier access of the structure directing reagent to the secondary particles. In the final crystallisation step the secondary particles are slowly transformed into TS-1 crystals. During this step crystalline edges appear on the surface of the secondary particles and hence the final size and shape of the TS-1 crystals is related to the morphology of the secondary particles.

Thus the transformation of the cogel precursor into a framework material occurs via a solid phase transformation process, unlike the conventional crystal growth mechanism previously described of nucleation and growth.

1.3 Zeolite Activity

The complexity of the heteroatom inserted framework materials results in these materials being active in a variety of ways. The types of activity considered herein are hydrophilic and catalytic activity.

1.3.1 Hydrophilic / Hydrophobic Activity

The materials considered within this work are the amorphous cogel precursors and the framework structures synthesised from them. Thus when the hydrophilic nature of these materials is discussed it is done so on a limited scale, being compared to each other (and analogous materials with different heteroatoms).

It has previously been reported that the cogel materials and comparable xerogel materials are more hydrophilic than their framework counterparts.[35] The higher concentration of terminal silanol groups on the amorphous surface results in a greater interaction with water, and hence higher hydrophilicity than for the framework materials.

The hydrophilicity of a material can affect its catalytic reactivity and selectivity, the actual affect is dependant upon specific reaction conditions such as the chemical nature of the solvent, reagents and products. However, caution must be taken when altering the

hydrophilicity of a material, for example it has been reported that upon silylation catalysts can become too hydrophobic which can result in the limited release of products hence lowering catalytic activity.[36] A balance between the hydrophobic and hydrophilic nature of the material must therefore be ascertained when altering the nature of a material in this manner. Considering an aqueous system, for example, if the altered catalyst is too hydrophobic, the active site will not release any organic products from the catalytic sites. However, if the hydrophilic nature of the catalyst were to be increased too much, water molecules would bind too strongly to the active sites, thus preventing any catalytic reaction from occurring.

1.3.2 Catalytic Activity

A catalyst is a material which increases the rate of a reaction, without being consumed during the process. Catalysts only alter the rate of a reaction (the kinetics), they do not effect either the thermodynamics or equilibrium composition of the reaction. Therefore, if the thermodynamics of a reaction state that a reaction can occur, the catalyst only alters the rate at which it occurs.

A catalyst lowers the energy barrier (activation energy) a reaction must overcome to form products (Figure 1.13). The lowering of the activation energy results in a faster reaction rate for the catalysed reaction.

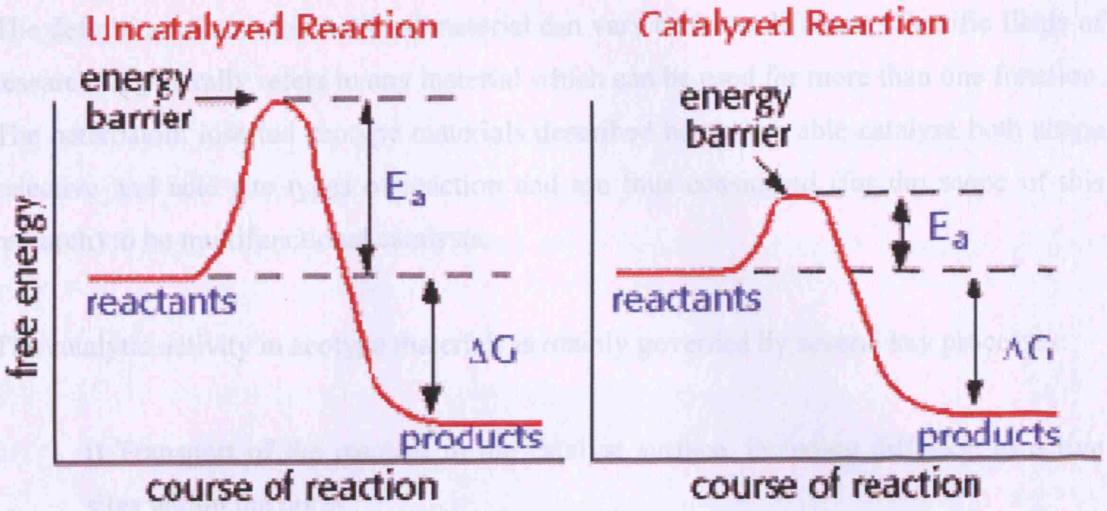

Figure 1.13: Energy pathways for an uncatalysed (left) and catalysed (right) reaction.[37]

During heterogeneous catalysis the reactant molecules (substrates) are absorbed onto the active sites on the surface of the catalyst. After reaction the products must desorb from the surface and diffuse away from the catalyst. Frequently this transport of reactants and products plays a dominant role in limiting the reaction rate.

The different types of catalysis undertaken by heteroatom inserted zeotype materials can be broadly split into two types, shape selective and active site catalysis. For shape selective reactivity the three-dimensional framework acts as a molecular sieve to catalyse a reaction. Whilst for active site reactivity, specific sites on the surface of the zeotype enable catalytic reaction. For the work reported herein these specific sites are either the inserted heteroatoms themselves or protons which occur due to changes in the framework caused by heteroatom insertion. The chemical nature of these heteroatom active sites, determines the type of reaction which can be catalysed (Table 1.2).

Table 1.2: The catalytic nature of the inserted heteroatom active sites.

Heteroatom	Catalytic Reactivity
Titanium	Oxidative
Aluminium	Acidic
Iron	Acidic or Oxidative

The definition of a multifunctional material can vary between different scientific fields of research, it generally refers to any material which can be used for more than one function. The heteroatom inserted zeotype materials described herein are able catalyse both shape selective and acid site types of reaction and are thus considered (for the scope of this research) to be multifunctional catalysts.

The catalytic activity in zeotype materials is mainly governed by several key processes:

i) Transport of the reactant to the catalyst surface, including diffusion to active sites within the pores.
ii) Adsorption of the reactant onto an active site.
iii) Chemical reaction of the adsorbed reactant to form an adsorbed product,
iv) Desorption of the product.
v) Diffusion of the products away from the interior active sites to the outer surface of the catalyst.
vi) transfer of the product away from the surface.

1.3.2.1 Shape Selective Catalysis

The pores and cavities of a zeotype material can be exploited to control the molecules which enter and leave the framework. Thus such framework materials are widely employed in shape selective catalysis for either reactant or product selectivity (Figure 1.14).

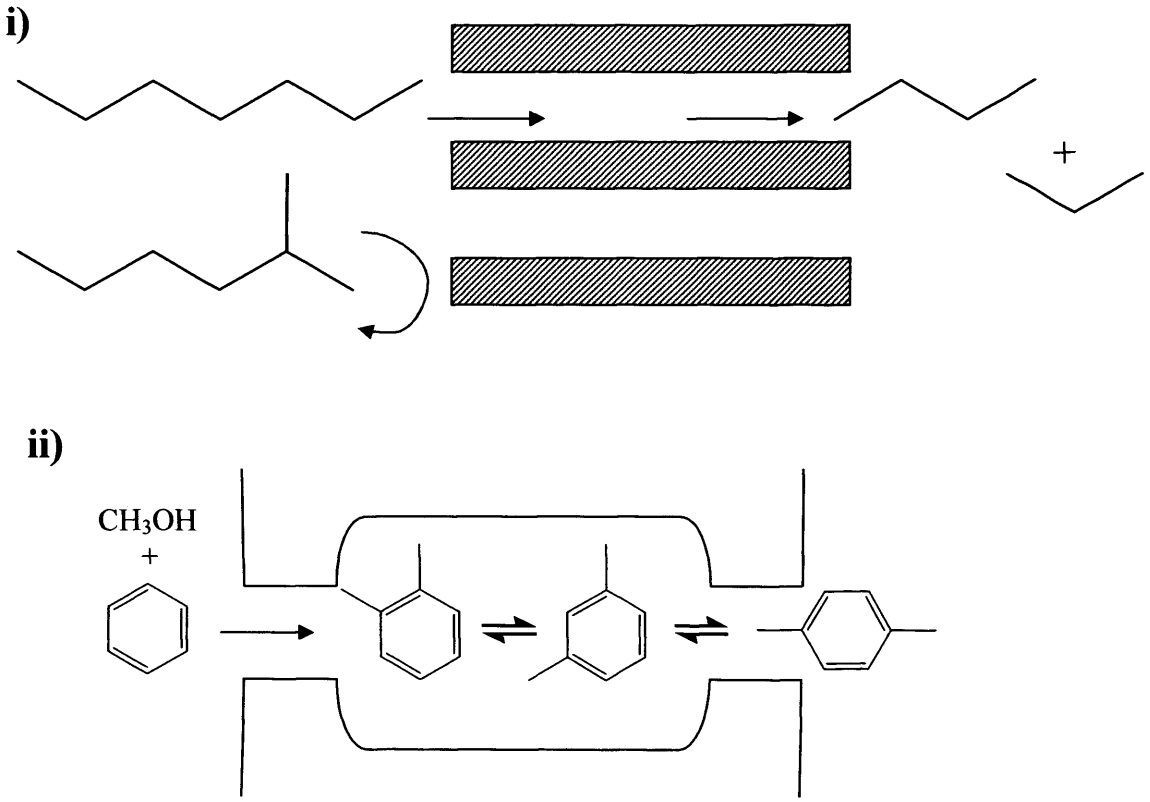

Figure 1.14: Shape selective catalysis (i) reactant selectivity, ii) product selectivity).

A common example reaction of shape selective catalysis is the Methanol To Gasoline (MTG) process developed by the Mobil Oil Company. In this reaction a stream of gaseous methanol is passed over a HZSM-5 catalyst and a dehydration-polymerisation reaction takes place inside the pores. The resulting effect is a sharp cut off of product distribution at C_{11} (gasoline) length fractions, the largest length of hydrocarbon that can fit inside the zeolite pore. A result of this cut off is that no further processing is required to remove heavier residues. The impact of this has been immense, countries with no

natural source of crude oil such as New Zealand are generating their own gasoline via the MTG process.[22]

1.3.2.2 Oxidative Catalysis Activity

The catalysts employed for oxidative catalysis within the scope of this work are titanosilicate materials which have previously demonstrated remarkable catalytic activity using the environmentally benign, aqueous hydrogen peroxide as the oxidant.[38,16] Dilute hydrogen peroxide is one of the most convenient oxidants due to its ease of handling, high active oxygen content and absence of by-products. The addition of hydrogen peroxide to titanosilicate materials brings about the formation of titanium peroxo complexes, which have been proposed to be the active species for the transfer of oxygen from the oxidant to the reactant. The hydrogen peroxide molecules act as bidentate ligands and are able to displace other ligands to form this peroxo species.

The nature of the framework titanium species to which the hydrogen peroxide ligand binds was reported (by To and co-workers) to have a tripodal structure.[39] It was demonstrated, via computational methods, that such tripodal species were converted from tetrapodal species which were the precursors to the peroxo intermediate sites, used for oxidation catalysis with hydrogen peroxide (Figure 1.15). The tripodal species is stabilised by the solvent, commonly depicted as water, although any ROH molecule could also give stability.

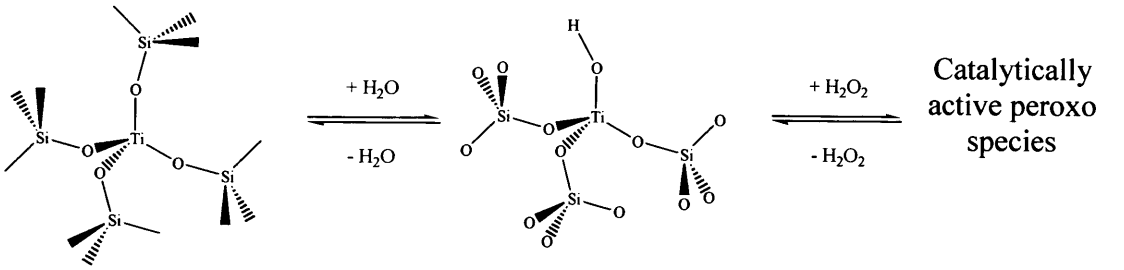

Figure 1.15 Interconversion of tetrapodal (left) and tripodal (middle) tetrahedral titanium sites in TS-1.

The precise nature of the catalytically active peroxo-titanium species for oxidation reactions (with hydrogen peroxide) has been widely debated, with several structures proposed from both theoretical and experimentally obtained data.[16,40] Research reported by Sankar and co-workers demonstrated that from the various proposed models, two structures (Ti-η^1-OOH and Ti-η^2-OOH) best fitted the experimental data describing the titanium active site (Figure 1.16).[41]

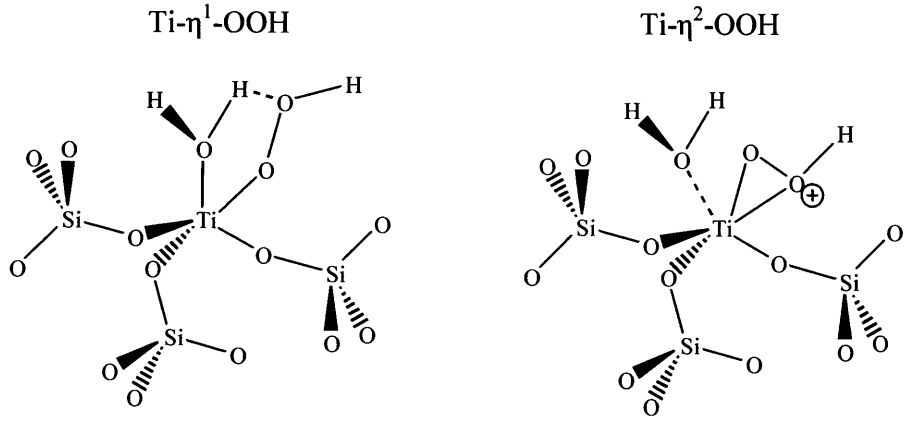

Figure 1.16: Proposed models of the titanium (IV) catalytically active sites, known as Ti-η^1-OOH (left) and Ti-η^2-OOH (right).

The peroxide species interacts with the titanium centre to form either of the Ti-η^1-OOH and Ti-η^2-OOH intermediates, which are energetically easily interconvertible. The Ti-η^1-OOH and Ti-η^2-OOH species catalyse the formation of the same products, just via different (although energetically similar) routes (Figure 1.17).[42] The main function of the catalyst in its active Ti-η^1-OOH and Ti-η^2-OOH forms, is to reduce the electron density at the peroxide O-O bond, making it more susceptible to attack by nucleophiles, such as alkenes.

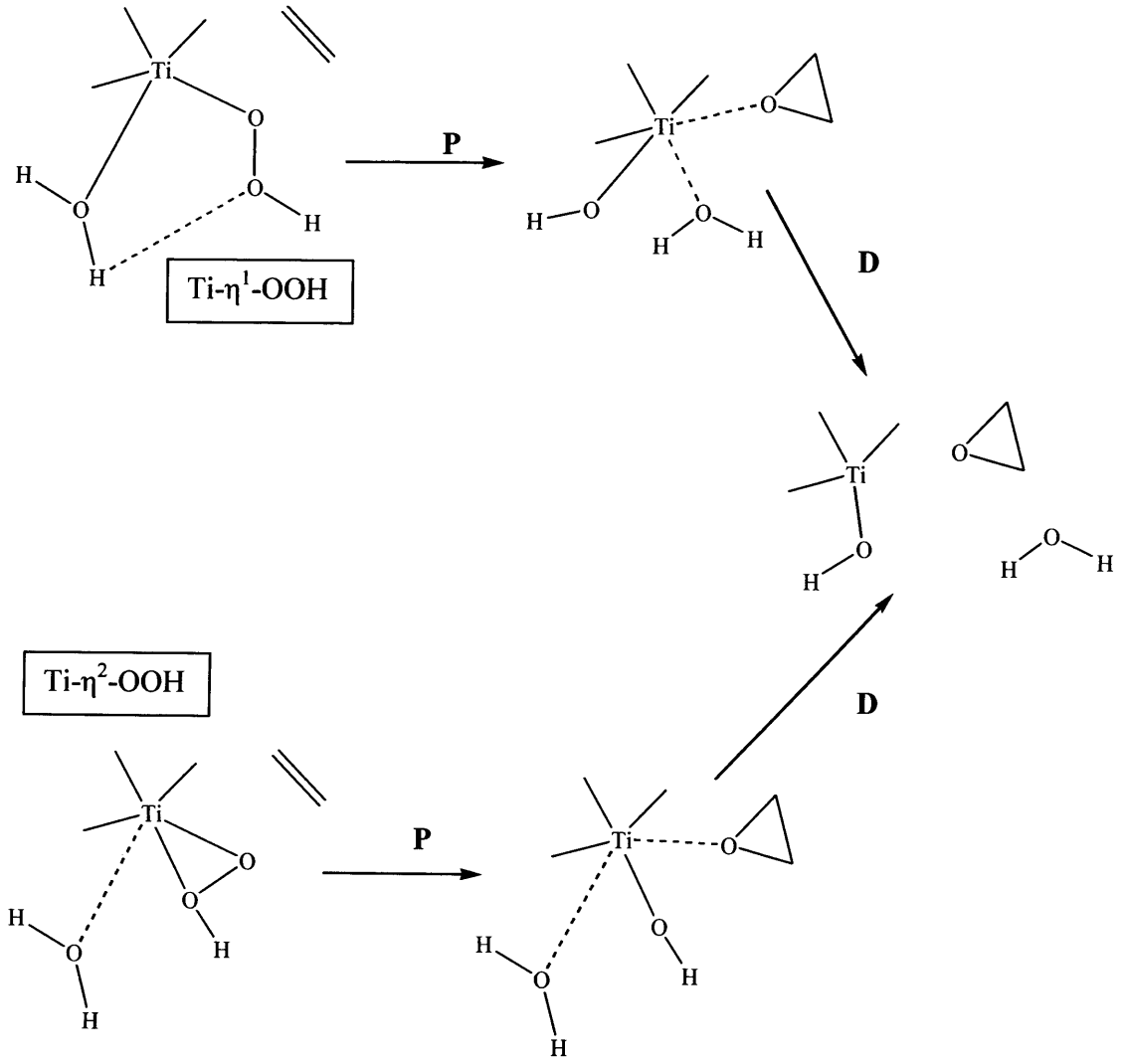

*Figure 1.17: Proposed mechanism of alkene epoxidation, utilising Ti-η^1-OOH and Ti-η^2-OOH catalytically active sites on TS-1 (Physisorption (**P**) and desorption (**D**)steps are shown).*

The oxidation reactions reported within this thesis are the epoxidation of cyclohexene, the formation of adipic acid and the hydroxylation of phenol (Chapter 2.3).

1.3.2.3 Acidic Catalysis Activity

Within this research the heteroatoms employed for acid catalysis were iron and aluminium. Acidic heteroatom inserted zeotype materials typically exhibit two types of acidic behaviour, Brønsted and Lewis acidity (Chapter 2.2.6.1). The acid site required for active catalysis is principally caused by a proton bound to oxygen bridging a silicon (IV) and aluminium / iron (III) atom within the framework (Figure 1.18). This proton is a strong Brønsted acid site, compared to those caused by a terminal silanol group. The nature of this acid site is such that the silicon atom could still accept a lone pair of electrons, thus making the site in activity both a Brønsted and Lewis acid site.

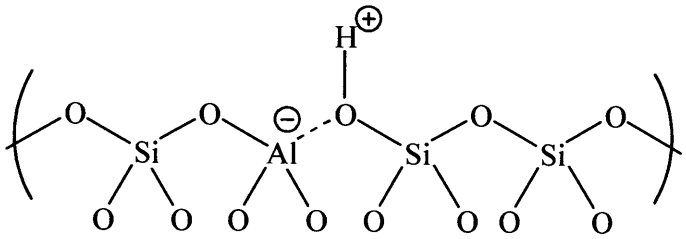

Figure 1.18: Catalytically reactive acid site in zeotype framework.

One of the main advantages of using such solid acid catalysts is that they are easily removable and therefore environmentally friendly. Thus, zeotype acid catalysts exhibit not only the advantages of being a solid acid catalyst (facile catalyst regeneration, limited reactor and plant corrosion) but also other unique advantages due to their frameworks (control over number and strength of acid sites, high adsorption capacity).

The only solely acid catalysis reaction undertaken in this work is the alkylation of benzene with ethanol (Chapter 2.3.4) and was undertaken for aluminium and iron inserted materials. The mechanism of this reaction can be likened to that of a Friedel-Crafts alkylation reaction. Friedel-Crafts alkylation reactions use Lewis mineral acids (such as HCl), whilst the active sites of the zeotype catalyst are also Brønsted acid sites (Figure 1.19). The mechanism outlined can continue to form a range of products employing both ethanol and benzene reagents.

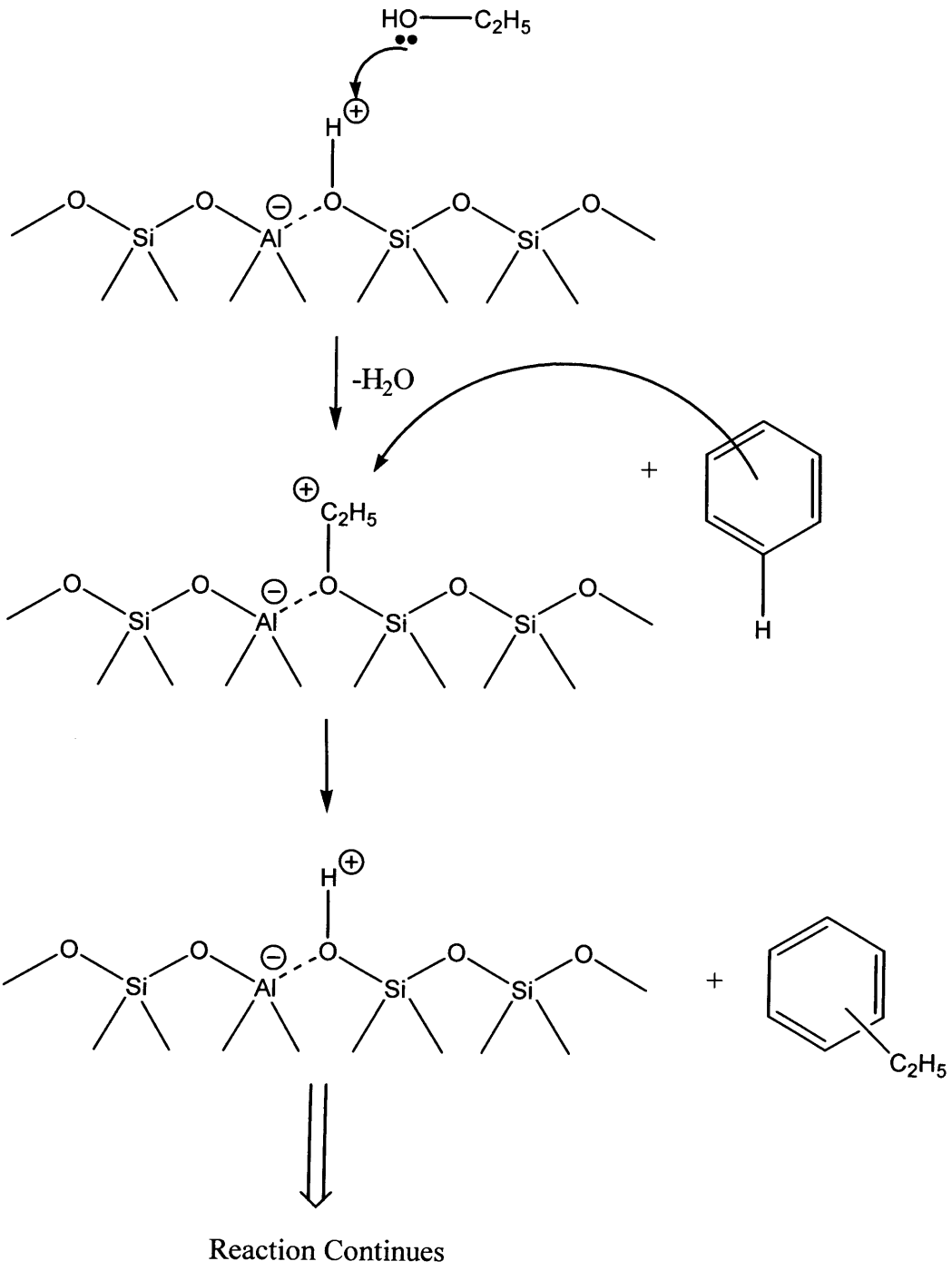

Figure 1.19: Friedel-Crafts alkylation type, acid catalysed reaction.

1.4 Research Hypothesis

The research reported herein intended to improve the qualities of heteroatom inserted zeotype materials. The materials produced contained titanium, aluminium, or iron heteroatoms initially and then a combination of two of these heteroatoms.

The synthetic procedure employed utilised a precursor, known as a *cogel* due to the way it was synthesised from a *co*-precipitated *gel*. This cogel consisted of an amorphous silica matrix, in which the desired heteroatom was inserted with tetrahedral coordination geometry (so as to be catalytically active). Thus, theoretically a range of zeolite materials can then be formed by subjecting a cogel to hydrothermal conditions in the presence of a specific organic structure directing agent.

By utilising the cogel precursor to produce framework materials it was envisaged that these product materials would exhibit different properties to those prepared by conventional methods. Common synthesis problems encountered with conventional synthesis techniques can include heteroatom clustering, the formation of extra-framework species and the limited heteroatom concentration incorporated within the framework. The cogel material itself would theoretically contain isolated heteroatoms in the predefined coordination geometry most reactive for catalysis. The heteroatoms would also be isolated and the concentration of these heteroatoms could be carefully controlled. From a single cogel precursor a range of framework materials could theoretically be produced, highlighting the flexibility of this synthesis method. The framework materials produced from the cogel precursors would similarly exhibit no heteroatom clustering, the formation of heteroatom oxides would be unlikely and, as stated the coordination geometry of the heteroatom is already predefined.

The physical properties of the framework materials synthesised were characterised and compared to analogous materials prepared by conventional methods. The catalytic properties of these materials were also analysed by either oxidative or acid catalysis depending on the nature of the inserted heteroatom.

1.5 Research Aims

- Reproducibly synthesise a range of cogel precursors containing either titanium, aluminium, or iron.

- Synthesise different framework materials from aforementioned cogel precursors and compare their physical and catalytic properties to those of analogous materials produced by a conventional process.

- Alteration of the properties of the synthesised materials and comparison with unaltered materials.

- Characterisation of the physical and catalytic properties of the cogel precursors and comparison with resultant framework materials.

- Evaluation of the potential for synthesising bimetallosilicate cogel precursors and from those framework materials.

1.6 References

(1) Bekkum, H. v.; Flanigen, E. M. *Introduction to Zeolite Science and Practice*; First ed.; Elsevier, **2001**.
(2) Uguina, M. A.; Serrano, D. P.; Ovejero, G.; Grieken, R. V.; Camacho, M. *Applied Catalysis A: General* **1995**, *124*, 391.
(3) Cronstedt, A. F. *Akad. Handl. Stockholm* **1756**, *18*, 120.
(4) Barrer, R. M. *Journal of the Chemical Society* **1948**, 2158.
(5) Stostack, R. *Molecular Sieves*; London: Blackie Academic and Professional, **1992**.
(6) Robson, H.; Lillerud, K. P. *Verified Syntheses of Zeolitic Materials*; 2nd ed.; Elsevier, **2001**.
(7) Atkins, P. W. *Physical Chemistry*; Fourth ed.; Oxford University Press, **1990**.
(8) http://www.iza-structure.org.
(9) Barrer, R. M. *Pure and Applied Chemistry* **1979**, *51*, 1091.
(10) Dyer, A. *An Introduction to Zeolite Molecular Sieves*; John Wiley and Sons, **1988**.
(11) Weitkamp, J. *Solid State Ionics* **2000**, *131*, 175.
(12) Gabelica, Z.; Valange, S. *Microporous and Mesoporous Materials* **1999**, *30*, 57.
(13) Hu, S.; Willey, R. J.; Notari, B. *Journal of Catalysis* **2003**, *220*, 240.
(14) Beck, C.; Mallat, T.; Burgi, T.; Baiker, A. *Journal of Catalysis* **2001**, *204*, 428.
(15) Serrano, D. P.; Grieken, R. v.; Melero, J. A.; Garcia, A. *Applied Catalysis A: General* **2004**, *269*, 137.
(16) Ratnasamy, P.; Srinivas, D. *Advances in Catalysis* **2004**, *48*, 1.
(17) Khouw, C. B.; Davis, M. E. *Journal of Catalysis* **1995**, *151*, 77.
(18) Perego, C.; Carati, A.; Ingallina, P.; Mantegazza, M. A.; Bellussi, G. *Applied Catalysis A: General* **2001**, *221*, 63.
(19) Perez-Ramirez, J.; Kapteijin, F.; Bruckner, A. *Journal of Catalysis* **2003**, *218*, 234.
(20) Mao, R. L. v.; Fairbairn, T. S. L.; Muntaser, A.; Xiao, S.; Denes, G. *Applied Catalysis A: General* **1999**, *185*, 41.
(21) Cundy, C. S.; Henry, M. S.; Plaisted, R. J. *Zeolites* **1995**, *15*, 400.
(22) Byrappa, K.; Yoshimura, M. *Handbook of Hydrothermal Synthesis*; 1st ed.; Noyes Publications, **2001**.
(23) Tatsumi, T.; Nakamura, M.; Yuasa, K.; Tominaga, H. *Catalysis Letters* **1991**, *10*, 259.
(24) Cundy, C. S.; Cox, P. A. *Microporous and Mesoporous Materials* **2005**, *82*, 1.
(25) Bronic, J.; Subotic, B. *Microporous Materials* **1995**, *4*, 239.
(26) Lechart, H.; Kacirek, H. *Zeolites* **1993**, *13*, 192.
(27) Derouane, E. G.; Gabelica, Z. *Journal of Solid State Chemistry* **1986**, *64*, 296.
(28) Schuth, F. *Current Opinion in Solid State and Materials Science* **2001**, *5*, 389.
(29) Padovan, M.; Leofanti, G.; Roffia, P.; 0311.983: European Patent, **1989**.
(30) Uguina, M. A.; Ovejero, G.; Grieken, R. V.; Serrano, D. P.; Camacho, M. *Journal of the Chemical Society, Chemical Communications* **1994**, 27.
(31) Walther, K. L.; Wokham, A.; Handy, B. E.; Baiker, A. *Journal of Non-Crystalline Solids* **1991**, *134*, 47.

(32) Serrano, D. P.; Uguina, M. A.; Ovejero, G.; Grieken, R. V.; Camacho, M. *Microporous Materials* **1995**, *4*, 273.
(33) Ahn, W. S.; Kang, K. K.; Kim, K. Y. *Catalysis Letters* **2001**, *72*, 229.
(34) Serrano, D. P.; Uguina, M. A.; Ovejero, G.; Grieken, R. V.; Camacho, M. *Microporous Materials* **1996**, *7*, 309.
(35) Camblor, M. A.; Corma, A.; Martinez, A.; Perez-Pariente, J. *Journal of the Chemical Society, Chemical Communications* **1992**, 589.
(36) Legrand, A. P. *The Surface Properties of Silicas*; 1st ed.; John Wiley and Sons, **2000**.
(37) http://www.biology.arizona.edu/biochemistry.
(38) Notari, B. *Advances in Catalysis* **1996**, *41*, 253.
(39) To, J.; Sherwood, P.; Sokol, A. A.; Bush, I. J.; Catlow, C. R. A.; Dam, H. J. J. v.; French, S. A.; Guest, M. F. *Journal of Materials Chemistry* **2006**, *16*, 1.
(40) Langhendries, G.; Vos, D. E. D.; Baron, G. V.; Jacobs, P. A. *Journal of Catalysis* **1999**, *187*.
(41) Sankar, G.; Thomas, J. M.; Catlow, C. R. A.; Barker, C. M.; Gleeson, D.; Kaltsoyannis, N. *Journal of Physical Chemistry B* **2001**, *105*, 9028.
(42) Romano, U.; Esposito, A.; Maspero, F.; Neri, C.; Clerici, M. G. *Studies of Surface Science and Catalysis* **1990**, *55*, 33.

Chapter 2: Experimental

2.0 Summary

This chapter details the experimental procedures employed during this research to enable reproduction or continuation of this work. Further from this details of material (both amorphous and framework) characterisation are given as well as any methods of results analysis.

Many different experimental procedures were utilised in the research reported herein, they have been split into three categories: synthesis, characterisation and catalysis. Each category outlines procedures utilised either in more than one chapter or extensively throughout one chapter. Where necessary specific details were further outlined in the appropriate chapter. Unless otherwise stated all reagents were purchased from Sigma-Aldrich and were used as received. (Throughout this chapter, M refers to a metal heteroatom.)

2.1 Synthesis

The main synthesis procedures employed to form a variety of heteroatom inserted materials are summarised below. In addition, several materials were produced with the heteroatom omitted from the synthesis, these 'blank' materials were used as experimental controls. The cogel synthetic procedure was similar to work reported by Serrano and co-workers, which described a method of converting a dried gel into TS-1 or zeolite β (Section 1.2.2).[1-4]

Once synthesised the products framework identity was confirmed utilising X-ray diffraction (XRD, Section 2.2.1), the pattern produced was compared to that reported in the literature and those obtained of standard materials (Figure 2.1).[5]

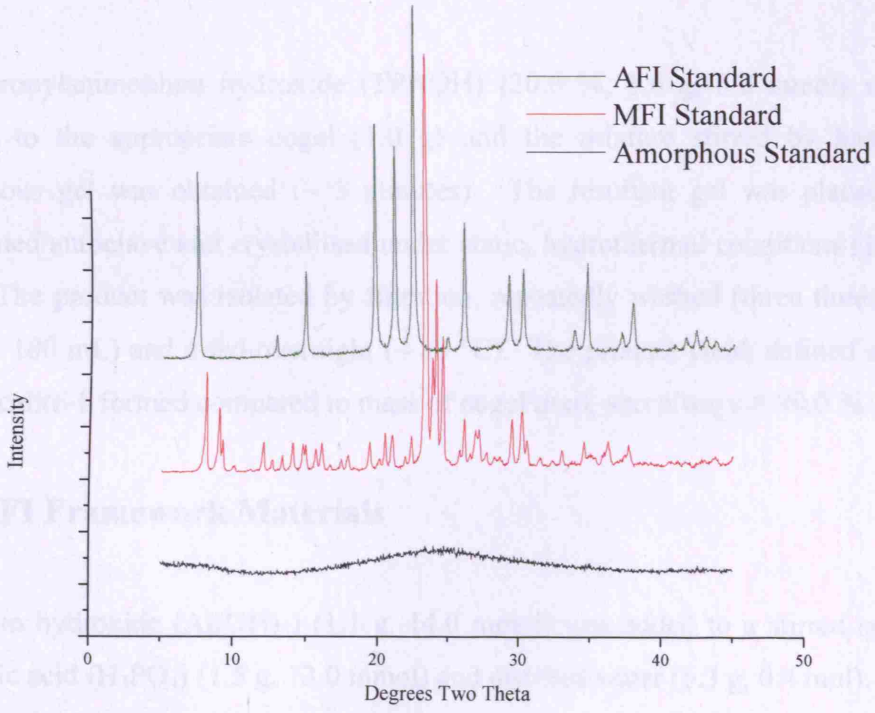

Figure 2.1: XRD patterns of standard materials.

2.1.1 Cogel Precursors

Tetraethylorthosilicate (TEOS) (98 %, 49.8 g, 0.2 mol) was slowly added dropwise to a stirred solution of distilled water (20.0 g, 1.1 mol) and dilute hydrochloric acid (0.1 M, 20.0 g, 0.5 mol), the resultant solution was stirred for 45 minutes. A separate solution of the heteroatom source* and isopropyl alcohol (110.0 g, 1.8 mol), was vigorously stirred for ~ 4 hours. The two solutions were then mixed and further agitated* whilst an aqueous solution of the ammonium salt* was added dropwise until gelation occurred. The transparent white gel was then dried overnight ~ 80 °C, calcined (if required) (3 °C min^{-1} to 535 °C, 4 hours maintained) crushed (by hand) and the resultant white powder (~ 40.0 g) stored under ambient conditions.

2.1.2 MFI Framework Materials

Tetra-*n*-propylammonium hydroxide (TPAOH) (20.0 %, 1.6 g, 3.2 mmol) was added dropwise to the appropriate cogel (1.0 g) and the mixture stirred by hand until a homogenous gel was obtained (~ 5 minutes). The resultant gel was placed inside a Teflon-lined autoclave and crystallised under static, hydrothermal conditions (170 °C, 24 hours). The product was isolated by filtration, repeatedly washed (three times, distilled water, 3x 100 mL) and dried overnight (~ 80 °C). The product yield, defined as mass of metal silicalite-1 formed compared to mass of cogel used, was always > 90.0 %.

2.1.3 AFI Framework Materials

Aluminium hydroxide ($Al(OH)_3$) (1.1 g, 14.0 mmol) was added to a stirred solution of phosphoric acid (H_3PO_4) (1.5 g, 13.0 mmol) and distilled water (6.3 g, 0.4 mol). To this a stirred solution of cogel (85.0 mg) and N-methyldicyclohexylamine (MCHA) (2.3 g, 11.0

*This method had several variations which are outlined specifically in the relevant chapter.

mmol) was added and the mixture covered and stirred for 1 hour. The resultant gel was placed inside a Teflon-lined autoclave and crystallised under static, hydrothermal conditions (150 °C, 16 hours). The product was isolated by filtration, repeatedly washed (three times, distilled water, 3x 100 mL) and dried overnight (~ 80 °C). The product yield, defined as mass of material formed compared to mass of cogel used, was always > 90.0 %.

The standard synthesis expected to produce AFI framework materials of the component ratio:

$$0.8 \text{ Template} : 0.9 \text{ P} : 0.1 \text{ Cogel} : 1.0 \text{ Al} : 25.0 \text{ } H_2O$$

2.1.4 Blank Materials

Both cogel and framework materials without the heteroatom were also synthesised. The blank cogel materials were synthesised as outlined in section 2.1.1 but the heteroatom source was omitted from the isopropyl alcohol mixture. From this precursor blank framework materials were synthesised, as outlined in sections 2.1.2 and 2.1.3. These materials were produced for use as comparative standards.

2.1.5 Silylation

Cogel and TS-1 materials were silylated with either tricholoromethylsilane (TCMS) or trimethylchlorosilane (TMCS). All glassware used was flame dried prior to use and all solvents were contained under an inert atmosphere prior to use.

Anhydrous hexane (excess) and the silylating reagent (dried, 9.0 g, TCMS: 58.6 mmol or TMCS: 82.8 mmol) were added to the pre-calcined, dehydrated titanosilicate material (5.0 g) under a nitrogen atmosphere. The resulting solution was stirred at reflux (4 hours) and

the product isolated by filtration, repeatedly washed (excess hexane) and dried overnight (~ 110 °C).

2.2 Characterisation

Several techniques have been used to identify and characterise the materials synthesised, their principles and applications are discussed herein.

2.2.1 X-Ray Diffraction (XRD)

This technique does have limitations as it only gives an average depiction of a structure. Additionally, it cannot identify localised defects or define the positions of small quantities of dopants (such as heteroatoms) and hence it was used in conjunction with other characterisation techniques.[6] Most zeolite and zeotype materials are polycrystalline and their crystal sizes are too small for single crystal X-ray analysis, thus only powder X-ray diffraction techniques were employed. Powder X-ray diffraction is a powerful technique which allows phase determination and structure identification.

X-ray diffraction is commonly used to establish phase purity, via the study of long-range order, within a material. Within this work the XRD pattern obtained from a material was compared to published crystallographic data of a material with the predicted framework type as well as those of the standard materials (Section 2.1).[7]

2.2.1.1 Principles of XRD

Every crystalline material produces a unique diffraction pattern which can be used as a means of identification. Crystals diffract X-rays since the wavelength of X-rays are similar to the atomic spacing between atoms within a crystal. Bragg proposed a mathematical formula to explain why the faces of crystals reflect X-ray beams.[8] Bragg's

Law stated that the diffraction of X-rays could be explained in terms of reflection from imaginary planes which extended throughout the crystal (Figure 2.2).

$$n\lambda = 2d \sin\theta$$

n = Integral Number of Wavelengths

λ = X-ray Wavelength

d = Distance between Successive Planes

θ = Angle which the Incident Beam of X-rays makes with the same Planes

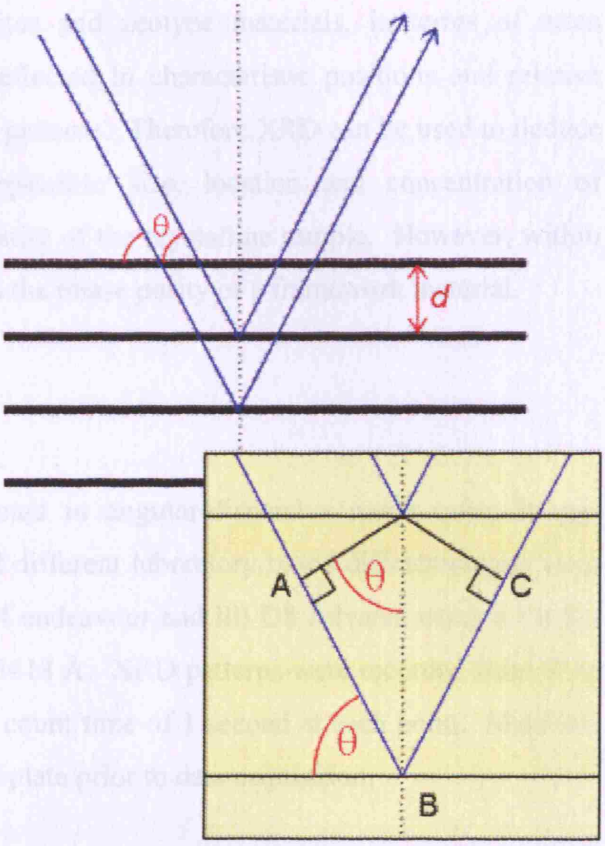

Figure 2.2: Bragg's Law (left) and Bragg reflection from a set of crystal planes (right).[8]

Using this idea of crystal planes it was observed that when two incident beams hit a crystalline material in parallel, at the same point but at different atomic planes, the path-lengths they must to travel to remain in phase were different. If an X-ray beam were considered as a wave and the components of that wave were to become out of phase then destructive rather than constructive interference would occur. Thus one component has to travel further than the other by AB + BC, which is dependant upon the glancing angle, θ, to remain in phase (Figure 2.2). Therefore, the path length difference of the two rays shown would be AB + BC = 2d sinθ. Thus X-ray waves that are reflected from the lattice planes in phase interfere constructively and give rise to strong signals (peaks) in a diffraction pattern. Similarly, for many glancing angles the path length difference was not

an integer number of wavelengths and the waves interfere destructively, which would result in weak or non-existent signals in a diffraction pattern.

The unique structure of different zeolites and zeotype materials, in terms of atom positions and unit cell dimensions, is reflected in characteristic positions and relative intensities of the peaks observed in XRD patterns. Therefore XRD can be used to deduce information about crystal structure, crystallite size, location and concentration of exchanged cations and degree of crystallinity of the crystalline sample. However, within this thesis XRD was used purely to assess the phase purity of a framework material.

2.2.1.2 XRD Data Collection

Powder diffraction patterns were collected in angular-dispersive mode using Bragg-Brentano geometry (Figure 2.3). Several different laboratory based diffractometers were used, **i)** Siemens D500, **ii)** Bruker axs D4 endeavour and **iii)** D8 Advana, using a Cu Kα radiation source with a wavelength of 1.5418 Å. XRD patterns were recorded from 0° to 45° (2θ) with a resolution of 0.02° and a count time of 1 second at each point. Materials were finely ground and mounted on a flat plate prior to data acquisition.

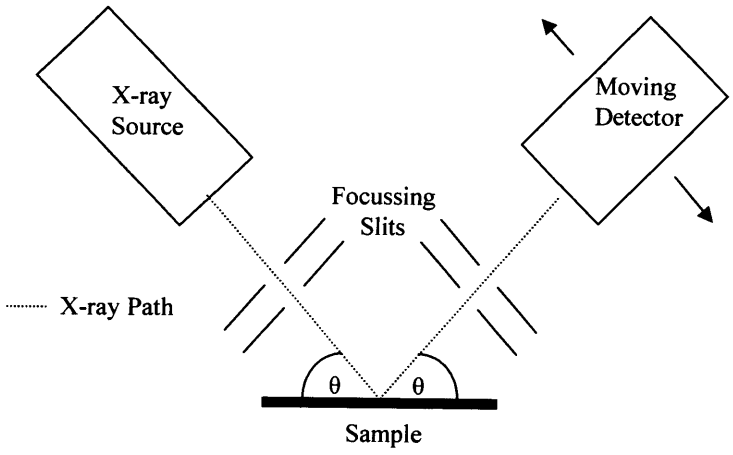

Figure 2.3: Laboratory based angular-dispersive XRD machine using Bragg-Brentano Geometry. (The arrows depict the stepwise movement of the detector).

2.2.2 Infrared (IR) Spectroscopy

Molecular vibrations and rotations occur in the infrared region of the electromagnetic spectrum and individual functional groups have characteristic absorption frequencies. IR spectroscopy utilises this to analyse chemical composition and structure of a material. This technique was used to **i)** confirm zeolite framework type, **ii)** provide qualitative information about the hydrophilic nature and **iii)** determine the degree of titanium tetrahedral incorporation upon lattice sites.[4,9]

The IR absorption band at 960 cm^{-1} is present in titanium silicalite-1 (TS-1, chapter 3) and absent from the spectrum of silicalite-1, thus it was initially considered to be a fingerprint for the characterisation of TS-1 materials. The intensity of the 960 cm^{-1} band was thought to be linearly correlated with the amount of titanium (IV) incorporated on framework positions, although it was experimentally extremely difficult to establish quantitative correlations between the intensity of the 960 cm^{-1} band and the titanium content of TS-1 and/or its catalytic activity.[10]

However, recent work has shown that this band was also present in many other silica compounds, therefore its relation to titanium (IV) is not straightforward.[9] The 960 cm^{-1} band had been considered to be a critical (although not necessarily sufficient), condition for the catalytic activity of titanium silicalites in the H_2O_2 oxidation of hydrocarbons.[11] Thus for a TS-1 material to be catalytically active in the oxidation of hydrocarbons, the corresponding IR spectrum must exhibit a peak at 960 cm^{-1} regardless of the cause of this vibration.[12]

2.2.2.1 Principles of IR

Typically when a molecule is exposed to infrared radiation it absorbs specific frequencies of radiation dependant upon both the functional groups within the molecule and the symmetry of the molecule. IR radiation can only be absorbed by bonds within a molecule

if the radiation has exactly the right energy to induce a vibration of the bond, hence the technique is used to diviluge chemical functionality.

In an IR spectrometer a source of infrared radiation is split into two beams of equal intensity, one beam is passed through the sample and the other is passed through air and used as a reference beam. Each beam is then analysed by the detector and a spectrum produced (Figure 2.4). The spectrum obtained denotes the vibrations within molecules via characteristic absorption peaks plotted against wavelength or frequency.

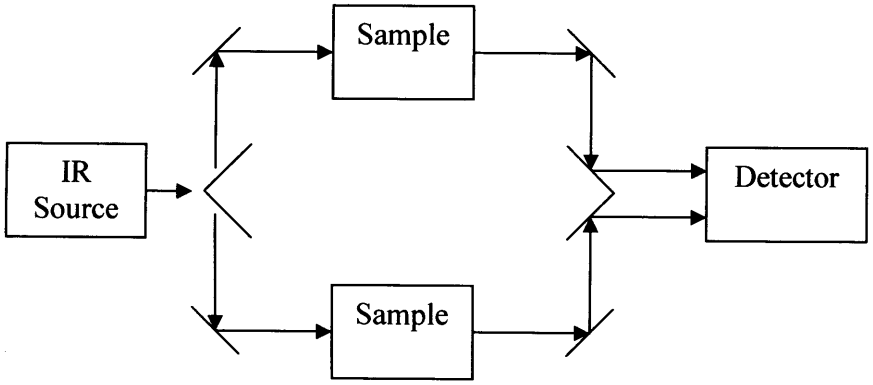

Figure 2.4: Schematic of an IR spectrometer.[13]

2.2.2.2 IR Data Collection

Self supporting wafers (25 mm diameter, ~ 100 mg) were analysed using PerkinElmer Spectrum One, FTIR spectrometer (100 cycles). Unless otherwise stated all materials were pre-calcined to prevent interference by organic molecules and dehydrated (300 °C for 1 hour) prior to experimentation.

2.2.3 Solid State Nuclear Magnetic Resonance (NMR) Spectroscopy

NMR spectroscopy is one of the most powerful tools for investigating the structure and dynamics of molecular systems. Within the scope of this reported research NMR spectroscopy was exploited to gain information regarding the coordination environment of two different nuclei, ^{27}aluminium and ^{29}silicon. Since high-resolution solid state NMR spectroscopy gives, in general, information on the local order of the structure and can be applied to crystalline and amorphous products and is a valuable complement to techniques such as XRD (which probe the long range order of crystalline materials).[14]

2.2.3.1 Principles of NMR

NMR spectroscopy is concerned with the magnetic properties of specific atomic nuclei, only nuclei that have a spin number greater than zero are NMR active. When an external magnetic field is applied across NMR active nuclei, the nuclei align with or against the applied field. The resonance produced for solids is broad, due to the orientation of the rigid nuclei related to the applied magnetic field.[15] To overcome this, the samples are spun around an axis to average the range of different orientations of nuclei within the material to zero. The angle about which the sample is spun is 54.74° and is known as the 'magic angle' (Figure 2.5).

Figure 2.5: In magic angle spinning, the sample spins at 54.74° to the applied magnetic field. Rapid motion at this angle averages dipole-dipole interactions and chemical shift anisotropies to zero.[8]

High resolution solid state ^{29}Si NMR was able to distinguish between four possible silicon-containing building blocks. Each block was represented by a Q^n designation, where n was the number of other silicon atoms joined to the central silicon via oxygen bridges (Figure 2.6).[16]

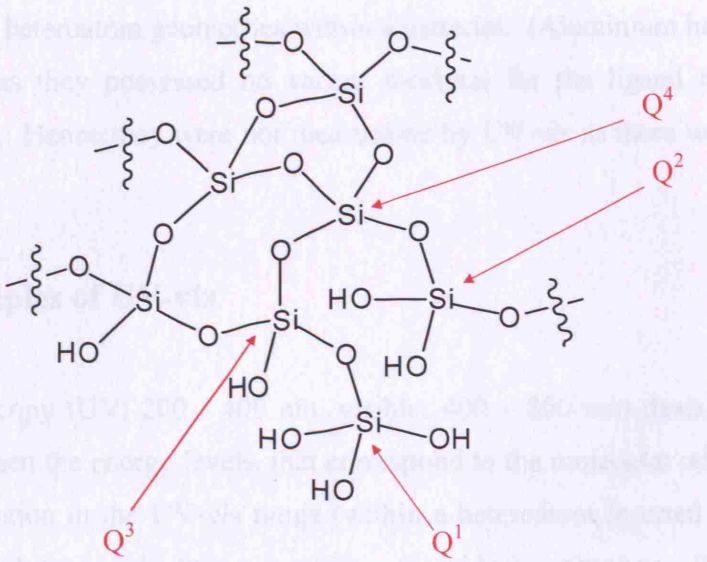

Figure 2.6: Demonstrating four different silicon Q^n environments within silica framework, which can be differentiated by ^{29}Si NMR.

2.2.3.2 NMR Data Collection

All NMR data reported in this thesis were obtained through department services, based at the Chemistry Department, University College London. High resolution solid state ^{29}Si MAS NMR spectra were recorded on a Varian 400 VRX spectrometer working at 79.5 MHz, with a pulse width of 6 μs, a pulse delay of 400 s, a spinning frequency of 4 kHz and 1000 scans. The ^{27}Al MAS NMR experiments were run on a Varian Infinity plus AS400 spectrometer at 104.26 MHz, with a pulse width of 0.5 μs, radio frequency field strength of 50 G, a pulse delay of 0.5 s, a spinning rate of 4 kHz and 85,000 scans.

2.2.4 Diffuse Reflectance Ultra Violet – Visible (UV-vis) Spectroscopy

UV-vis spectroscopy was used to identify the coordination geometry of both titanium and iron inserted heteroatoms. Quantitative results were obtained which demonstrated the ratio of different heteroatom geometries within a material. (Aluminium heteroatoms were not considered as they possessed no vacant d-orbital for the ligand to metal charge transfer to occur. Hence they were not measurable by UV-vis as there was no electronic transition.)

2.2.4.1 Principles of UV-vis

UV-vis spectroscopy (UV: 200 - 400 nm, visible: 400 – 800 nm) deals with electronic excitations between the energy levels, that correspond to the molecular orbitals within the system.[1] Absorption in the UV-vis range (within a heteroatom inserted material) arises because of ligand to metal charge transfer. Considering titanium silicalite-1 (TS-1, chapter 3) for example, the absorption at 215 nm is due to the transfer of charge from oxygen (II) to tetrahedrally coordinated titanium (IV). This charge transfer occurs due to electron transfer from the oxygen ligand to the vacant orbital of titanium species in the framework and therefore it is directly related to the titanium incorporation within the framework. A change in the band position is directly related to a change in coordination state of titanium (IV) within the framework. Hence, the presence of the band at 215 nm is accepted as evidence for the presence of isolated titanium (IV) species whereas a band at 280–330 nm (if present), is taken as evidence of extra framework species.[17]

2.2.4.2 UV-vis Data Collection

Data was collected on a PerkinElmer Precisely, Lambda 35 UV-vis spectrometer, under ambient conditions using $BaSO_4$ as a standard. Data was collected in reflectance mode and the intensities evaluated using the Kubelka-Munk function.[18]

2.2.5 Temperature Programmed Desorption – Mass Spectroscopy (TPD-MS)

Temperature programmed desorption of ammonia was used to investigate the nature of solid acid sites. By employing mass spectrometry to monitor the adsorbed species whilst the temperature was increased, quantitative information was derived about the strength and concentration of these acid sites.

2.2.5.1 Principles of TPD-MS

Acid sites on the surface of an oxide material are the direct consequence of the termination of the bulk and exposure of either metal cations or oxygen atoms. The nature of these acid sites results in them being either weak acid sites or strong acid sites. When ammonia was adsorbed onto the surface of one of the solid acid materials reported herein, it could have bound to both of these acid site types.

Weaker acid sites desorb ammonia at lower temperatures than the stronger acid sites, thus qualitative information can be gained about them (Figure 2.7).[19] The most predominate weak acid site type for all the materials studied was terminal silanol groups. These groups are normally considered as Lewis acids due to the ability of the silicon atom to accept a lone pair of electrons. However, it is also feasible for the species to donate a proton, thus also making the site a weak Brønsted acid. The stronger acid sites are predominantly caused by a proton bound to oxygen bridging a silicon (IV) and aluminium / iron (III) atom. This proton would be a strong Brønsted acid site (compared to the terminal silanol group). The nature of this acid site however, is such that the silicon atom could still accept a lone pair of electrons, thus making the site a Lewis acid site as well.

Thus complete resolution of the TPD peaks is difficult as the nature of acid sites causes them overlap. Hence, quantitative information about the acid strength of a material could not be obtained.

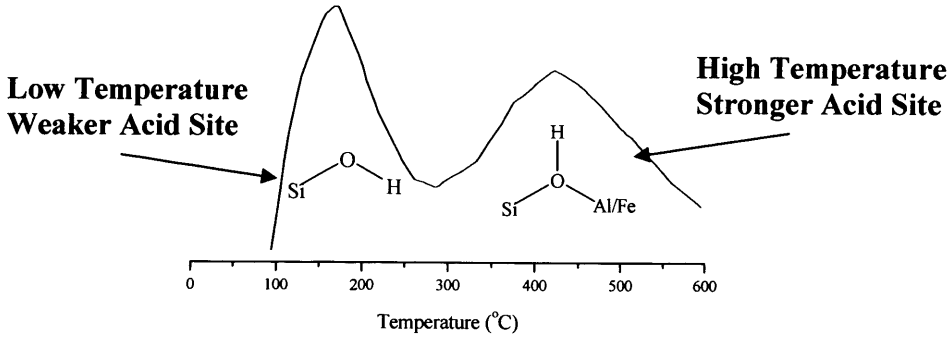

Figure 2.7: Example TPD profile indicating the two predominate acid sites in the silicate based materials synthesised.

2.2.5.2 TPD-MS Data Collection

Sieved pellets of a pre-calcined sample (400 mg) were dehydrated under a flow of nitrogen (350 °C, 1 hour). Once cool (< 100 °C) the system was then flushed with ammonia and the adsorption reaction allowed to equilibrate under a flow of ammonia (40 cm^3 min^{-1}, 2 hours). The system was then flushed with nitrogen to remove the ammonia atmosphere and ensure equilibrium conditions (50 cm^3 min^{-1}, 2 hours).[20] TPD experiments were then undertaken with a temperature ramp of 5 °C min^{-1}, to a final temperature of 600 °C (high enough to allow complete desorption of the probe) whilst still under a flow of nitrogen. A fresh sample was loaded for every run. (Figure 2.8).

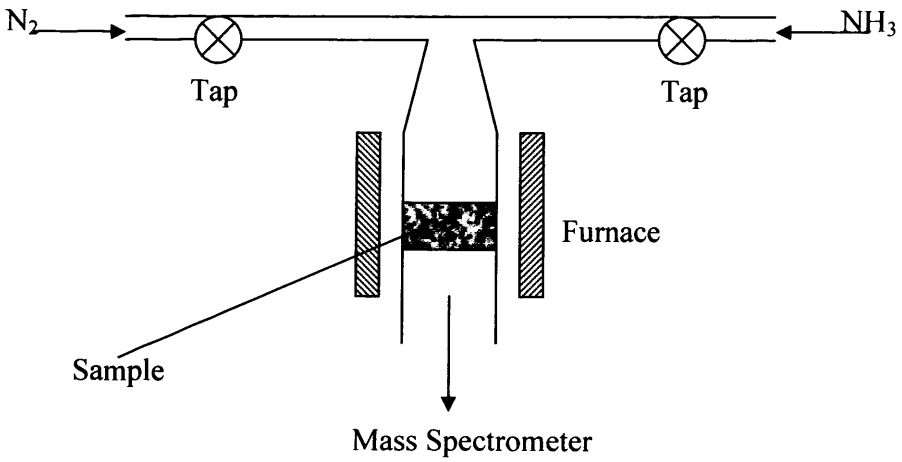

Figure 2.8: TPD-MS apparatus (built in house).

2.2.6 Scanning Electron Microscopy (SEM)

Scanning electron microscopy produces a largely magnified image using electrons instead of light to form an image. This image can give detailed information about a sample, specifically morphology, crystal size, surface area and topography. From this information it is possible to predict the catalytic reactivity of the material examined.

2.2.6.1 Principles of SEM

In SEM an electron beam is focused into a fine probe and subsequently scanned over a small area of the sample. As the beam interacts with the sample it creates various signals (secondary electrons, internal currents, photon emissions etc.), all of which can be appropriately detected. By using these signals to modulate the brightness of a cathode ray tube, which is scanned in synchronism with the electron beam, an image is formed.[21] All the materials examined were electrically non-conductive (negatively charged), which disturbs the image, thus they were gold coated to reduce the charge build up which repels or deflects the approaching beam causing image imperfections.

2.2.6.2 SEM Data Collection

SEM data was collected using the equipment of the Department of Archaeology, University College London. Samples were loaded onto stubs and spin coated with gold, for analysis on a JEOL JSM-5200 microscope using a 15 KV electron beam.

2.2.7 Energy Dispersive X-ray Analysis (EDX)

EDX chemical analysis was undertaken to determine the inserted heteroatom concentration and environment within a sample.

2.2.7.1 Principles of EDX

EDX is a non-destructive technique which detects most elements. Within this technique an X-ray beam impinging on a sample causes electrons to be ejected, leaving atoms ionised or in excited states. If the X-ray energy is sufficient, electrons can be ejected resulting in the emission of an X-ray photon specific to the element. Only the local surface area is scanned by the electron beam, thus no information is obtained about the bulk of the material.[22] However, quantitative information about heteroatom concentration (in relation to other heteroatoms) can be derived for a specific area and conclusions about regional clustering further derived from the heteroatom concentration within a specific area.

2.2.7.2 EDX Data Collection

EDX data was collected from samples which had been spin coated in gold, on a JEOL JSM-8900 electron microprobe scanning electron microscope. Dr. Kevin Reeves, Department of Archaeology, University College London aided in the collection of this data.

2.3 Catalysis Experiments

Oxidative (liquid phase) and acidic (both liquid and gas phase) catalysis experiments were undertaken as outlined below. (All catalysts were calcined prior to use.)

2.3.1 Epoxidation of Cyclohexene

Epoxides are important chemicals in synthetic organic chemistry, where they are used in many important organic transformation reactions.[23] They are also widely employed in industry for manufacturing products ranging from perfumery chemicals to polymeric materials.[24] The selective synthesis of various epoxides, by environmentally friendly processes using solid recyclable catalysts, is an area of great research interest.[25-27]

The formation of the epoxide product from cyclohexene (in this research) was undertaken using titanium inserted catalysts. The titanium heteroatoms within the catalysts behave as an active site, which upon the addition of the peroxide oxidant catalyses the transformation of cyclohexene into the desired epoxide product. The reaction pathway for the epoxidation of cyclohexene can continue after the epoxide has been formed. Additionally, a common side reaction can occur to form both mono-alcohol and ketone side-products (Figure 2.9). The presence of acidic hydroxyl groups on the surface of the titanium inserted catalyst, can cause the desired epoxide product to further hydrolyse to form the less desired diol (hence the reaction should not be undertaken in an aqueous solvent).[28]

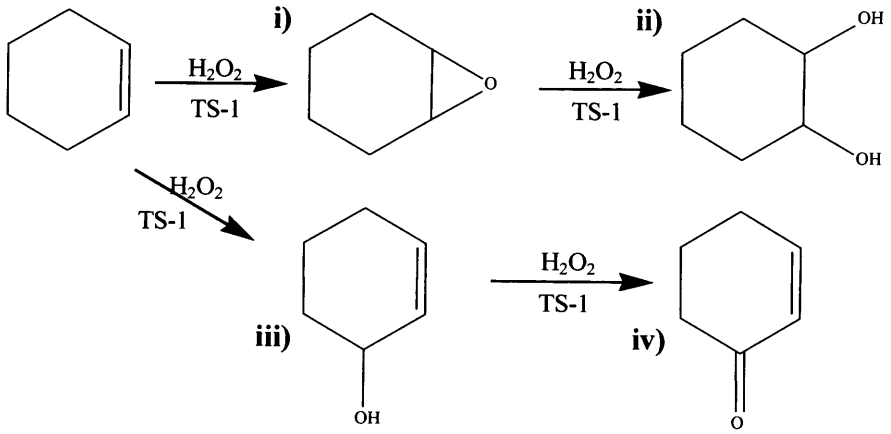

Figure 2.9: Epoxidation of cyclohexene to form products ***i)*** *epoxide and* ***ii)*** *diol as well as side products* ***iii)*** *mono-alcohol and* ***iv)*** *ketone (TS-1 = Titanium silicalite-1, Chapter 3).*

2.3.1.1 Experimental

The catalyst (100 mg), solvent (anhydrous acetonitrile, 99.8 %, 6.0 g, 0.1 mol) internal standard (mesitylene, 99.8 %, 500 mg, 4.2 mmol) and cyclohexene (500 mg, 99.5 %, 6.1 mmol) were stirred under reflux conditions and allowed to equilibrate (60 °C, 30 minutes). The oxidising reagent (hydrogen peroxide, 30 % (aq), 0.6 g, 6.1 mmol) was then carefully injected into the sealed mixture. Aliquots (~ 0.5 mL) were periodically removed from the mix and quenched (clean syringe equipped with micro-filter, 0.5 mL aliquot), over six hours. The aliquots were kept sealed and under refrigerated conditions until analysed by gas chromatography (GC, Section 2.4). The reactions were carried out in a 100 mL round bottomed flask equipped with reflux condenser and magnetic stirrer, an oil bath was used to maintain constant temperature.

2.3.2 Phenol Hydroxylation

The hydroxylation of phenol with hydrogen peroxide, catalysed by titanium containing silicalite materials, produces a mixture of catechol (*o*-dihydroxybenzene), hydroquinone (*p*-dihydroxybenzene), p-benzoquinone (Figure 2.10). Water and undetectable tar

compounds are the major by-products from this reaction.[29] Catechol and hydroquinone are both widely used in the chemical, pharmaceutical and food industries.[29] The major applications of catechol are as an electroplate additive and in hair dye, whilst the major uses of hydroquinone are as a reducing agent or photographic developer.[30] EniChem developed the synthesis of catechol and hydroquinone to use on an industrial scale and a plant producing over 10,000 tonnes per year of diphenols is in operation in Ravenna, Italy.[31]

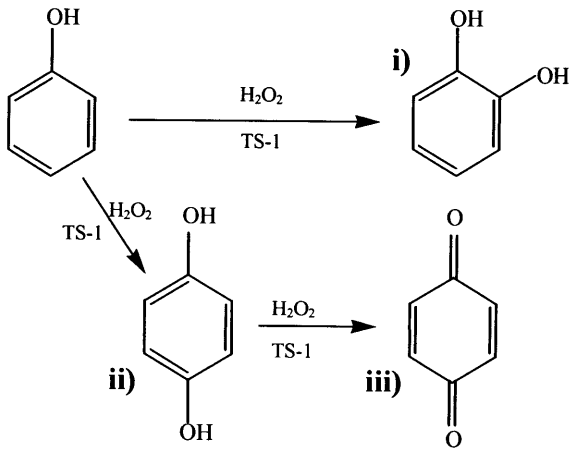

Figure 2.10: Hydroxylation of phenol to form products ***i)*** *catechol,* ***ii)*** *hydroquinone and* ***iii)*** *p-benzoquinone.*

2.3.2.1 Experimental

A stirred solution containing the catalyst (100 mg), water (distilled, ~ 20 g, 1.1 mol) and phenol (500 mg, 5.3 mmol) was allowed to equilibrate under reflux conditions (60 °C, 30 minutes). Hydrogen peroxide (30 % (aq), 600 mg, 5.3 mmol) was then carefully injected into the solution. Aliquots (~ 0.5 mL) were regularly removed from the reaction mix, quenched (micro-syringe filter) and subsequently the internal standard was added (4-fluorophenol, 99.0 %, 50 mg, 0.4 mmol) and the sample vessel sealed. Samples were kept under refrigerated conditions prior to GC characterisation. Reactions were performed in a 100 mL round bottomed flask equipped with reflux condenser and magnetic stirrer, an oil

bath was used to ensure constant temperature. All of the glassware used was covered to prevent product formation by a separate, light induced radical mechanism.[32]

2.3.3 Adipic Acid (AA) Formation

In industry adipic acid (AA) is mainly produced by oxidation of cyclohexane with air and nitric acid, following a homogenous two-step route.[33] However, this process leads to the formation of nitrous oxide, a greenhouse gas that has to be decomposed. Thus, the preparation of adipic acid by the heterogeneous one-step oxidation of cyclohexene is an attractive possibility. AA is an important building block for a variety of commercially useful products such as polyamides (nylon 6,6) and urethanes.[34,35] The reaction pathway to form AA from cyclohexene has many reaction steps hence the reported product yield can be lower than perhaps first expected (Figure 2.11).

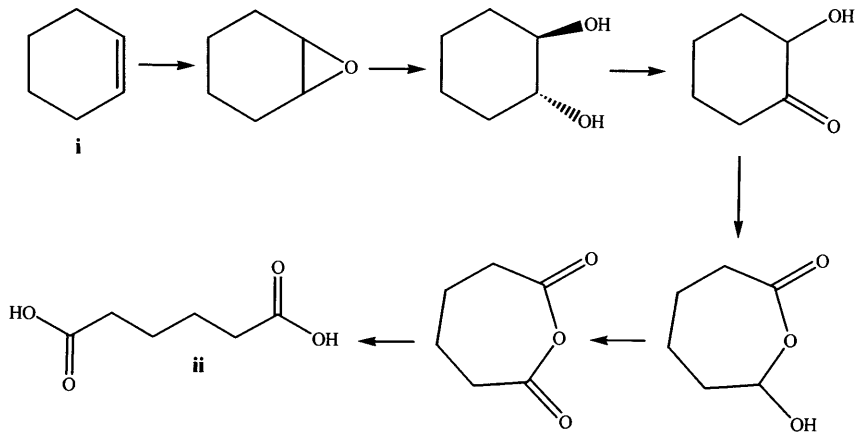

Figure 2.11: Reaction pathway for the oxidation of cyclohexene (i) to adipic acid (ii).

2.3.3.1 Experimental

The catalyst (100 mg) was added to a stirred solution containing methanol (99.8%, 6.0 g 0.2 mol), mesitylene (99.8 %, 500 mg, 4.2 mmol) and cyclohexene (99.5 %, 500 mg, 6.1 mmol) the temperature of the reaction mix was then allowed to equilibrate under reflux conditions (60 °C, 30 minutes). Hydrogen peroxide (30 % (aq), 2.4 g, 24.4 mmol) was

then carefully injected into the mix. Aliquots (~ 0.5 mL) were periodically removed from the mix, quenched (micro-syringe filter) and part of the aliquot esterified*. Aliquots were stored in sealed containers under refrigerated conditions until analysed by GC. The reactions were carried out in a 100 mL round bottomed flask equipped with reflux condenser and magnetic stirrer, an oil bath was used to maintain constant temperature.

*The esterification of adipic acid to diethyl adipate was necessary as adipic acid has previously been shown to interact with GC columns to produce false readings.[9] Methanol (dried, 5.0 g, 0.2 mol), concentrated sulphuric acid (95.0 %, 0.3 g, 3.1 mmol) and the aliquot (0.25 mL) were stirred in a gently heated (40 °C, 2 hours) closed system. The mixture was then cooled (ice bath) and the solvent removed in-vacuo. The resultant liquid was then analysed as normal (GC) and the results calibrated against the internal standard.

2.3.4 Ethylation of Benzene

In many industrial processes the alkylation of aromatics is performed using catalysts which exhibit several major drawbacks. Often such catalysts are strong mineral or Lewis acids, which are highly toxic and corrosive. They are dangerous to handle and to transport as they corrode storage and disposal containers. Often products need to be separated from the acid with a difficult and energy consuming process. Additionally, these acids frequently are neutralised after reaction necessitating the disposable of the salts as well. In order to avoid these problems efforts have been devoted to the production solid acid catalysts which are selective, safe, environmentally friendly and reusable.[36,37] This reaction was undertaken in a fixed bed reactor, unlike the batch testing undertaken for the previously described catalysis reactions.

The ethylation of benzene can yield a range of products, ethyl benzene (EB) being the most significant (Figure 2.12). The type of catalysts employed for this reaction were acid catalysts, thus within the scope of this research they contained either aluminium or iron heteroatoms. EB is the key intermediate in the manufacture of styrene, which in turn is

one of the most important industrially used monomers, with ~ 20 million tonnes produced globally each year.[38]

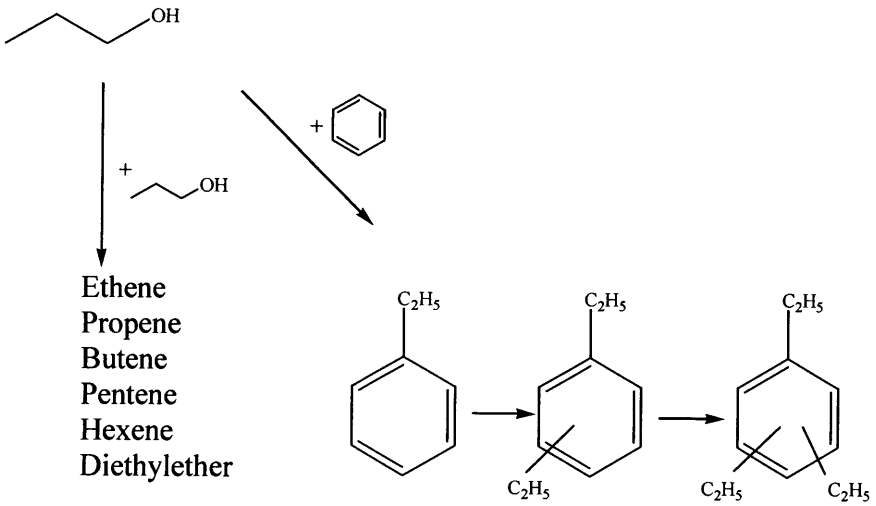

Figure 2.12: Possible products for the ethylation of benzene reaction.

2.3.4.1 Experimental

The catalyst (400 mg, pelletised) was activated (500 °C for 1 hour,) in air, then cooled (300 °C) and allowed to equilibrate (30 minutes). Under a flow of nitrogen, the freshly prepared feed mix (2:1 benzene:ethanol) was injected over the catalyst at a constant flow rate using a syringe infusion pump (4 mL / hour). The resultant vapour was condensed and aliquots of both gas and liquid phase were taken hourly and analysed using GC. This catalysis reaction was carried out using equipment built and tested in-house. The temperature of the system was monitored by a thermocouple linked to the heating control.

Catalyst activity was recorded as a function of both benzene and ethanol conversion normalised via data collected from a series of calibration runs. Reagent conversions can appear misleading when using a fixed bed reactor as reagents (which may not have reacted) can become hindered in passing through the reaction bed. Thus by normalising data obtained with data from experiments in which just benzene or ethanol was used as the reagent, the delay of reagents leaving the reactor can be negated.

The benzene to ethanol (2:1) ratio of the feed mixed had previously been found by our research group to afford the maximum benzene conversion and EB selectivity and was hence unaltered for this work.

2.4 Gas Chromatography (GC)

As a catalytic reaction proceeded aliquots were analysed using GC to elucidate the composition of the reaction mixture at time, *t*. These aliquots were either gas or liquid phase depending on the nature of the reagents and products formed. By deriving the specific composition of the reaction (at a precise time) information regarding the reactivity and selectivity of the catalyst was ascertained. Strictly both gas chromatography (solid stationary phase) and gas-liquid chromatography (GLC) (porous solid plus viscous liquid, stationary phase) were employed, but both are frequently referred to as GC.

2.4.1 Principles of GC

In GC a small volume of the reaction mixture is vaporised and injected onto the head of the chromatographic column, where it is then carried through the column by a flow of inert gas (Figure 2.13). The column contains a stationary phase which causes the components (solutes) of the sample to separate according to their affinity for this stationary phase. Solutes which have a high affinity for the stationary phase will move more slowly along the column than those with less affinity. Thus the components will separate and reach the detector at different times, allowing separate detection and identification.[39,40]

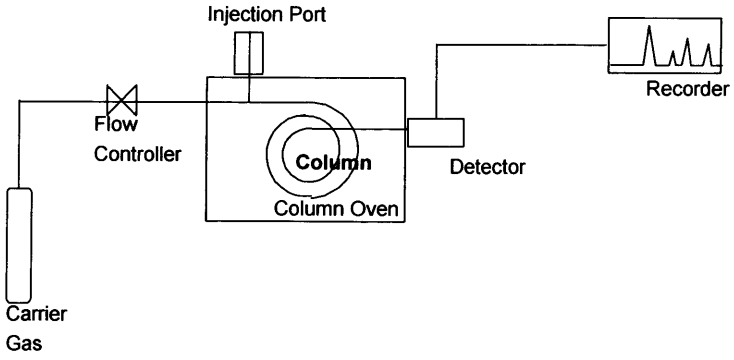

Figure.2.13: Schematic of gas chromatograph.

2.4.2 GC Data Collection

The method of data collection for GC varied according to the specific catalytic experiment under investigation (Section 2.3). Reaction mixtures were characterised on either **i)** Varian 3400 CX, equipped with flame ionisation detector and 25 metre capillary column (BPX5, crossbond) (liquid phase analysis) or **ii)** Clarus 500, PerkinElmer equipped with flame ionisation detector and 30 metre capillary column (Ellite-1, crossbond 100% polysiloxane) (both liquid and gas phase analysis). The carrier gas used was always helium and the ignition gases were always hydrogen and air.

2.5 References

(1) Serrano, D. P.; Uguina, M. A.; Ovejero, G.; Grieken, R. V.; Camacho, M. *Microporous Materials* **1996**, *7*, 309.

(2) Serrano, D. P.; Uguina, M. A.; Ovejero, G.; Grieken, R. V.; Camacho, M. *Microporous Materials* **1995**, *4*, 273.

(3) Uguina, M. A.; Ovejero, G.; Grieken, R. V.; Serrano, D. P.; Camacho, M. *Journal of the Chemical Society, Chemical Communications* **1994**, 27.

(4) Uguina, M. A.; Serrano, D. P.; Ovejero, G.; Grieken, R. V.; Camacho, M. *Applied Catalysis A: General* **1995**, *124*, 391.

(5) Millini, R.; Massara, P.; Perego, G.; Bellusi, G. *Journal of Catalysis* **1992**, *137*, 497.

(6) Robson, H.; Lillerud, K. P. *Verified Syntheses of Zeolitic Materials*; 2nd ed.; Elsevier, **2001**.

(7) Treacy, M. M. J.; Higgins, J. B. *Collection of Simulated XRD Powder Patterns for Zeolites*; 4th ed.; Elsevier, **2001**.
(8) Atkins, P. W. *Physical Chemistry*; Fourth ed.; Oxford University Press, 1990.
(9) Ratnasamy, P.; Srinivas, D. *Advances in Catalysis* **2004**, *48*, 1.
(10) Legrand, A. P. *The Surface Properties of Silicas*; 1st ed.; John Wiley and Sons, **2000**.
(11) Huybrechts, D. R. C.; Buskens, P. L.; Jacobs, P. A. *Journal of Molecular Catalysis* **1992**, *71*, 129.
(12) Eley, D. D.; Hagg, W. O.; Gates, B. *Advances in Catalysis*; 1st ed.; Academic Press, **1996**.
(13) Harwood, L. M.; Claridge, T. D. W. *Introduction to Organic Spectroscopy*; 2nd ed.; Oxford University Press, **2000**.
(14) Duer, M. J. *Solid-State NMR Spectroscopy*; 1st ed.; Blackwell Science, **2002**.
(15) Iggo, J. A. *NMR: Spectroscopy in Inorganic Chemistry*; 5th ed.; Oxford University Press, **2004**.
(16) Cheng, C.-H.; Shantz, D. F. *Journal of Physical Chemistry B* **2005**, *110*, 313.
(17) Liu, Z.; Davis, R. J. *Journal of Physical Chemistry B* **1994**, *98*, 1253.
(18) Deglass, W. H.; Haller, G. L.; Kellerman, R.; Lunsford, J. H. *Spectroscopy in Heterogeneous Catalysis*; 2nd ed.; Academic Press, **1979**.
(19) Selli, E.; Forni, L. *Microporous and Mesoporous Materials* **1999**, *31*, 129.
(20) Auroux, A.; Monaci, R.; Rombi, E.; Solinas, V.; Sorrentino, A.; Santacesaria, E. *Thermochimica Acta* **2001**, *379*, 227.
(21) Lawes, G. *Scanning electron microscopy and microanalysis*; 1st ed.; John Wiley and Sons, **1987**.
(22) Christian, G. D. *Analytical Chemistry*; 5th ed.; John Wiley and Sons, **1994**.
(23) Laha, S. C.; Kumar, R. *Journal of Catalysis* **2002**, *208*, 339.
(24) Kochkar, H.; Figueras, F. *Journal of Catalysis* **1997**, *171*, 420.
(25) Waal, J. C. v. d.; Bekkum, H. v. *Journal of Molecular Catalysis A: Chemical* **1997**, *124*, 137.
(26) Thomas, J. M.; Sankar, G.; Klunduk, M. C.; Atfield, M. P.; Maschmeyer, T.; Johnson, B. F. G.; Bell, R. G. *Journal of Physical Chemistry B* **1999**, *103*, 8809.
(27) Xia, Q. H.; Chem, X.; Tatsumi, T. *Journal of Molecular Catalysis A: Chemical* **2001**, *176*, 179.
(28) Welch, A.; Shiju, N. R.; Watts, I. D.; Sankar, G.; Nikitenko, S.; Bras, W. *Catalysis Letters* **2005**, *105*, 179.
(29) Yokoi, T.; Wu, P.; Tatsumi, T. *Catalysis Communications* **2003**, *4*, 11.
(30) Villa, A. L.; Caro, C. A.; Correa, C. M. d. *Journal of Molecular Catalysis A: Chemical* **2005**, *228*, 233.
(31) Ma, N.; Ma, Z.; Yue, Y.; Gao, Z. *Journal of Molecular Catalysis A: Chemical* **2002**, *184*, 361.
(32) Klaewkla, R.; Rirksomboon, T.; Kulprathipanja, S.; Nemeth, L.; Rangsunvigit, P. *Catalysis Communications* **2006**, *7*, 260.
(33) Lapisardi, G.; Chiker, F.; Launay, F.; Nogier, J. P.; Bonardet, J. L. *Microporous and Mesoporous Materials* **2005**, *78*, 289.
(34) Dugal, M.; Sankar, G.; Raja, R.; Thomas, J. M. *Angewandte Chemie International Edition* **2000**, *39*, 2310.

(35) Thomas, J. M.; Raja, R.; Sankar, G.; Bell, R. G. *Nature* **1999**, *398*, 227.
(36) Halgeri, A. B.; Das, J. *Applied Catalysis A: General* **1999**, *181*, 347.
(37) Corma, A.; Costa-Vaya, V. I.; Diaz-Cabanas, M. J.; Llopsi, F. J. *Journal of Catalysis* **2002**, *207*, 46.
(38) Perego, C.; Ingallina, P. *Catalysis Today* **2002**, *73*, 3.
(39) Skoog; West; Holler *Fundamentals of Analytical Chemistry*; 7th ed., **1996**.
(40) Skoog; Leary *Principles of Instrumental Analysis*; 4th ed., **1992**.

Chapter 3: Titanosilicates

3.0 Summary

In this chapter the synthesis of titanium silicalite-1 (TS-1) from a titanosilicate cogel precursor is reported. The synthesis parameters were altered to optimise both the cogel and resultant framework material. The titanosilicate materials were characterised using a range of techniques including: EDX analysis, XRD, ^{29}Si NMR, IR, UV-vis, and SEM (Chapter 2). Those materials which demonstrated the most catalytic potential were used as catalysts for the epoxidation of cyclohexene reaction, in which the use of aqueous hydrogen peroxide (H_2O_2) and a urea-H_2O_2 adduct, were compared. In addition to this the titanosilicate catalysts were silylated and these new materials were then employed as catalysts for the same epoxidation reaction. The catalytic ability of the titanosilicate materials was further tested by their use as catalysts for the hydroxylation of phenol and for the formation of adipic acid reactions.

It was shown that the cogel precursors themselves exhibited some catalytic activity and selectivity for all of the catalysis reactions exploited. However, the TS-1 materials were more catalytically active, which highlighted the need of the ordered framework for the most effective catalysis. The TS-1 materials prepared from the cogel precursors exhibited similar catalytic ability to those analogous standard materials prepared via conventional processes. Thus TS-1 preparation by the cogel route was shown to be a viable alternative preparation method to the conventional synthesis process.

3.1 Introduction

In 1983, Taramasso and co-workers reported the formation of a new material, via the isomorphous substitution of silicon (IV) by titanium (IV), with the crystalline structure of silicalite-1 (MFI).[1] The catalytic properties of titanium silicalite-1 (TS-1) appeared to be unique and were attributed to the location of the titanium atoms on isolated lattice sites within a hydrophobic framework (Figure 3.1). It was reported that in oxidation reactions, with aqueous H_2O_2 as the oxidant, many organic compounds could be oxidised with high selectivity and reactivity. Additionally, partial oxidation products could be obtained in high yields and almost all the oxygen available from H_2O_2 was used to produce the desired products.[2]

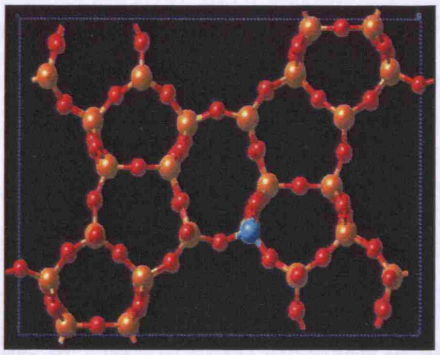

Figure 3.1: Titanium silicalite-1 (MFI) framework highlighting inserted titanium atom on a lattice site (blue). (Channel dimensions are [100] 5.1 x 5.5 Å, [010] 5.3 x 5.6 Å.)

Since industrialisation of the TS-1 catalyst, carried out successfully by EniChem in the mid-eighties, big efforts have been made towards the study of reactions involving this class of catalyst (Figure 3.2).[3-5] TS-1 is currently used for two processes on an industrial scale (phenol hydroxylation and cyclohexanone ammoximation) and several companies are developing a third process, propylene epoxidation.

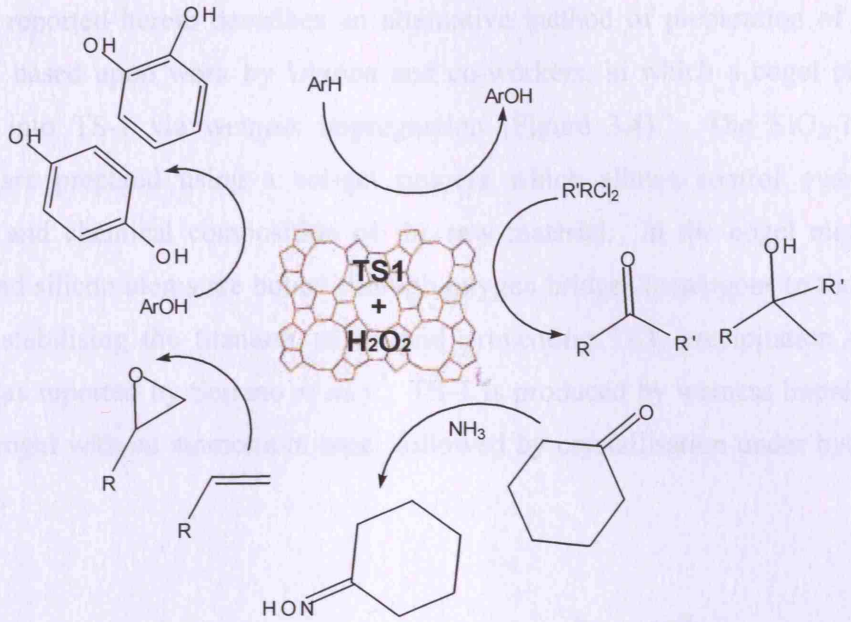

Figure 3.2: Common catalytic applications of TS-1.

According to the conventional synthesis, preparation of TS-1 has to be performed under carefully controlled conditions. The silicon and titanium alkoxides are hydrolysed by the dropwise addition of tetra-*n*-propylammonium hydroxide (TPAOH) at 0 °C, under a nitrogen atmosphere and in the absence of alkali-metal cations. Even with these precautions a white precipitate of TiO_2, is often observed in the liquid gel. Details of the conventional TS-1 synthesis are given below (Figure 3.3).

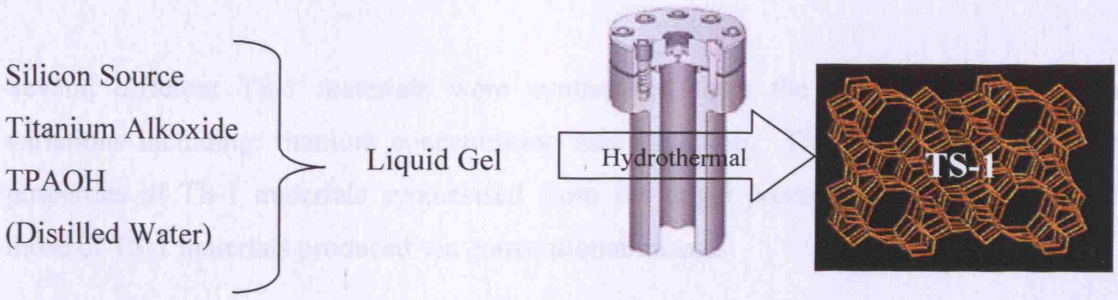

Figure 3.3: Schematic representation of conventional TS-1 synthesis.

The work reported herein describes an alternative method of preparation of TS-1. Its premise is based upon work by Uguina and co-workers, in which a cogel precursor is converted into TS-1 via wetness impregnation (Figure 3.4).[6] The SiO_2-TiO_2 cogel materials are prepared using a sol-gel process which allows control over both the properties and chemical composition of the raw material. In the cogel materials, the titanium and silicon atoms are bound through oxygen bridges (analogous to those present in TS-1), stabilising the titanium atoms and preventing TiO_2 precipitation during the synthesis (as reported by Serrano *et al.*).[7] TS-1 is produced by wetness impregnation of the dried cogel with an ammonium base, followed by crystallisation under hydrothermal conditions.

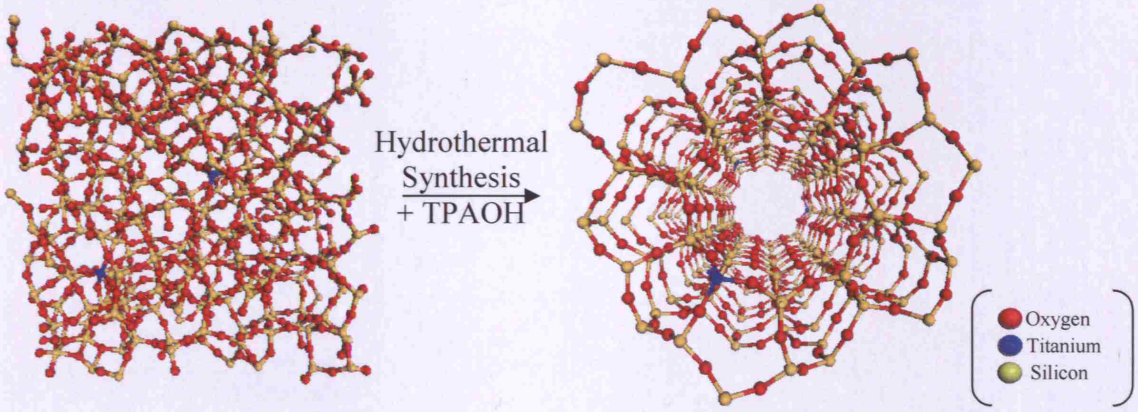

Figure 3.4: Transformation of amorphous cogel (left) into TS-1 (right) via a wetness impregnated, hydrothermal synthesis route.

Several different TS-1 materials were synthesised from the cogel precursors, with variations including: titanium concentration and silylation. The physical and catalytic properties of TS-1 materials synthesised from the cogel precursors were compared to those of TS-1 materials produced via conventional means.

3.2 Aims

- Synthesise TS-1 materials from cogel precursors and compare their physical and catalytic properties to those of TS-1 materials produced by a conventional process.

- Alteration of the chemical properties (by silylation, titanium concentration etc.) of the synthesised TS-1 materials and comparison with unaltered TS-1 materials.

- Characterisation of the physical and catalytic properties of the cogel precursors and comparison with resultant TS-1 materials.

3.3 Experimental

3.3.1 Cogel Synthesis

Further details regarding the cogel synthesis procedure are given in chapter 2.1.1. The table below (Table 3.1) gives specific details of the titanium cogel materials formed (TPAOH: tetra-*n*-propylammonium hydroxide, TEAOH: tetra-*n*-ethylammonium hydroxide).

Table 3.1: Specific synthesis details of titanium cogel materials produced.

Cogel Code	Heteroatom Source	Si:Ti	Ti	Condensation Method	Condensation Reagent
1	Titanium butoxide	10	8.14 g 23.00 mmol	Stirring	TPAOH
2	Titanium butoxide	80	1.02 g 2.88 mmol	Stirring	TPAOH
3	Titanium butoxide	10	8.14 g 23.00 mmol	Sonocation	TPAOH
4	Titanium butoxide	80	1.02 g 2.88 mmol	Sonocation	TPAOH
5	Titanium butoxide	10	8.14 g 23.00mmol	Stirring	TEAOH
6	Titanium butoxide	80	1.02 g 2.88 mmol	Stirring	TEAOH
7	Titanium butoxide	10	8.14 g 23.00 mmol	Sonocation	TEAOH
8	Titanium butoxide	80	1.02 g 2.88 mmol	Sonocation	TEAOH
9	Titanium isopropoxide	10	6.54 g 23.00 mmol	Stirring	TEAOH
10	Titanium isopropoxide	80	0.82 g 2.88 mmol	Stirring	TEAOH
11	Titanium isopropoxide	10	6.54 g 23.00 mmol	Sonocation	TEAOH
12	Titanium isopropoxide	80	0.82 g 2.88 mmol	Sonocation	TEAOH
13	Titanium ethoxide	10	5.25 g 23.00mmol	Stirring	TEAOH
14	Titanium ethoxide	80	0.66 g 2.88 mmol	Stirring	TEAOH

3.3.2 TS-1 Synthesis

TS-1 materials were synthesised from the cogel precursors as outlined in chapter 2.1.2, these framework materials were prepared from both the calcined and as-prepared cogel precursors (Table 3.2). Standard TS-1 was obtained from the National Chemical Laboratory, Pune, India, according to procedures given in the patent literature and was treated as a standard for comparison.[1]

Table 3.2: Details of TS-1 materials produced.

Cogel Source	TS-1 Code	Calcined / As Prepared Cogel
1	1-1	As Prepared
	1-2	Calcined
2	2-1	As Prepared
	2-2	Calcined
3	3-1	As Prepared
	3-2	Calcined
4	4-1	As Prepared
	4-2	Calcined
5	5-1	As Prepared
	5-2	Calcined
6	6-1	As Prepared
	6-2	Calcined
7	7-1	As Prepared
	7-2	Calcined
8	8-1	As Prepared
	8-2	Calcined
9	9-1	As Prepared
	9-2	Calcined
10	10-1	As Prepared
	10-2	Calcined
11	11-1	As Prepared
	11-2	Calcined
12	12-1	As Prepared
	12-2	Calcined
13	13-1	As Prepared
	13-2	Calcined
14	14-1	As Prepared
	14-2	Calcined

3.3.3 Blank Material Synthesis

Framework materials containing no titanium were synthesised from cogel precursors as outlined in chapter 2.1.4.

3.4 Results and Discussion

3.4.1 Titanosilicate Materials

All of the cogel and TS-1 materials synthesised were fine white powders, however upon addition of aqueous H_2O_2 their colour changed to yellow. This colour change was more pronounced for TS-1 than cogel materials and more prominent still for materials with a higher titanium concentration. The formation of this yellow colour when TS-1 is brought in contact with aqueous H_2O_2 (and its disappearance during hydrocarbon oxidations) has been previously well documented.[8] It is therefore unsurprising that the same colour change occurs with cogel materials, the yellow colour being due to the formation of a peroxy group containing a titanium ion. It is noteworthy that as the cogel materials exhibit evidence of this peroxy group, they also have potential catalytic reactivity.

EDX Characterisation:

EDX analysis was performed to evaluate the elemental composition of all TS-1 and cogel materials (Figure 3.5). All of the materials were pre-calcined to remove any organic residues. The percentage titanium atomic composition of all of the materials was to within 3.0 % of the expected values (EDX accuracy ~ 1.0 %). Although this technique only observes the surface of the material there was no evidence of titanium clustering. Several publications have previously stated a limit to the ratio of silicon to titanium atoms within the framework, the materials produced were within this range.[9]

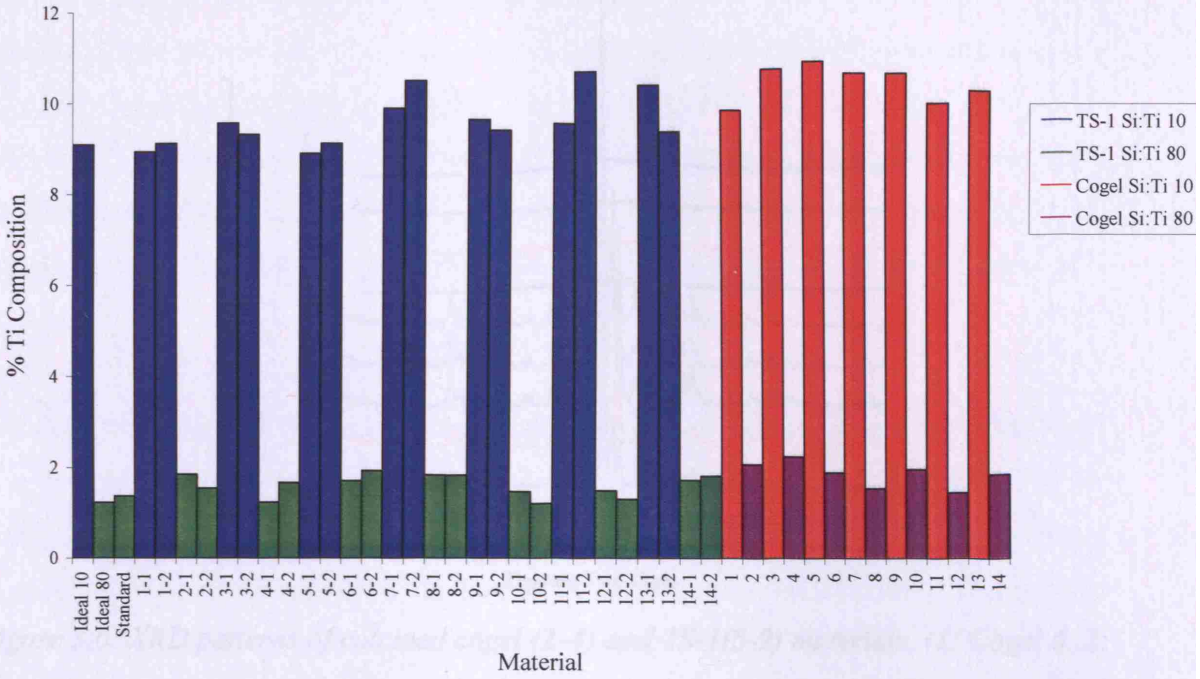

Figure 3.5: Titanium composition (%) of TS-1 (blue) and cogel (red) materials of both Si:Ti 10 (solid colour) and Si:Ti 80 (striped).

XRD Characterisation:

The XRD patterns of the cogel materials are broad and centred around 25 degrees two theta. This is typical for amorphous materials which suggests that the cogel materials have no long range order (Figure 3.6). Conversely all of the TS-1 materials produced were crystalline and of framework type MFI. The XRD patterns obtained were compared to those reported in the literature.[10] The XRD patterns of TS-1 materials were examined before and after calcination, both were found to be identical which would suggest no structural degradation or loss after calcination.

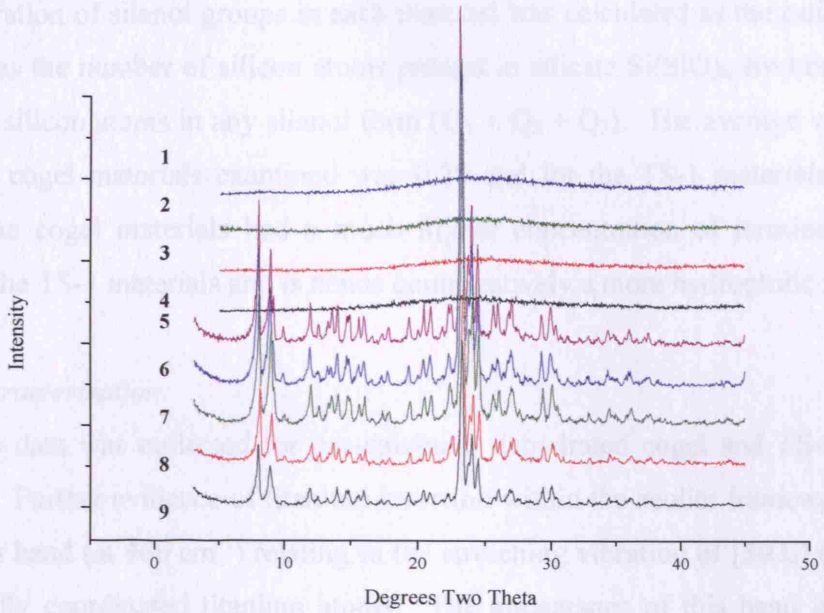

*Figure 3.6: XRD patterns of calcined cogel (**1-4**) and TS-1(**5-9**) materials. (**1**: Cogel 6, **2**: Cogel 1, **3**: Cogel 10, **4**: Cogel 14.)(**5**: TS-1 standard, **6**: TS-1 6-2, **7**: TS-1 1-2, **8**: TS-1 10-1, **9**: TS-1 14-2.)*

^{29}Si NMR Characterisation:

^{29}Si NMR was employed to evaluate the different types of silicon environment within the titanosilicate materials (Figure 3.7). The spectra of the cogel materials exhibited three peaks, relating to three different Q_n environments within the material, whilst the TS-1 materials only revealed two (Section 2.2.3.1). Thus, the less ordered cogel materials exhibited a wider range of silicon environments than the corresponding ordered framework material.

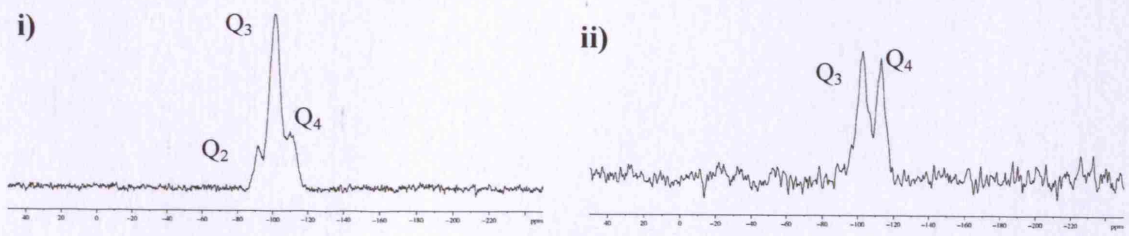

*Figure 3.7: ^{29}Si NMR spectra of **i)** Cogel 8 and **ii)** TS-1 8-2.*

The concentration of silanol groups in each material was calculated as the ratio of Q_4/Q_n. Where Q_4 was the number of silicon atoms present in silicate $Si(SiO)_4$ environments and Q_n relates to silicon atoms in any silanol form ($Q_1 + Q_2 + Q_3$). The average value of this ratio for the cogel materials examined was 0.28 and for the TS-1 materials was 0.75. Therefore, the cogel materials had a much higher concentration of terminal hydroxyl groups than the TS-1 materials and is hence comparatively a more hydrophilic material.[11]

Infrared Characterisation:

Infrared (IR) data was collected for pre-calcined, dehydrated cogel and TS-1 materials (Figure 3.8). Further evidence of titanium insertion within the zeolite framework was the presence of a band (at 960 cm^{-1}) relating to the stretching vibration of $[SiO_4]$ units bound to tetrahedrally coordinated titanium atoms. The appearance of this band in the cogel spectrum confirmed that the cogel contained titanium centres of the desired tetrahedral coordination geometry, prior to crystallisation. It was notable that upon addition of aqueous H_2O_2 the intensity of the band at 960 cm^{-1} decreased, this was attributed to coordination of H_2O_2 at the titanium sites. However, the 960 cm^{-1} band could be recovered by calcination, which removed the coordinated H_2O_2. Thus indirectly providing more evidence that the incorporated titanium heteroatoms were capable of forming the peroxy species necessary for effective catalysis. The signal at 550 cm^{-1} is characteristic of the orthorhombic MFI framework and was visible in the IR spectra of all TS-1 materials.

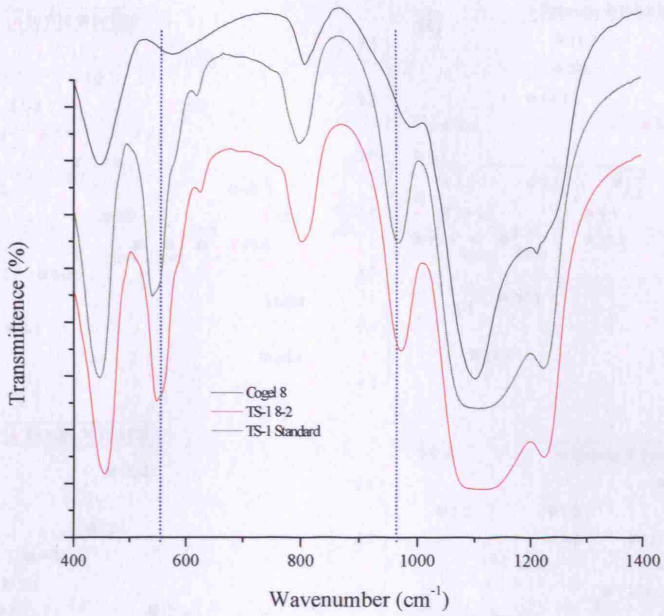

Figure 3.8: IR spectra of titanosilicate materials. (Dashed line: 550 cm^{-1} and 960 cm^{-1}.)

The degree of titanium incorporation within TS-1 materials was assessed using the 550 cm^{-1} band as a reference. This reference band (characteristic of the MFI structure) was evident in the IR spectra of TS-1 and absent in the cogel materials. The ratio of intensities of the 960 cm^{-1} and 550 cm^{-1} bands (I_{960}/I_{550}) was higher for TS-1 materials prepared from cogel precursors with a higher titanium concentration, suggesting a higher degree of titanium incorporation (Figure 3.9). However the relationship between titanium concentration and the intensity of the 960 cm^{-1} band has not been completely determined in the literature, thus no quantitative conclusions were drawn.[12] Typical I_{960}/I_{550} ratio values for catalytically active TS-1 have been reported between 1.3 to 1.7 for materials with ~ Si:Ti 80.[13]

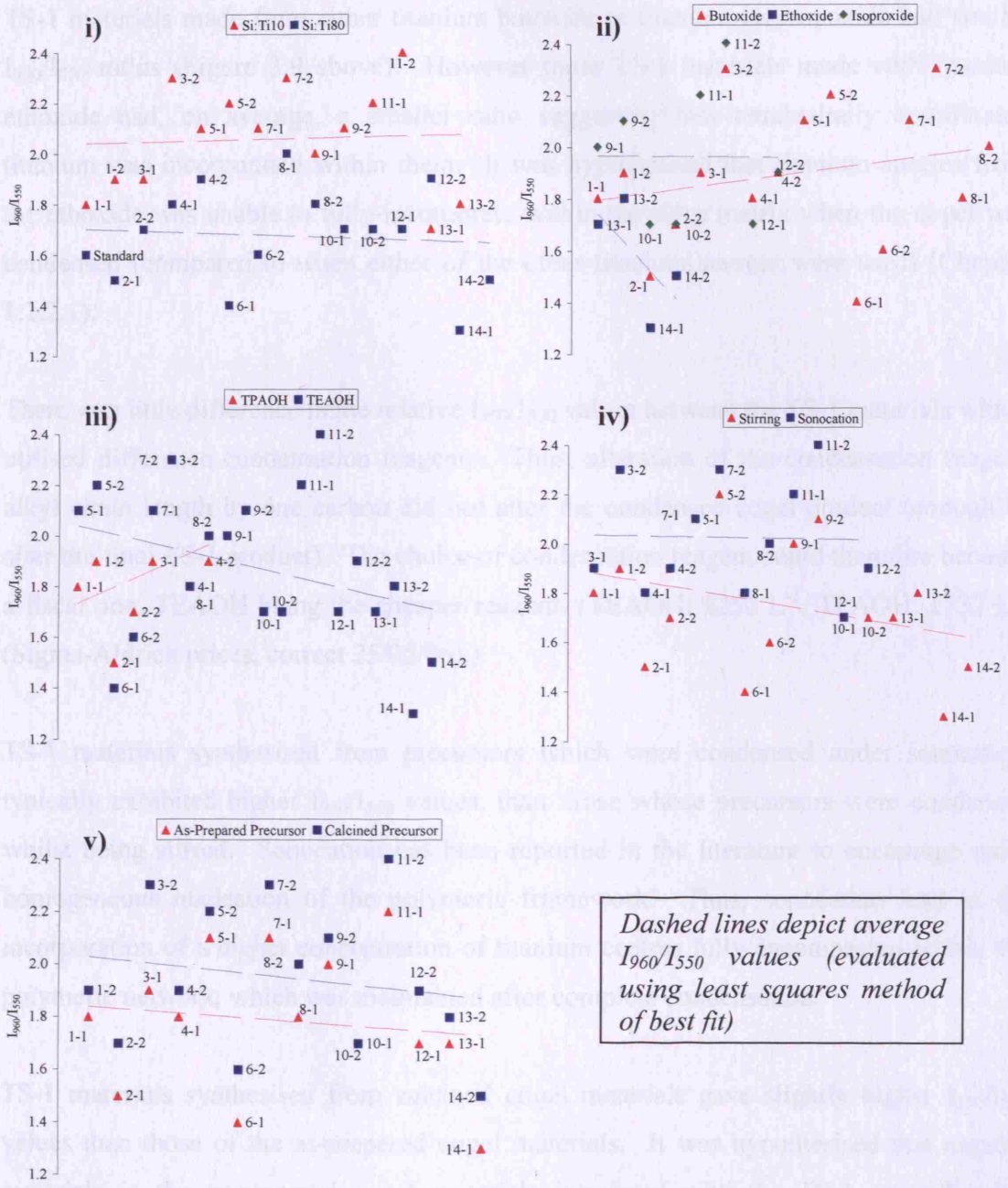

Figure 3.9: I_{960}/I_{550} values for different TS-1 materials. (Material distinctions: ***i)*** *titanium concentration* ***ii)*** *titanium source* ***iii)*** *condensation reagent* ***iv)*** *condensation method* ***v)*** *as-prepared or calcined precursor.)*

TS-1 materials made from either titanium butoxide or titanium isopropoxide had similar I_{960}/I_{550} ratios (Figure 3.9 above). However those TS-1 materials made with titanium ethoxide had, on average, a smaller ratio suggesting less tetrahedrally coordinated titanium was incorporated within them. It was hypothesised that titanium species from the ethoxide was unable to fully incorporate within the silica matrix when the cogel was condensed (compared to when either of the other titanium sources were used) (Chapter 1.2.2.1).

There was little difference in the relative I_{960}/I_{550} values between the TS-1 materials which utilised difference condensation reagents. Thus, alteration of the condensation reagent alkyl chain length by one carbon did not alter the condensed cogel product (enough to alter the final TS-1 product). The choice of condensation reagent could therefore become a fiscal one, TEAOH being the cheaper reagent. (TEAOH: £250 L^{-1}, TPAOH: £732 L^{-1} (Sigma-Aldrich prices, correct 25/05/06).)

TS-1 materials synthesised from precursors which were condensed under sonocation typically exhibited higher I_{960}/I_{550} values, than those whose precursors were condensed whilst being stirred. Sonocation has been reported in the literature to encourage more homogeneous nucleation of the polymeric framework. Thus, sonocation lead to the incorporation of a higher concentration of titanium centres fully encompassed within the polymeric network, which was maintained after complete condensation.

TS-1 materials synthesised from calcined cogel materials gave slightly higher I_{960}/I_{550} values than those of the as-prepared cogel materials. It was hypothesised that organic materials in the as-prepared cogel materials interfered with the TS-1 crystallisation process, via interaction either with the organic structure directing reagent or the titanium heteroatoms.

UV-vis Characterisation:

UV-vis spectroscopy is the most widely applied technique in the literature, to determine the quality of titanium-containing molecular sieves, since the presence of bulk TiO_2 can be detected by the appearance of an absorption band at ~ 330 nm. Additionally, a narrow band centred ~ 220 nm is considered indicative of titanium atoms being tetrahedrally bound within a silica network.[7]

Figure 3.10 depicts the UV-vis spectra of the standard TS-1, TS-1 8-2 and the corresponding precursor cogel 8. In all cases there was no appreciable adsorption band at ~ 330 nm thus portraying an absence of bulk TiO_2 phases (although the presence of small TiO_2 clusters cannot be completely discarded). The comparably narrow bands of the TS-1 materials, centred at ~ 220 nm, confirmed that the titanium atoms occupied mostly tetrahedral positions within the framework.

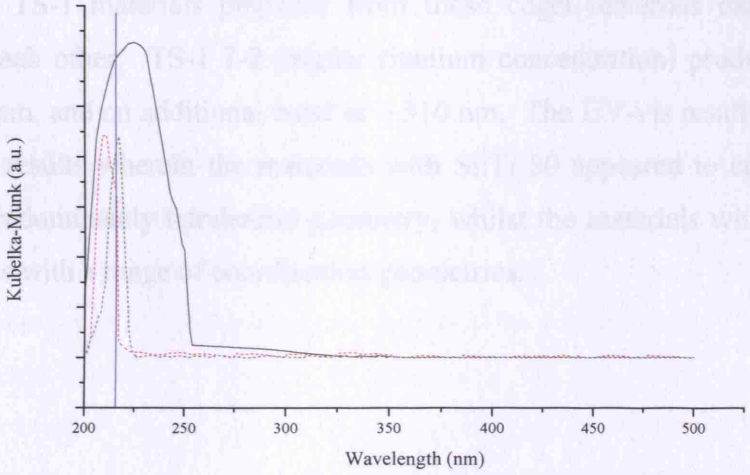

Figure 3.10: UV-vis spectra of cogel 8 (black), TS-1 8-2 (green) and standard TS-1 (red). (Navy line = 220 nm.)

The cogel UV-vis spectrum depicted a broader band (than for TS-1) shifted to a high wavelength, which suggested that the titanium atoms were present in configurations other than the desired tetrahedral geometry. These alternative titanium configurations may have resulted from incomplete condensation of the cogel. Alternatively, these other configurations may have been due to the hydrophilic nature of the cogel materials,

whereby the reversible hydrolysis of the Si-O-Ti bonds and subsequent adsorption of two molecules of water could have changed the titanium coordination from tetrahedral to octahedral.[14] It was theorised to have been a combination of these two effects as the dehydrated cogel materials exhibited a comparably narrower band. A slight narrowing of the TS-1 band was evident after dehydration, but the effect was much less pronounced than that of the cogel materials, relating to the more hydrophobic nature of TS-1 and the more fixed heteroatom geometry within the framework structure.

As expected, UV-vis spectra of the cogel materials containing different titanium concentrations, exhibited broad bands in the range 200 to 300 nm, which demonstrated that different titanium environments coexisted within these materials (Figure 3.11). This band was broader in the spectrum of cogel 7, which had a higher titanium concentration than cogel 8. Additionally, cogel 7 produced another band at ~ 310 nm which was attributed to either extra framework titanosilicate species or bulk TiO_2. The spectra obtained from TS-1 materials prepared from these cogel materials exhibited similar properties to each other. TS-1 7-2 (higher titanium concentration) produced a broader band at ~ 220 nm, and an additional band at ~ 310 nm. The UV-vis results obtained thus echoed the IR results wherein the materials with Si:Ti 80 appeared to contain titanium centres with predominately tetrahedral geometry, whilst the materials with Si:Ti 10 had titanium centres with a range of coordination geometries.

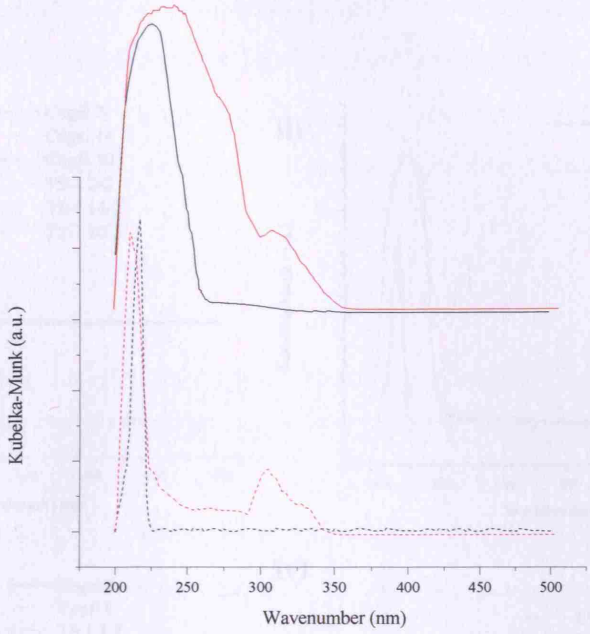

Figure 3.11: UV-vis spectra of cogel and TS-1 materials with varying titanium concentrations: Cogel 7 (Si:Ti 10, solid red line), Cogel 8 (Si:Ti 80, solid black line), TS-1 7-2 (Si:Ti 10, dashed red line), TS-1 8-2 (Si:Ti 80, dashed black line).

Alteration of the titanium source made little difference to the UV-vis spectra of either the cogel or the TS-1 materials (Figure 3.12). The materials made from the titanium ethoxide source gave rise to slightly wide bands (compared to those produced by materials from other titanium sources), indicating that these materials contained a broad range of titanium coordination environments. UV-vis results also showed that alteration of the condensation reagent made little difference to the titanium environment within the final TS-1 materials (Figure 3.12). However, the cogel materials formed when TPAOH was used as the condensation reagent showed very slightly broader bands (relating to a wider range of titanium coordination geometries) than those formed utilising TEAOH as the condensation reagent.

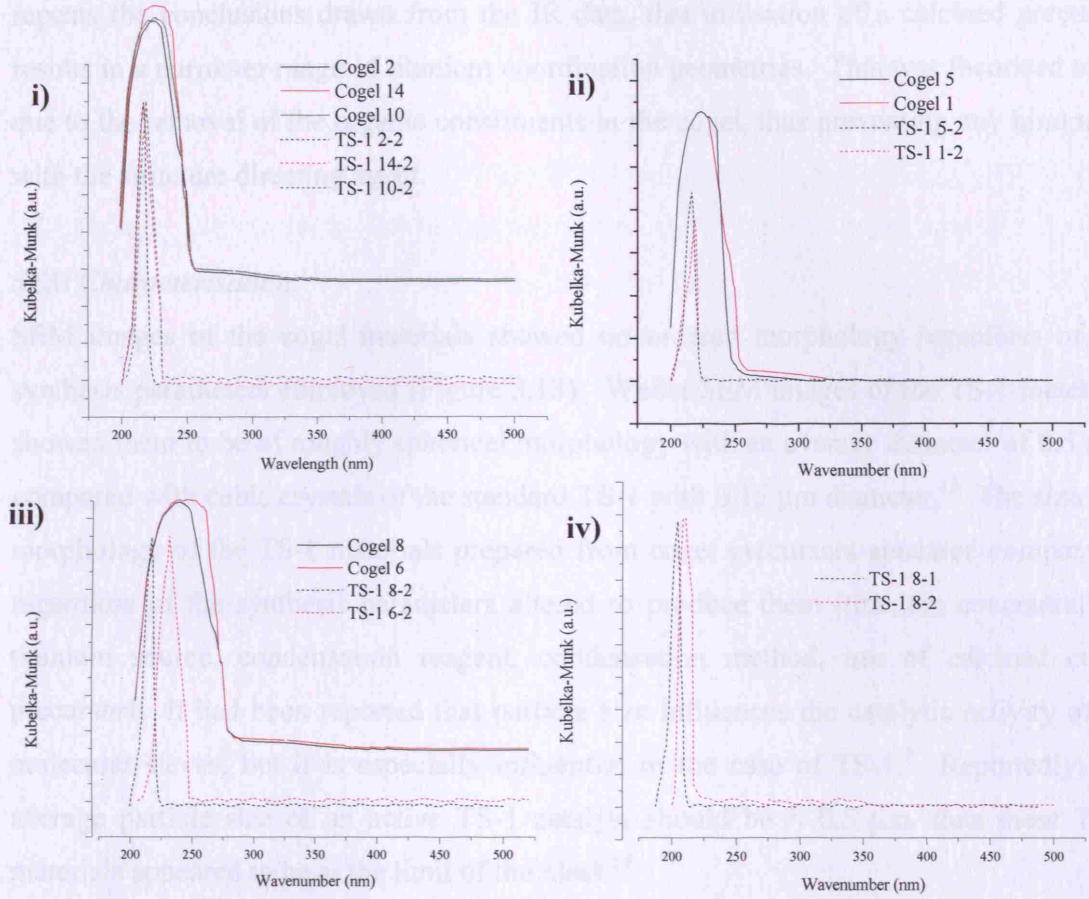

Figure 3.12: UV-vis spectra of cogel materials (solid line) and TS-1 (dashed line) materials with different preparation methods: ***i)*** *titanium source (Black: butoxide, Red: ethoxide, Green: isopropoxide)* ***ii)*** *Condensation reagent (Black: TEAOH, Red: TPAOH)* ***iii)*** *Condensation method (Black: Sonocation, Red: Stirring)* ***iv)*** *TS1 materials prepared from calcined (black) or uncalcined (red) cogel precursor.*

In general, irrespective of titanium source and composition, the cogel materials (and the corresponding TS-1 materials) formed whilst condensed under sonocation conditions, exhibited narrow UV-vis bands compared to cogel materials (and TS-1 materials) which were stirred during condensation (Figure 3.12 above). This suggested that sonocation of the condensing gel directed more titanium atoms towards tetrahedral coordination geometry, which was maintained during TS-1 synthesis. The UV-vis spectra of TS-1 materials prepared from calcined or as-prepared cogel precursors were similar: the ~ 220

nm band was partially narrower for materials prepared using the calcined cogel. Which repeats the conclusions drawn from the IR data, that utilisation of a calcined precursor results in a narrower range of titanium coordination geometries. This was theorised to be due to the removal of the organic constituents in the cogel, thus preventing any hindrance with the structure directing agent.

SEM Characterisation:

SEM images of the cogel materials showed no ordered morphology regardless of the synthesis parameters employed (Figure 3.13). Whilst SEM images of the TS-1 materials showed them to be of roughly spherical morphology with an average diameter of 0.5 μm, compared with cubic crystals of the standard TS-1 with 0.15 μm diameter.[13] The size and morphology of the TS-1 materials prepared from cogel precursors appeared comparable regardless of the synthesis parameters altered to produce them (titanium concentration, titanium source, condensation reagent, condensation method, use of calcined cogel precursor). It had been reported that particle size influences the catalytic activity of all molecular sieves, but it is especially influential in the case of TS-1.[5] Reportedly, the average particle size of an active TS-1 catalyst should be < 0.5 μm, thus these TS-1 materials appeared to be at the limit of the ideal.[14]

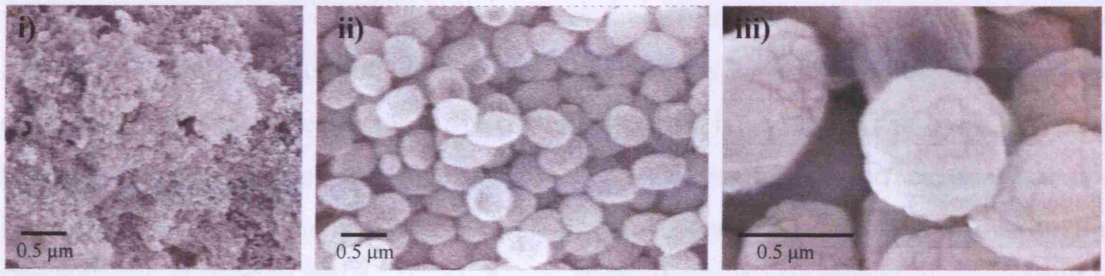

Figure 3.13: Typical SEM images of ***i)*** *Cogel 8,* ***ii) and iii)*** *TS-1 8-2.*

The surface of the TS-1 materials produced, appeared coarse and was archetypal of materials formed via an aggregate process. A main advantage of a catalyst formed in this manner is the higher surface area produced, which can result in higher catalytic activity. The formation of the TS-1 materials via an aggregate process concurred with the

mechanism of growth from cogel materials, proposed by Serrano *et al.* (Chapter 1.2.2.2).[15]

BET Characterisation:

BET surface area measurements were carried out on selected samples using the facility at NCL, India. The results found the cogel (10) material to have a surface area of 694 m^2g^{-1} and the corresponding TS-1 (10-2) to have a surface area of 416 m^2g^{-1}. The surface area of TS-1 was close to the values reported in the literature of for TS-1 materials: ~ 400 m^2g^{-1}.[7] The surface area of the cogel was higher than that of the TS-1 and was close to the value of ~ 700 m^2g^{-1} reported for comparable xerogels in the literature.[16] The high surface area of these titanosilicates was encouragingly similar to catalytically reactive materials, wherein the higher the surface area the more easily assessable the active sites are for the reagent materials.

Bulk Density Characterisation:

Measurements of the packed bulk density of the calcined titanosilicate materials showed that the cogel materials were more dense than the corresponding TS-1 materials (Figure 3.14). This difference in density was theorised to be the result of two factors, firstly, although both materials were porous, the repeating unit cell and larger pore dimensions of the framework materials could have resulted in them being less dense. Additionally, the higher concentration of terminal hydroxyl groups (Figure 3.7 above) on the surface of the cogel materials (compared to the TS-1 materials) could have resulted in more hydrogen bonding between surfaces within the material, thus attracting the surfaces together and increasing the cogel density. As expected the cogel and TS-1 materials with a higher titanium concentration were more dense than their lower titanium concentration counterparts. The standard TS-1 and comparable TS-1 materials synthesised from cogel precursors had analogous bulk densities.

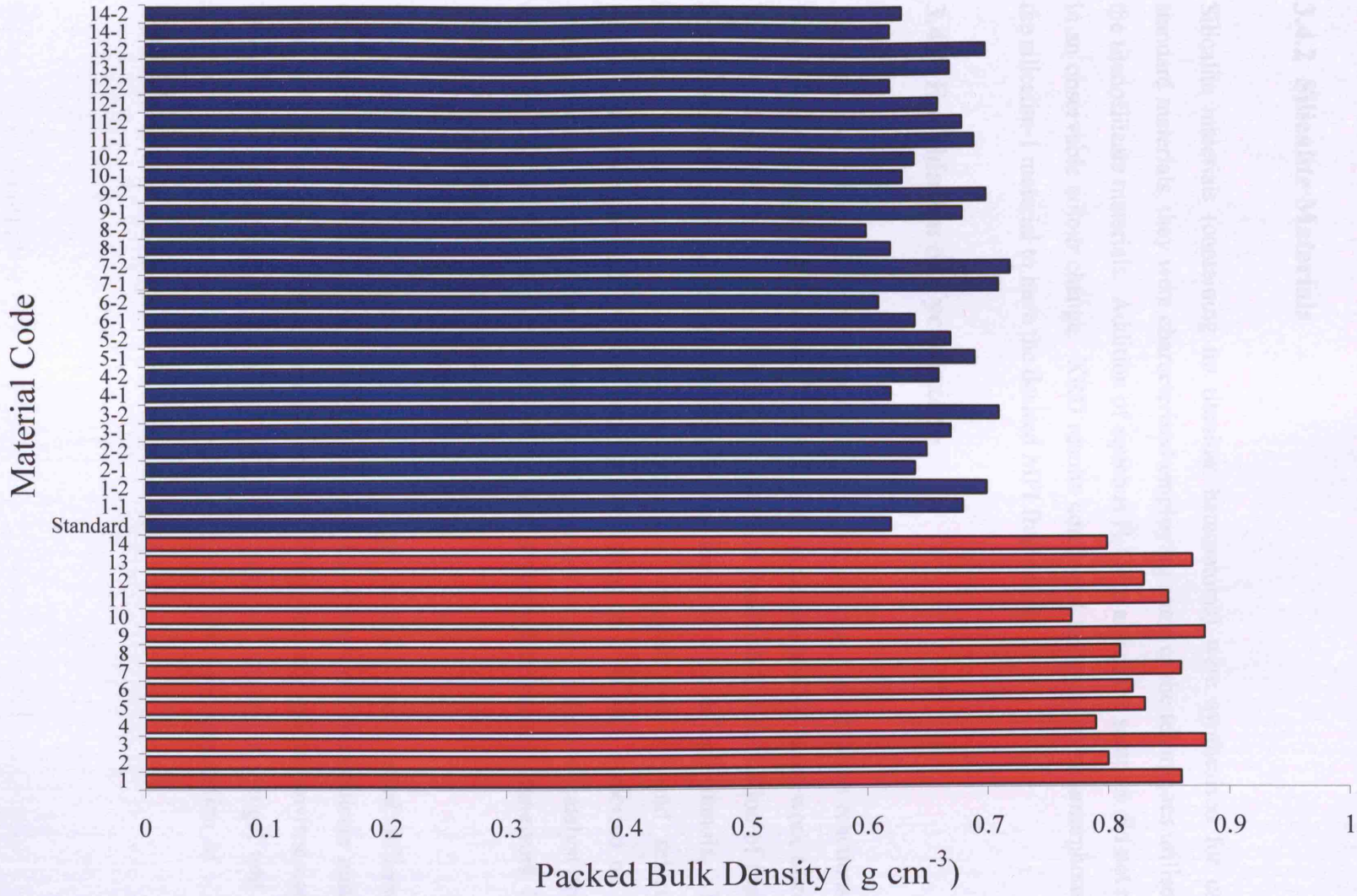

Figure 3.14: Packed bulk density of all titanosilicate materials (Red: Cogel, Blue: TS-1).

3.4.2 Silicalite Materials

Silicalite materials (containing no titanium heteroatoms) were synthesised for use as standard materials, they were characterised employing some of the techniques utilised for the titanosilicate materials. Addition of aqueous H_2O_2 to any of the samples did not result in an observable colour change. XRD results confirmed the cogel to be amorphous and the silicalite-1 material to have the desired MFI framework.

3.4.3 Epoxidation of Cyclohexene

The catalytic activity of titanosilicate materials, for a variety of different reactions, has been well recognised and reported.[17] The surface structure of TS-1 framework materials has been described both in terms of **i)** the state and framework coordination of titanium and **ii)** surface hydroxyl groups present in the form of silanols and titanols. These structural characteristics influence the materials' catalytic activity and selectivity. Similarly an amorphous TiO_2-SiO_2 catalyst consisting of 2 % TiO_2 dispersed on high-surface area silica has been reported to be an active and selective catalyst for the epoxidation of alkenes, thus demonstrating that a three-dimensional framework is not necessarily essential for active catalysis.[18,19]

The catalytic activity of both the TS-1 and cogel materials were tested utilising the epoxidation of cyclohexene reaction (Chapter 2.3.1). Only those titanosilicate materials with Si:Ti 80 which exhibited titanium centres in the desired optimal environment for catalysis were employed as catalysts. After six hours of reaction the cogel and TS-1 materials showed similar catalytic reactivity, with a cyclohexene conversion of ~ 20 % (Figure 3.15).

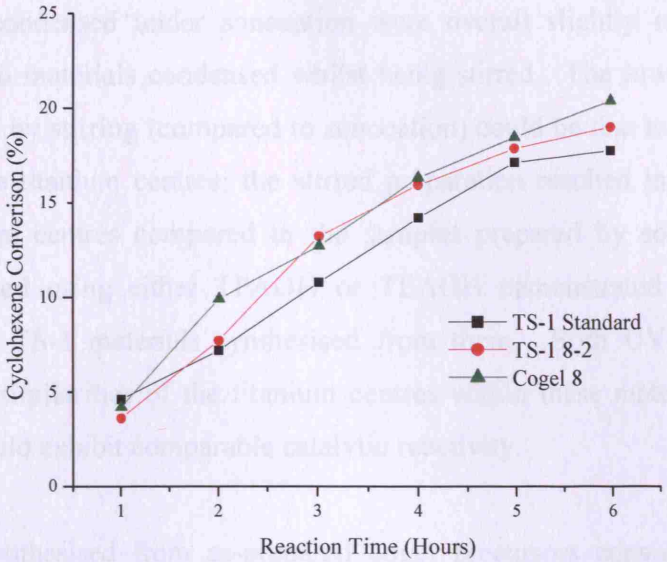

Figure 3.15: Typical cyclohexene conversion (%) of titanosilicate materials over six hours.

The percentage conversion of cyclohexene by the standard TS-1 (17.7 %, mean value) and the cogel prepared TS-1 materials (16.8 %, mean value) were comparable (Figure 3.16).

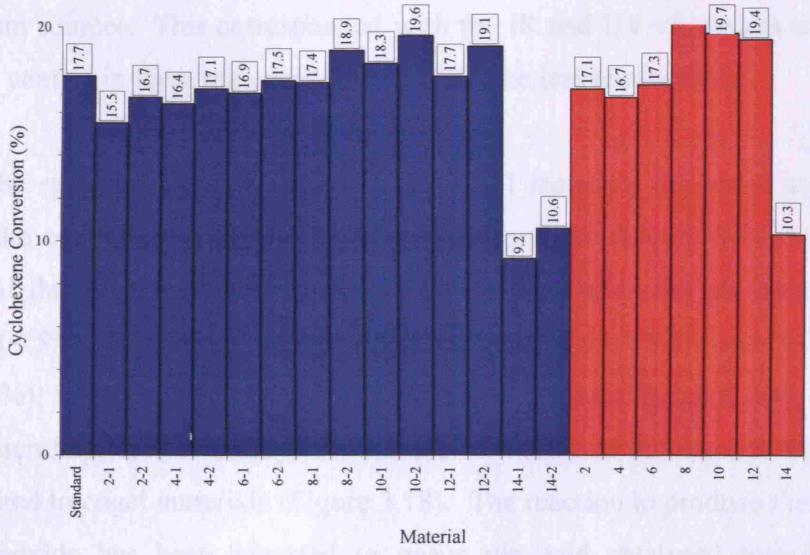

Figure 3.16: Cyclohexene conversion (%) for TS-1 (blue) and cogel (red) materials after six hours of reaction (Numbers show the percentage conversion of cyclohexene after six hours of reaction).

Cogel materials condensed under sonocation were overall slightly more catalytically active compared to materials condensed whilst being stirred. The lower activity of the materials prepared by stirring (compared to sonocation) could be due to the nature of the catalytically active titanium centres; the stirred preparation resulted in less numbers of tetrahedral titanium centres compared to the samples prepared by sonocation. Cogel materials condensed using either TPAOH or TEAOH demonstrated similar catalytic reactivities to the TS-1 materials synthesised from them. Both UV-vis and IR data demonstrated the similarities of the titanium centres within these materials, thus it was expected they should exhibit comparable catalytic reactivity.

TS-1 materials synthesised from as-prepared cogel precursors consistently had lower catalytic activity compared to similar materials prepared from calcined precursors. This is consistent with the IR and UV-vis results which showed that the titanium centres were on average more tetrahedral in TS-1 materials prepared from calcined cogel precursors.

Both the cogel and corresponding TS-1 materials which contained titanium from a titanium ethoxide source (cogel materials 13 and 14, TS-1 13-1, 13-2, 14-1, 14-2) had lower catalytic activity (cyclohexene conversion) than those materials synthesised using other titanium sources. This corresponded with the IR and UV-vis results which showed the titanium centres in these materials on average to be less tetrahedral.

In general the epoxide selectivity of cogel and TS-1 materials decreased as the reaction continued, the epoxide degraded to form the diol product (Figure 3.17). The epoxide selectivity of the cogel was initially very low (~ 10%) and after six hours, decreased further still (< 5%). Conversely the epoxide selectivity of the TS-1 materials was initially high (~ 75 %), which again decreased (~ 60 %) to produce the diol over six hours of reaction. Therefore, the selectivity towards the formation of the epoxide was higher for TS-1 compared to cogel materials (Figure 3.18). The reaction to produce the diol product from the epoxide has been reported to occur via acid catalysed hydrolysis of the epoxide.[20] The TS-1 synthesised from the cogel precursor exhibited analogous catalytic selectivity to the TS-1 prepared by conventional means (~ 60 %). No notable differences

in the epoxide selectivity of all TS-1 or all cogel materials were observed, regardless of the alteration of the synthesis parameters (Figure 3.18).

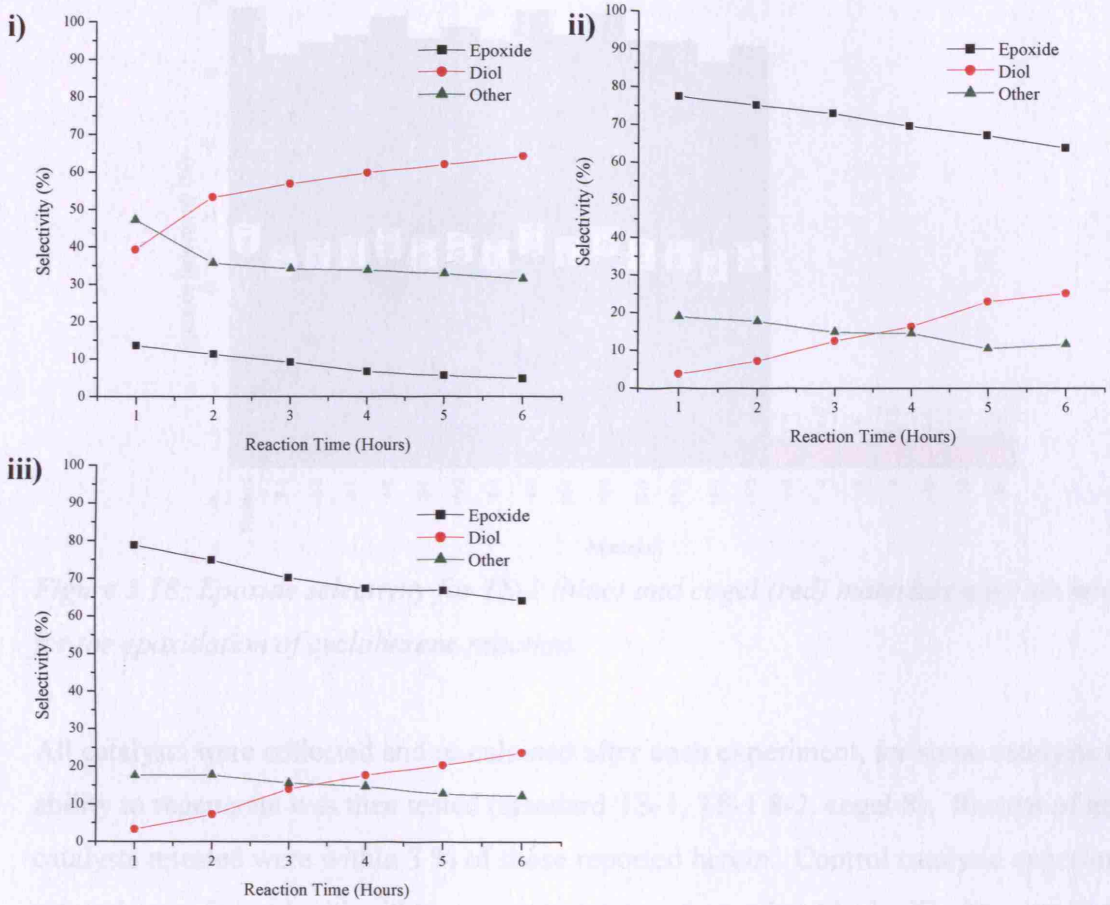

Figure 3.17: The typical catalytic selectivity of ***i)*** *cogel 8,* ***ii)*** *TS-1 8-2,* ***iii)*** *standard TS-1, for the epoxidation of cyclohexene. (Other denotes combined ketone and mono-alcohol selectivity.)*

The breaking down of the epoxide to diol is likely to be due to the highly disordered structure of the cogel materials which contain a higher concentration of hydroxyl groups (required for epoxide degradation), in contrast to the crystalline TS-1 materials. Thus the product selectivities were more dependant upon the concentration of terminal hydroxyl groups than the geometry of the titanium species. The NMR results shown above demonstrate the that the average Q_4/Q_n value for the cogel materials was 0.75, whilst for

the TS-1 materials it was 0.28 (Section 3.4.1). This shows the cogel materials to be comparatively more hydrophilic than the framework TS-1 materials.

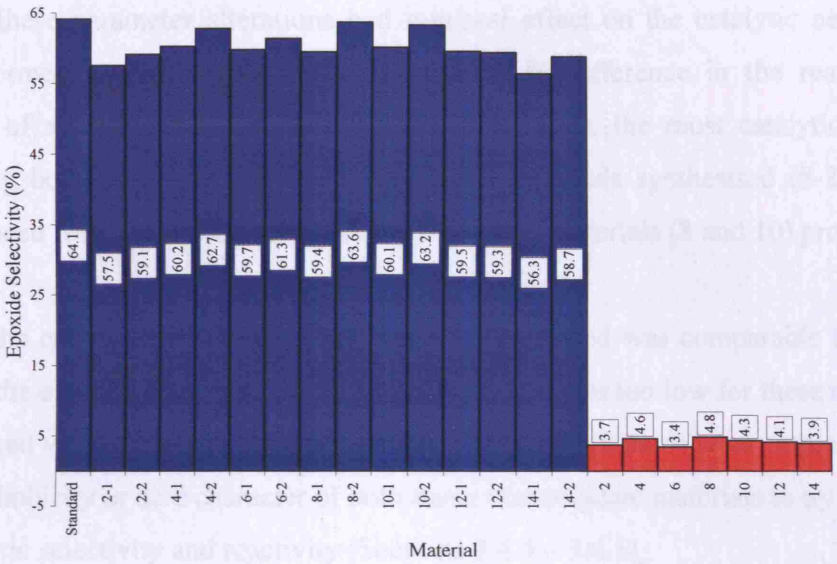

Figure 3.18: Epoxide selectivity for TS-1 (blue) and cogel (red) materials after six hours for the epoxidation of cyclohexene reaction.

All catalysts were collected and re-calcined after each experiment, for some catalysts their ability to regenerate was then tested (standard TS-1, TS-1 8-2, cogel 8). Results of all the catalysts retested were within 3 % of those reported herein. Control catalytic experiments were also performed with either no catalyst present or using blank silicalite materials as the catalyst (Section 3.3.3), these yielded no products.

Leeching experiments were undertaken for the standard TS-1, TS-1 8-2 and cogel 8 materials. After one hour of reaction the catalyst was removed by filtration and the experiment continued with the filtrate. No further reaction occurred, hence no titanium leeching of the catalysts was reported, or leeched titanium did not participate in the reaction.

The parameters altered during the cogel synthesis have an effect upon the catalytic activity of the material formed for the epoxidation of cyclohexene. For maximum

catalytic activity the ideal cogel synthesis parameters should be altered so that condensation occurs under sonocation, the titanium source used is either the butoxide or isopropoxide and the resultant cogel should be calcined prior to use as a precursor. However, these parameter alterations had minimal effect on the catalytic nature of the material formed, typically there was less than 5 % difference in the reactivity and selectivity of all the cogel materials formed. However, the most catalytically active (considering both reactivity and selectivity) TS-1 materials synthesised (8-2 and 10-2) were produced form the most catalytically active cogel materials (8 and 10) produced.

Although the catalytic activity of cogel materials produced was comparable to the TS-1 materials, the epoxide selectivity of the cogel materials was too low for these materials to be considered viable catalysts for this reaction. Different methods were employed to alter the hydrophobicity or acid character of both these titanosilicate materials to try to improve their catalytic selectivity and reactivity (Sections 3.4.4 – 3.4.5).

3.4.4 Urea-H_2O_2 Adduct Alteration

It has been reported that to enhance epoxide selectivity a non-aqueous source of H_2O_2 can be used, specifically a urea-H_2O_2 adduct, which slowly releases H_2O_2 into solution.[21] Additionally, the urea adduct can bind to terminal hydroxyl groups on the catalyst, thus preventing these sites being employed as acid centres for epoxide degradation.

Whilst the catalytic activity of the TS-1 materials under the altered conditions were comparable with each other they were vastly different from the activity of the cogel materials. In figure 3.19 a comparison is made between the conventionally synthesised TS-1, TS-1 synthesised from the cogel precursor and the cogel itself; for the epoxidation of cyclohexene in the presence of urea-H_2O_2. After six hours of reaction the TS-1 materials showed ~ 30 % cyclohexene conversion whilst the cogel showed < 5 %. This dramatic decrease in cogel activity could be due to the binding of the urea adduct to the titanium centres. It has been reported that urea interacts very strongly with titanium centres, in some systems preventing any catalytic reaction occurring.[5] The binding of the

adduct to the highly concentrated silanols on the cogel surface, could have hindered access to the titanium active sites of the bulky cyclohexene reagent.

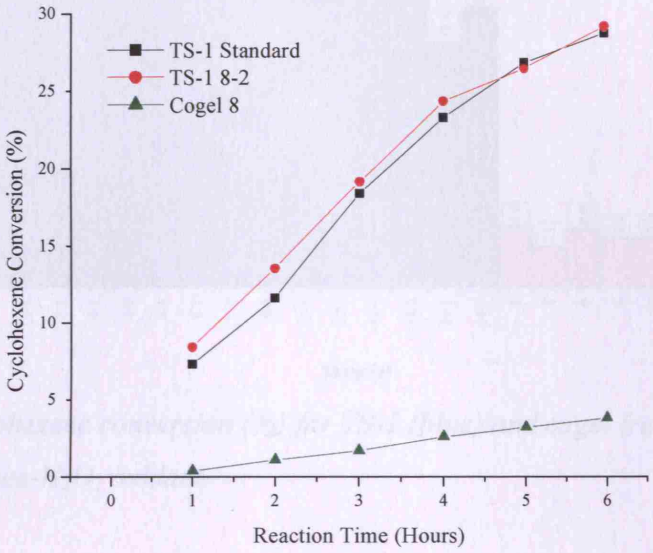

Figure 3.19: Cyclohexene conversion (%) of titanosilicate materials over six hours, using urea-H_2O_2 oxidant.

In general irrespective of the preparative method and titanium source; alteration of the oxidant from aqueous H_2O_2 to the urea-H_2O_2 adduct greatly altered the activity of all of the titanosilicate materials (Figure 3.20). The reactivity of the TS-1 materials increased from ~ 20 % cyclohexene conversion to ~ 30 %. It has been proposed that the comparative increase in hydrophilicity of the reaction medium, enabled release of the organic products formed from the more hydrophobic TS-1 material.[5]

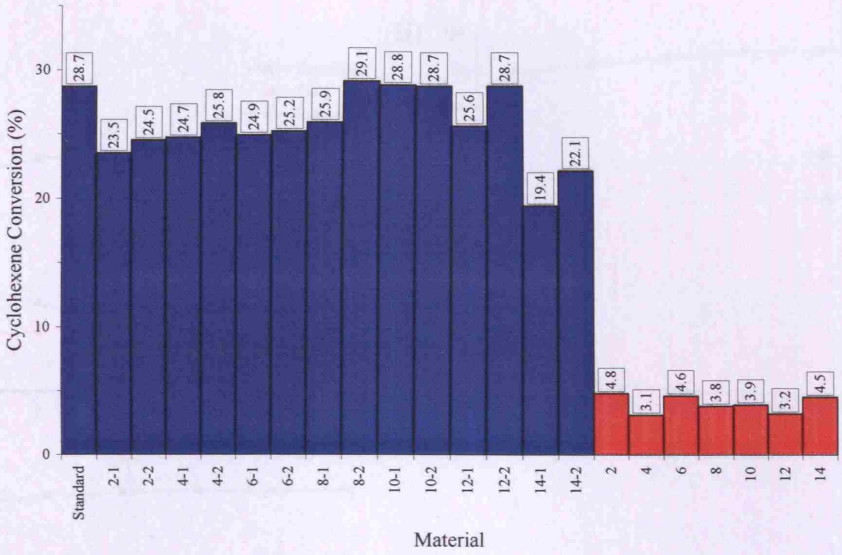

Figure 3.20: Cyclohexene conversion (%) for TS-1 (blue) and cogel (red) materials after six hours, using urea-H_2O_2 oxidant.

The catalytic selectivity of cogel and TS-1 materials towards epoxide formation remained approximately constant as the reaction continued, with no obvious epoxide degradation to the diol (Figure 3.21). Compared to results utilising aqueous H_2O_2, the epoxide selectivity of the TS-1 materials increased from ~ 60 % to ~ 90 %. The cogel materials also exhibited increased (to a larger extent) epoxide selectivity, rising from ~ 5 % to ~ 60 %.

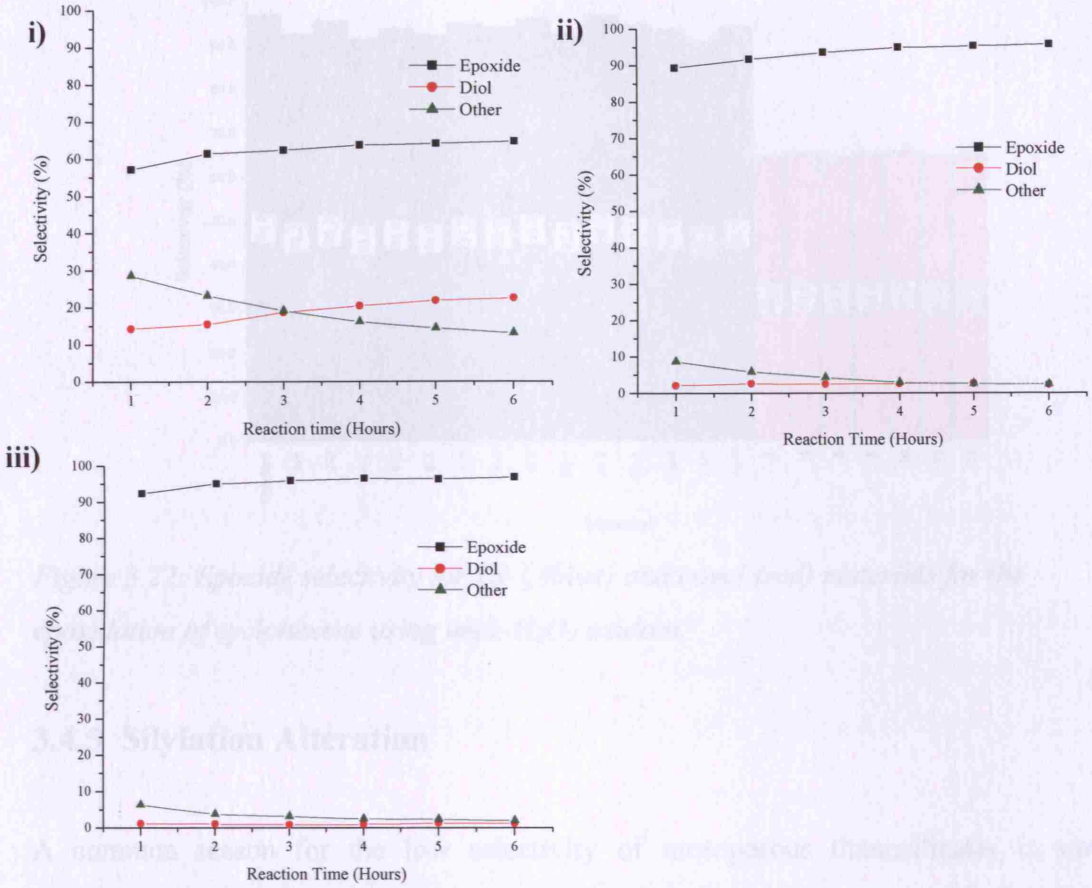

Figure 3.21: Catalytic selectivity of ***i)*** *cogel 8,* ***ii)*** *TS-1 8-2,* ***iii)*** *TS-1 standard, for the epoxidation of cyclohexene using urea-H_2O_2 oxidant. (Other denotes combined ketone and mono-alcohol formation (%))*

Irrespective of the method of preparation or titanium source, the epoxide selectivity of the TS-1 materials remained higher than that for the cogel materials and appeared stable over the reaction time (Figure 3.22). It was therefore concluded that by altering the oxidant to the urea-H_2O_2 adduct, the acid sites of the titanosilicate materials were prevented from catalysing the degradation of the epoxide.[22] It was shown that the cogel materials contain a higher concentration of terminal hydroxyl groups (Figure 3.7) which catalyse diol formation. Potentially not all of these groups were neutralised by the urea adduct, thus explaining the lower epoxide selectivity of these materials.

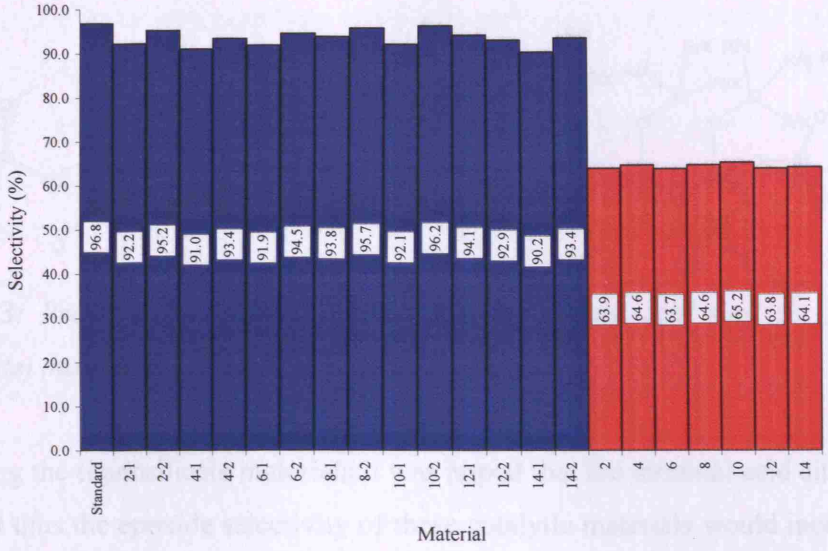

Figure 3.22: Epoxide selectivity for TS-1 (blue) and cogel (red) materials for the epoxidation of cyclohexene using urea-H_2O_2 oxidant.

3.4.5 Silylation Alteration

A common reason for the low selectivity of mesoporous titanosilicates is surface hydrophilicity, caused by a high concentration of surface hydroxyl groups.[5] One method of reducing this hydroxyl concentration is by silylation, which has been shown to improve both catalytic selectivity and reactivity (Figure 3.23). Specifically, silylation has been shown to improve epoxide selectivity in cyclohexene epoxidation for titanium MCM-41 and titanium MCM-48 catalysts.[23] Although in these cases the surface hydrophilicity of the material was decreased, there was little control over whether silanol or titanol groups were capped. The elimination of titanol groups by silylation can lead to a decrease in catalytic activity as the formation of the catalytically active titanium peroxy group can be hindered or prevented on the tripodal titanium sites. This titanol capping however should only affect those groups (if any) on the outer surface of the material, those sites in the pores should remain largely unaltered.

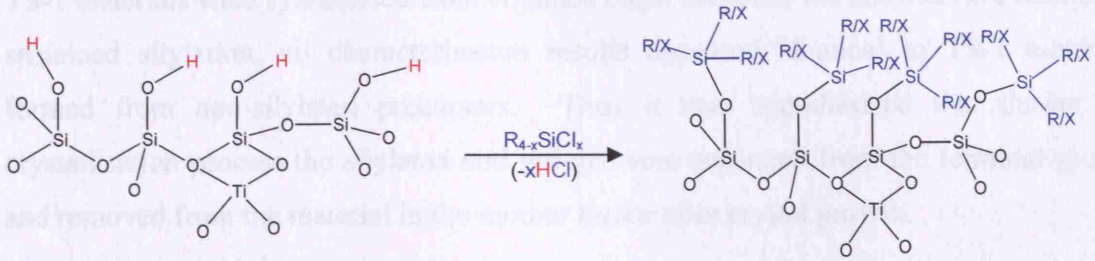

Figure 3.23: Premise of silylation: the capping of surface acid sites in (for example titanosilicate) materials.

By silylating the titanosilicate materials it was hoped that the terminal acid sites would be capped and thus the epoxide selectivity of these catalytic materials would increase for the epoxidation of cyclohexene reaction. Both the cogel and TS-1 materials were silylated with either TMCS or TCMS* (Chapter 2.1.5) details of the transformed materials are given in table 3.3. Methyl groups were chosen as the alkyl chain on the silylated reagents to minimise steric bulk which can potentially block either the titanium active sites or the pore openings.

Table 3.3: Silylated titanosilicate materials synthesised.

Product Code	Material Type	Titanosilicate Reagent	Silylating Reagent
6-TMCS	Cogel	6	TMCS
8-TMCS	Cogel	8	TMCS
10-TMCS	Cogel	10	TMCS
12-TMCS	Cogel	12	TMCS
6-TCMS	Cogel	6	TCMS
8-TCMS	Cogel	8	TCMS
10-TCMS	Cogel	10	TCMS
12-TCMS	Cogel	12	TCMS
6-2-TMCS	TS-1	6-2	TMCS
8-2-TMCS	TS-1	8-2	TMCS
10-2-TMCS	TS-1	10-2	TMCS
12-2-TMCS	TS-1	12-2	TMCS
6-2-TCMS	TS-1	6-2	TCMS
8-2-TCMS	TS-1	8-2	TCMS
10-2-TCMS	TS-1	10-2	TCMS
12-2-TCMS	TS-1	12-2	TCMS

* TMCS = Trimethylchlorosilane, TCMS = Trichloromethylsilane.

TS-1 materials were synthesised from silylated cogel materials but showed no evidence of sustained silylation, all characterisation results appeared identical to TS-1 materials formed from non-silylated precursors. Thus it was hypothesised that during the crystallisation process the silylated end groups were separated from the terminal groups and removed from the material in the mother liquor after crystal growth.

All of these altered materials were fine white powders which upon addition of aqueous H_2O_2 changed colour to yellow, depicting the formation of the catalytically active titanium peroxy species. As with the non-silylated materials the yellow colour was more prominent in TS-1 materials than for their cogel counterparts.

XRD Characterisation:

XRD patterns of the silylated titanosilicate materials showed an unaltered structure when silylated. The TS-1 materials maintained their framework structure, similarly the amorphous cogel materials remained unchanged (Figure 3.24).

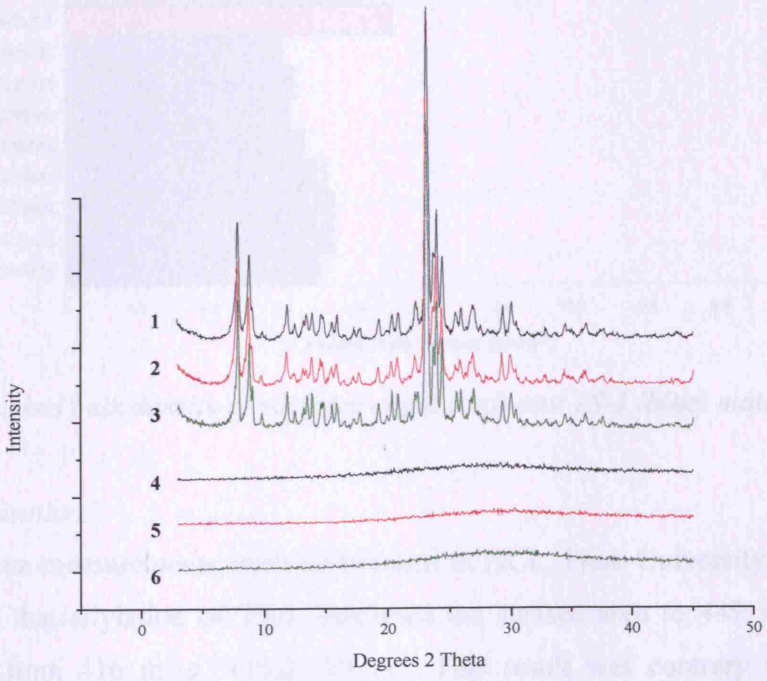

*Figure 3.24: XRD patterns of cogel 8 (**4**) and TS-1 8-2 (**1**), silylated with **i)** TMCS to form cogel 8-TMCS (**5**) and TS-1 8-2-TMCS (**2**) and **ii)** TCMS to form cogel 8-TCMS (**6**) and TS-1 8-2-TCMS (**3**).*

Packed Bulk Density Characterisation:

The cogel materials had a greater packed bulk density than the TS-1 materials after silylation (Figure 3.25). However, the overall packed bulk density of the silylated materials was less than for their non-silylated counterparts. The packed bulk density of the cogel materials decreased from (an average value of) ~ 0.75 g cm^{-3} to ~ 0.35 g cm^{-3} upon silylation. Similarly, the packed bulk density of the TS-1 materials decreased from (an average value of) ~ 0.60 g cm^{-3} to ~ 0.45 g cm^{-3} after silylation. The decrease in packed bulk density for the silylated materials was expected; as upon silylation the materials gain bulk, therefore the surfaces cannot get as close together, resulting in a decrease in density.

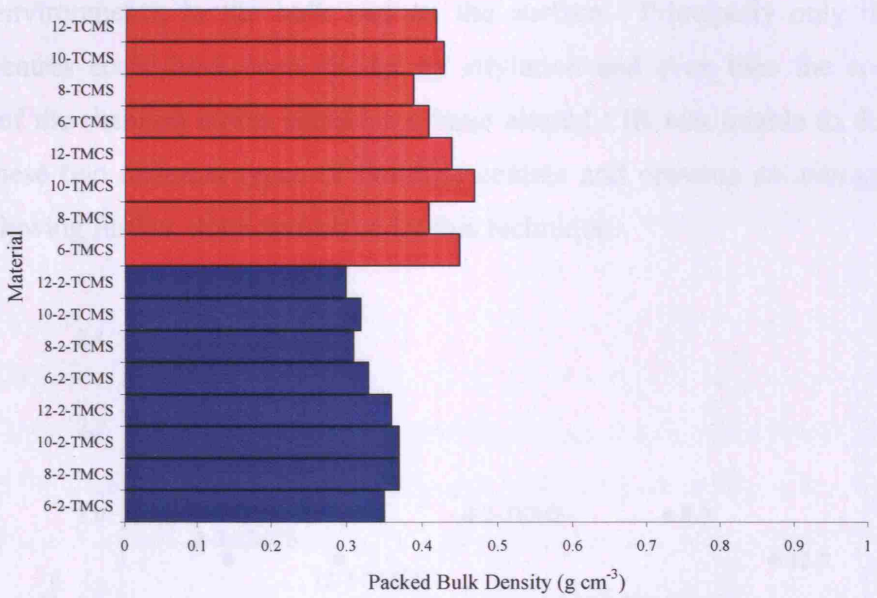

Figure 3.25: Packed bulk density of silylated cogel (red) and TS-1 (blue) materials.

BET Characterisation:

BET surface area measurements were undertaken at NCL, Pune University, India. The results showed that silylation of TS-1 increased the surface area to 449 m^2 g^{-1} (10-2-TCMS, TS-1) from 416 m^2 g^{-1} (10-2, TS-1). This result was contrary to what was expected, it was thought that silylation would add a layer of molecules to the surface of the material including the pores themselves. This would reduce the diameter of the pores

and thus reduce the overall surface area of the material. However, the layer added by silylation could itself be thought of as porous, as it was only added to the terminal hydroxyl groups. Thus, the surface area of the material would (as shown) increase compared to the non-silylated material.

IR Characterisation:

IR measurements (using the I_{960}/I_{550} ratio outlined before, figure 3.11) taken of the silylated materials showed no alteration of the titanium environment when TS-1 materials were silylated (Figure 3.26). The average I_{960}/I_{550} ratio for the silylated TS-1 materials was 1.75 and 1.78 for TMCS and TCMS respectively, compared to 1.80 for the non-silylated TS-1 materials. Within the framework the titanium centres were present in two different environments, in the bulk and on the surface. Principally only the surface titanium centres could have been altered by silylation and even then the coordination geometry of the titanium atoms should not have altered. IR was unable to differentiate between these two different types of titanium centres and presents an average of them thus not allowing further characterisation by this technique.

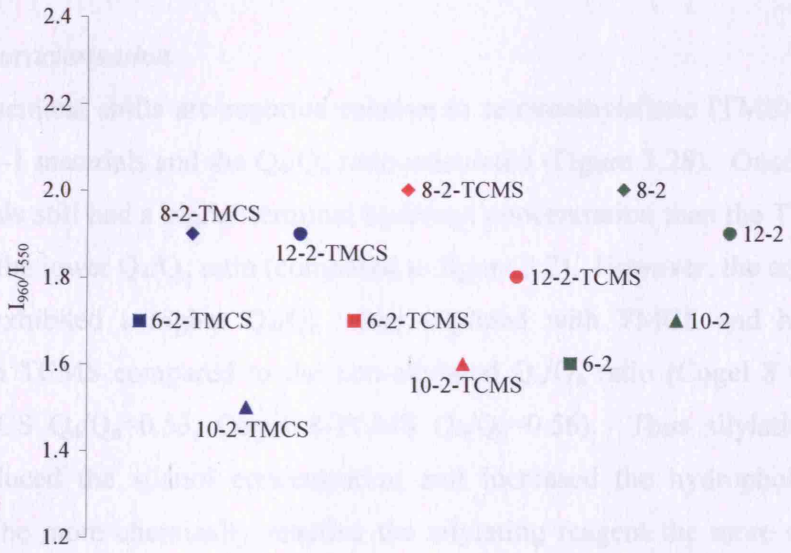

Figure 3.26: I_{960}/I_{550} ratios for different TS-1 materials. (Blue: TS-1 silylated with TMCS, Red: TS-1 silylated with TCMS, Green: TS-1 non-silylated).

UV-vis Characterisation:

Data collected from UV-vis measurements confirmed the IR results that the titanium coordination geometry appeared unaltered after silylation (Figure 3.27).

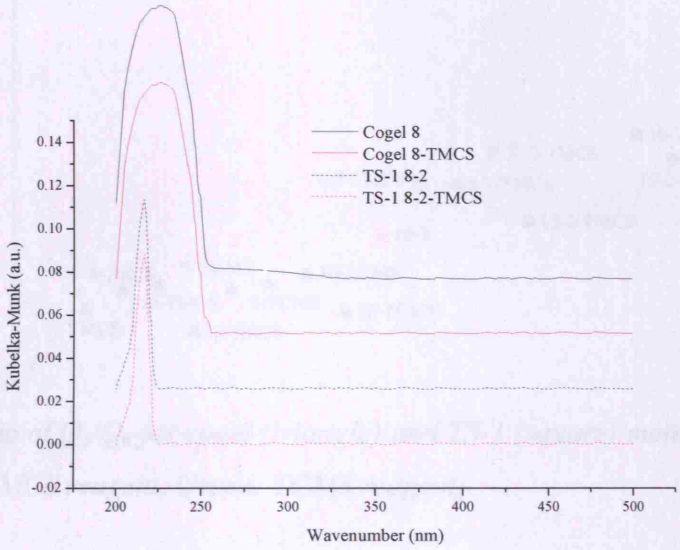

Figure 3.27: UV-vis spectra of cogel 8 and TS-1 8-2 materials before and after silylation with TMCS.

^{29}Si NMR Characterisation:

^{29}Si NMR chemical shifts are reported relative to tetramethylsilane (TMS) for silylated cogel and TS-1 materials and the Q_4/Q_n ratio calculated (Figure 3.28). Once silylated the cogel materials still had a higher terminal hydroxyl concentration than the TS-1 materials as shown by the lower Q_4/Q_n ratio (compared to figure 3.7). However, the cogel materials themselves exhibited a higher Q_4/Q_n when silylated with TMCS and higher still if silylated with TCMS compared to the non-silylated Q_4/Q_n ratio (Cogel 8 Q_4/Q_n= 0.28, Cogel 8-TMCS Q_4/Q_n=0.53, Cogel 8-TCMS Q_4/Q_n=0.56). Thus silylating the cogel materials reduced the silanol concentration and increased the hydrophobicity of the materials. The more chemically reactive the silylating reagent the more silanols were capped and the greater the increase in the resultant cogel materials hydrophobicity. The same was shown for the TS-1 materials which became more hydrophobic upon silylation, the hydrophobicity being greatest when the TCMS silylating reagent was used.

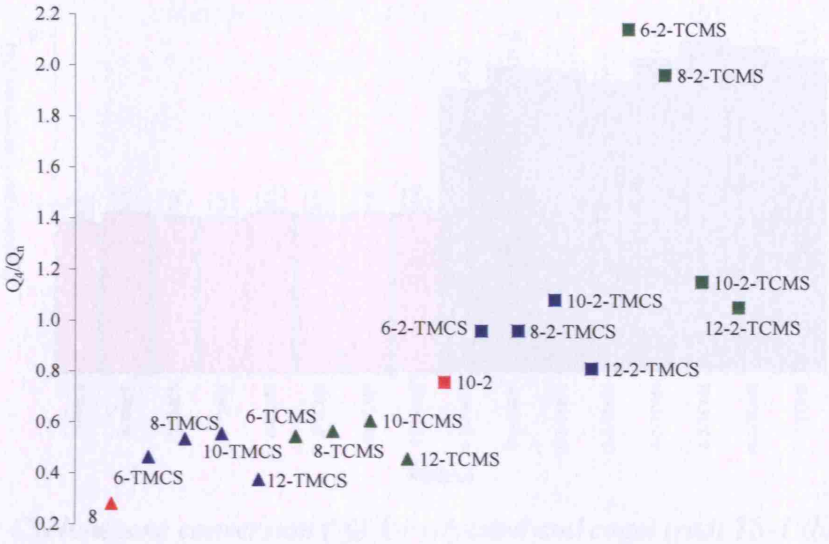

Figure 3.28: Ratio of Q_4/Q_n for cogel (triangle) and TS-1 (square) materials. (Red: Non-silylated, Blue: TMCS reagent, Green: TCMS reagent).

Catalytic Activity:

All the silylated titanosilicate materials demonstrated some catalytic activity for the epoxidation of cyclohexene reaction (Figure 3.29). The reactivity of the cogel materials decreased from an average of ~ 17 % to < 10 % cyclohexene conversion upon silylation, whilst the average TS-1 reactivity increased marginally from ~ 17 % to ~ 18 % upon silylation.

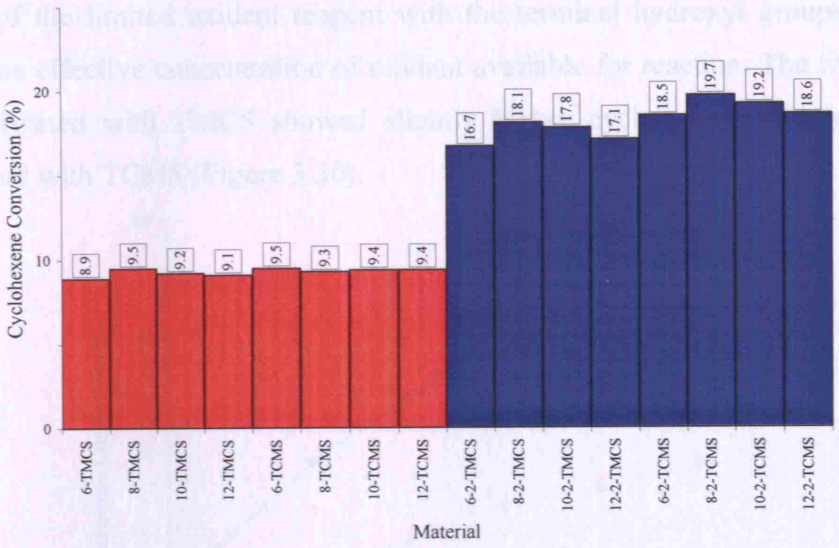

Figure 3.29: Cyclohexene conversion (%) for silylated and cogel (red) TS-1 (blue) materials after six hours reaction.

An explanation for the poor activity of the cogel materials could be that the added bulk around the titanium centres prevented interaction with the reagents themselves. Accordingly, it could be that either the titanium peroxy species was unable to form, or that the bulky cyclohexene could not interact with it. Evidence from the colour change when H_2O_2 (aq) was added to the materials would suggest that the titanium peroxy species was able to form. Whilst the increased surface area measurements agreed with the bulk hindrance argument, thus it was more likely that the low reactivity was due to poor interaction of cyclohexene with the active site. Further *in-situ* experiments which monitor the titanium centres (i.e. XANES/ UV-vis etc.) would be required to provide direct evidence.

The cyclohexene conversion for the silylated TS-1 materials (average ~ 18.2 %) was marginally better than for the non-silylated framework (average ~ 17.6 %) materials. The lower concentration of hydroxyl groups on the surface of the non-silylated framework materials (compared to the cogel precursors) resulted in less hindering bulk on the surface of the materials upon silylated. Thus, it was far less likely for steric effects to hinder or prevent reaction. The slight increase in reactivity was attributed to the decreased

interaction of the limited oxidant reagent with the terminal hydroxyl groups, therefore increasing the effective concentration of oxidant available for reaction. The titanosilicate materials silylated with TMCS showed slightly higher cyclohexene conversions than those silylated with TCMS (Figure 3.30).

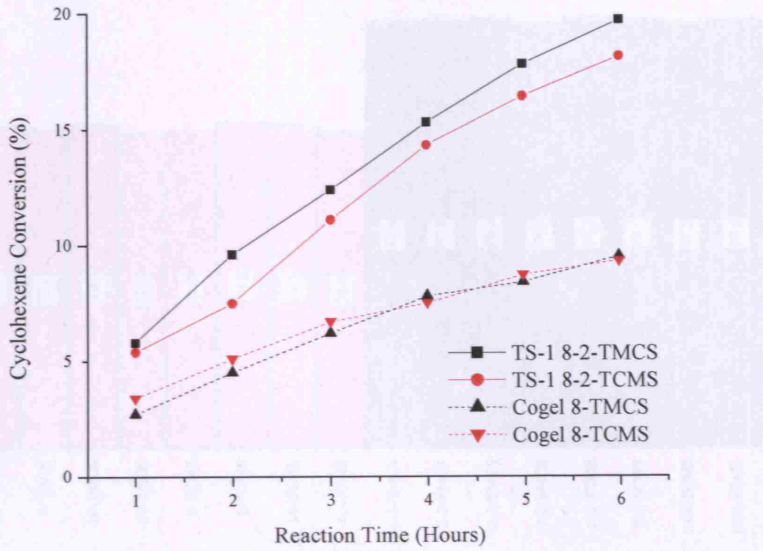

Figure 3.30: Cyclohexene conversion (%) of silylated titanosilicate materials over six hour reaction (Black: TMCS, Red: TCMS).

This difference in catalytic activity was possibly due to the different size of the resultant surface groups after silylation with each reagent (Figure 3.31). For TCMS, assuming that all of the chlorine groups have reacted with surface silanol groups, the resultant surface group is likely to be more bulky and rigid. Therefore access to the pores and the active sites may be restricted when the TCMS silylating reagent was used, compared to the TMCS reagent.

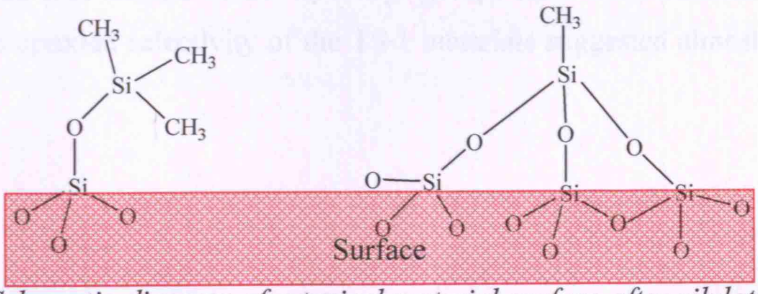

Figure 3.31: Schematic diagram of a typical material surface after silylation with TMCS (left) and TCMS (right).

The epoxide selectivity for all titanosilicate materials improved upon silylation (Figure 3.32). The selectivity has increased from ~ 5 % to ~ 75 % for cogel materials and from ~ 60 % to > 95 % for TS-1 materials.

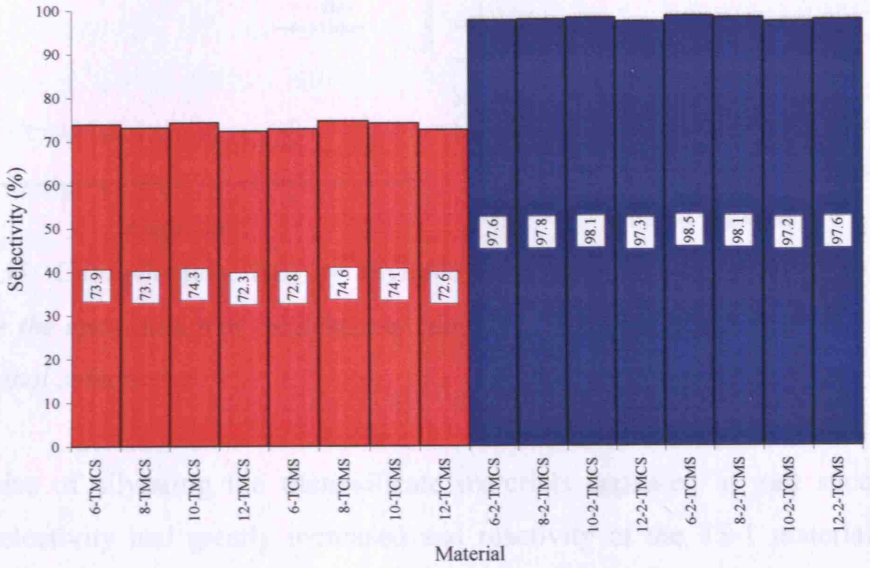

Figure 3.32: Epoxide selectivity for cogel (red) and TS-1 (blue) silylated materials, after six hours reaction.

The selectivity of the titanosilicate materials demonstrated that once the epoxide product had been formed it was stable towards degradation to the diol product (Figure 3.33). This high selectivity was evidence that the acid sites had been capped, and thus the hydrophobicity of the materials increased. Although the epoxide selectivity for the cogel materials had dramatically increased it was still not as high as that for the TS-1 materials, which suggested that not all of the hydroxyl groups have been altered. Similarly the extremely high epoxide selectivity of the TS-1 materials suggested almost complete acid site removal.

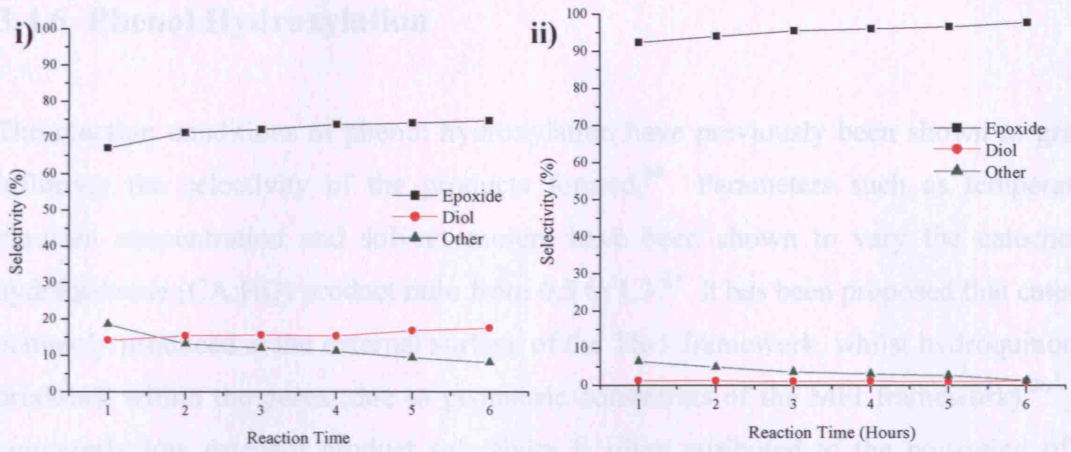

Figure 3.33: Catalytic selectivity of silylated material ***i)*** *Cogel 8-TMCS,* ***ii)*** *TS-1 8-2-TMCS, for the epoxidation of cyclohexene reaction. (Other denotes combined ketone and mono-alcohol selectivity)*

The premise of silylating the titanosilicate materials appeared in part successful, the epoxide selectivity had greatly increased and reactivity of the TS-1 materials had also increased. However, in other ways the premise appeared limited: the reactivity of the cogel materials decreased and the titanosilicate catalysts cannot be reused. Calcination of these materials resulted in the thermal removal of all silylated groups and both the catalytic activity and selectivity returned to that of their non-silylated counterparts. Therefore, further work would be required to establish a method of regenerating the catalyst without permanent loss of the silylated groups. One possible method of catalyst regeneration could be to alter the reaction setup to employ a fixed bed reactor. This would mean that after catalysis reaction the catalyst can be calcined *in-situ* and then re-silylated by passing the vapour of a passivating reagent through the catalyst. Such a reagent could be hexamethylsilazane (HMDS), although further studies would be required to confirm that the catalysts activity was unaltered.

3.4.6 Phenol Hydroxylation

The reaction conditions of phenol hydroxylation have previously been shown to greatly influence the selectivity of the products formed.[24] Parameters such as temperature, titanium concentration and solvent moiety have been shown to vary the catechol to hydroquinone (CA:HQ) product ratio from 0.5 to 1.3.[25] It has been proposed that catechol is mainly produced at the external surface of the TS-1 framework, whilst hydroquinone is produced within the pores (due to geometric constraints of the MFI framework).[26] The commonly low catechol product selectivity is often attributed to the poisoning of the external active sites by organic deposits (tars) which are not dissolved by highly polar solvents. Cogel 8, the corresponding TS-1 (8-2), and silylated materials cogel 8-TMCS and TS-1 8-2-TMCS were used as catalysts for this reaction (Chapter 2.3.2).

The cogel materials were less catalytically active than the framework counterparts, despite these materials containing the same concentration of titanium centres (Figure 3.34). Silylation of the cogel and TS-1 materials resulted in an increase in catalytic activity, although the cogel was still less active than the framework material. This increase in activity was unexpected for the cogel, as during the epoxidation of cyclohexene reaction the catalytic activity had dramatically decreased (due to added bulk preventing reagent access to the titanium centres).

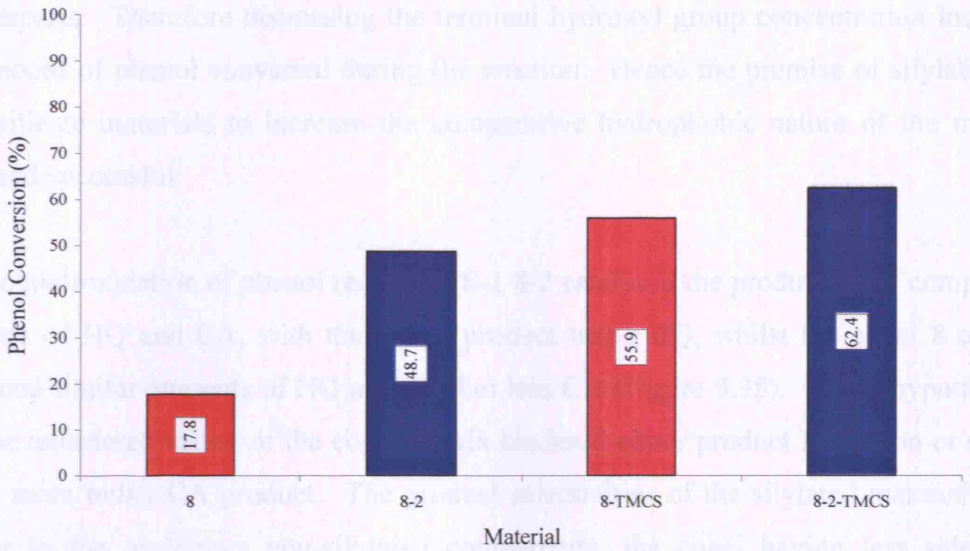

Figure 3.34: Phenol conversion (%) after six hours for cogel (red) and TS-1 (blue) materials.

Therefore, increase of the catalytic activity upon silylation, was possibly due to the decrease in terminal hydroxyl concentration, resulting in a higher effective concentration of available reagents for catalysis. Both the phenol and hydrogen peroxide reagents are able to interact with the terminal hydroxyl groups on the surface of the catalyst, which reduces the concentration of reactants available for reaction. As the amount of these reagents was limited within the system, their effective concentration had a notable effect on the catalytic activity of the system. This was shown by both the increase in reactivity of the silylated cogel and TS-1 materials relative to their non-silylated analogues. The TS-1 materials which contained fewer hydroxyl groups before silylation (Q_4/Q_n values, Figure 3.28) consequently showed a smaller increase in catalytic ability after silylation compared to the cogel.

The hydroxylation of phenol reaction is complex with the conversion of phenol depends on interaction of the catalyst surface with not only phenol and hydrogen peroxide but also insoluble tars formed during the reaction. These results demonstrate that the cogel materials catalyse lower phenol conversions than the framework counterparts, and that silylated materials exhibited higher phenol conversions than their non-silylated

counterparts. Therefore decreasing the terminal hydroxyl group concentration increased the amount of phenol converted during the reaction. Hence the premise of silylating the titanosilicate materials to increase the comparative hydrophobic nature of the material appeared successful.

For the hydroxylation of phenol reaction TS-1 8-2 catalysed the production of comparable amounts of HQ and CA, with the minor product being BQ, whilst the cogel 8 catalyst produced similar amounts of HQ and BQ but less CA (Figure 3.35). It was hypothesised that the unordered nature of the cogel matrix hindered either product formation or release of the more bulky CA product. The product selectivities of the silylated materials were similar to the analogous non-silylated counterparts, the cogel having less selectivity towards the CA product.

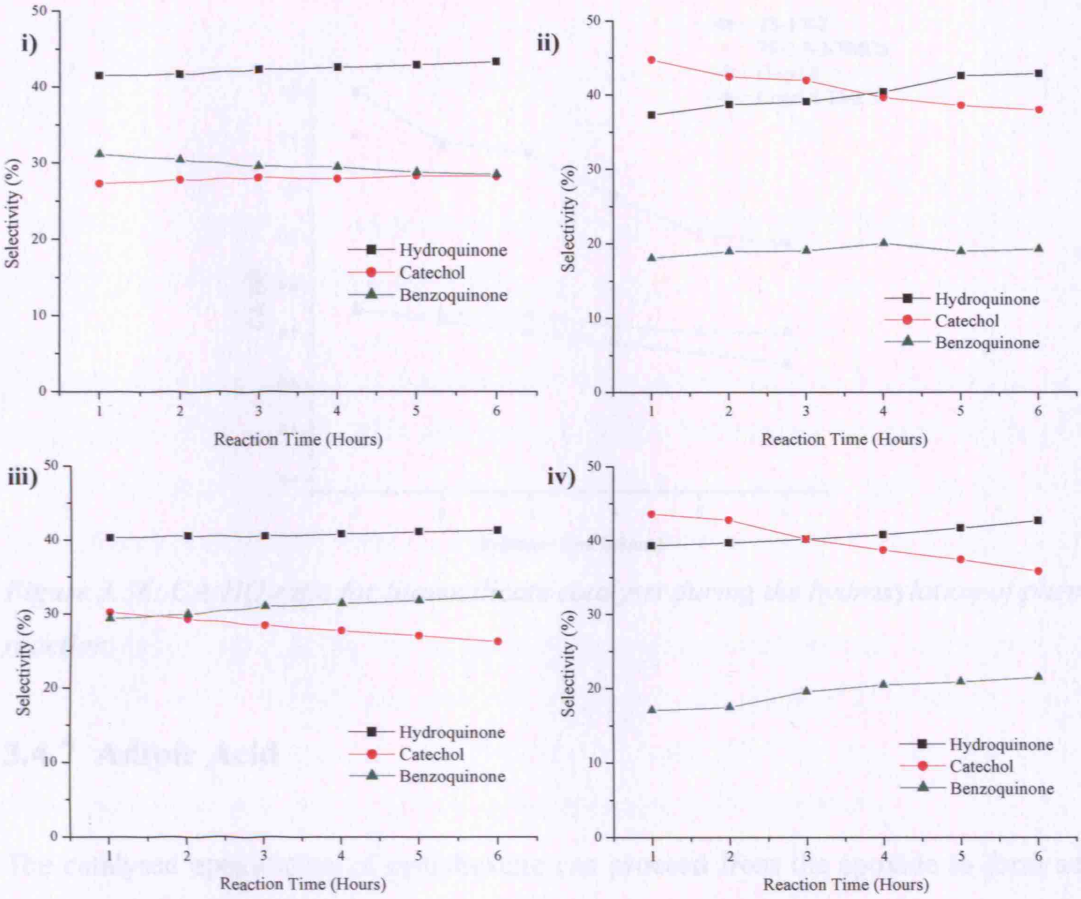

Figure 3.35: Product selectivity (%) for phenol hydroxylation reaction using different catalysts: ***i)*** *Cogel 8,* ***ii)*** *TS-1 8-2,* ***iii)*** *Cogel 8-TMCS,* ***iv)*** *TS-1 8-2-TMCS.*

The CA:HQ ratio decreased throughout the phenol hydroxylation reactions (Figure 3.36). The framework TS-1 materials were shown to be more selective for CA formation than their amorphous cogel counterparts, with a CA:HQ ratio of ~ 0.85 after six hours of reaction, this was comparable with standard values reported in the literature.[5]

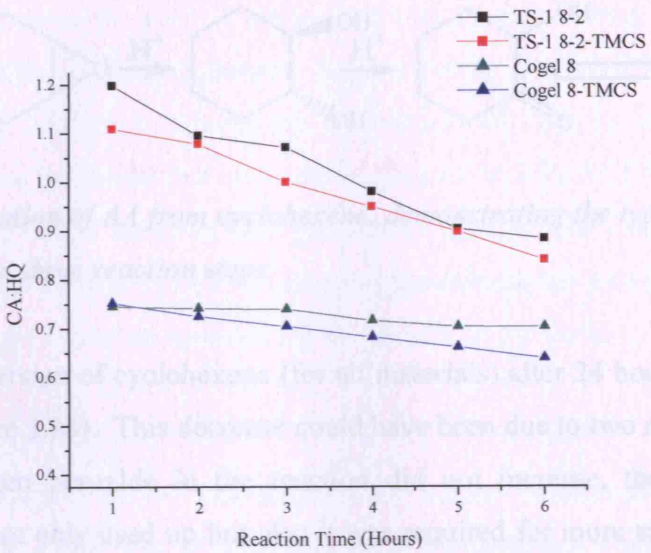

Figure 3.36: CA:HQ ratio for titanosilicate catalysts during the hydroxylation of phenol reaction.

3.4.7 Adipic Acid

The catalysed epoxidation of cyclohexene can proceed from the epoxide to form adipic acid (AA) an important precursor for Nylon 6,6 in turn used extensively to form a range of products (Chapter 2.3.3).[27] Currently the main method of AA production is a costly multi-step process involving homogeneous catalysts and aggressive oxidants, resulting in the production of the greenhouse gas nitrous oxide. Thus the need for a catalyst which provides a cleaner and cheaper production method is evident. The most effective catalysts reported for this reaction have been multi-functional, they have been able to facilitate both oxidative and acidic catalysis. The formation of AA from cyclohexene has been demonstrated to be most effective when the first catalysed step was oxidative and the next two catalysed steps acidic (Figure 3.37).[28] For this reason reactivity of previously reported titanosilicate catalysts has been low, hence the reactions undertaken herein were continued for extended periods of 24, 48 and 72 hours.[29,30] AA production was undertaken using cogel 8, TS-1 8-2 and silylated materials cogel 8-TMCS and TS-1 8-2-TMCS as catalysts.

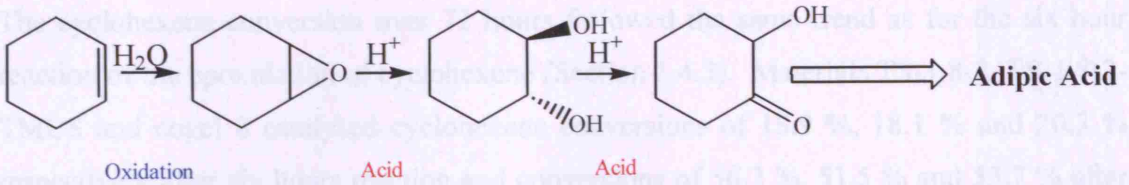

Figure 3.37: Formation of AA from cyclohexene, demonstrating the type of catalysis most effective for the first three reaction steps.

The catalytic conversion of cyclohexene (for all materials) after 24 hours reaction slowed dramatically (Figure 3.38). This decrease could have been due to two main reasons, **i)** the amount of hydrogen peroxide in the reaction did not increase, thus as the reaction proceeded it was not only used up but also it was required for more steps in the reaction pathway. Four equivalents of hydrogen peroxide are required for each cyclohexene to be fully converted into AA, but this assumes no side products are formed. **ii)** the number of catalytically active titanol sites remains constant as the number of reaction processes requiring these sites increases, thus competitive reactions other than the conversion of cyclohexene or further reaction of the epoxide may have been ongoing.

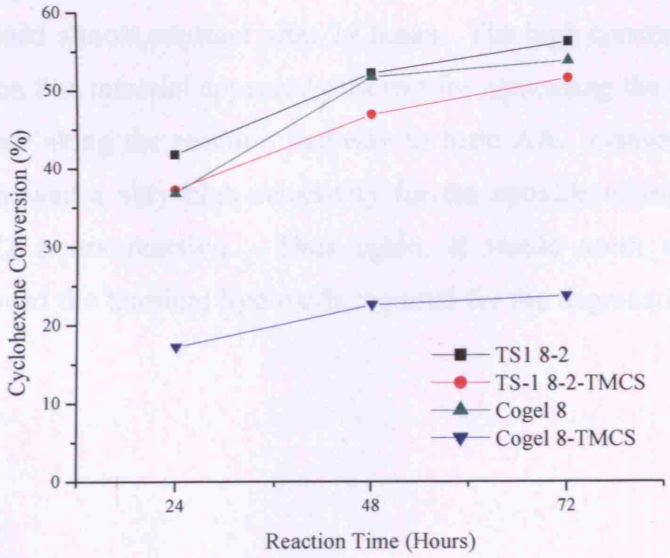

Figure 3.38: Cyclohexene conversion (%) for adipic acid formation utilising titanosilicate catalysts over 72 hours.

The cyclohexene conversion over 72 hours followed the same trend as for the six hour reaction of the epoxidation of cyclohexene (Section 3.4.3). Materials TS-1 8-2, TS-1 8-2-TMCS and cogel 8 catalysed cyclohexene conversions of 18.9 %, 18.1 % and 20.3 % respectively after six hours reaction and conversions of 56.2 %, 51.5 % and 53.7 % after 72 hours. Cogel 8-TMCS however catalysed lower cyclohexene conversions after both six hours (9.5 %) and 72 hours (23.7 %), possibly confirming the previous hypothesis that silylation of the cogel materials appends too much bulk to the surface, preventing reaction at the active sites.

The product distributions for the formation of AA varied considerably according to the catalyst used (Figure 3.39). The selectivity of TS-1 8-2 remained almost constant after 24 hours, despite the cyclohexene conversion (%) still increasing, suggesting that the limited peroxide was being used for the more favourable oxidative reaction to form the epoxide. Catalyst TS-1 8-2-TMCS, demonstrated a very high selectivity for the epoxide, even after 72 hours. This suggested that the silylation of this material, as designed, had destroyed the majority of the terminal acid sites required for the reaction pathway to form AA. Cogel 8 produced a range of products over 72 hours of reaction and the product distribution remained almost constant after 24 hours. The high concentration of terminal hydroxyl groups on this material appeared efficient for converting the epoxide product to the diol and further along the reaction pathway to form AA. Conversely, the silylated cogel 8-TMCS showed a very high selectivity for the epoxide which remained largely unaltered over 72 hours reaction. Thus again, it would seem that silylation has successfully removed the terminal hydroxyls required for the degradation for the epoxide product.

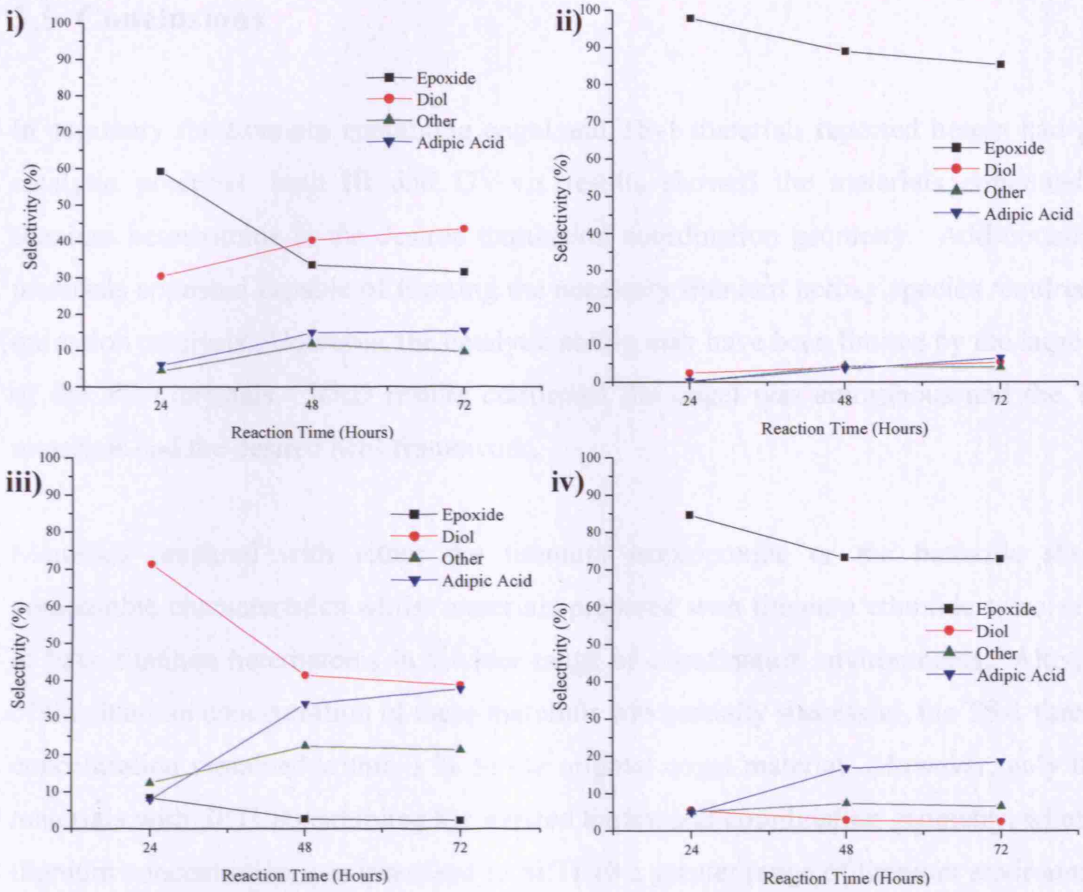

Figure 3.39: Selectivity (%) of adipic acid over 72 hours for titanosilicate materials: ***i)*** *TS-1 8-2,* ***ii)*** *TS-1 8-2-TMCS,* ***iii)*** *Cogel 8,* ***iv)*** *Cogel 8-TMCS.*

Overall the selectivity of the titanosilicate catalysts for AA formation was poor (Table 3.4), literature values for multifunctional materials have reported AA selectivity to be ~ 65 %.[31]

Table 3.4: Summary of adipic acid selectivity for all titanosilicate materials tested after 72 hours of reaction.

Material	AA Selectivity (%)
TS-1 8-2	15.3
TS-1 8-2-TMCS	6.1
Cogel 8	37.6
Cogel 8-TMCS	18.4

3.5 Conclusions

In summary the titanium containing cogel and TS-1 materials reported herein had good catalytic potential, both IR and UV-vis results showed the materials contained the titanium heteroatoms in the desired tetrahedral coordination geometry. Additionally all materials appeared capable of forming the necessary titanium peroxy species required for oxidation catalysis. However, the catalytic ability may have been limited by the large size of the TS-1 crystals. XRD results confirmed the cogel was amorphous and the TS-1 materials had the desired MFI framework.

Materials prepared with either the titanium isopropoxide or the butoxide showed comparable characteristics whilst materials prepared with titanium ethoxide were shown to have titanium heteroatoms in a wider range of coordination environments. Alteration of the titanium concentration of these materials was partially successful, the TS-1 titanium concentration remained within 3 % of the original cogel material. However, only those materials with Si:Ti 80 exhibited the desired tetrahedral coordination geometry, when the titanium concentration was increased to Si:Ti 10 a greater range of titanium environments were shown. Thus further work would be required to evaluate the maximum titanium concentration which could be successful incorporated within the zeolite framework.

Alteration of the ammonium alkyl salt used to initiate the cogel condensation by one carbon chain length, made no appreciable difference to the materials produced. Sonocation of the cogel solution during condensation produced materials with titanium centres that were more tetrahedral than when the solution was condensed whilst stirred. Cogel precursors which were calcined prior to use produced materials with more ideal titanium coordination geometry.

The epoxidation of cyclohexene reaction using these titanosilicate materials demonstrated that alteration of these synthesis parameters (titanium source, titanium concentration, condensation reagent, condensation method, as-prepared/calcined cogel) only had a minor effect upon the catalytic properties of the materials produced. Although the most

catalytically active cogel materials produced the most catalytically active TS-1 materials tested. For epoxidation of cyclohexene reaction, the cogel and TS-1 materials exhibited similar catalytic activity but vastly different selectivity. The epoxide selectivity of the TS-1 materials was comparable to values reported in the literature (~ 60 %), whilst the epoxide selectivity of the cogel was extremely poor (< 5 %). The epoxide selectivity of all of the titanosilicate materials decreased over time due to the acid catalysed formation of the diol.

To discourage diol formation the oxidant was altered to a urea adduct, which slowly released H_2O_2 into the reaction system as well as reducing the acidic hydroxyl site concentration by binding to them. Alteration of the oxidant increased the TS-1 activity to ~ 30 % but tremendously decreased the cogel activity to < 5 %. However, the epoxide selectivity of the catalysts increased the TS-1 materials (~ 90 %) being more selective than the cogel materials (~ 60 %). Alteration of the oxidant prevented epoxide degradation to the diol for all titanosilicate materials, additionally it resulted in the activity of the TS-1 materials increasing and conversely the activity of the cogel materials being greatly diminished.

Silylation of the titanosilicate materials appeared successful with no apparent alteration of the titanium coordination geometry for either the TS-1 or cogel materials. By silylating the materials it was shown that the terminal hydroxyl concentration was reduced but it was not conclusively determined whether the titanol groups were also silylated. The activity of the TS-1 materials for the epoxidation of cyclohexene slightly increased after the catalysts were silylated. Conversely the activity of the cogel materials decreased from ~ 17 % to < 10 %, thus suggesting some of the titanol groups were silylated preventing catalytic reaction at these centres. The premise of silylating the titanosilicate materials to reduce the epoxide degradation was successful. The epoxide selectivity for the TS-1 materials increased from ~ 60 % to ~ 95 %, whilst the selectivity for the cogel materials increased from ~ 5 % to ~ 75 %. Although the activity of the cogel materials decreased after silylation, the decrease was not as pronounced as when the oxidant was altered to the urea-adduct.

Similar trends occurred when the titanosilicate materials were used as catalysts for the hydroxylation of phenol. The TS-1 materials were always more active than the cogel materials, and once silylated the activity of these materials increased further. Similarly to the epoxidation of cyclohexene reaction the product selectivity of the TS-1 materials was more favourable than for the cogel materials.

Further catalysis experiments to produce AA demonstrated similar catalytic activity to those for the epoxidation of cyclohexene reaction. The TS-1 and non-silylated cogel materials exhibiting approximately identical activity, the silylated cogel had lower activity. The product selectivity also demonstrated the differing properties of the TS-1 and cogel materials. The cogel material with remaining acid sites were able to catalyse the formation of AA, whilst the more hydrophobic framework materials cannot.

Thus the cogel precursor and the framework TS-1 material exhibited different properties. Some control over the hydrophilic nature of the cogel materials was possible by either employing an urea-adduct as an oxidant or by silylation of these materials. Although the cogel materials demonstrated some catalytic activity, the most active and selective catalysts were the TS-1 materials. Thus the three-dimensional framework is important for the materials catalytic ability.

The catalytic ability of the TS-1 materials prepared from the cogel precursors is comparable to those TS-1 materials prepared from conventional means. Thus this synthetic method employed to form the TS-1 materials is an effective alternative to the standard method reported.

3.6 References

(1) Tatamasso, M.; Perego, G.; Notari, B.; 4,410,501: U.S. Patent, **1983**.
(2) Romano, U.; Esposito, A.; Maspero, F.; Neri, C.; Clerici, M. G. *Studies of Surface Science and Catalysis* **1990**, *55*, 33.
(3) Jung, K. T.; Shul, Y. G. *Microporous and Mesoporous Materials* **1998**, *21*, 281.
(4) Serrano, D. P.; Uguina, M. A.; Ovejero, G.; Grieken, R. V.; Camacho, M. *Microporous Materials* **1995**, *4*, 273.
(5) Ratnasamy, P.; Srinivas, D. *Advances in Catalysis* **2004**, *48*, 1.
(6) Uguina, M. A.; Ovejero, G.; Grieken, R. V.; Serrano, D. P.; Camacho, M. *Journal of the Chemical Society, Chemical Communications* **1994**, 27.
(7) Serrano, D. P.; Uguina, M. A.; Ovejero, G.; Grieken, R. V.; Camacho, M. *Microporous Materials* **1996**, *7*, 309.
(8) U.Schuchardt; Cardoso, D.; Sercheli, R.; Pereira, R.; Cruz, R. S. d.; Guerrerio, M. C.; Mandelli, D.; Spinace, E. V.; Pires, E. L. *Applied Catalysis A: General* **2001**, *211*, 1.
(9) Huybrechts, D. R. C.; Buskens, P. L.; Jacobs, P. A. *Journal of Molecular Catalysis* **1992**, *71*, 129.
(10) Treacy, M. M. J.; Higgins, J. B. *Collection of Simulated XRD Powder Patterns for Zeolites*; 4th ed.; Elsevier, **2001**.
(11) Beck, C.; Mallat, T.; Burgi, T.; Baiker, A. *Journal of Catalysis* **2001**, *204*, 428.
(12) Uguina, M. A.; Serrano, D. P.; Ovejero, G.; Grieken, R. V.; Camacho, M. *Applied Catalysis A: General* **1995**, *124*, 391.
(13) Notari, B. *Advances in Catalysis* **1996**, *41*, 253.
(14) Geobaldo, F.; Bordiga, S.; Zecchina, A.; Gianello, E.; Leofanti, G.; Petrini, G. *Catalysis Letters* **1992**, *16*, 109.
(15) Wilkenhoner, U.; Langhendries, G.; Laar, F. v.; Baron, G. V.; Gammon, D. W.; Jacobs, P. A.; Steen, E. v. *Journal of Catalysis* **2001**, *203*, 201.
(16) Keshavaraja, A.; Ramaswamy, V.; Soni, H. S.; Ramaswamy, A. V.; Ratnasamy, P. *Journal of Catalysis* **1995**, *157*, 501.
(17) Kim, K. Y.; Ahn, W. S.; Park, D. W.; Oh, J. H.; Lee, C. M.; Tai, W. P. *Bulletin of the Korean Chemical Society* **2004**, *25*, 634.
(18) Eley, D. D.; Hagg, W. O.; Gates, B. *Advances in Catalysis*; 1st ed.; Academic Press, **1996**.
(19) Hutter, R.; Dutoit, D. C. M.; Mallat, T.; Schneider, M.; Baiker, A. *Journal of the Chemical Society, Chemical Communications* **1995**, 163.
(20) Lafond, V.; Mutin, P. H.; Vioux, A. *Journal of Molecular Catalysis A: Chemical* **2002**, *182*, 81.
(21) Xia, Q. H.; Chem, X.; Tatsumi, T. *Journal of Molecular Catalysis A: Chemical* **2001**, *176*, 179.
(22) Laha, S. C.; Kumar, R. *Journal of Catalysis* **2002**, *208*, 339.
(23) Welch, A.; Shiju, N. R.; Watts, I. D.; Sankar, G.; Nikitenko, S.; Bras, W. *Catalysis Letters* **2005**, *105*, 179.
(24) Tatsumi, T.; Koyano, K. A.; Ignarashi, N. *Journal of the Chemical Society, Chemical Communications* **1998**, *325*.

(25) Perego, C.; Carati, A.; Ingallina, P.; Mantegazza, M. A.; Bellussi, G. *Applied Catalysis A: General* **2001**, *221*, 63.
(26) Bellussi, G.; Carati, A.; Clerici, M. G.; Maddinelli, G.; Millini, R. *Journal of Catalysis* **1992**, *133*, 220.
(27) Tozzola, G.; Mantegazza, M. A.; Ranghino, G.; Petrini, G.; Bordiga, S.; Ricchiardi, G.; Lamberti, C.; Zulian, R.; Zecchina, A. *Journal of Catalysis* **1998**, 64.
(28) Raja, R.; Lee, S.; Sanchez-Sanchez, M.; Sankar, G.; Harris, K. D. M.; Johnson, B. F. G.; Thomas, J. M. *Topics in Catalysis* **2002**, *20*, 85.
(29) Lapisardi, G.; Chiker, F.; Launay, F.; Nogier, J. P.; Bonardet, J. L. *Microporous and Mesoporous Materials* **2005**, *78*, 289.
(30) Chiker, F.; Nogier, J. P.; Launay, F.; Bonardet, J. L. *Applied Catalysis A: General* **2003**, *243*, 209.
(31) Chiker, F.; Launay, F.; Nogier, J. P.; Bonardet, J. L. *Green Chemistry* **2003**, *5*, 3.

Chapter 4: Aluminosilicates

4.0 Summary

The aim of the work reported within this chapter was to utilise the information gained from the titanosilicate research (Chapter 3) to produce framework materials from aluminium containing cogel precursors. Two different types of framework material were synthesised **i)** ZSM-5, which is an aluminosilicate framework of the same MFI framework type as TS-1 **ii)** a new variation of Al SAPO-5, which is referred to as an aluminium silicoaluminophosphate framework of AFI framework type. The materials produced were characterised using a suite of techniques including, XRD, packed bulk density measurements, SEM and ^{27}Al NMR. Those materials which demonstrated the greatest acid catalyst properties were further characterised by ammonia absorption and employed as catalysts for the alkylation of benzene reaction.

Similarly to the titanosilicate materials synthesised the aluminosilicate cogels demonstrated some catalytic activity and selectivity. The ZSM-5 materials synthesised are more active catalysts than their amorphous precursors, their catalytic ability being comparable to commercial HZSM-5 materials. Therefore, the synthesis of ZSM-5 materials from cogel precursors produced catalysts of comparable activity to the conventional ZSM-5 procedure. The results obtained also demonstrate that the Al SAPO-5 materials did not contain the cogel incorporated aluminium heteroatoms in a catalytically active form. The Al SAPO-5 materials prepared from cogel precursors were less catalytically active and selective than the standard AlPO5 and SAPO-5 materials tested. Therefore, the preparation of Al SAPO-5 materials from cogel precursors requires further optimisation in order to become a valid alternate synthesis procedure.

4.1 Introduction

The strict composition of a zeolite material is that of SiO_4 and AlO_4 tetrahedra, the AlO_4 tetrahedra cause the zeolite framework to possess negative charges. Positive charges are required to balance the negative framework and attain charge neutrality for the zeolite. Such positive charges are typically metal cations or protons, whose presence results in either cation exchange or acidic properties within the material.

Aluminosilicates have both Brønsted and Lewis acid sites, the definitions being that Brønsted acid sites can donate protons, whilst Lewis acid sites can accept pair of electrons.[1] Brønsted acid sites in aluminosilicates can be changed into Lewis sites through dehydration upon heating, the reverse reaction occurs in the presence of water (Figure 4.1).

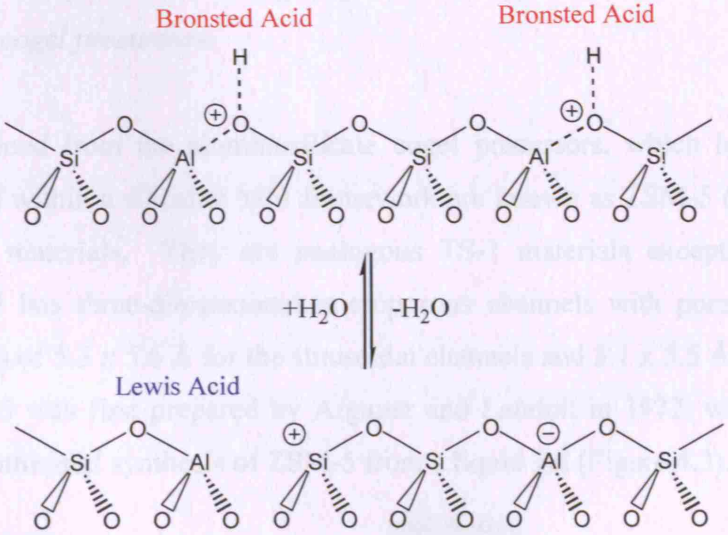

Figure 4.1: Conversion of Brønsted and Lewis acid sites by dehydration.

The conventional ZSM-5 synthesis is via the formation of a liquid gel (containing an aluminium and silicon source, a structure directing reagent and water) which is then subjected to hydrothermal conditions. The work reported herein adopts a similar *co-precipitated gel* (cogel) procedure as exploited for the synthesis of framework TS-1 in chapter 3. In this chapter the synthesis of ZSM-5 framework materials from

aluminosilicate cogel precursors (for use as acid catalysts), is reported. The activity and product selectivity of acidic catalysts depends on the number, strength and nature of the acid sites present and on the shape and size of the micropores which can induce different shape selectivity effects on product distribution.[2] Thus using the cogel precursors two different types of framework materials were synthesised of framework types MFI (identical to that of TS-1) and AFI (Figure 4.2).

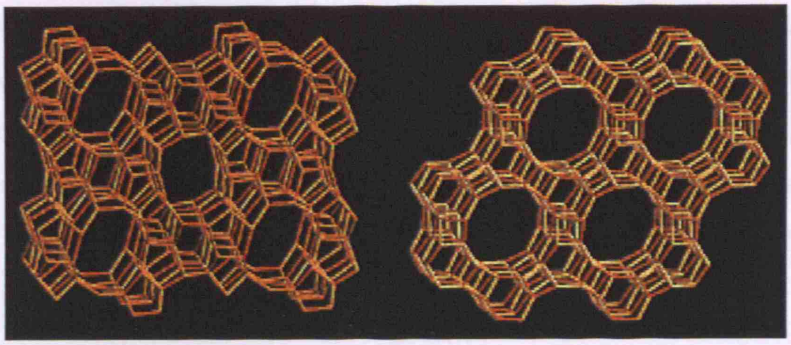

Figure 4.2: MFI (left) and AFI (right) framework types synthesised from identical aluminosilicate cogel precursors.

Materials produced from the aluminosilicate cogel precursors, which have aluminium atoms dispersed within a silicalite MFI framework are known as ZSM-5 (Zeolite Socony Mobil – Five) materials. They are analogous TS-1 materials excepting heteroatom identity, ZSM-5 has three-dimensional microporous channels with pore openings (10-membered rings) of 5.3 x 5.6 Å for the sinusoidal channels and 5.1 x 5.5 Å for the straight channels. ZSM-5 was first prepared by Argauer and Landolt in 1972, who reported the successful hydrothermal synthesis of ZSM-5 from a liquid gel (Figure 4.3).[3]

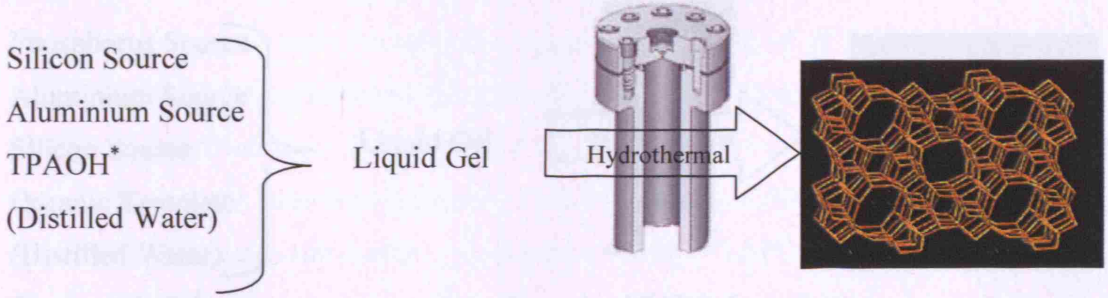

*Figure 4.3: Schematic representation of standard ZSM-5 synthesis (*other organic templates also are widely used).*

ZSM-5 is a commonly used acid catalyst and has several industrial uses such as benzene alkylation, xylene isomerisation and toluene disproportionation.[4,5]

The materials produced in this work from the aluminosilicate cogel precursors with AFI framework contain phosphorus, silicon and aluminium and they are referred to as aluminium silico-alumino-phosphate structure type-5 (Al SAPO-5) materials. AlPO-5 materials have a framework made of alternating phosphorus (V) and aluminium (III) atoms connected through oxygen bridges; when silicon atoms are substituted into this framework the material becomes a SAPO (Figure 4.4). The substitution of silicon (IV) for phosphorus (V) creates a charge imbalance on the framework which is stabilised by a proton, thus creating a Brønsted acid site and many potential applications as an acid catalyst.

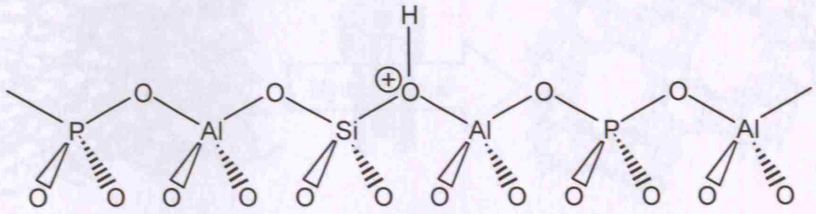

Figure 4.4: Substitution of phosphorous atom (V) by a silicon atom (IV) in an AlPO framework to form a SAPO material.

During the standard synthesis of SAPO-5 a liquid gel is subjected to hydrothermal conditions (Figure 4.5).[6] The AFI type framework has one dimensional pores 7.3 x 7.3 Å which are larger than those of ZSM-5.

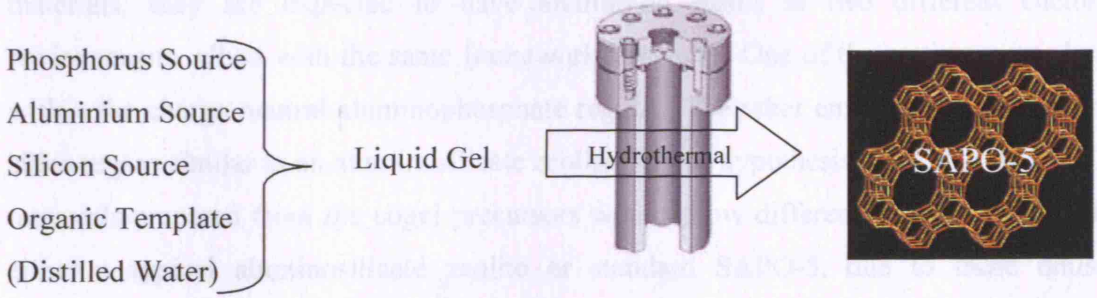

Figure 4.5: Schematic representation of standard SAPO-5 synthesis.

For the work reported herein, the cogel precursor was used as the aluminosilicate source to form the liquid gel, which was then converted into Al SAPO-5 via a hydrothermal process. The heteroatom coordination within the cogel was maintained within the product framework, hence the aluminium atoms remained bound within the silica matrix. Thus, the SAPO-5 framework as described above was prevented from forming, instead an aluminophosphate framework was built around silica framework-islands containing the aluminium (the whole framework having the AFI structure) (Figure 4.6). The synthesis procedure employed was expected to produce materials of the component ratio:

0.8 Template : 0.9 P : 0.1 Cogel : 1.0 Al : 25H_2O.

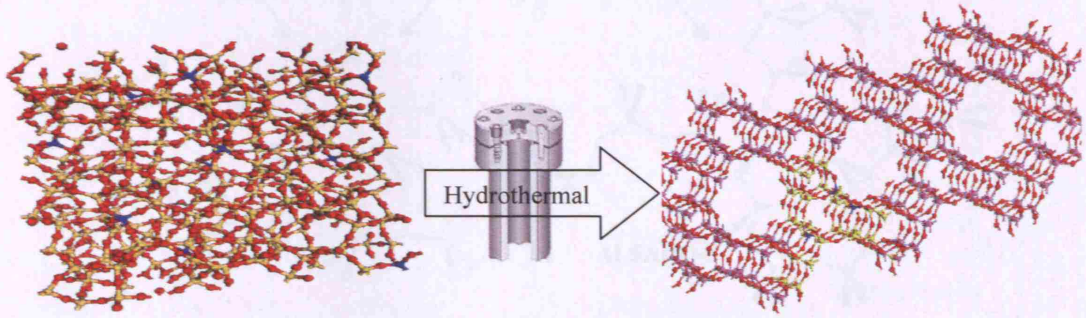

*Figure 4.6 Schematic representation of aluminosilicate cogel conversion into Al SAPO-5 via hydrothermal synthesis (**Cogel Atom Key:** Blue: Inserted Aluminium, Yellow: Silicon, Red: Oxygen. **Al SAPO-5 Atom Key:** Red: Oxygen, Purple: Framework Aluminium and Phosphorus)*

Therefore, the materials synthesised from the cogel precursor are not strictly SAPO-5 materials, they are expected to have aluminium atoms in two different chemical environments, albeit with the same framework structure. One of the environments being within the charge neutral aluminophosphate region. The other environment being in the silica region similar to an aluminosilicate zeolite. It was hypothesised that the Al SAPO-5 materials prepared from the cogel precursors would show different activity compared to either a typical aluminosilicate zeolite or standard SAPO-5, due to these unusual aluminium environments.

Various synthesis parameters were altered to produce the most effective ZSM-5 catalysts possible from the aluminosilicate cogels. The work undertaken to form the AFI materials was a preliminary study, to prove the premise of the procedure, further work is necessary for the material to be optimised. However, the same cogel materials were used to synthesise both the MFI and AFI framework materials (Figure 4.7).

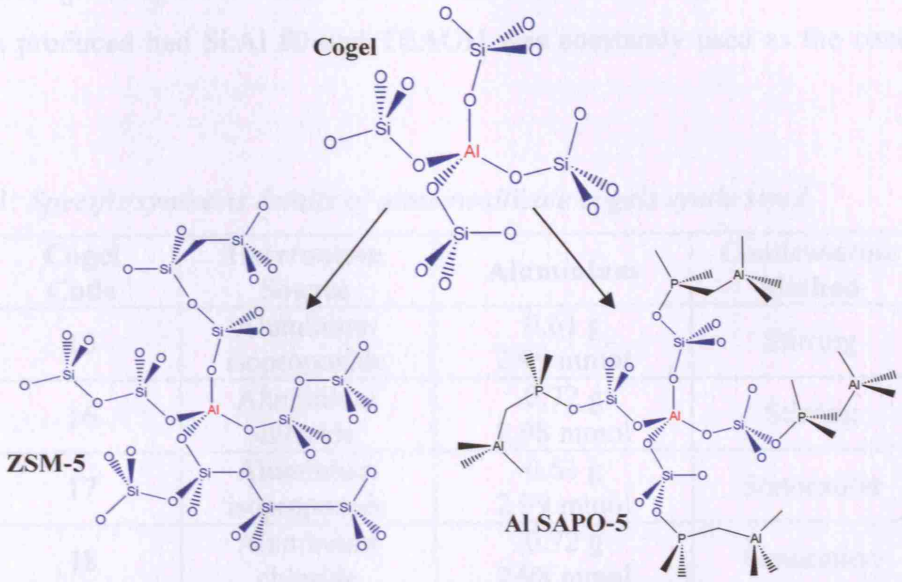

Figure 4.7: Schematic showing the same cogel precursor forming different framework types.

4.2 Aims

- Synthesise ZSM-5 and Al SAPO-5 materials from cogel precursors and compare their physical and catalytic properties.
- Prepare AlPO-5 materials by standard processes and SAPO-5 materials from blank cogel precursors, to compare with Al SAPO-5 materials prepared from cogel precursors.
- Characterisation of the physical and catalytic properties of the cogel precursors and comparison with analogous framework materials.

4.3 Experimental

4.3.1 Cogel Synthesis

Further details regarding the cogel synthesis are given in chapter 2.1.1. The table below (Table 4.1) gives specific details of the aluminosilicate cogels formed. All cogel materials produced had Si:Al 80 and TEAOH was constantly used as the condensation reagent.

Table 4.1: Specific synthesis details of aluminosilicate cogels synthesised.

Cogel Code	Heteroatom Source	Aluminium	Condensation Method
15	Aluminium isopropoxide	0.61 g 2.99 mmol	Stirring
16	Aluminium chloride	0.72 g 2.98 mmol	Stirring
17	Aluminium isopropoxide	0.61 g 2.99 mmol	Sonocation
18	Aluminium chloride	0.72 g 2.98 mmol	Sonocation

4.3.2 ZSM-5 Synthesis

ZSM-5 materials were synthesised from the cogel precursors as outlined in chapter 2.1.2, these framework materials were prepared using both the calcined and as-prepared cogel precursors (Table 4.2).

Table 4.2: Details of ZSM-5 materials produced.

Cogel Source	ZSM-5 Code	Calcined / As Prepared Cogel
15	15-1	As Prepared
	15-2	Calcined
16	16-1	As Prepared
	16-2	Calcined
17	17-1	As Prepared
	17-2	Calcined
18	18-1	As Prepared
	18-2	Calcined

4.3.3 Al SAPO-5 Synthesis

Cogel precursors were utilised to produce Al SAPO-5 materials as outlined in chapter 2.1.3, specific details of the products are given below (Table 4.3).

Table 4.3: Details of Al SAPO-5 materials produced.

Cogel Source	Al SAPO-5 Code	Calcined / As Prepared Cogel
15	15-3	As Prepared
	15-4	Calcined
16	16-3	As Prepared
	16-4	Calcined
17	17-3	As Prepared
	17-4	Calcined
18	18-3	As Prepared
	18-4	Calcined

4.3.4 Standard Materials

Blank MFI (ZSM-5 standard) and AFI (SAPO-5 standard) materials were synthesised as outlined in 2.1.4. Additionally, AlPO-5 (AlPO-5 standard) was prepared using the method outlined in chapter 2.1.3, with the cogel source omitted from the synthesis.

4.4 Results and Discussion

4.4.1 Aluminosilicate Materials

XRD Characterisation:

XRD patterns of the aluminosilicate cogel precursors demonstrated that they were amorphous materials (Figure 4.8). The XRD patterns of both the ZSM-5 and Al SAPO-5 materials demonstrated them to be crystalline with different framework structures of MFI and AFI respectively. The XRD patterns of the crystalline materials were evaluated against those previously reported in the literature and model materials, to ensure standardised framework construction. The XRD patterns demonstrated that the premise of employing one cogel as a precursor to produce different crystalline materials had been achieved. As for the titanosilicate materials (Chapter 3) the use of either as-prepared or calcined cogel precursors made no obvious structural difference to the framework materials synthesised from them.

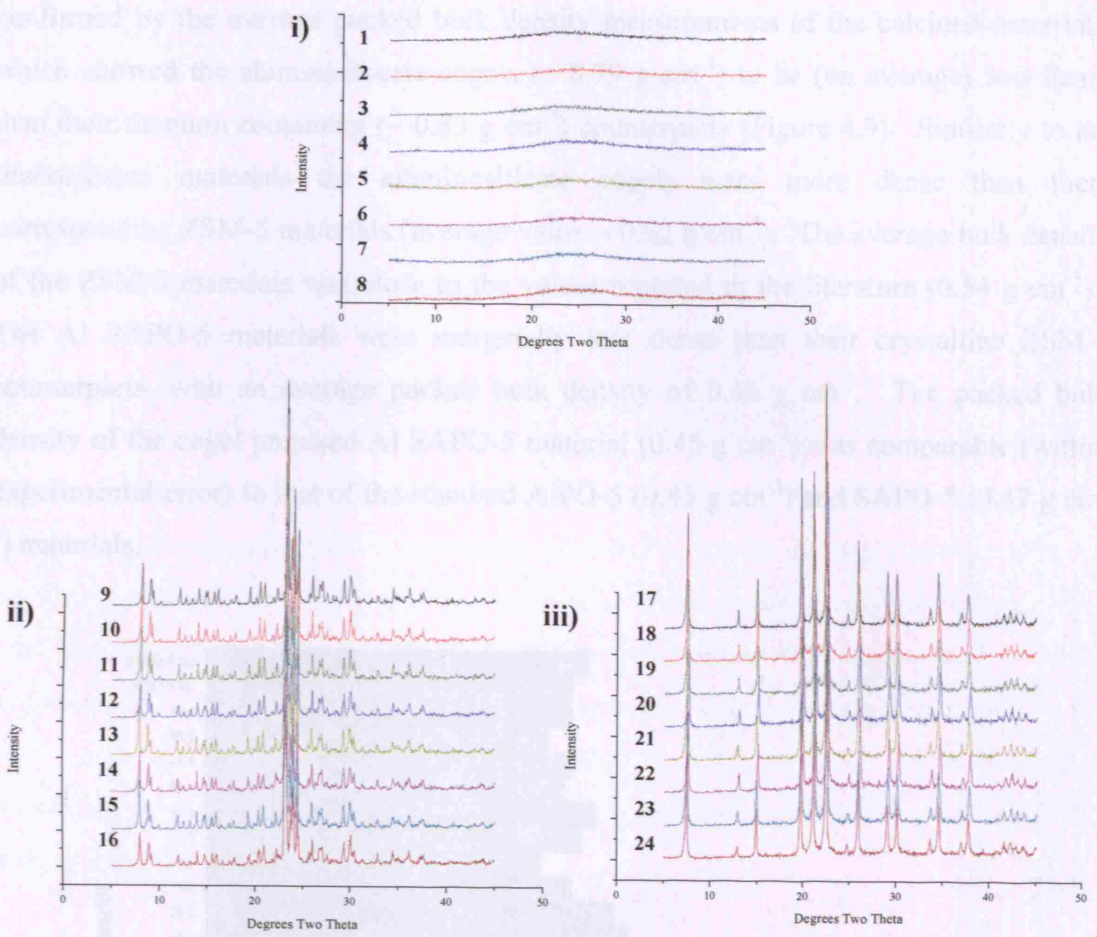

Figure 4.8: XRD patterns of ***i)*** *cogel (**1-8**),* ***ii)*** *ZSM-5 (**9-16**) and* ***iii)*** *Al SAPO-5 (**16-24**) materials. (**1:** Cogel 15 as-prepared, **2:** Cogel 15 calcined, **3:** Cogel 16 as-prepared, **4:** Cogel 16 calcined, **5:** Cogel 17 as-prepared, **6:** Cogel 17 calcined, **7:** Cogel 15 as-prepared, **8:** Cogel 15 calcined) (**9:** ZSM-5 15-1, **10:** ZSM-5 15-2, **11:** ZSM-5 16-1, **12:** ZSM-5 16-2, **13:** ZSM-5 17-1, **14:** ZSM-5 17-2, **15:** ZSM-5 18-1, **16:** ZSM-5 18-2) (**17:** Al SAPO-5 15-3, **18:** Al SAPO-5 15-4, **19:** Al SAPO-5 16-3, **20:** Al SAPO-5 16-4, **21:** Al SAPO-5 17-3, **22:** Al SAPO-5 17-4, **23:** Al SAPO-5 18-3, **24:** Al SAPO-5 18-4).*

Bulk Density Characterisation:

All of the aluminosilicate materials were similar in appearance, they were fine white powders of similar consistency. It was noteworthy however, that the aluminosilicate cogel materials appeared less substantial their titanium counterparts. This assertion was

confirmed by the average packed bulk density measurements of the calcined materials, which showed the aluminosilicate cogels (~ 0.79 g cm^{-3}) to be (on average) less dense than their titanium containing (~ 0.83 g cm^{-3}) counterparts (Figure 4.9). Similarly to the titanosilicate materials the aluminosilicate cogels were more dense than there corresponding ZSM-5 materials (average value ~ 0.52 g cm^{-3}). The average bulk density of the ZSM-5 materials was close to the values reported in the literature (0.54 g cm^{-3}).[8] The Al SAPO-5 materials were marginally less dense than their crystalline ZSM-5 counterparts, with an average packed bulk density of 0.45 g cm^{-3}. The packed bulk density of the cogel prepared Al SAPO-5 material (0.45 g cm^{-3}) was comparable (within experimental error) to that of the standard AlPO-5 (0.45 g cm^{-3}) and SAPO-5 (0.47 g cm^{-3}) materials.

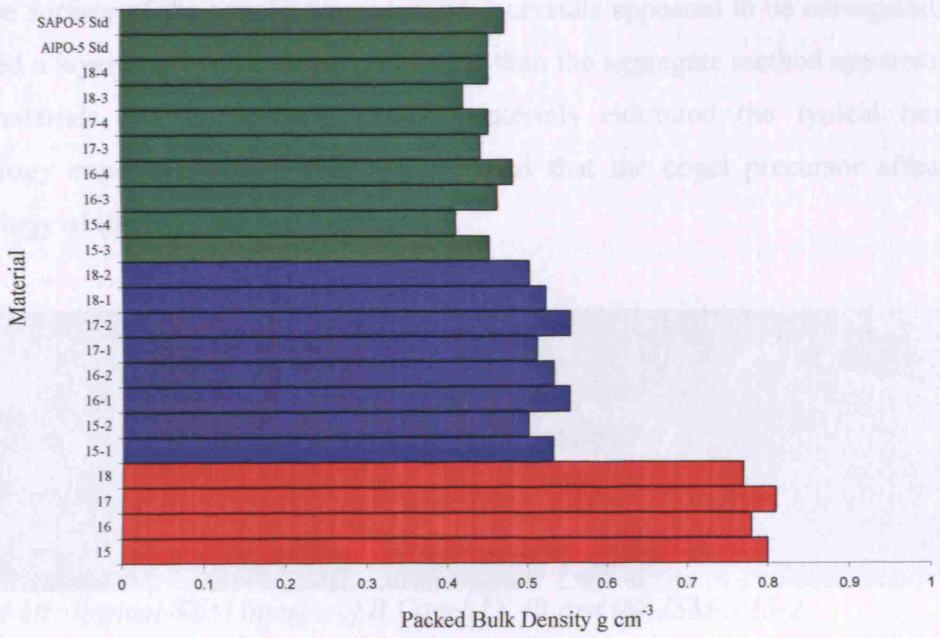

*Figure 4.9: Packed bulk density for all aluminium containing materials synthesised. (**Red:** Cogel materials, **Blue:** ZSM-5, **Green:** Al SAPO-5).*

It was hypothesised that the lower density of the crystalline materials was due to the more ordered nature of the materials. Although, all of the materials produced were porous, the repeating unit cell and reportedly larger pore dimensions of the crystalline materials

resulted in them being less dense. Further from this, the Al SAPO-5 materials have larger pore dimensions hence they are on average less dense than the ZSM-5 materials.

SEM Characterisation:

SEM images of the all aluminosilicate cogels prepared demonstrated these materials to have no ordered morphology regardless of the synthesis parameters employed (Figure 4.10). The appearance of both the titanium and aluminosilicate cogels was indistinguishable.

The morphology of all the ZSM-5 materials was spherical, the same as for the TS-1 materials. However, the ZSM-5 materials exhibited a smaller average diameter of ~ 0.3 μm (compared to ~ 0.5 μm for the TS-1 materials) within a narrow range of 0.8 μm to 0.3 μm. The surface of the cogel prepared ZSM-5 crystals appeared to be corrugated, which suggested a layered growth mechanism, rather than the aggregate method apparent for the TS-1 materials. The standard ZSM-5 materials exhibited the typical hexagonal morphology expected, thus it was hypothesised that the cogel precursor affected the morphology of the final product crystals.

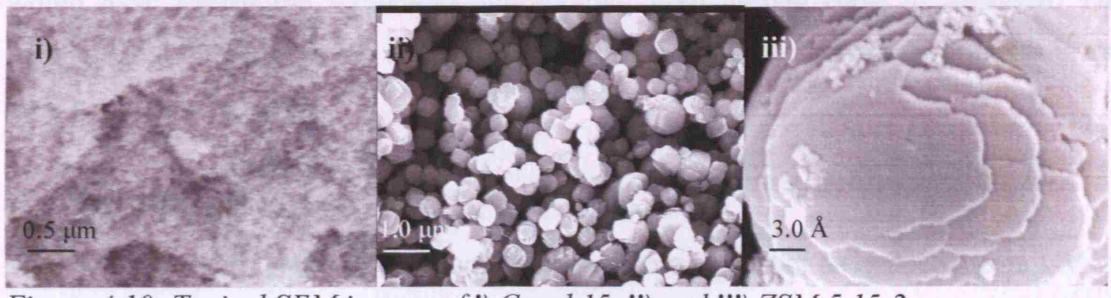

Figure 4.10: Typical SEM images of ***i)*** *Cogel 15,* ***ii)*** *and* ***iii)*** *ZSM-5 15-2.*

The SEM images of all of the Al SAPO-5 materials demonstrated the morphology of these materials to be loosely cuboid (Figure 4.11). The approximate average size of these cuboid crystals was 1.0 μm, but the range in all of the Al SAPO-5 materials was between 0.2 μm to 2.5 μm. The surface of these materials was smooth, thus it was hypothesised that these crystals were grown via a single crystal growth mechanism.

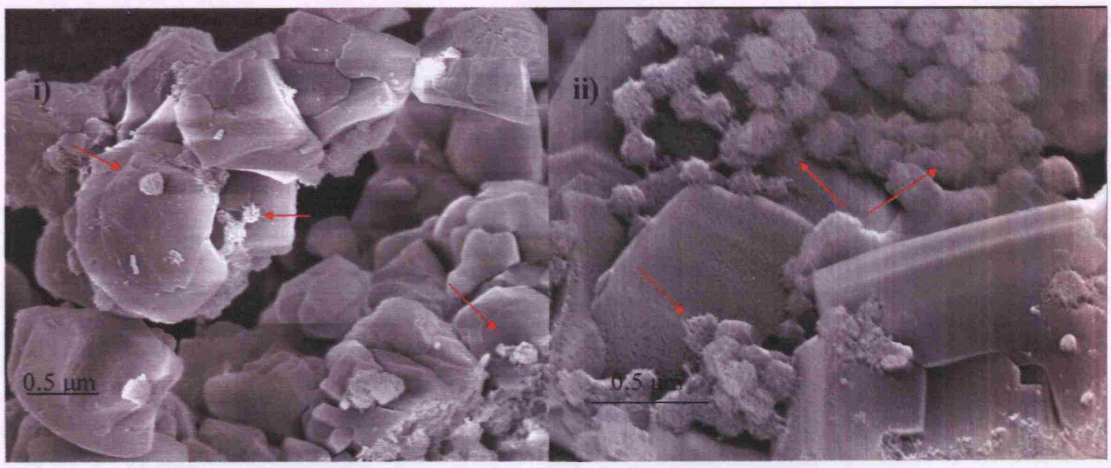

Figure 4.11: Typical SEM images of Al SAPO-5 15-4.

In all of the Al SAPO-5 materials, smaller spherical structures could be viewed. The surface of these spheres (red arrows on figure 4.11) appeared to exhibit comparable texture to that of the cogel materials. However, the low concentration of cogel material added to the Al SAPO-5 synthesis could not explain the apparently high concentration of these spherical structures. It was tentatively hypothesised that the spherical structures could be a form of AlPO-5 which had entrapped the silica islands (from the cogel precursor). Further from this, that addition of the silica atoms to the AlPO-5 framework would have altered the framework morphology from pseudo cubic to spherical. This hypothesis would explain the smaller size of the spheres to the cuboid structures and also their high concentration.

^{27}Al NMR Characterisation:

The bonding environment of the aluminium heteroatoms cannot be deduced from UV-vis analysis, thus ^{27}Al NMR data was collected for all of the aluminium containing materials. Three main signals were expected for the solely aluminosilicate materials, two of them at approximately 60, and 0 ppm which were assigned to tetrahedral and octahedral coordinated aluminium centres, respectively.[9,10] The third predicted peak at ~ 30 ppm has been reportedly assigned either as aluminium in AlO_5 polyhedra or as distorted AlO_4 tetrahedra.[11]

The NMR data collected from the as-prepared cogel materials exhibited one signal at ~ 50 ppm attributed to tetrahedrally coordinated aluminium heteroatoms (Figure 4.12). For all of the cogel materials the peak was broad, which was indicative of no long range order within the amorphous matrix. The calcined cogel materials gave rise to an even broader peak shifted to comparable, but slightly lower, ppm values. Additionally, the calcined cogel displayed an extra peak at ~ 0 ppm, which was assigned to octahedrally coordinated aluminium atoms.

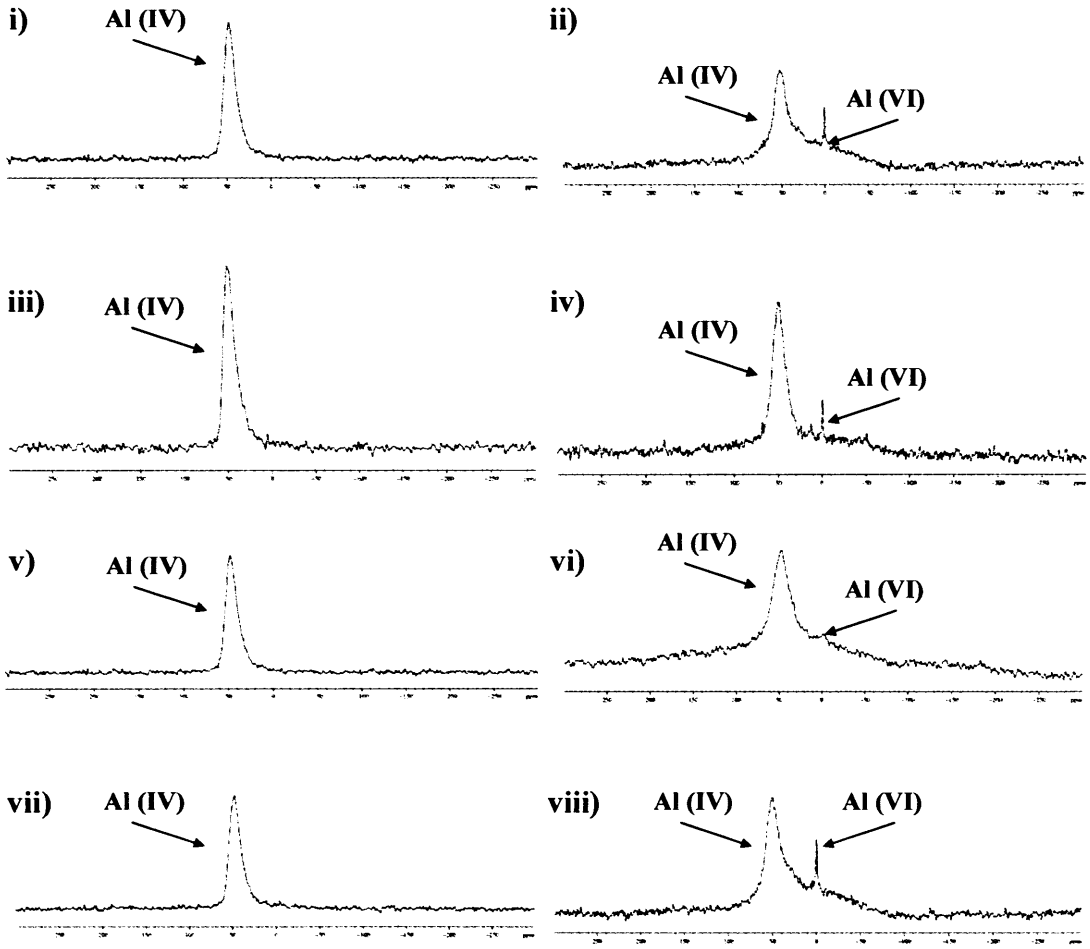

Figure 4.12: ^{27}Al NMR spectra of cogel materials: ***i)*** *Cogel 15 as-prepared,* ***ii)*** *Cogel 15 calcined,* ***iii)*** *Cogel 16 as-prepared,* ***iv)*** *Cogel 16 calcined,* ***v)*** *Cogel 17 as-prepared,* ***vi)*** *Cogel 17 calcined,* ***vii)*** *Cogel 18 as-prepared,* ***viii)*** *Cogel 18 calcined.*

Thus the as-prepared cogel materials contained aluminium atoms bound within the amorphous silica matrix in predominantly tetrahedral coordination geometry. After calcination the cogel silica matrix had degraded to a less ordered material (broader signal ~ 50 ppm) and some of the aluminium atoms were removed from the matrix (and became octahedrally coordinated centres). When aluminium centres are pulled from the amorphous matrix they are commonly bound by water ligands and thus their coordination geometry alters from tetrahedral to octahedral. This coordination alteration may have indicated that the cogel matrix was somehow dependant upon the organic constituents for stability, as once these were removed the structure collapsed. Further work could be done via alteration of the calcination parameters to elucidate a conclusive explanation. There was no other obvious difference between the cogel precursors produced regardless of the alterations to the synthesis parameters.

Unlike the cogel materials, the ZSM-5 materials did not show any increase in disorder upon calcination (confirmed by XRD patterns of the calcined materials), conversely the predominant signal narrowed and shifted position to slightly higher ppm values (Figure 4.13). Additionally, the aluminium centres continued to exhibit the coordination environment.

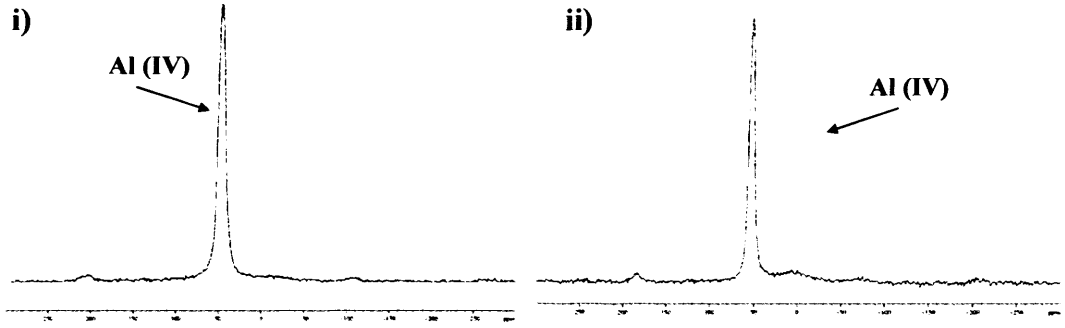

*Figure 4.13: ^{27}Al NMR spectra of ZSM-5 15-1 **i)** as-prepared and **ii)** calcined.*

The NMR spectra of the ZSM-5 materials allowed identification of the most potentially reactive catalysts (those materials whose NMR spectra depicted all of the aluminium centres to be in tetrahedral sites were proposed to be more catalytically reactive). ZSM-5 materials 16-1, 18-1 and 18-2 produced NMR spectra which exhibited the narrowest sole

peak of all the materials examined, indicative of them being the most crystalline and with solely tetrahedral aluminium centres (Figure 4.14).

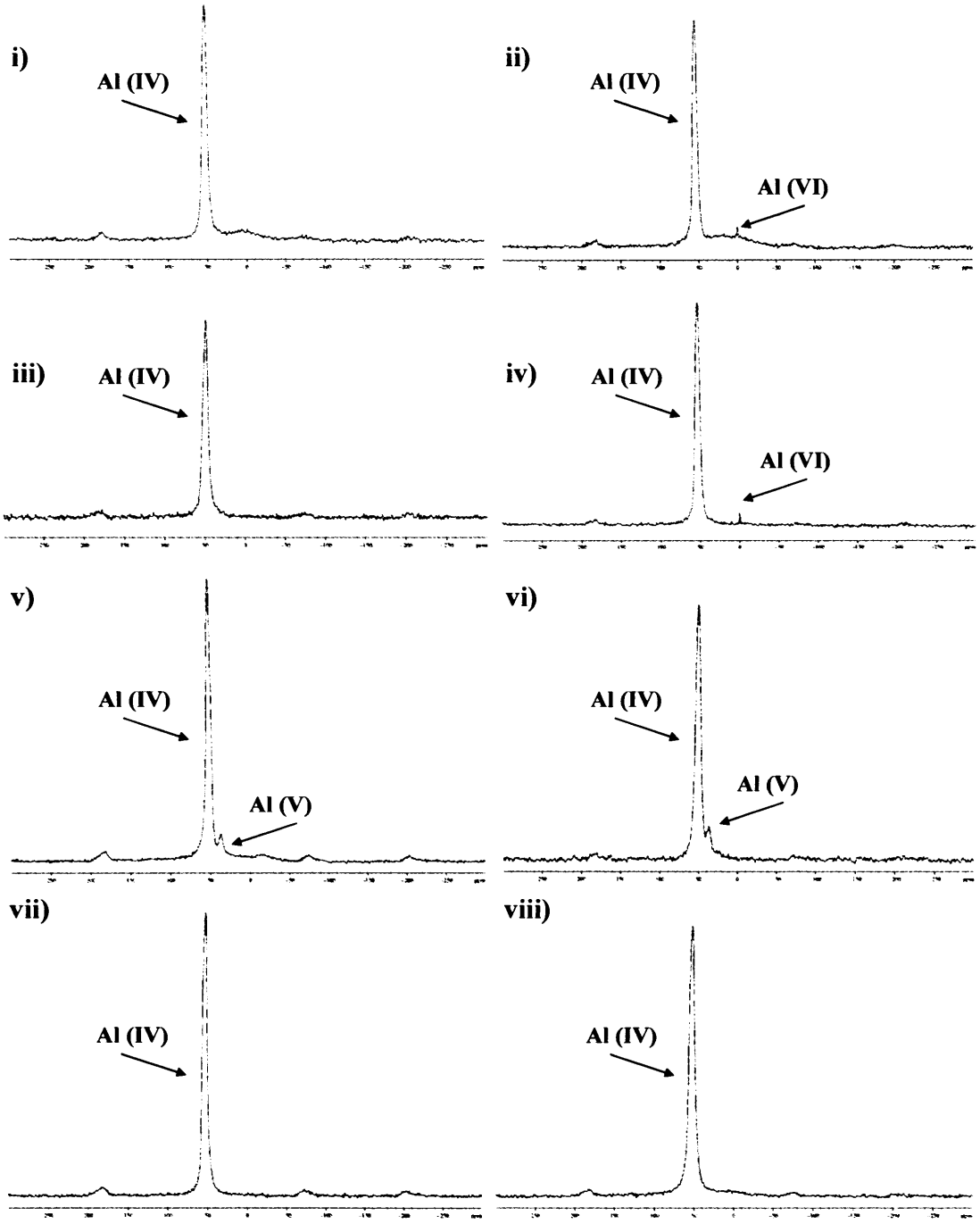

Figure 4.14: ^{27}Al NMR spectra of calcined ZSM-5 materials: ***i)*** *ZSM-5 15-1,* ***ii)*** *ZSM-5 15-2,* ***iii)*** *ZSM-5 16-1,* ***iv)*** *ZSM-5 16-2,* ***v)*** *ZSM-5 17-1,* ***vi)*** *ZSM-5 17-2,* ***vii)*** *ZSM-5 18-1,* ***viii)*** *ZSM-5 18-2.*

The signals produced from ZSM-5 material 15-1 had a principal peak at ~ 50 ppm and a small peak at ~ 0 ppm which suggested that whilst the majority of the aluminium heteroatoms were tetrahedrally coordinated, a minority were in octahedral sites. The NMR spectra of ZSM-5 materials 15-2 and 16-2 (Table 4.2) exhibited similar signals, each showed a main peak at ~ 50 ppm and a smaller peak at ~ 0 ppm, indicative of tetrahedral and octahedral aluminium coordination respectively. Materials 17-1 and 17-2 (Table 4.2) displayed the most clearly defined extra peak at ~ 30 ppm, as well as the expected signal at ~ 50 ppm. This extra peak was assigned to either aluminium in a five coordinated site or a distorted four coordinate site, whichever model is taken, the peak was described as due to aluminium centres removed from framework sites.[11]

The ZSM-5 materials prepared using aluminium chloride as the source, exhibited potential for catalytic activity (more than those prepared from aluminium isopropoxide), their NMR spectra appearing more crystalline with fewer extra signals. Additionally, materials prepared from the as-prepared cogel precursors were less likely to contain aluminium centres in non-tetrahedral environments. This substantiates the NMR data collected from the cogel materials which showed they degrade upon calcination to contain aluminium centres in a range of coordination environments.

The ZSM-5 materials prepared from cogel precursors which underwent sonocation during condensation, exhibited fewer superfluous signals than those prepared from cogel materials which were stirred during condensation. Therefore from these results, theoretically the most reactive ZSM-5 catalyst should be made from an as-prepared cogel produced from aluminium chloride, which was condensed under sonocation; ZSM-5 18-1.

The examination of Al SAPO-5 NMR spectra was not as clear-cut as for solely silicalite materials; the aluminium centres investigated are in two distinct chemical environments. The aluminium centres within the silicate environment could potentially give rise to identical peaks as the cogel and ZSM-5 materials, (within the ranges of ~ 50 to 80, ~ 30 to 40 and ~ -10 to 15 ppm for four, five and six coordinated centres respectively). Whilst those aluminium heteroatoms within the phosphate region can theoretically give rise to

peaks within the ranges ~ 35 to 40, ~ 20 to 25 and ~ -21 to -10 ppm for four, five and six coordinated centres respectively.[12,13] Thus there was potential for the peaks pertaining to these two separate environments to overlap and thus confuse the identity of the aluminium species resonsible.[14] Additionally, the concentration of aluminium in these two samples was widely different, making it easier for the silicalite environment aluminium atoms to be hard to distinguish.

The NMR spectra of the as-prepared Al SAPO-5 materials appeared similar regardless of the difference in preparative method employed (Figure 4.15). The principal signal in all of the spectra related to tetrahedrally bound aluminium in a phosphorous environment (~ 35 ppm). A minor peak attributed to octahedrally coordinated aluminium also in a phosphorus environment was also visible (~ -5 ppm); though sometimes as a shoulder rather than as an independent peak. The signal at ~ 10 ppm, related to the aluminium heteroatoms within the silicate environment, demonstrated the aluminium atoms to be octahedrally coordinated.

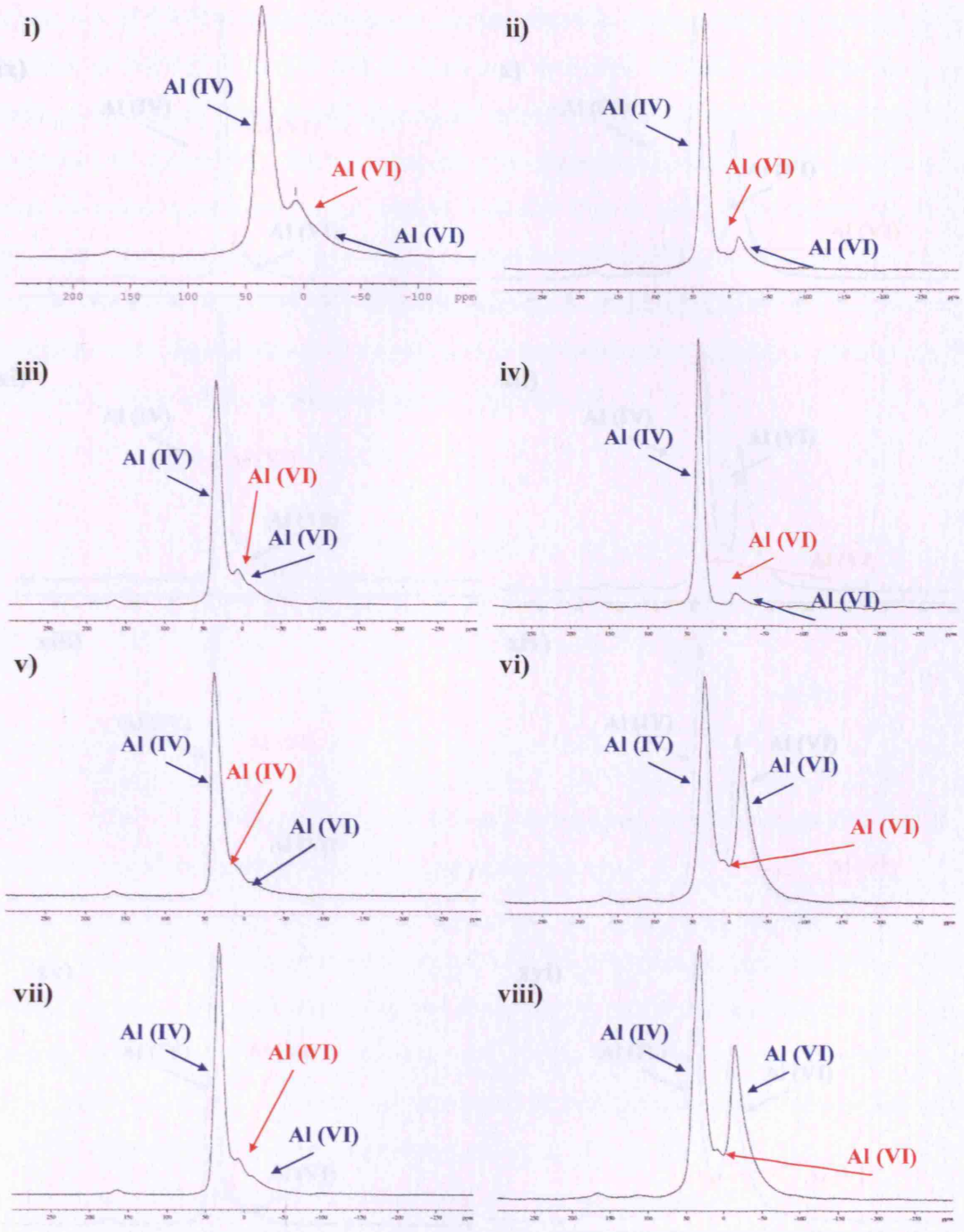

Figure 4.15(1 of 2): ^{27}Al NMR spectra (ap = as-prepared, c= calcined):

***i)** Al SAPO-5 15-3 ap, **ii)** Al SAPO-5 15-3 c, **iii)** Al SAPO-5 15-4 ap, **iv)** Al SAPO-5 15-4 c **v)** Al SAPO-5 16-3 ap, **vi)** Al SAPO-5 16-3 c, **vii)** Al SAPO-5 16-4 ap **viii)** Al SAPO-5 16-4 c. (**Red:** silicate environment, **Blue:** phosphorous environment).*

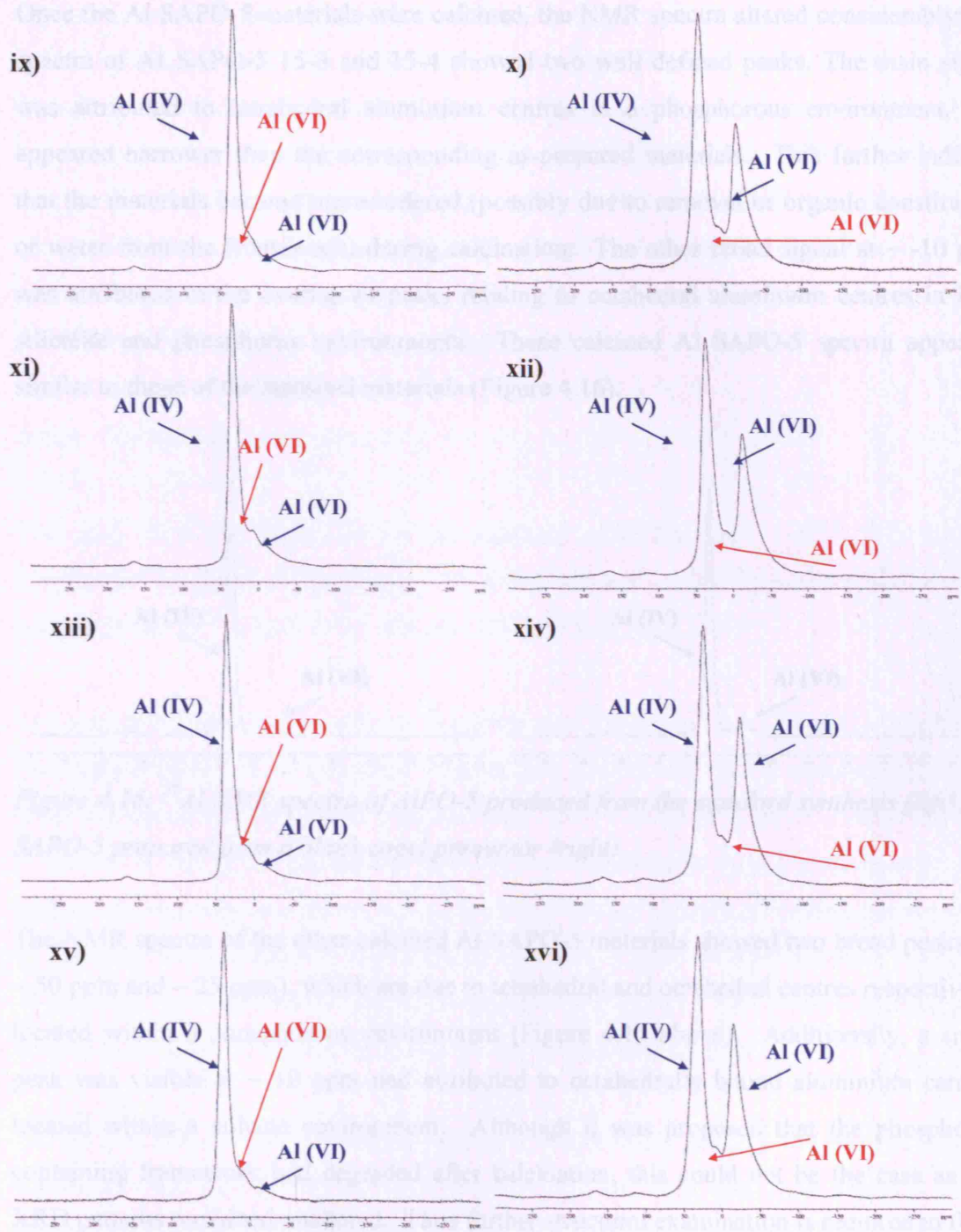

Figure 4.15(2 of 2): ^{27}Al NMR spectra (ap = as-prepared, c= calcined):

***ix)** Al SAPO-5 17-3 ap, **x)** Al SAPO-5 17-3 c, **xi)** Al SAPO-5 17-4 ap, **xii)** Al SAPO-5 17-4 c, **xiii)** Al SAPO-5 18-3 ap, **xiv)** Al SAPO-5 18-3 c, **xv)** Al SAPO-5 18-4 ap, **xvi)** Al SAPO-5 18-4 c. (**Red:** silicate environment, **Blue:** phosphorous environment).*

Once the Al SAPO-5 materials were calcined, the NMR spectra altered considerably: the spectra of Al SAPO-5 15-3 and 15-4 showed two well defined peaks. The main signal was attributed to tetrahedral aluminium centres in a phosphorous environment, and appeared narrower than the corresponding as-prepared materials. This further indicted that the materials became more ordered (possibly due to removal or organic constituents or water from the framework) during calcination. The other broad signal at ~ -10 ppm was attributed to the overlap of peaks relating to octahedral aluminium centres in both silicalite and phosphorus environments. These calcined Al SAPO-5 spectra appeared similar to those of the standard materials (Figure 4.16).

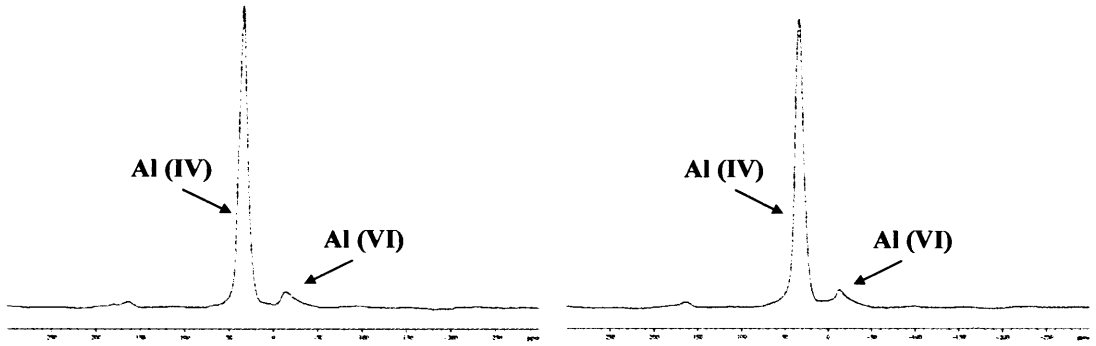

Figure 4.16: ^{27}Al NMR spectra of AlPO-5 produced from the standard synthesis (left) and SAPO-5 prepared from a blank cogel precursor (right).

The NMR spectra of the other calcined Al SAPO-5 materials showed two broad peaks (at ~ 50 ppm and – 25 ppm), which are due to tetrahedral and octahedral centres respectively, located within a phosphorous environment (Figure 4.15 above). Additionally, a small peak was visible at ~ 10 ppm and attributed to octahedrally bound aluminium centres located within a silicate environment. Although it was proposed that the phosphorus containing framework had degraded after calcination, this could not be the case as the XRD patterns remained unaltered. Thus further structural examination is required to fully evaluate the materials structure.

In summary there was no evidence of tetrahedrally bound aluminium atoms within a silicate environment, suggesting that utilising the cogel precursor did not produce the

expected material. It was hypothesised that the cogel completely degraded during the AlPO framework synthesis, to further investigate this *in-situ* NMR studies could be utilised to follow the crystallisation of Al SAPO-5 from a cogel precursor. It has also been reported that silicon incorporation within a SAPO material is unlikely if the pH of the synthesis gel is not carefully controlled. Therefore, it is possible that the aluminosilicate cogel did not take part in the synthesis of the framework itself. The cogel may either have been removed in the mother liquor after synthesis, or remained trapped within the cavities of the newly formed framework.

4.4.2 Ammonia Absorption

The acid sites of the following pre-calcined materials were evaluated using the temperature programmed desorption (TPD) of ammonia: cogel (15 and 18), ZSM-5 (18-1 and 18-2) and Al SAPO-5 (15-3 and 15-4) (Chapter 2.2.6).

The acidity of some aluminosilicate materials was studied to enable further prediction of the catalytic ability of the materials. In principle, TPD of ammonia elucidates information about the concentration of acid sites and their relative acidic strengths.[15] However, TPD is limited in that it can distinguish sites by sorption strength only, it cannot completely distinguish Brønsted and Lewis acid sites (acid sites are capable of exhibiting both types of acidity). Additionally, the desorption of ammonia may occur simultaneously from sites of different types resulting in the overlapping of the recorded TPD bands, although this may be minimised by employment of a slower temperature ramp rate.[12]

The TPD profiles of the cogel materials showed one major band (~ 170 °C) and a small subsidiary band (~ 420 °C) at higher temperature consistent with those reported in the literature (Figure 4.17).[16] The small band at high temperature displayed in the profile of cogel 18 was more well-defined than that exhibited for the cogel 15 (although only a qualitative comparison could be made due the overlap of these bands, which introduced some uncertainty into the band area). For both cogel profiles the small band in the high temperature region were attributed to the desorption of ammonia from strong (Brønsted

and Lewis) acid sites: these acid sites have been demonstrated to be mainly responsible for the acid catalysed reaction in hydrocarbon transformations.[17] Assignment of the band at low temperature (~ 150 °C) is still controversial with varying research groups proposing that it was attributed to desorption from weakly acidic silanol groups, extra framework alumina species such as $Al(OH)_2^+$ and $Al(OH)^{2+}$ exhibiting weak Lewis acidity, or the release of ammonia which was hydrogen bound to NH_4^+ cations.[18] The presence of a more intense band at low temperature suggested that the most common type of acidity exhibited by both the cogel materials was not that of the catalytically desired strong acid sites, although a band was evident in both profiles for the higher acid strength sites. Hence it was expected that the cogel materials would exhibit some catalytic activity; as this band was more defined for cogel 18 than 15, it was expected that cogel 18 would exhibit higher catalytic activity. Although the NMR results suggest that there is loss of tetrahedral coordination of the aluminium centres upon calcination, the TPD profiles indicate that there are strong acid sites in the cogel materials.

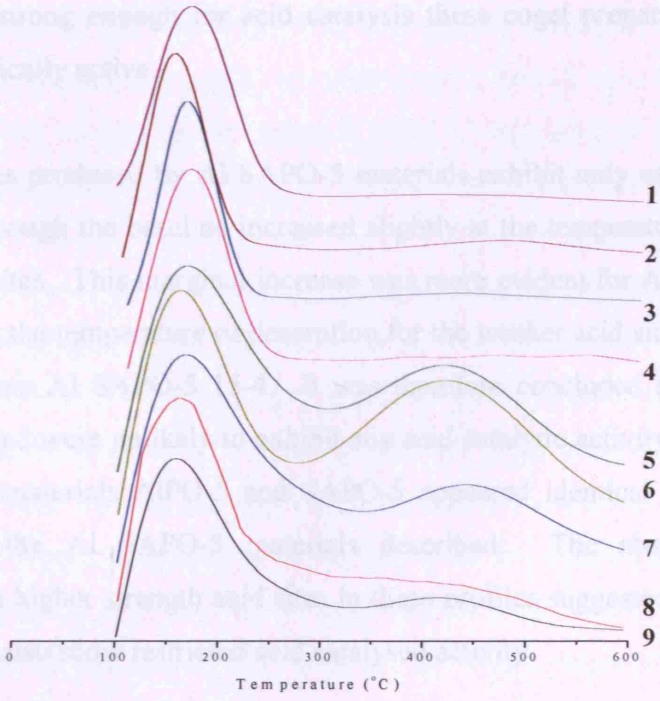

Figure 4.17: TPD profiles of aluminium containing materials: ***1)*** *Al SAPO-5 15-3* ***2)*** *Al SAPO-5 15-4,* ***3)*** *Standard SAPO-5,* ***4)*** *AlPO-5 Standard,* ***5)*** *ZSM-5 18-1,* ***6)*** *ZSM-5 18-2,* ***7)*** *Commercial HZSM-5,* ***8)*** *Cogel 15,* ***9)*** *Cogel 18.*

The bands relating to the weaker acid sites of the ZSM-5 materials were comparable in size to those of the cogel materials. The ZSM-5 materials prepared from different cogel precursors produced almost identical graphs, with both bands having similar approximate areas. The HZSM-5 commercial material, produced a profile similar to those of the ZSM-5 prepared from cogel materials. The band corresponding to the weaker acid sites (low temperature) was shifted to a slightly higher temperature for ZSM-5 18-1, suggesting that the average strength of the weaker acid sites was stronger for this material than for either ZSM-5 18-2 or the commercial HZSM-5. In addition to the low temperature band, the band at high temperature (~ 420 °C) was observed in all crystalline HZSM-5 materials. This high temperature band is related to the strong acid sites and the area under this band (curves 5 and 6) is much higher compared to the ones seen for the corresponding cogel materials. However, the area of the graphs of the cogel prepared ZSM-5 materials was greater than that of the commercial ZSM-5 material, suggesting that they contained a higher concentration of strong acid sites. Therefore, it was expected that so long as these acid sites were strong enough for acid catalysis these cogel prepared ZSM-5 materials would be catalytically active.

The TPD profiles produced by Al SAPO-5 materials exhibit only one clear band at low temperature, although the baseline increased slightly at the temperature of desorption for the strong acid sites. This marginal increase was more evident for Al SAPO-5 15-4 than 15-3, conversely the temperature of desorption for the weaker acid sites was higher for Al SAPO-5 15-3 than Al SAPO-5 15-4. It was therefore concluded that the Al SAPO-5 materials produced were unlikely to exhibit any acid catalytic activity. The TPD profiles of the standard materials AlPO-5 and SAPO-5 appeared identical to one another and comparable to the Al SAPO-5 materials described. The absence of any band corresponding to higher strength acid sites in these profiles suggested that these standard materials would also show restricted acid catalysed activity.

4.4.3 Acid Catalysis

The ability of the aluminosilicate materials produced to behave as acid catalysts was tested by the alkylation of benzene with ethanol (Chapter 2.3.2). The products from this reaction were formed in both liquid and gaseous phases, although all were detectable by GC. The products formed from the reaction of benzene with ethanol are ethyl benzene (EB), diethyl benzene (DEB) and triethyl benzene (TEB). The reaction of ethanol molecules alone produces diethyl ether (DEE), ethene, propene, butene, pentane and hexene. The results presented herein are after two hours of reaction. These catalysis reactions were repeated to ensure reproducibility and additionally catalysts were re-calcined to prove reusability.

Of all of the catalysts tested the ZSM-5 materials were the most catalytically active for this reaction (Figure 4.18). These results echo what was expected from the TPD experiments, whereby the ZSM-5 materials demonstrated a higher concentration of the strong acid sites required for acid catalysis. The catalytic activity of the ZSM-5 materials prepared from cogel precursors, and the commercial HZSM-5 were all comparable. The percentage benzene conversion for materials ZSM-5 18-1, ZSM-5 18-2 and commercial HZSM-5 were 20.2 %, 23.4 % and 23.8 % respectively, whilst the ethanol conversions were 63.8 %, 64.2 % and 56.3 % respectively. A higher concentration of ethanol was shown to have been converted than that of benzene, as ethanol was employed to produce a higher number of product types. Although the percentage benzene conversions are only slightly different for the cogel and commercial prepared ZSM-5 materials, the ethanol conversion are approximately 10 % greater for the cogel prepared ZSM-5 materials. Therefore, the active sites in the cogel prepared ZSM-5 materials are more active for ethanol than benzene conversion, when compared to the commercial ZSM-5 material. This differing reactivity was theorised to be due to the large benzene reagent being more hindered in locating the active acid sites in the cogel prepared materials than the commercial ZSM-5.

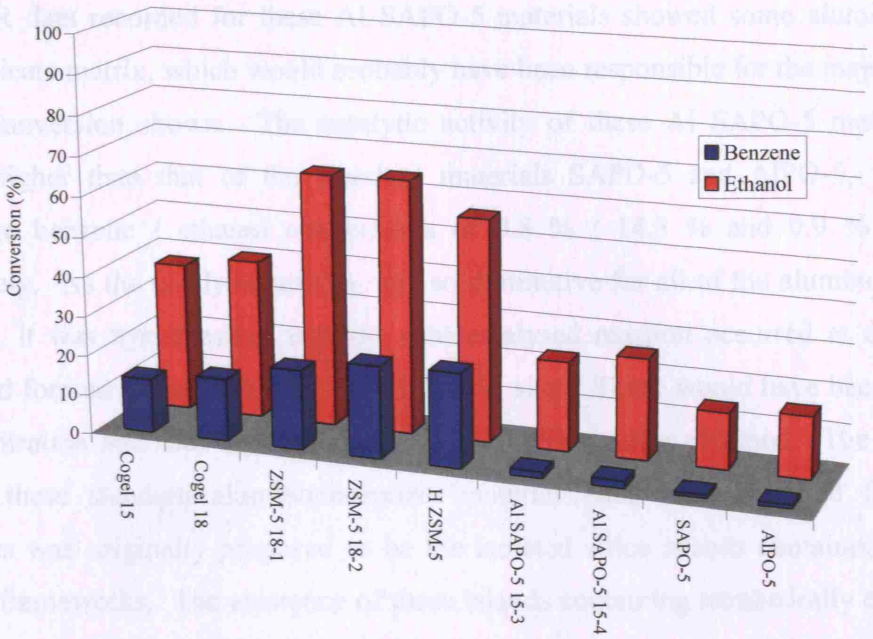

Figure 4.18: Benzene and ethanol conversion (%) after two hours reaction for all aluminium containing materials.

The cogel materials were less catalytically active than the ZSM-5 materials for both benzene and ethanol conversion. The benzene conversion for cogel 15 and cogel 18 was 13.7 % and 15.8 % respectively and 37.5 % and 40.2 % for ethanol conversion. This was in agreement with the results expected from TPD experiments, which showed the cogel materials had less strong acid sites which are required for this catalytic reaction. Additionally, previous NMR results obtained showed there to be a wider range of coordination geometries of the aluminium centres within the cogel materials, than those within the ZSM-5 materials. Thus, as fewer of the aluminium centres were tetrahedrally bound, there was a lower concentration of active aluminium sites in the cogel materials.

The Al SAPO-5 materials were the least catalytically active of the all the aluminosilicates examined. The percentage benzene conversion for Al SAPO-5 15-3 and Al SAPO-5 15-4 was 1.6 % and 1.8 %, whilst the ethanol conversion was 22.7 % and 25.6 % respectively. The pore dimensions of the AFI framework are larger than that of the MFI materials, hence a higher catalytic activity may have been expected. However, the TPD results of these materials showed little evidence of the strong acid sites required for active catalysis.

The NMR data recorded for these Al SAPO-5 materials showed some aluminium (IV) within silicate matrix, which would probably have been responsible for the majority of the reagent conversion shown. The catalytic activity of these Al SAPO-5 materials was slightly higher than that of the standard materials SAPO-5 and AlPO-5, which had percentage benzene / ethanol conversions of 0.8 % / 14.3 % and 0.9 % / 15.7 % respectively. As the catalytic activity was so diminutive for all of the aluminophosphate materials, it was hypothesised that the acid catalysed reaction occurred at defect sites which had formed strong Brønsted or Lewis acid sites. These would have been very low in concentration and thus barely evident on the TPD profiles obtained. The difference between these standard aluminophosphate materials and those prepared from cogel precursors was originally proposed to be the isolated silica islands contained in the Al SAPO-5 frameworks. The existence of these islands containing tetrahedrally coordinated aluminium centres, would explain the slightly higher activity of the Al SAPO-5 materials compared the standard materials. However, the islands would have to have existed in very low concentrations (if at all) or the TPD results would have shown a stronger response.

The ZSM-5 materials were the most selective catalysts for the formation of EB and for other ethyl benzene derivatives (Figure 4.19). The EB selectivity for ZSM-5 18-1 and ZSM-5 18-2 was 42.3 % and 45.0 % respectively. These figures are comparable to the commercial HZSM-5 material with an EB selectivity of 45.7 %. This high alkyl benzene selectivity was indicative of a well formed framework with active sites which are assessable to the bulky benzene reagent.

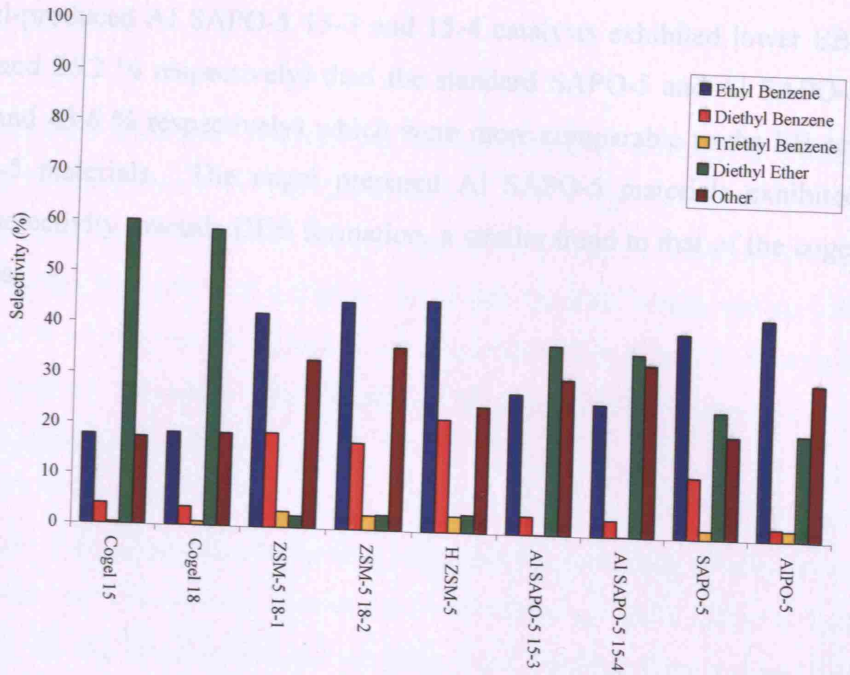

Figure 4.19: Product selectivity for aluminium containing catalysts after two hours reaction.

The selectivity of the cogel materials was different from that of the ZSM-5, the major product for the cogel catalysed reactions being DEE. Cogel 15 and cogel 18 had DEE selectivity of 60.2 % and 58.5 % respectively, compared to only 17.8 % and 18.4 % EB selectivity. In actuality over 75.0 % of the products created from the reactions the cogel materials catalysed contained no component from the benzene reagent. It hypothesised that this ethanol preference could be due to a combination of two explanations: **i)** that the benzene reagent was prevented from getting to the active sites, due to its larger size compared to ethanol. The cogel NMR data obtained suggested that the active tetrahedral sites degraded upon calcination, which could have blocked access to the active sites. Additionally, the amorphous nature of the cogel materials equates to there being no ordered channels or pores, which could again restrict access to the active sites. **ii)** the cogel materials have been shown to be comparatively hydrophilic and thus are more likely to react with polar materials than non-polar materials. Ethanol is more hydrophilic than benzene and hence a higher ethanol conversion could be expected.

The cogel-produced Al SAPO-5 15-3 and 15-4 catalysts exhibited lower EB selectivity (27.8 % and 26.2 % respectively) than the standard SAPO-5 and Al SAPO-5 materials (40.4 % and 43.6 % respectively) which were more comparable to the EB selectivity of the ZSM-5 materials. The cogel prepared Al SAPO-5 materials exhibited a higher catalytic selectivity towards DEE formation, a similar trend to that of the cogel materials themselves.

4.5 Conclusions

ZSM-5 materials have been synthesised via utilisation of aluminium containing cogel precursors, as have novel Al SAPO-5 materials. The cogel precursor which produced ZSM-5 materials with the most catalytic potential (tetrahedral aluminium centres and strong acid sites) was prepared using an aluminium chloride source and condensed under sonocation. Whilst the cogel utilised in the synthesis of the Al SAPO-5 samples with the greatest catalytic potential, was produced from aluminium isopropoxide and was condensed whilst being stirred.

Although the cogel materials themselves catalysed the formation of ethyl benzene, they were neither as catalytically active nor selective as their ZSM-5 counterparts. Additionally, as the NMR results demonstrated, the aluminium environments within the cogel materials degraded upon calcination, unlike the stable ZSM-5 materials. Thus it was concluded that for the aluminosilicate catalysts to be most catalytically efficient, the framework structure is required. The ZSM-5 materials prepared from a cogel precursor were analogous to the commercial ZSM-5, thus the cogel preparation route is a viable alternative way of preparing equivalent materials.

The Al SAPO-5 materials synthesised utilising the cogel precursors did not exhibit the desired catalytic activity. The catalytic activity demonstrated was lower than expected, the NMR results obtained showed some of the samples to contain the desired tetrahedrally coordinated aluminium centres required for catalysis. Feasibly there could be distinct areas of amorphous cogel material (containing the tetrahedral aluminium centres) within the framework which would reduce the catalytic ability of the material. Additionally, SEM images depicted some structures of spherical morphology within the Al SAPO-5 materials, thus it was concluded that two different types of materials were forming during the crystallisation process. Although further characterisation of these materials would be required to fully determine the properties of the Al SAPO-5 materials produced, it was surmised that they were different from the standard SAPO-5 and AlPO-5 materials. Despite evidence that at least some of the cogel precursor was encompassed within the

framework, the concentration of the aluminium centres within the cogel may not have been great enough to show any catalytic activity. Therefore, alteration of the aluminium concentration within the cogel material, or an increase in the cogel concentration used, would provide further information regarding the Al SAPO-5 materials.

4.6 References

(1) Auroux, A.; Monaci, R.; Rombi, E.; Solinas, V.; Sorrentino, A.; Santacesaria, E. *Thermochimica Acta* **2001**, *379*, 227.

(2) Triantafyllidis, K. S.; Nalbandian, L.; Trikalitis, P. N.; Ladavos, A. K.; Mavromoustakos, T.; Nicolaides, C. P. *Microporous and Mesoporous Materials* **2004**, *75*, 89.

(3) Argauer, R. J.; Landolt, G. R.; 3,702,886: US Patent, **1969**.

(4) Ovejero, G.; Grieken, R. V.; Uguina, M. A.; Serrano, D. P.; Melero, J. A. *Catalysis Letters* **1996**, *41*, 69.

(5) Armaroli, T.; Bevilacqua, M.; Trombetta, M.; Milella, F.; Gutierrez, A.; Ramirez, J.; Notari, B.; Willey, R. J.; Busca, G. *Applied Catalysis A: General* **2001**, *216*, 59.

(6) Tuel, A. *Zeolites* **1995**, *15*, 228.

(7) Louis, B.; Kiwi-Minsker, L. *Microporous and Mesoporous Materials* **2004**, *74*, 171.

(8) Treacy, M. M. J.; Higgins, J. B. *Collection of Simulated XRD Powder Patterns for Zeolites*; 4th ed.; Elsevier, **2001**.

(9) Sang, S.; Chang, F.; Liu, Z.; He, C.; He, Y.; Xu, L. *Catalysis Today* **2004**, *93*, 729.

(10) Freude, D.; Ernst, H.; Wolf, I. *Solid State Nuclear Magnetic Resonance* **1994**, *3*, 271.

(11) Peeters, M. P. J.; Kentgens, A. P. M. *Solid State Nuclear Magnetic Resonance* **1997**, *9*, 203.

(12) Okada, K.; Tomita, T.; Kameshima, Y.; Yasumori, A.; MacKenzie, K. J. D. *Journal of Colloid and Interface Science* **1999**, *219*, 195.

(13) Prakask, A. M.; Hartmann, M.; Zhu, Z.; Kevan, L. *Journal of Physical Chemistry B* **2000**, *104*, 1610.

(14) Tan, J.; Liu, Z.; Bao, X.; Liu, X.; Han, X.; He, C.; Zhai, R. *Microporous and Mesoporous Materials* **2002**, *53*, 97.

(15) Freude, D.; Ernst, H.; Hunger, M.; Pfeifer, H. *Chemical Physics Letters* **1988**, *143*, 477.

(16) Lonyi, F.; Valyon, J. *Microporous and Mesoporous Materials* **2001**, *47*, 293.

(17) Salker, A. V.; Weisweiler, W. *Applied Catalysis A: General* **2000**, *203*, 221.

(18) Inui, T.; Matsuba, K.; Tanaka, Y. *Catalysis Today* **1995**, *23*, 317.

Chapter 5: Ferrisilicates

5.0 Summary

The premise of utilising a cogel precursor was again employed, a range of Fe-MFI materials with different iron concentrations were synthesised. All the ferrisilicate materials produced were characterised using a suite of techniques including XRD, bulk density measurements, SEM and UV-vis. Those materials which indicated the most potential as acid catalysts were further characterised by ammonia absorption. The temperature programmed desorption of ammonia was employed to elucidate the nature of the acid sites within the materials. These TPD results demonstrated that the iron containing materials have stronger acid sites than their aluminium containing counterparts (Chapter 4).

A selection of the ferrisilicate materials were further utilised as catalysts for the alkylation of benzene with ethanol. As was expected the cogel materials were catalytically active, but less so than the analogous framework materials. The ferrisilicate materials with a higher concentration of iron heteroatoms demonstrated similar catalytic activity to comparable materials which contained a lower concentration of iron. This confirmed the preliminary characterisation results, that not all of the iron centres were bound in the desired coordination. Overall, the ferrisilicate materials demonstrated similar acid catalytic activity and selectivity to the aluminosilicate materials.

5.1 Introduction

In recent years iron containing microporous zeolites, particularly those of MFI framework type, have been recognised as highly efficient catalysts for a number of reactions: notably the selective oxidation of benzene to phenol and propane oxidative dehydrogenation to propylene.[1] However, within this research our interest in iron containing MFI materials (Fe-MFI) is related to their use as acid catalysts. Fe-MFI materials are analogous to TS-1 and ZSM-5, wherein the heteroatom is incorporated within an ordered silica framework. The main catalytically active iron sites within Fe-MFI, for redox catalysis, is thought to be related to extra framework iron species (iron oxide, binuclear iron sites and oxohydroxide aggregates) formed during ion exchange and solid-solid treatments.[2] Whilst the predominate catalytically active iron sites within Fe-MFI for acid catalysis is protonic Fe(OH)Si sites, analogous to those in ZSM-5.[3]

An ideal Fe-MFI catalyst would have tetrahedrally coordinated iron (III) within the MFI three dimensional framework. The pore openings (10-membered rings) of 5.3 x 5.6 Å for the sinusoidal channels and 5.1 x 5.5 Å for the straight channels ideally would only be minimally altered by the incorporation of iron onto the lattice sites (Figure 5.1).

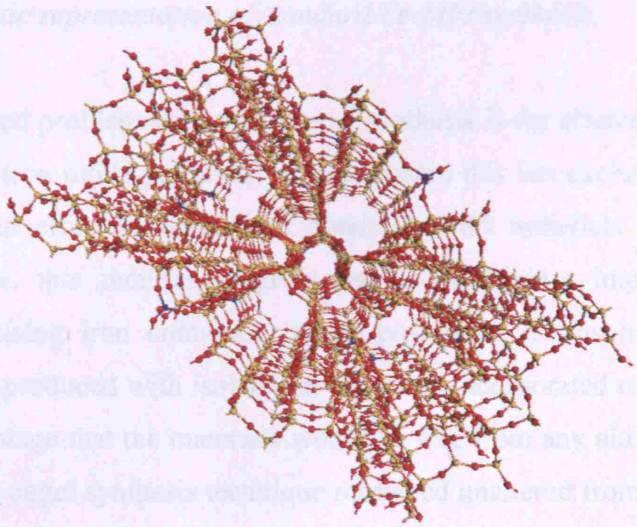

Figure 5.1: Fe-MFI framework. (Red: Oxygen, Yellow: Silicon, Blue: Iron).

These iron heteroatoms behave as active sites for acid catalysis, in a similar manner to ZSM-5 (Chapter 4). The main difference between these two materials is the size of the heteroatom, iron being far larger; the crystal radii for iron and aluminium being 0.72 Å and 0.53 Å respectively. For both Fe-MFI and ZSM-5 the heteroatom is inserted onto the lattice site of a silicon (crystal radius: 0.4 Å) atom. Thus the difference in size of the heteroatom can affect the framework dimensions, commonly leading to framework instability and expanded unit cell dimensions.[4]

Previously iron heteroatoms have been incorporated into tetrahedral framework sites, of MFI dimensions, during a crystallisation process (Figure 5.2).[5] The concentration of substituted iron has reportedly been low and it has been shown to be dependant upon the synthesis parameters (pH, crystallisation time, temperature, etc.) employed.

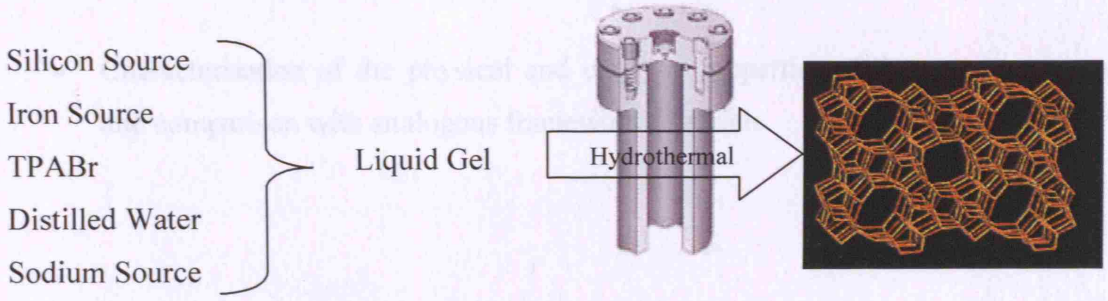

Figure 5.2: Schematic representation of standard Fe-MFI synthesis.

A commonly reported problem with this type of synthesis is the clustering of iron species into large, inactive iron oxide particles.[6] To overcome this ion exchange of ZSM-5 has been reported as an effective method to obtain Fe-MFI materials with isolated iron centres.[5] However, this recurrently gives rise to aluminium impurities within the materials. By utilising iron containing cogel precursors it was hoped that Fe-MFI materials would be produced with isolated iron centres incorporated on lattice sites, with the additional advantage that the materials would be free from any aluminium impurities. The principle of the cogel synthesis technique remained unaltered from that employed for titanium or aluminium containing materials. An amorphous cogel containing the desired

heteroatom in tetrahedral coordination geometry was crystallised to produce the desired framework structure with the heteroatom geometry unaltered.

The synthesis parameters altered for the cogel materials produced, were iron concentration and condensation method. The iron source was fixed (iron chloride hexahydrate) as iron isopropoxide (analogous to titanium and aluminium isopropoxide utilised in chapters 3 and 4) was prohibitively expensive (£ 38 g^{-1}, Sigma-Aldrich, price correct 02/2005).

5.2 Aims

- Synthesise Fe-MFI materials from cogel precursors and compare their physical and catalytic properties.

- Characterisation of the physical and catalytic properties of the cogel precursors and comparison with analogous framework materials.

5.3 Experimental

5.3.1 Cogel Synthesis

Further details regarding the cogel synthesis are given in chapter 2.1.1. The table below (Table 5.1) gives specific details of the iron cogel materials produced. All cogel materials produced used iron chloride hexahydrate as the iron source and TEAOH was used as the condensation reagent.

Table 5.1: Synthesis details of iron cogel materials.

Cogel Code	Si:Fe	Iron	Condensation Method
19	10	6.46 g 23.89 mmol	Stirring
20	80	0.81 g 3.00 mmol	Stirring
21	10	6.46 g 23.89 mmol	Sonocation
22	80	0.81 g 3.00 mmol	Sonocation

5.3.2 Fe-MFI Synthesis

Fe-MFI materials were synthesised from both the calcined and as-prepared cogel precursors as outlined in chapter 2.1.2 (Table 5.2).

Table 5.2: Fe-MFI materials synthesised.

Cogel Source	Fe-MFI Code	Calcined / As Prepared Cogel
19	19-1	As Prepared
	19-2	Calcined
20	20-1	As Prepared
	20-2	Calcined
21	21-1	As Prepared
	21-2	Calcined
22	22-1	As Prepared
	22-2	Calcined

5.3.3 Standard Materials

MFI containing no iron was synthesised from a blank cogel as outlined in chapter 2.1.4.

5.4 Results and Discussion

5.4.1 Ferrisilicate Materials

The colour of the as-prepared and calcined ferrisilicate materials was off-white, upon calcination those materials with Si:Fe 80 became white. However, those materials with Si:Fe 10 turned shades of red, the Fe-MFI materials became very light pink whilst the cogel materials turned a dark rust colour. The appearance of these red hues was indicative of iron (III) oxide, it was interesting that the Fe-MFI materials were a lighter shade (thus less iron (III) was present) which suggested that the MFI framework aided stabilisation of the iron heteroatom.

XRD Characterisation:

XRD patterns of the as-prepared and calcined cogel materials demonstrated them to be amorphous (Figure 5.3). Whilst the XRD patterns of the calcined Fe-MFI materials demonstrated them to be crystalline and of the expected framework type MFI. The XRD patterns of these crystalline materials were compared against MFI frameworks previously reported in the literature.[7]

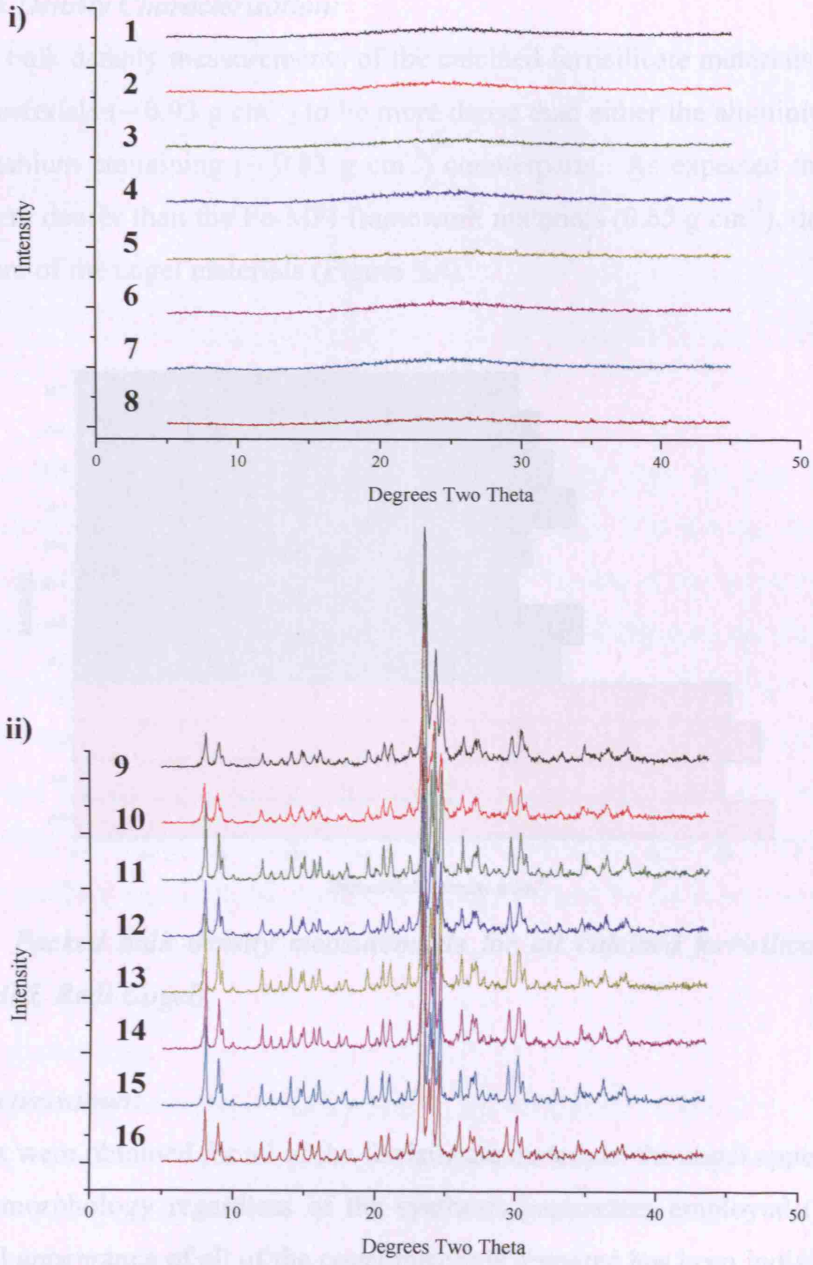

Figure 5.3: XRD patterns of ***i)*** *cogel (**1-8**),* ***ii)*** *calcined Fe-MFI (**9-16**) materials. (**1:** Cogel 19 as-prepared, **2:** Cogel 19 calcined, **3:** Cogel 20 as-prepared, **4:** Cogel 20 calcined, **5:** Cogel 21 as-prepared, **6:** Cogel 21 calcined, **7:** Cogel 22 as-prepared, **8:** Cogel 22 calcined) (**9:** Fe-MFI 19-1, **10:** Fe-MFI 19-2, **11:** Fe-MFI 20-1, **12:** Fe-MFI 20-2, **13:** Fe-MFI 21-1, **14:** Fe-MFI 21-2, **15:** Fe-MFI 22-1, **16:** Fe-MFI 22-2.)*

Packed Bulk Density Characterisation:

The packed bulk density measurements of the calcined ferrisilicate materials, showed the iron cogel materials (~ 0.93 g cm^{-3}) to be more dense than either the aluminium (~ 0.79 g cm^{-3}) or titanium containing (~ 0.83 g cm^{-3}) counterparts. As expected the iron cogel materials were denser than the Fe-MFI framework materials (0.65 g cm^{-3}), due to the less open structure of the cogel materials (Figure 5.4).

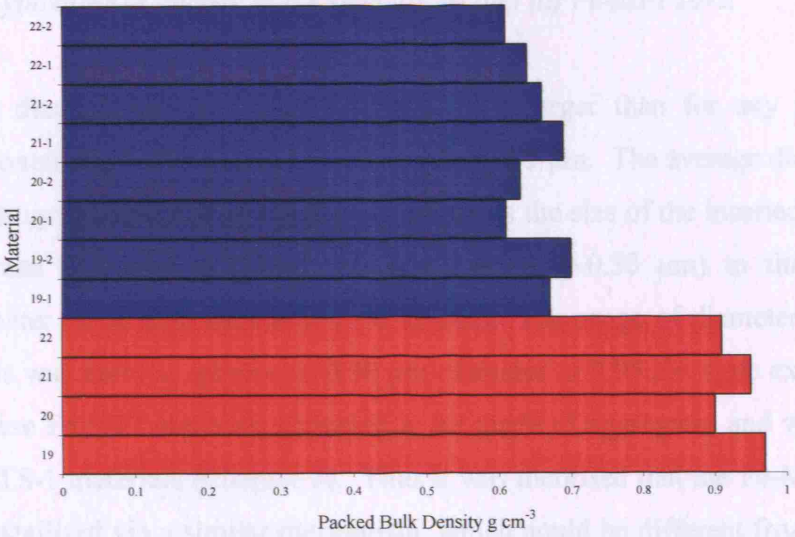

*Figure 5.4: Packed bulk density measurements for all calcined ferrisilicate materials (**Blue:** Fe-MFI, **Red:** Cogel).*

SEM Characterisation:

SEM images were obtained for all of the ferrisilicate materials, the cogel appeared to have no ordered morphology regardless of the synthesis parameters employed (Figure 5.5). The physical appearance of all of the cogel materials prepared has been indistinguishable, regardless of the moiety of the heteroatom encompassed within the amorphous silica matrix. The morphology of all the Fe-MFI materials synthesised was roughly spherical, the same for all of the other heteroatom inserted MFI framework materials produced. This was noteworthy as various other morphologies are common for the MFI framework, thus confirming previously stated conclusions that the cogel precursor must, a least partly, direct the crystal morphology.

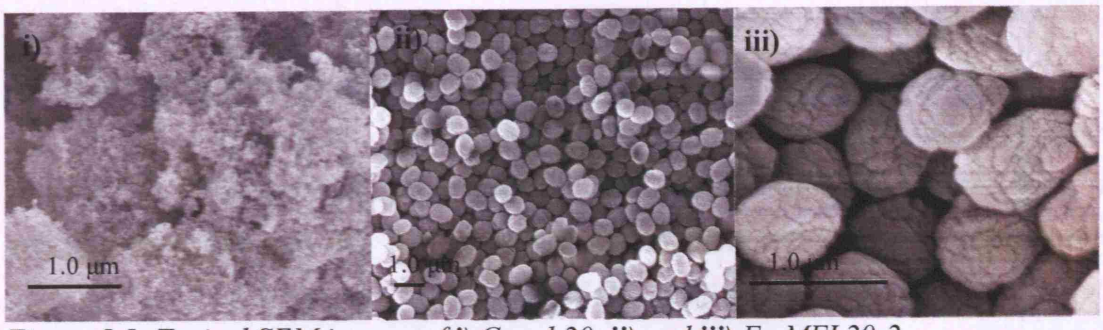

Figure 5.5: Typical SEM images of ***i)*** *Cogel 20,* ***ii)*** *and* ***iii)*** *Fe-MFI 20-2.*

The average diameter of the Fe-MFI crystals was larger than for any of the other heteroatom containing MFI materials synthesised ~ 0.75 μm. The average diameter of the MFI materials synthesised follows the same pattern as the size of the inserted heteroatom, increasing from aluminium (ZSM-5 average diameter ~0.30 μm) to titanium (TS-1 average diameter ~0.50 μm) then iron (~ 0.75 μm). The range of diameters for the Fe-MFI materials was narrow, spheres of 0.50 μm diameter to 0.95 μm were exhibited. The surface of these Fe-MFI materials appeared to be made of aggregates and was similar to the reported TS-1 materials (Chapter 3). Thus it was theorised that the Fe-MFI and TS-1 materials crystallised via a similar mechanism, which could be different from the ZSM-5 materials.

UV-vis Characterisation:

UV-vis spectroscopy was employed to assess the nature and distribution of iron (III) species in the calcined ferrisilicate materials prepared. The typical *d-d* transitions of iron (III) (which are expected between 350 to 550 nm), are symmetry and spin forbidden, hence they are not seen on the spectra collected. Typically bands between 200 to 300 nm are assigned to isolated iron centres, whilst lower energy bands between 300 to 450 nm are attributed to small oligonuclear iron species $(FeO)_n$. Tetrahedrally bound iron heteroatoms within a silicate matrix produce signals which are observed at 220 and 240 nm. Whilst octahedrally bound iron species have broad signal regions of 185 to 235 nm and 240 to 305 nm. Resolution of these bands can be problematic as the increased size of

the iron species commonly results in deviation from regular symmetry and wide overlap of the signals occurs.[6]

The UV-vis spectra of the calcined and as-prepared cogel materials were comparable (Figure 5.6). The calcined spectra had almost identical band positions, yet there was greater overlap of the bands. This showed that the environment of the iron species altered upon calcination, to exhibit a broader range of coordination geometries.

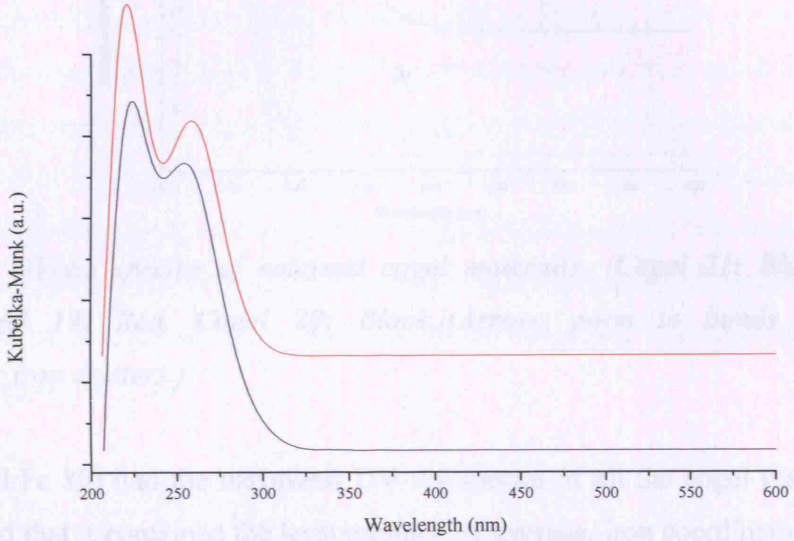

Figure 5.6: UV-vis spectra of Cogel 20 (Si:Fe 80) , as-prepared (red) and calcined (black).

The UV-vis spectra of the calcined cogel materials commonly exhibit *at least* one band below 300 nm relating to isolated iron centres within the amorphous cogel matrix (Figure 5.7). Those cogel materials with Si:Fe 80 had an additional band which trailed slightly after 300 nm, which suggested that most of these iron environments were isolated centres. Whilst the maxima of the second band, exhibited by the cogel materials with Si:Fe 10, was at ~ 300 nm, which suggested that they contained higher concentration of oligonuclear iron heteroatoms than for the Si:Fe 80 ratio materials. Additionally, the Si:Fe 10 cogel materials exhibited a third UV-vis at ~ 350 nm (arrows, Figure 5.8), relating to solely multinuclear iron clusters, confirming that for these materials not all of the iron centres were isolated within the silica matrix.

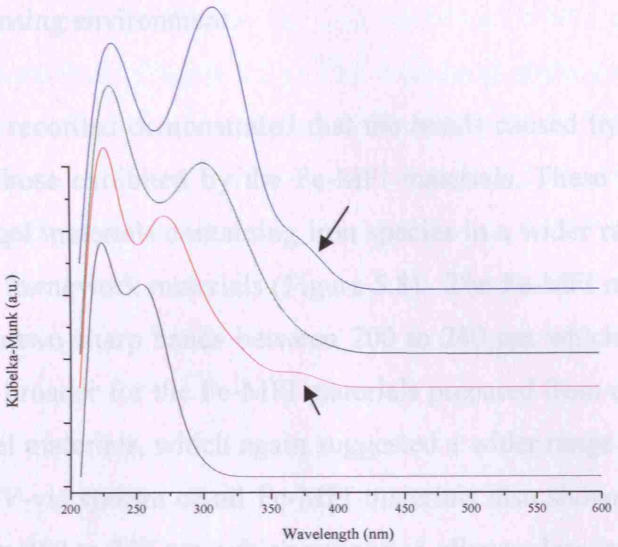

*Figure 5.7: UV-vis spectra of calcined cogel materials. (**Cogel 21:** Blue, **Cogel 22:** Green, **Cogel 19:** Red, **Cogel 20:** Black.)(Arrows point to bands arising from oligonuclear iron clusters.)*

Cogel 20 (Si:Fe 80) had the narrowest UV-vis spectra of all the cogel materials, which demonstrated that it contained the least number, of average, iron coordination geometries. Whilst cogel 22 (Si:Fe 80) also narrower than cogel 21 (Si:Fe 10), which suggested that there was a maximum concentration of iron which could be successfully incorporated within the cogel matrix and that the maximum was somewhere between the two concentrations produced. The cogel materials condensed whilst being stirred produced UV-vis spectra which were narrower than those produced from the cogel materials which were subjected to sonocation during condensation. Thus it was concluded that condensation under sonocation lead to a greater number of iron coordination environments than under stirring conditions. This contradictory to the titanium containing cogel materials (Chapter 3), it was hypothesised that the heavier (than silicon or titanium) iron heteroatoms had sunk during condensation of the cogel under sonocation and hence a wider range of oligonuclear clusters were produced. Conversely, when the cogel materials were stirred during condensation, the stirring motion originated at the bottom of

the reaction vessel, thus preventing the deposition of the heavier iron species at the bottom of the condensing environment.

The UV-vis spectra recorded demonstrated that the bands caused by the cogel materials were broader than those exhibited by the Fe-MFI materials. These broader bands were indicative of the cogel materials containing iron species in a wider range of coordination geometries than the framework materials (Figure 5.8). The Fe-MFI materials gave rise to UV-vis spectra with two sharp bands between 200 to 240 nm which overlapped. These bands were slightly broader for the Fe-MFI materials prepared from calcined (as opposed to as-prepared) cogel materials, which again suggested a wider range of iron coordination geometries. The UV-vis spectra of all Fe-MFI materials also showed some less intense broad bands between 250 to 350 nm, which suggested oligonuclear iron clusters were also present in these materials. These less intense bands appeared more resolved when the material was calcined, which suggested that organic materials had been interacting with these iron centres.

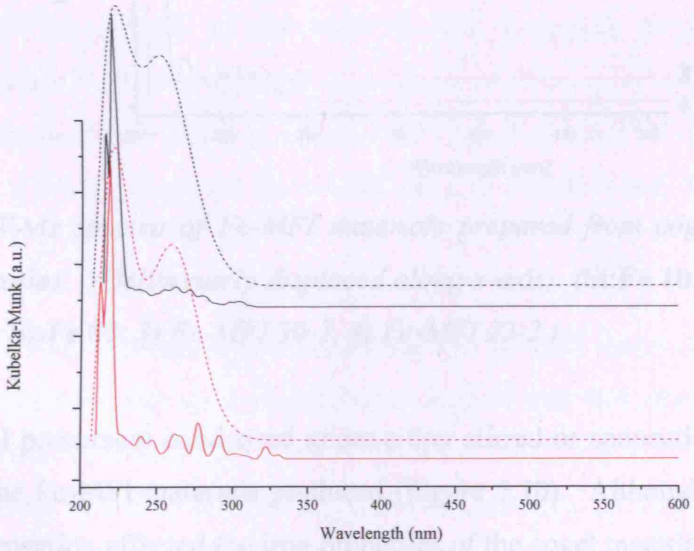

*Figure 5.8: UV-vis spectra of cogel 20 (**dashed line**, **black:** calcined, **red:** as-prepared) and calcined Fe-MFI 20-1 (**solid line**, **black**) and Fe-MFI 20-2 (**solid line**, **red**).*

The UV-vis spectra of the Fe-MFI materials containing Si:Fe 10 exhibited a greater range of iron coordination environments than the corresponding Fe-MFI materials with lower (Si:Fe 80) iron concentration (Figure 5.9). These findings mimicked those reported for the iron cogel precursor materials, thus again it was hypothesised that there was a maximum concentration of iron which could be coordinated within the framework and remain isolated from other such centres.

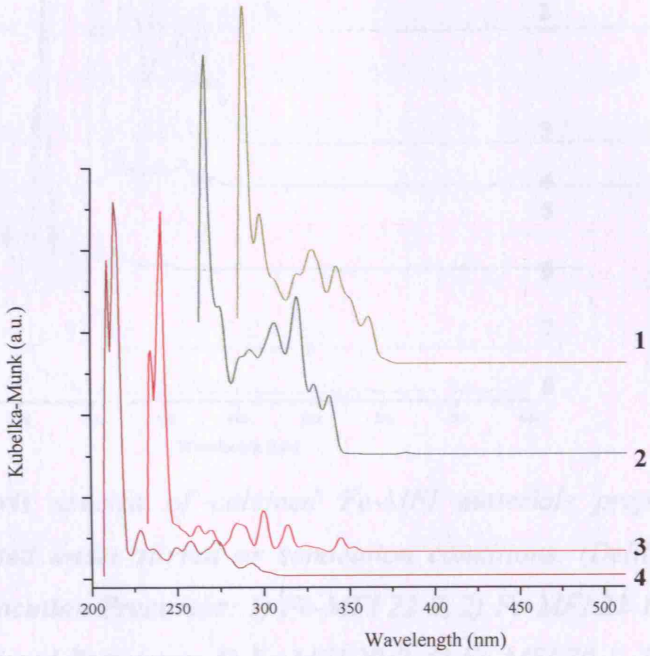

Figure 5.9: UV-vis spectra of Fe-MFI materials prepared from cogel materials with different Si:Fe ratios. (Deliberately displaced along x-axis). ***(Si:Fe 10**: **1)** Fe-MFI 19-2, **2)** Fe-MFI 21-2,* **Si:Fe 80**: ***3)** Fe-MFI 20-2, **4)** Fe-MFI 22-2.)*

The use of cogel precursors condensed under either stirred or sonocation conditions had little effect on the Fe-MFI materials produced (Figure 5.10). Although alteration of the method of condensation affected the iron properties of the cogel materials themselves this appeared not to have as greater effect upon the crystalline Fe-MFI materials produced.

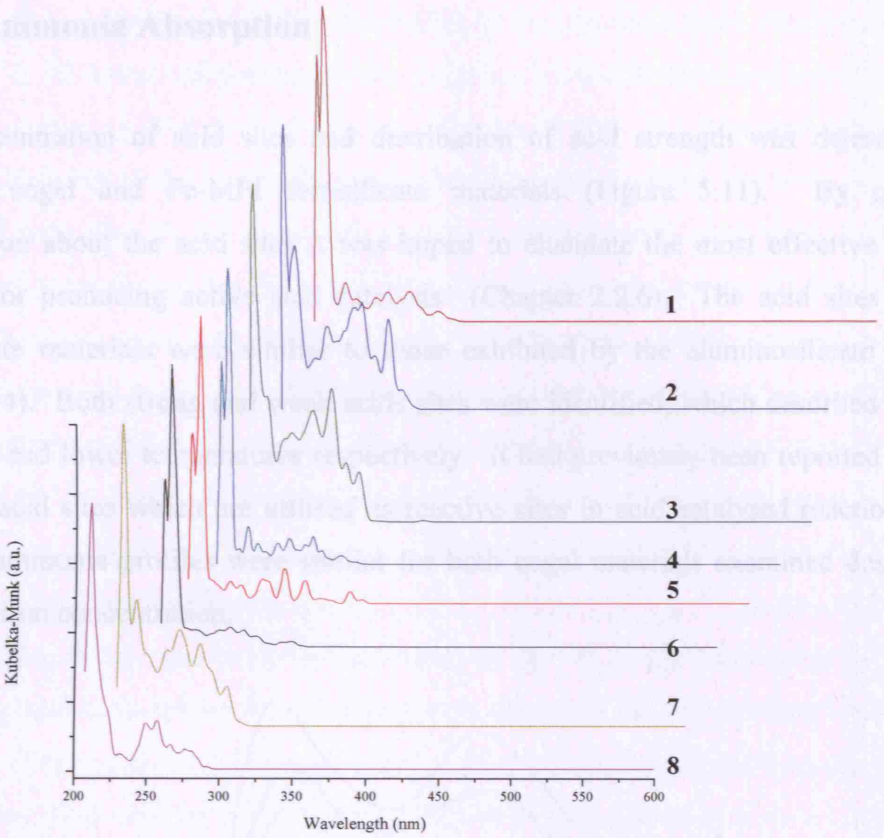

Figure 5.10: UV-vis spectra of calcined Fe-MFI materials prepared from cogel precursors condensed under stirred or sonocation conditions. (Deliberately displaced along x-axis). ***(Sonocation Precursor**: 1) Fe-MFI 22-2, **2)** Fe-MFI 22-1, **3)** Fe-MFI 21-2, **4)** Fe-MFI 21-1, **Stirred Precursor**: **5)** Fe-MFI 20-2, **6)** Fe-MFI 20-1, **7)** Fe-MFI 19-2, **8)** Fe-MFI 19-1.)*

From the UV-vis data obtained it was concluded that Fe-MFI materials with lower iron concentrations exhibited the most isolated iron centres and that alteration of the iron concentration had the greatest effect on the heteroatom environment within the crystalline materials. However, accurate theories regarding the potential catalytic activity of these materials cannot be made, as it is impossible to distinguish between tetrahedral and octahedral iron centres. Thus, whilst the Fe-MFI materials with lower iron concentrations may have more isolated iron centres, they may still have a small concentration of non-catalytically active centres.

5.4.2 Ammonia Absorption

The concentration of acid sites and distribution of acid strength was determined for calcined cogel and Fe-MFI ferrisilicate materials (Figure 5.11). By examining information about the acid sites it was hoped to elucidate the most effective synthesis method for producing active acid catalysts (Chapter 2.2.6). The acid sites on these ferrisilicate materials were similar to those exhibited by the aluminosilicate materials (Chapter 4). Both strong and weak acids sites were identified, which desorbed ammonia at higher and lower temperatures respectively. It had previously been reported to be the stronger acid sites which are utilised as reactive sites in acid catalysed reactions.[8] The TPD of ammonia profiles were similar for both cogel materials examined despite their differing iron concentration.

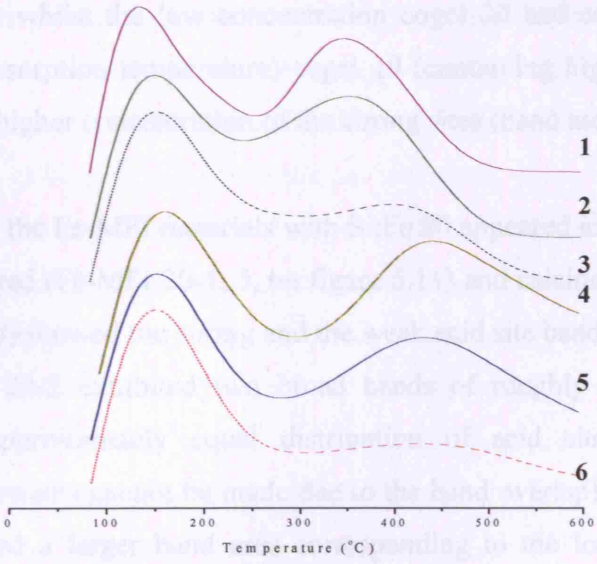

*Figure 5.11: TPD of ammonia for ferrisilicate materials. **(1)** Fe-MFI 19-2, **2)** Fe-MFI 19-1, **3)** Fe Cogel 19, **4)** Fe-MFI 20-2, **5)** Fe-MFI 20-1, **6)** Fe Cogel 20.)*

All of the TPD spectra produced exhibited two bands, the band at a low temperature relates to the concentration of weak acid sites and the band at high temperature relates strong acid sites on the catalyst.

For both of the cogel materials the desorption of the ammonia from the strong acid sites occurred at different temperatures (the position of the high temperature band is at different positions) (Figure 5.11 above). The cogel with low iron concentration (iron cogel 20, 6 in figure 5.11) desorbed ammonia from these strong acid sites at ~ 450 °C, compared with 400 °C for the cogel material containing high iron concentration (iron cogel 19, 3 in figure 5.11). The strong acid sites on cogel 20 were therefore comparatively stronger than those on cogel 19. Therefore, (despite cogel 19 containing more iron centres), it was hypothesised that the active iron centres within cogel 20 would be more effective for acid catalysis. However, the strong acid site band appeared smaller in amplitude for cogel 20 than for cogel 19, which suggested a comparatively lower concentration of these strong acid sites. Yet due to the overlap between the strong and weak acid site types a definite evaluation of the concentration of each type of acid site is not possible. Thus, prediction of the catalytic ability of these precursor materials is further complicated; whilst the low concentration cogel 20 had comparatively stronger acid sites (higher desorption temperature) cogel 19 (containing high iron concentration) had demonstrated a higher concentration of the strong sites (band area).

The TPD profiles of the Fe-MFI materials with Si:Fe 80 appeared identical, both (Fe-MFI made from as-prepared (Fe-MFI 20-1, 5, on figure 5.11) and calcined (Fe-MFI 20-2, 4 on figure 5.11) cogel 20) showed the strong and the weak acid site bands expected. The TPD spectra of Fe-MFI 20-2 exhibited two broad bands of roughly uniform area, which demonstrated an approximately equal distribution of acid site strength (although quantitative measurements cannot be made due to the band overlap). The TPD profile of Fe-MFI 20-1 showed a larger band area corresponding to the low strength acid sites (compared to the higher temperature band), which suggested that the catalyst had a comparatively greater weak acid site concentration.

The Fe-MFI materials with higher iron concentration (Si:Fe 10) (Fe-MFI 19-1, 2 on figure 5.11 and Fe-MFI 19-2, 1 on figure 5.11) exhibited similar TPD profiles, with two overlapping bands which related to the weak and strong acid sites. The overlap of these

bands appeared more prominent for these Fe-MFI materials with higher iron concentration than for the lower iron concentration framework materials.

The low temperature band appeared to be in approximately the same position for all the Fe-MFI and cogel materials (~ 150 °C), whilst the temperature at which the strong acid sites desorbed ammonia, appeared dependant upon the iron concentration and nature of the material studied. Those ferrisilicate materials with low iron concentrations (Si:Fe 80) desorbed ammonia from the strong acid sites at higher temperature than those ferrisilicate materials with a higher iron concentration. The strong acid site band position was the same (~ 450 °C) for both the Si:Fe 80, cogel and Fe-MFI materials, thus both these materials contain comparable strong acid sites which are required for catalysis. However, the high iron concentration materials desorbed ammonia from the strong acid sites at different temperature for the Fe-MFI (~ 350 °C) and cogel (~ 400 °C) materials. This temperature difference suggests that the iron environments within these materials are different to the materials with lower iron concentration. The UV-vis results have previously shown that the cogel materials contain iron in oligomeric environments, whilst the iron heteroatoms in Fe-MFI materials appeared isolated. Thus, the higher temperature of desorption of ammonia from the iron species could be an effect of this iron clustering with the cogel matrix. Although the iron centres within the Fe-MFI materials had been demonstrated to be isolated, information which related to their precise coordination geometry and framework position has not been established. Thus it is feasible that the lower temperature of desorption from these acid sites was related to the iron centres having a non-ideal bonding environment.

The TPD of ammonia from the Si:Fe 80 ferrisilicate materials occurred from the weak and strong acid sites at ~ 150 °C and ~ 450 °C respectively. The ammonia desorption temperatures were different from those reported for comparable *aluminosilicate* materials of ~ 170 °C and ~ 420 °C for the weak and strong acid sites.[8] Thus the weak acid sites are weaker for the ferrisilicate, rather than aluminosilicate materials, whilst conversely the strong acid sites (those used for acid catalysis) are stronger for the ferrisilicates materials, than for aluminosilicate materials.

It has been reported that isomorphous substitution within a silicate matrix, of silicon by iron, generates an acid site weaker than that by aluminium.[9,3,2] Many researchers have accepted the acid site strength sequence B < Fe < Ga < Al in corresponding metallosilicates, because this order agreed well with the catalytic reactivity observed for the typical acid catalysed reactions. However, there is some controversy with other research groups publishing conflicting acid strength sequences. Katada *et al.* report that at low iron concentrations, isomorphous substitution of iron into the silicate framework results in the strong acid site being stronger than that of the comparable aluminium silicate.[5] The TPD results reported herein are consistent with the conclusions drawn by Katada and co-workers, hence it was concluded that the ferrisilicate materials exhibited more potential acid catalytic activity then analogous aluminosilicate materials.

5.4.3 Acid Catalysis

The catalytic ability of the ferrisilicate materials synthesised was investigated by the alkylation of benzene with ethanol (Chapter 2.3.2). Not all of the ferrisilicate materials produced were tested, only those materials which had shown the greatest catalytic potential. Both the liquid and gas phase products synthesised during the catalytic reaction were quantitatively characterised by gas chromatography. The catalytic reactions were performed for two hours, after which the catalysts were collected, re-calcined and reused to confirm their reusability. The products formed from the reaction of benzene with ethanol are ethyl benzene (EB), diethyl benzene (DEB) and triethyl benzene (TEB). The reaction of ethanol molecules alone produces diethyl ether (DEE), ethene, propene, butene, hexene and pentene. A higher concentration of ethanol was shown to have been converted than that of benzene for all the materials tested, this was expected as ethanol is utilised to produce a higher number of products than benzene.

The catalytic activity was different for the iron cogel materials of different iron concentrations (Figure 5.12). The percentage conversion for cogel 19 (Si:Fe 10) was 11.6 % and 34.1 % for benzene and ethanol respectively, compared to 19.8 % and 58.5 % for

cogel 20 (Si:Fe 80). Thus, the cogel material with the higher iron concentration was least catalytically active. The TPD results predicted this trend, as cogel 20 (Si:Fe 80) exhibited stronger catalytically active acid sites than cogel 19 (Si:Fe 10).

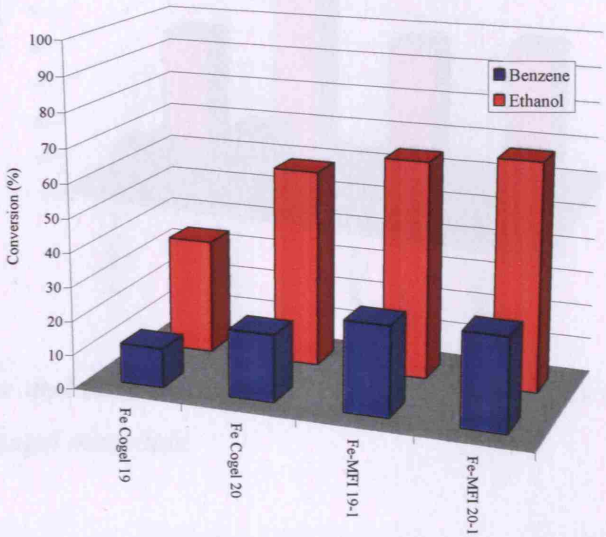

Figure 5.12: Benzene and ethanol conversion (%) after two hours reaction for calcined ferrisilicate materials.

The TPD results also predicted the ferrisilicate materials with isolated iron centres would be more active acid catalysts than corresponding aluminosilicate materials. A comparison of the cogel activity results agreed with these predictions; iron cogel 20 which contained the highest proportion of isolated iron centres (UV-vis results) was indeed more catalytically active than the aluminium cogel materials (Figure 5.13). The most active aluminium cogel had percentage benzene and ethanol conversions of 15.8 % and 40.2 % respectively (compared with 19.8 % and 58.5 % for iron cogel 20). However, iron cogel 19, which had fewer isolated iron centres, was less active than the aluminium cogel materials.

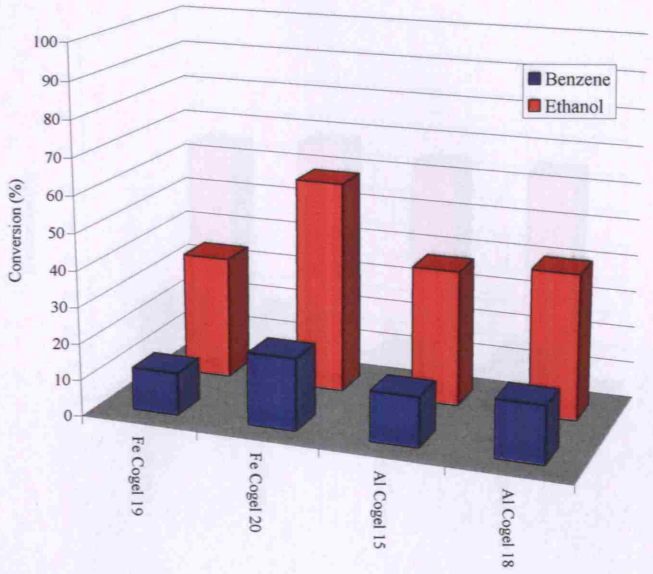

Figure 5.13: Benzene and ethanol conversion (%) after two hours reaction for calcined iron and aluminium cogel materials.

Both the Fe-MFI framework materials employed as catalysts demonstrated very similar activity (Figure 5.12, above) despite Fe-MFI 19-1 having a higher iron concentration (Si:Fe 10) than Fe-MFI 20-1 (Si:Fe 80). Fe-MFI 19-1 and 20-1 exhibited percentage catalytic conversions for benzene of 26.5 % and 27.5 % and for ethanol of 64.4 % and 67.2 % respectively. Thus alteration of the iron concentration encompassed within the Fe-MFI materials had no appreciable effect upon catalytic activity. The activity of the Fe-MFI materials was higher than that of the cogel materials, as was predicted from both the UV-vis and TPD results.

Thus, the ferrisilicate materials are comparable to the aluminosilicate materials reported in chapter 4, which showed the three dimensional framework to be required for the most active catalysis. Both of the Fe-MFI catalysts tested were more active than the analogous aluminium containing ZSM-5 materials (Figure 5.14). ZSM-5 66h, the most reactive ZSM-5 material exhibited percentage benzene and ethanol conversions of 23.4 % and 64.2 % respectively (compared with 27.5 % and 67.2 % for Fe-MFI 20-1). These results mirror the cogel activity and also the results predicted from TPD measurements.

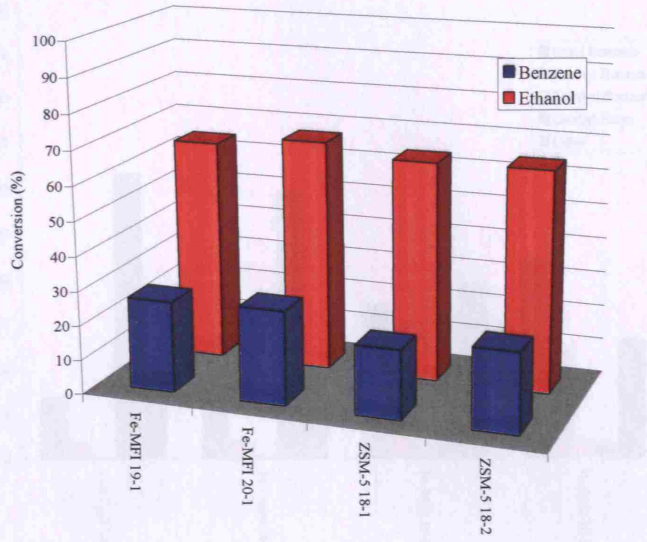

Figure 5.14: Benzene and ethanol conversion (%) after two hours reaction for Fe-MFI and ZSM-5 materials.

The product selectivity of the iron cogel materials were similar regardless of the iron concentration, the predominate product formed being DEE (Figure 5.15). The selectivity of EB was 13.7 % and 18.2 % for cogel materials 19 and 20, the total selectivity for the alkyl benzene products was 17.3 % and 22.5 % respectively. Thus the cogel catalysts were three times more effective in directing the formation of products which contained no benzene component (than any product which required the benzene reagent). Thus it was hypothesised that the amorphous nature of the silica matrix sterically hindered the interaction of benzene with the active iron sites.

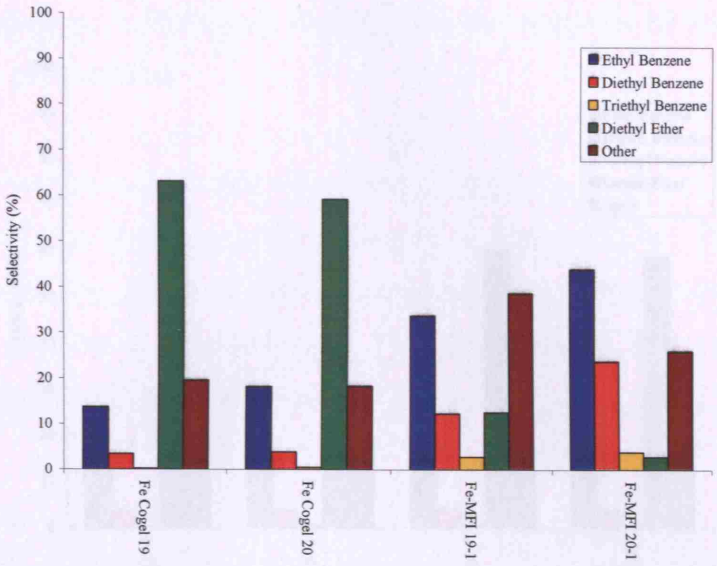

Figure 5.15: Product selectivity for ferrisilicate catalysts after two hours reaction.

The product selectivity of the iron containing cogel catalysts was very similar to those reported for the aluminium containing cogel materials (as reported in chapter 4)(Figure 5.16). The high DEE selectivity of the aluminium cogel materials was similarly attributed to the amorphous nature of the cogel, which hindered the benzene reagent in getting to the catalytically active sites. Additionally, the aluminium cogel structure was shown to degrade upon calcination which may have exacerbated steric constraints.

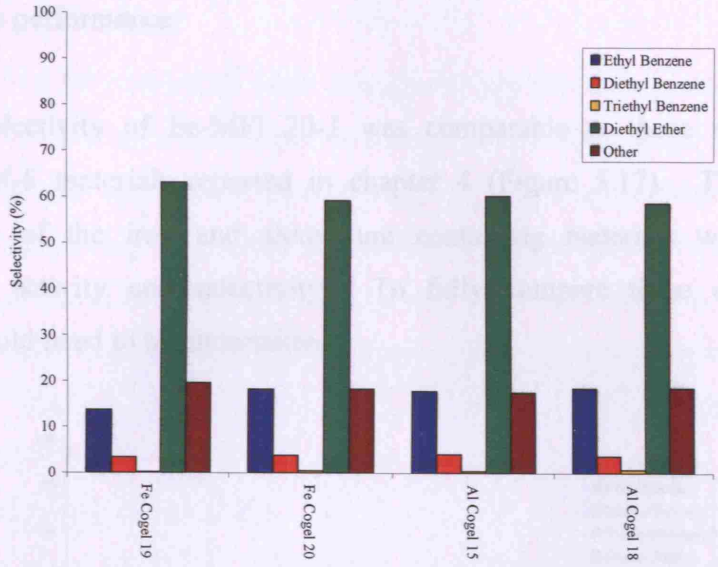

Figure 5.16: Product selectivity for iron and aluminium cogel catalysts after two hours reaction.

The product selectivity differed when Fe-MFI 19-1 and Fe-MFI 20-1 were employed as catalysts (Figure 5.15 above). Fe-MFI 19-1 (Si:Fe 10) produced more products without a benzene component than Fe-MFI 20-1 (51.2 % to 28.7 %). The predominate product formed from the reaction catalysed by Fe-MFI 19-1 was other (ethene, propene, butene, hexene and pentene), for Fe-MFI 20-1 it was EB. Thus the iron environments within these two Fe-MFI materials must be different for such variations in product distribution to occur. The smaller proportion of benzene containing products formed by the reaction catalysed with Fe-MFI 19-1, suggests that the bulky benzene reagent was hindered getting to or being released from the acid sites. Thus whilst Fe-MFI 19-1 contained a higher iron concentration either not all of the iron centres were accessible or they were in a catalytically unreactive form.

The product selectivity of the cogel and Fe-MFI materials varied, the Fe-MFI materials being more selective towards the desired EB product. This was theorised to be due to the ordered framework of the Fe-MFI materials allowing greater access within the material to

the active iron centres. This again demonstrates the necessity of the framework for optimal catalytic performance.

The product selectivity of Fe-MFI 20-1 was comparable to those reported for the aluminium ZSM-5 materials reported in chapter 4 (Figure 5.17). Thus, overall the catalytic ability of the iron and aluminium containing materials was very similar regarding both activity and selectivity. To fully compare these catalysts further experiments would need to be undertaken.

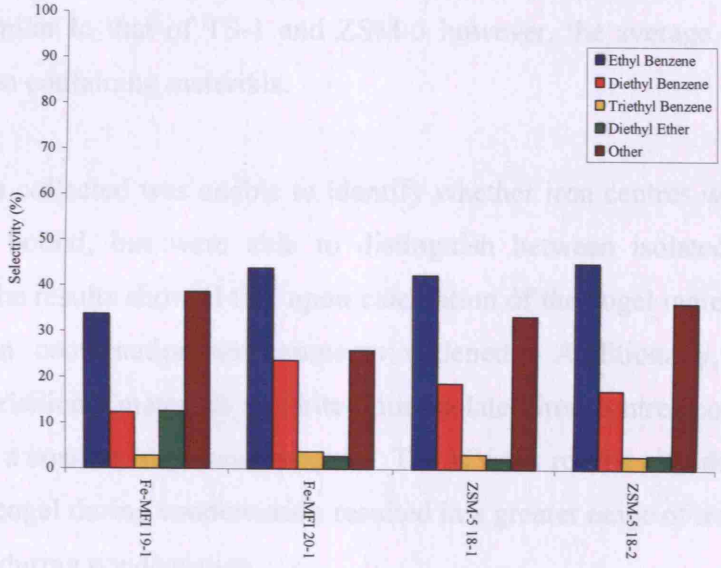

Figure 5.17: Product selectivity for Fe-MFI and ZSM-5 catalysts after two hours reaction.

Overall the most effective iron containing catalyst produced was Fe-MFI 20-1, which was prepared from an as-prepared cogel (which was stirred whilst condensed) of Si:Fe 80. Once again the cogel materials demonstrated difference catalytic abilities to the framework materials, highlighting their different properties. However, the three dimensional framework was demonstrated be essential for optimised catalytic ability.

5.5 Conclusions

The synthesis of Fe-MFI materials from amorphous iron containing cogel materials was reported herein. XRD results confirmed the structure of the framework materials formed, as well as stability after calcination. Bulk density measurements outlined the similarity of the iron containing materials with the aluminium and titanium materials already reported, wherein the cogel materials were denser than the framework materials. SEM images demonstrated similar comparisons, the amorphous iron cogel appeared identical to its aluminium and titanium counterparts. The framework Fe-MFI exhibited spherical morphology, similar to that of TS-1 and ZSM-5 however, the average crystal size was larger for the iron containing materials.

The UV-vis data collected was unable to identify whether iron centres were tetrahedrally or octahedrally bound, but were able to distinguish between isolated and bulk iron coordination. The results showed that upon calcination of the cogel materials the number of different iron coordination environments widened. Additionally, the more iron concentrated ferrisilicate materials exhibited non-isolated iron centres compared to those materials which a smaller iron concentration. The UV-vis results also demonstrated that sonocation of a cogel during condensation resulted in a greater range of iron environments than sonocation during condensation.

The TPD of ammonia occurred at two temperatures for all ferrisilicate materials. A low temperature corresponding to weak acid sites and a high temperature relating to strong acid sites (which have been shown to be utilised during acid catalysis). The TPD results of the cogel materials showed the band relating to the weak sites was more predominate than for the strong acid sites. The Fe-MFI framework materials also desorbed ammonia at two temperatures however as the ratio of iron within the material was decreased the temperature of desorption from the stronger acid sites increased. Thus the Fe-MFI materials with Si:Fe 80 has the strongest acid sites of all of the materials prepared and hence the greatest catalytic potential.

The acid catalysed reaction of benzene with ethanol was employing both the cogel and Fe-MFI materials as catalysts. The Fe-MFI materials were the more effective catalysts than the cogel materials, and the catalytic activity and product selectivity was comparable to those reported for the aluminium containing materials.

5.6 References

(1) Kumar, M. S.; Perez-Ramirez, J.; Debbagh, M. N.; Smarsly, B.; Bentrup, U.; Bruckner, A. *Applied Catalysis B: Environment* **2006**, *62*, 244.

(2) Urquieta-Gonzalez, E. A.; Martins, L.; Peguin, R. P. S.; Batista, M. S. *Materials Research* **2002**, *5*, 321.

(3) Kresnawahjuesa, O.; Kuhl, G. H.; Gorte, R. J.; Quierini, C. A. *Journal of Catalysis* **2002**, *210*, 106.

(4) Fejes, P.; Lazar, K.; Marsi, I.; Rockenbauer, A.; Korecz, L.; Nagy, J. B.; Perathoner, S.; Centi, G. *Applied Catalysis A: General* **2003**, *252*, 75.

(5) Katada, N.; Miyamoto, T.; Begum, H. A.; Naito, N.; Niwa, M. *Journal of Physical Chemistry B* **2000**, *104*, 5511.

(6) Perez-Ramirez, J.; Kapteijin, F.; Bruckner, A. *Journal of Catalysis* **2003**, *218*, 234.

(7) Treacy, M. M. J.; Higgins, J. B. *Collection of Simulated XRD Powder Patterns for Zeolites*; 4th ed.; Elsevier, **2001**.

(8) Yeom, Y. H.; Nam, S. S.; Kim, S. B.; Lee, K. W. *Bulletin of the Korean Chemical Society* **1999**, *20*, 781.

(9) Mohamed, M. M.; Ali, I. O.; Eissa, N. A. *Microporous and Mesoporous Materials* **2005**, *87*, 93.

Chapter 6: Bimetallosilicate Materials

6.0 Summary

Amorphous and crystalline metallosilicate materials containing two different metal heteroatoms were synthesised for use as catalysts. These materials, containing both oxidative and acidic centres, were capable of simultaneously catalysing both types of reaction. Three different approaches were employed to produce the cogel precursors used to synthesise the framework materials. These approaches were the mixing of powders, a one solution method and a two solution method. The materials formed contained two of the following heteroatoms: titanium, aluminium and iron. All of the metallosilicate materials produced were characterised using a range of techniques including XRD, packed bulk density measurements, SEM, UV-vis, IR and ^{27}Al NMR.

From the characterisation results collected, the metallosilicate materials synthesised using the two solution method were deemed to exhibit the most catalytic potential. These materials were thus further characterised by TPD of ammonia as well as being employed as catalysts.

The alkylation of benzene with ethanol was employed to evaluate the catalytic ability of the iron and aluminium centres incorporated within the metallosilicate materials. Both the iron and aluminium containing materials were shown to be active and selective catalysts. Similarly, the titanium centres were demonstrated to be both catalytically reactive and selective for the hydroxylation of phenol.

The formation of adipic acid (AA) reaction was employed to simultaneously evaluate both the acidic and oxidative catalytic ability of the metallosilicate materials. As predicted the cogel materials were less selective and marginally less catalytically active than the analogous framework materials. The framework materials demonstrated effective catalytic activity and selectivity, the TiFe materials being the most selective towards AA formation.

6.1 Introduction

In previous chapters it has been shown that by altering the chemical identity of the heteroatom inserted within the silicate MFI framework, the nature of the framework material alters. By incorporating a heteroatom such as titanium (Chapter 3) within a framework a redox catalyst is produced. Similarly by the addition of iron or aluminium onto the lattice sites of a framework material an acid catalyst is produced. The premise of this further research, was to further alter the nature of the silica MFI framework by encompassing two different heteroatoms within the material. The metallosilicate materials synthesised contained a combination of the heteroatoms already discussed: i) titanium and aluminium, ii) titanium and iron or iii) iron and aluminium. The framework materials produced containing titanium and either iron or aluminium contained both a redox and an acidic centre, therefore increasing the range of applications for these materials (Figure 6.1).

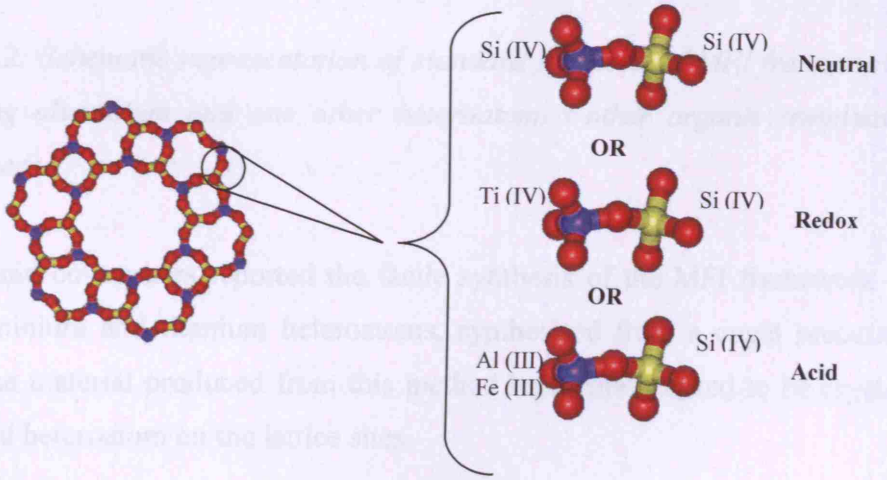

Figure 6.1: A typical example of how insertion of different heteroatoms within a generic framework can introduce catalytically sites into the framework.

[The framework materials synthesised in this chapter, were still mainly silica and thus should not be confused with mixed metal oxides (MMO). MMO are a series of materials

in which a metal is introduced into the framework of existing metal oxides, for example titania (TiO_2) doped with iron oxide.[1]]

These MFI framework materials containing titanium, aluminium and/or iron have previously been synthesised by a range of methods.[2-4] One such method is to employ commercially available ZSM-5 as a starting reagent, which undergoes ion exchange to incorporate the desired heteroatom within the existing ZSM-5 framework. Another method involves the addition of the desired heteroatom to the conventional ZSM-5 synthesis gel before crystallisation (Figure 6.2).

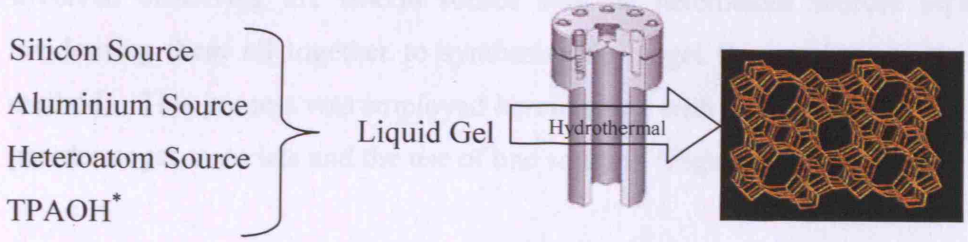

*Figure 6.2: Schematic representation of standard synthesis of MFI framework materials containing aluminium and one other heteroatom. (*other organic templates also are widely used).*

Ovejero and co-workers reported the facile synthesis of the MFI framework containing both aluminium and titanium heteroatoms, synthesised from a cogel precursor (Figure 6.3).[5] The material produced from this method was demonstrated to be crystalline with the desired heteroatom on the lattice sites.

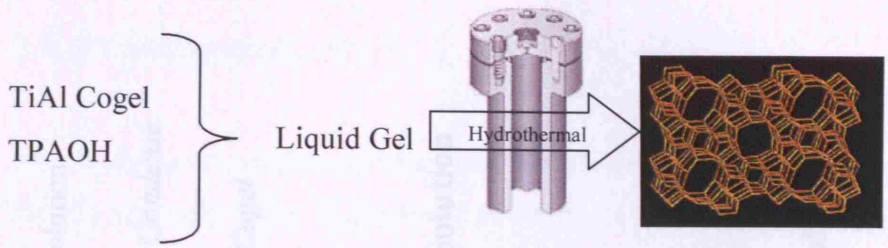

Figure 6.3: Schematic of cogel precursor method employed by Ovejero et al., to synthesise a silica based MFI framework material containing both titanium and aluminium heteroatoms.[5]

The method of formation of the bimetallosilicate cogel, reported by Ovejero *et al.*, involved dissolving the silicon source and the heteroatom sources separately before condensing them all together to synthesise the cogel (known here as the two solution method). This process was employed herein along with two other methods, the mixing of powder cogel materials and the use of one solution (Figure 6.4, next page).

In a similar manner to titanium silicalite-1, -S1 was used as the suffix for framework materials. Additionally specific nomenclature was adopted that would make the nature of the heteroatoms easily explicable. Thus MFI framework materials with incorporated titanium and aluminium centres were named TiAl-S1.

6.2 Aims

- Synthesise a range of cogel precursors containing two different heteroatoms, via different three procedures.

- Synthesise a range of MFI framework materials from cogel precursors and compare their physical and catalytic properties.

- Characterisation of the physical and catalytic properties of the cogel precursors and comparison with analogous framework materials.

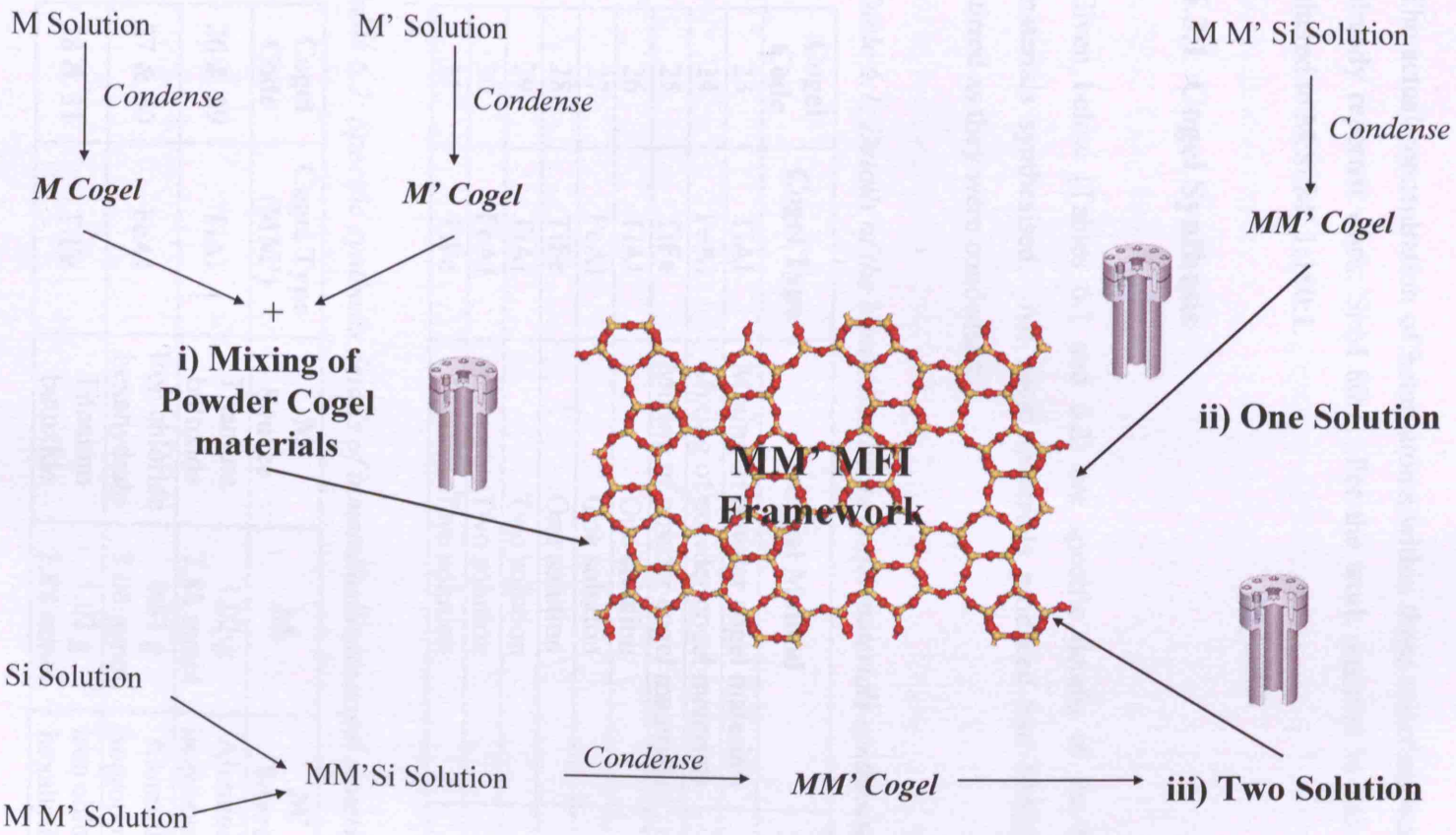

Figure 6.4: Schematic representation of the three synthesis pathways employed to produce bimetallosilicate materials.

6.3 Experimental

The actual concentration of heteroatoms within these materials was kept the same as for already reported work; Si:M 80:1. For the work reported in this chapter, the ratio was altered to M:Si:M' 1:160:1.

6.3.1 Cogel Synthesis

Given below (Tables 6.1 and 6.2) are specific details of the bimetallosilicate cogel materials synthesised. All cogel materials produced had M:Si:M' 1:160:1, and were stirred as they were condensed.

Table 6.1: Details of the bimetallosilicate cogel materials synthesised.

Cogel Code	Cogel Type	Cogel Method	Section
23	TiAl	Mixing of powder cogel materials	6.3.1.1
24	FeAl	Mixing of powder cogel materials	6.3.1.1
25	TiFe	Mixing of powder cogel materials	6.3.1.1
26	TiAl	One solution	6.3.1.2
27	FeAl	One solution	6.3.1.2
28	TiFe	One solution	6.3.1.2
29	TiAl	Two solution	6.3.1.3
30	FeAl	Two solution	6.3.1.3
31	TiFe	Two solution	6.3.1.3

Table 6.2: Specific synthesis details of bimetallosilicate cogel materials synthesised.

Cogel Code	Cogel Type (MM')	M Source	M	M' Source	M'
26 & 29	TiAl	Titanium butoxide	1.02 g 2.88 mmol	Aluminium isopropoxide	0.61 g 2.99 mmol
27 & 30	FeAl	Iron chloride hexahydrate	0.81 g 3.00 mmol	Aluminium isopropoxide	0.61 g 2.99 mmol
28 & 31	TiFe	Titanium butoxide	1.02 g 2.88 mmol	Iron chloride hexahydrate	0.81 g 3.00 mmol

6.3.1.1 Mixing of Powder Cogel Materials

Separate cogel materials were prepared for each of the heteroatoms concerned: titanium cogel 6 (Chapter 3.3.1), aluminium 15 (Chapter 4.3.1), iron 20 (Chapter 5.3.1). The bimetallosilicate cogel was prepared via thoroughly mixing by hand, identical weights of each calcined cogel.

6.3.1.2 One Solution

Tetraethylorthosilicate (TEOS) (98 %, 49.8 g, 0.2 mol) was slowly added to a stirred solution of distilled water (20.0 g, 1.1 mol), isopropyl alcohol (110.0 g, 1.8 mol) and dilute hydrochloric acid (0.1 M, 20.0 g, 0.5 mol). To this solution the first heteroatom source* was slowly added, followed by the second heteroatom source*, the resultant solution was vigorously stirred for ~ 4 hours. With continued stirring, aqueous TEAOH was added dropwise until gelation occurred. The transparent white gel was then dried overnight ~ 80 °C, calcined (3 °C min^{-1} to 535 °C, 4 hours maintained) crushed (by hand) and the resultant white powder (~ 40.0 g) stored under ambient conditions.

6.3.1.3 Two Solution

Tetraethylorthosilicate (TEOS) (98 %, 49.8 g, 0.2 mol) was slowly added to a stirred solution of distilled water (20.0 g, 1.1 mol) and dilute hydrochloric acid (0.1 M, 20.0 g, 0.5 mol) and the resultant solution stirred for 45 minutes. A separate solution of both the heteroatom sources* dissolved in isopropyl alcohol (110.0 g, 1.8 mol), was vigorously stirred for ~ 4 hours. The two solutions were then mixed and further stirred whilst an aqueous solution of TEAOH was added dropwise until gelation occurred. The transparent white gel was then dried overnight ~ 80 °C, calcined (3 °C min^{-1} to 535 °C, 4 hours maintained) crushed (by hand) and the resultant white powder (~ 40.0 g) stored under ambient conditions.

---

* Table 6.2

6.3.2 MM'-S1 Synthesis

MM'-S1 materials were synthesised from calcined cogel precursors as outlined in chapter 2.1.2 (Table 6.3).

Table 6.3: Details of MM'-S1 materials produced.

Cogel Source	MM'-S1Code	Material
23	23-1	TiAl-S1
24	24-1	FeAl-S1
25	25-1	TiFe-S1
26	26-1	TiAl-S1
27	27-1	FeAl-S1
28	28-1	TiFe-S1
29	29-1	TiAl-S1
30	30-1	FeAl-S1
31	31-1	TiFe-S1

6.4 Results and Discussion

6.4.1 Mixed Metallosilicate Materials

Packed Bulk Density Characterisation:

All of the bimetallosilicate materials prepared were fine white powders of comparable consistency. The packed bulk density measurements of these materials followed the same trend as for all of the other mono-heteroatom materials produced. The cogel materials were denser than the crystalline materials, thus agreeing with the hypothesis that the open framework of the crystalline materials reduces their internal bulk (Figure 6.5).

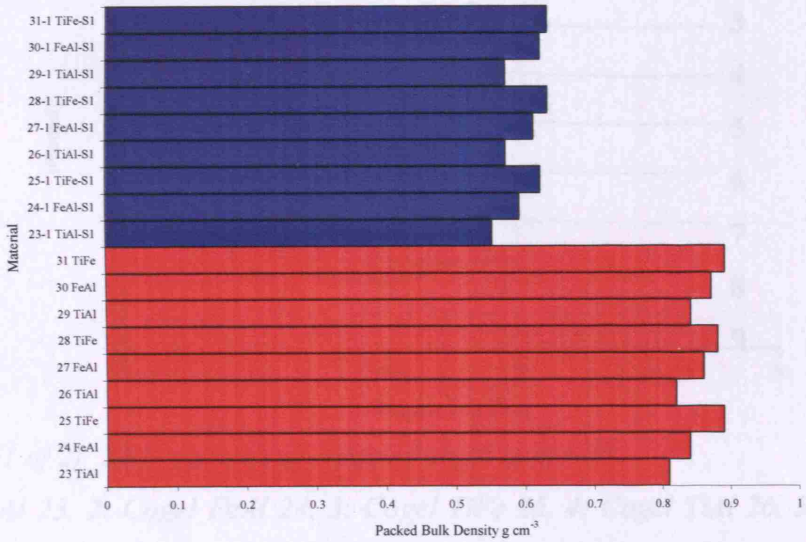

*Figure 6.5: Packed bulk density for all bimetallosilicate materials synthesised. (**Red:** Cogel materials, **Blue:** MM'-S1).*

The average bulk density of the TiAl cogel materials (0.82 g cm^{-3}) was the least of all of the cogel materials, with FeAl cogel materials (0.86 g cm^{-3}) and then TiFe cogel materials (0.89 g cm^{-3}) being similar. Therefore the materials containing the heaviest heteroatoms had the greatest bulk density. The average bulk density of the MM'-S1 materials followed an identical trend with the TiFe-S1 (0.63 g cm^{-3}) materials being the most dense, then FeAl-S1 (0.61 g cm^{-3}) with the least dense framework material being TiAl-S1 (0.56 g cm^{-3}). Although there was a notable trend in variation of packed bulk density with alteration

of heteroatom, there was little appreciable difference for the alternative methods of cogel preparation.

XRD Characterisation:

As reported for the mono-heteroatom materials reported XRD results demonstrated the cogel precursors to be amorphous and the crystalline materials to be of framework type MFI, as compared with previously reported data (Figure 6.6).[6]

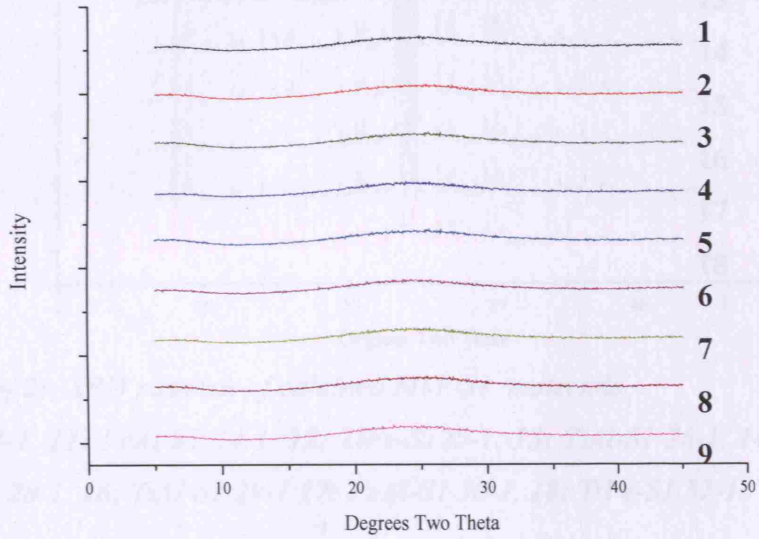

Figure 6.6 (1 of 2): XRD patterns of calcined cogel materials.

***1:** Cogel TiAl 23, **2:** Cogel FeAl 24, **3:** Cogel TiFe 25, **4:** Cogel TiAl 26, **5:** Cogel FeAl 27, **6:** Cogel TiFe 28, **7:** Cogel TiAl 29, **8:** Cogel FeAl 30, **9:** Cogel TiFe 31.*

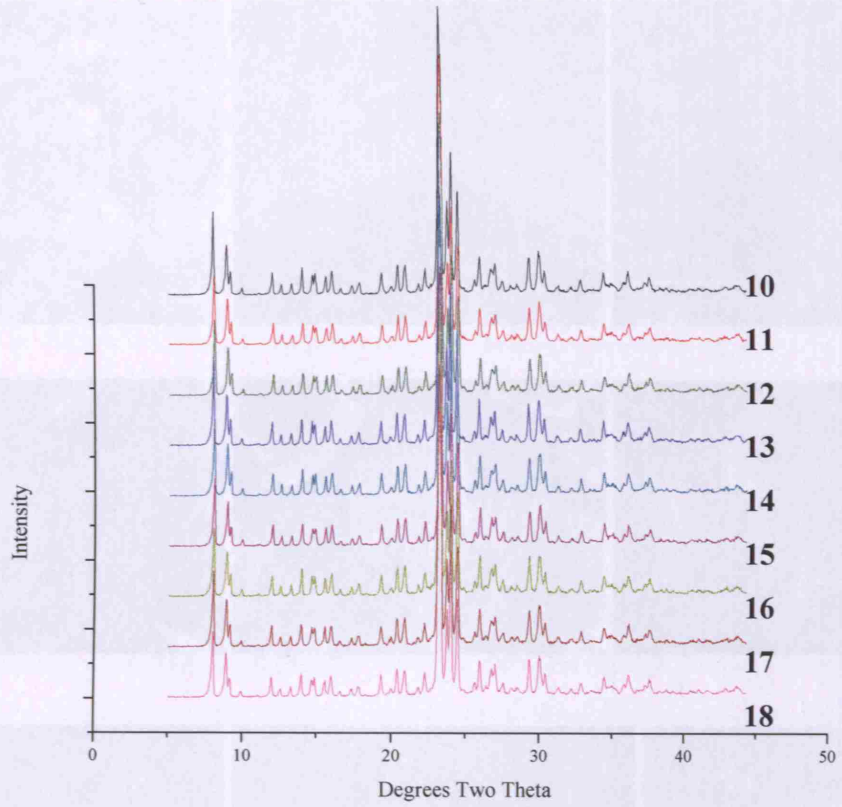

Figure 6.6 (2 of 2): XRD patterns of calcined MM'-S1 materials.
10: *TiAl-S1 23-1,* ***11:*** *FeAl-S1 24-1,* ***12:*** *TiFe-S125-1,* ***13:*** *TiAl-S1 26-1,* ***14:*** *FeAl-S1 27-1,* ***15:*** *TiFe-S1 28-1,* ***16:*** *TiAl-S1 29-1* ***17:*** *FeAl-S1 30-1,* ***18:*** *TiFe-S1 31-1*

SEM Characterisation:

SEM images of the all the bimetallosilicate cogel materials demonstrated they had no ordered morphology, regardless of the synthesis parameters employed (Figure 6.7). The cogel precursors appeared identical, not only to each other, but also to previously prepared cogel materials containing only one heteroatom. The morphology of all of the previously described MFI type framework materials was spherical, thus the range of different morphologies produced from the bimetallosilicate cogel precursors was unexpected. Additionally, the framework materials previously described, exhibited notably smaller average diameters (of 0.3 μm, 0.5 μm and 0.8 μm for TS-1, ZSM-5 and Fe-MFI respectively) than some of the MM'-S1 materials synthesised.

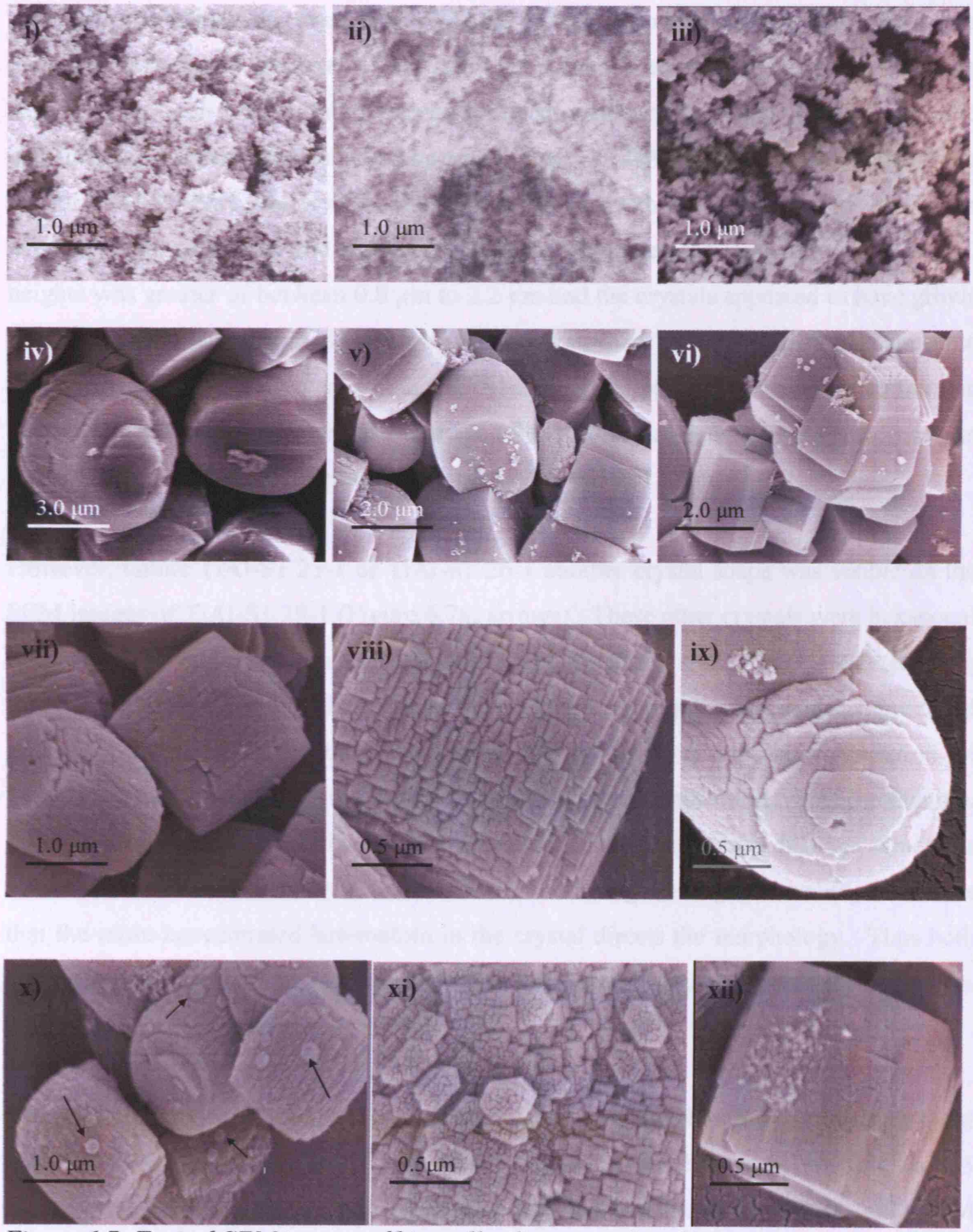

Figure 6.7: Typical SEM images of bimetallosilicate cogel and MM'-S1 materials. ***(i)*** *TiAl Cogel 26,* ***ii)*** *FeAl Cogel 27,* ***iii)****TiFe Cogel 28)* ***(iv)****TiAl-S1 23-1,* ***v)*** *FeAl-S1 24-1,* ***vi)*** *TiFe-S1 25-1,* ***vii)****TiAl-S1 26-1,* ***viii)*** *FeAl-S1 27-1,* ***ix)*** *TiFe-S1 28-1,* ***x)****TiAl-S1 29-1,* ***xi)*** *FeAl-S1 30-1,* ***xii)*** *TiFe-S1 31-1).*

SEM images showed the crystals of TiAl-S1 23-1 to be barrel shaped, with an average height of 2.0 μm and diameter of 3.0 μm. The range of crystal heights was moderately narrow of between 1.5 μm and 2.7 μm, and the smooth surfaces of the crystals suggested that they grew as single crystals. The morphology of TiAl-S1 26-1 was comparable to that of TiAl-S1 23-1, the crystals were barrel shaped, although slightly smaller with an average height of 1.3 μm and diameter of 0.8 μm. However, the range of average crystal heights was greater of between 0.8 μm to 2.2 μm and the crystals appeared to have grown from an aggregate method (as shown by the rough surfaces). TiAl-S1 29-1 also appeared to exhibit barrel morphology and akin to TiAl-S1 26-1 it appeared to have formed from an aggregate process. The average diameter of the barrel crystals was 0.7 μm, with an average height of 1.4 μm, over a range between 1.0 μm to 1.8 μm.

However, unlike TiAl-S1 23-1 or TiAl-S1 26-1 another crystal shape was visible on the SEM images of TiAl-S1 29-1 (Figure 6.7x, arrows). These other crystals were hexagonal in morphology and much smaller than the barrel structures, the average diameter being just 0.3 μm. These hexagonal structures were dispersed throughout the material produced and their surface showed they were also formed from aggregates. Alteration of heteroatom identity can alter the morphology of a material, thus conceivably the titanium and aluminium heteroatoms in TiAl-S1 are within the different two different structures shown. However, the lower concentration of the hexagonal crystals would necessitate that the more concentrated heteroatom in the crystal directs the morphology. Thus both heteroatoms are present in both morphologies but where one greatly predominates is was theorised that the crystal shape altered.

The morphology of FeAl-S1 24-1 was also barrel shaped, and the smooth surfaces suggest grown via a single crystal mechanism. The average height of these barrel crystals was 2.5 μm (between the ranges 1.1 μm to 3.4 μm) and the average diameter 1.8 μm. SEM images of FeAl-S1 27-1 showed the morphology of the crystals to be roughly cubic. The average length of one side was 2.0 μm, the range of sizes of these cubic structures was wide between 1.0 μm to 2.8 μm. The rough surface demonstrated the crystals to have been formed by an aggregate process. FeAl-S1 30-1 portrayed a different morphology to

the other FeAl-S1 materials described, the crystals appeared hexagonal. The hexagonal morphology was not always clearly definable, with some crystals appearing stretched or only half complete. These FeAl-S1 crystals again exhibited a rough surface indicative of an aggregate growth mechanism. The most surprising feature of these crystals was there size, with the average diameter of just 0.3 μm within a small range of 0.1 μm to 0.7 μm.

All of the FeAl-S1 materials synthesised exhibited a different morphology, additionally two of these materials appeared to have grown via an aggregate mechanism whilst the third via a single growth mechanism. The only difference between these materials was the method of preparation of the cogel precursor which highlighted the effect the cogel precursor had on the final MFI framework material.

SEM images of TiFe-S1 25-1 demonstrated the material to have a range of morphologies, some areas demonstrated hexagonal or cubic morphology whilst other areas appeared to show rounded edges and corners. The average size of TiFe-S1 25-1 was difficult to measure due to the intergrowth and overlap of the crystals, the approximate range being between 1.0 μm and 4.0 μm. The variety of morphologies may again have been the result of different areas of the material containing different concentrations of each heteroatom. Thus, whilst the iron and titanium heteroatoms in equal concentration may direct one morphology, an increase in concentration of either heteroatom may result in another morphology developing. The smooth edges of the structures infer that all of the crystals structures formed via a single crystal growth mechanism.

TiFe-S1 28-1, in contrast to TiFe-S1 25-1 exhibited approximately spherical morphology, with an average sphere diameter of 2.0 μm (range between 1.2 μm to 2.3 μm). The surface of the spheres suggested that they grew via a layered mechanism. The SEM images of TiFe-S1 31-1 showed the crystals to have cubic morphology with an average width of 1.0 μm over a range of cubic sizes 0.4 μm to 1.2 μm. The smooth surface of the cubic crystals suggested that they also grew via a single crystal growth mechanism.

The framework materials (prepared from cogel materials synthesised via the mixing of powders method), exhibited different morphologies, the TiAl-S1 and FeAl-S1 materials had barrel shaped crystals whilst TiFe-S1 exhibited a range of morphologies. The variations can be explained as the nature and concentration of the heteroatoms present within a crystal can direct product morphology. All of these crystals appeared to have grown via a single crystal growth mechanism. Whilst, the framework materials (prepared from cogel precursors which were synthesised via the one solution) exhibited different morphologies (TiAl-S1 barrel, FeAl-S1 cubic, TiFe-S1 spherical). However, these crystals appeared to have grown via different methods, the TiAl-S1 and FeAl-S1 via an aggregate process whilst the TiFe-S1 grew in layers. Therefore how the crystal morphology is influenced by the synthesis parameters of the cogel precursor and the nature of the heteroatoms is not straightforward. The MM'-S1 materials (synthesised from cogel materials prepared from the two solution method) exhibited different morphologies (TiAl-S1 barrel, FeAl-S1 hexagonal, TiFe-S1 cubic). Notably the growth methods were different again, with TiAl-S1 and FeAl-S1 being formed via an aggregate process and TiFe-S1 following a single crystal growth mechanism.

The methods of crystal growth only appeared the same for the materials prepared from cogel materials prepared from the mixing powder methods, which grew via single crystal growth mechanism. MM'-S1 materials prepared from cogel materials which were synthesised from the one or two solution method appear to have grown via an aggregate method if they contained aluminium and via a solution method if no aluminium heteroatoms were present. This was expected as the framework aluminosilicate materials were the only mono-heteroatom materials synthesised not to have grown via an aggregate process.

The crystallisation of TS-1 from cogel precursors was reported not to occur via the classical method of crystal growth around a previously formed nuclei by incorporation of soluble species (Chapter 1.2.2.2).[7] It has been assumed that the same method of solid-solid transformation growth occurred for all MFI framework synthesised from cogel precursors. This method of crystal growth occurs via the formation of amorphous

primary particles which aggregate to form secondary particles. These secondary particles transform into crystals, the morphology of which was reported to be primarily directed by the secondary particles themselves. Therefore the differences in the method of cogel preparation presumably have affected mechanism of crystal growth by alteration of these secondary particles. Further work is required to fully understand how these cogel alterations have altered the crystal morphology, specifically *in situ* studies relating to the crystal growth and characterisation of the primary and secondary particles.

The MFI framework materials which contained one heteroatom all exhibited spherical morphology, comparatively a vast range of morphologies were evident for the bimetallosilicate materials. This range has been attributed partly to the ability of the identity of a heteroatom to alter crystal shape and partly to the method of preparation of the cogel precursor.

UV-vis Characterisation:

UV-vis spectroscopy was utilised to identify the nature and environment of titanium and iron centres within calcined bimetallosilicate materials. Only materials containing either titanium *or* iron are reported herein as the overlap between bands of titanium and iron resulted in the spectra being indecipherable.

Both the TiAl containing cogel and crystalline materials were studied using UV-vis spectroscopy (Figure 6.8). The UV-vis spectra of the cogel materials were all similar, exhibiting one broad band between ~ 200 to 260 nm. Additionally all of the cogel spectra were free from extra framework titanium due to the absence a band around 330 nm. The band width broadened with differing methods of cogel synthesis, cogel 23-1 (prepared from mixing powders) had the narrowest band, whilst cogel 29-1 (prepared from the two solution method) had the broadest band inferring the widest range of titanium coordination geometries.

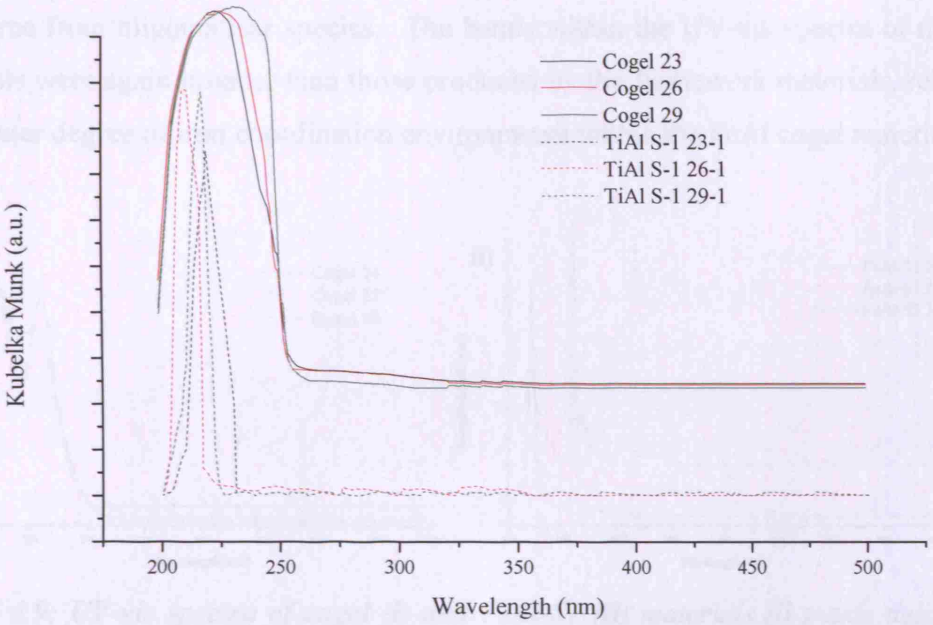

Figure 6.8: UV-vis spectra of cogel (solid line) and TiAl-S1 (dashed line) materials.

The TiAl-S1 materials all gave rise to similar UV-vis spectra containing one narrow band centred around 220 nm, which related to titanium centres on tetrahedral lattice sites. Similarly to the titanium containing cogel UV-vis spectra, there was no evidence of extra framework TiO_2 species. The bands relating to the framework materials were much narrower than those corresponding to the cogel materials, confirming the more ordered nature of the titanium centres within the framework. The band attributed to TiAl-S1 23-1 was notably wider than that of either TiAl-S1 26-1 or TiAl-S1 29-1, equating a wider range of titanium environments within the material. This was contrary to the width of the cogel bands wherein cogel 23 (the precursor for TiAl-S1 23-1) was the narrowest band.

The FeAl cogel materials all gave rise to comparable UV-vis spectra, consisting of two broad overlapping bands centred at approximately 220nm and 260 nm (Figure 6.9). These bands relate to isolated iron centres within the silica matrix, the exact coordination of these centres was unable to be determined. FeAl cogel 24 exhibited the most overlapped bands on the UV-vis spectrum, whilst FeAl cogel 30 gave rise to the most resolved signals and hence exhibited the least number of iron environments. None of the FeAl cogel UV-vis spectra exhibited bands between 300 to 450 nm, demonstrating them

to be free from oligonuclear species. The bands within the UV-vis spectra of the cogel materials were again broader than those produced by the framework materials, relating to the greater degree of iron coordination environments within the FeAl cogel materials.

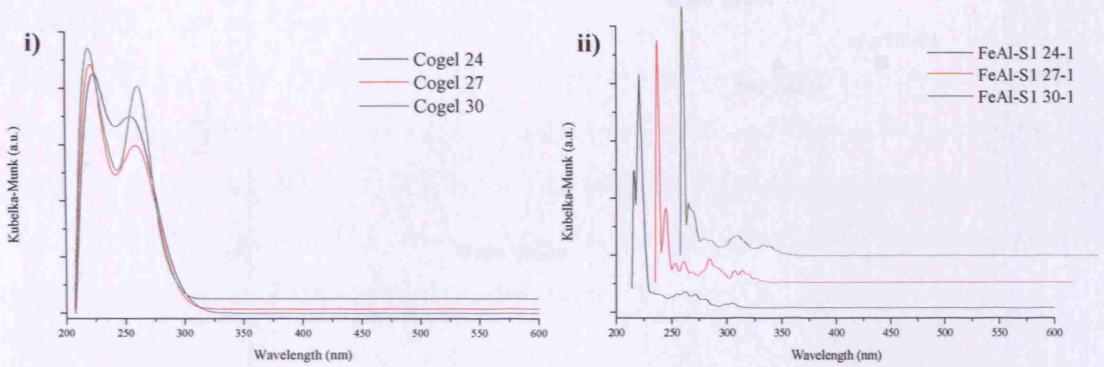

*Figure 6.9: UV-vis spectra of cogel (**i**) and FeAl-S1 (**ii**) materials (**ii** x-axis deliberately displaced.).*

The UV-vis spectra of the FeAl-S1 materials were again comparable, each spectra exhibited two main bands centred at 220nm and 240 nm, which related to isolated iron centres within the MFI framework (Figure 6.9). All of the FeAl-S1 materials had additional bands on the UV-vis spectra relating to other iron environments within the silica framework. The exact nature of these bands could not be determined, they are however at lower wavelengths than the region attributed to oligomeric species. The relative intensity of the two main bands in the FeAl-S1 spectra was the same for FeAl-S1 27-1 and FeAl-S1 30-1, the first band being much more intense than the second. However, for FeAl-S1 24-1 the second band was much more prominent than the first, which suggested that the iron was predominantly in a different environment within this material.

IR Characterisation:

IR data was collected for pre-calcined, dehydrated TiM-S1 materials (where M is either aluminium or iron). The ratio of intensities (I_{960}/I_{550}) of the bands at 960 cm^{-1} and 550 cm^{-1} were obtained and compared as evidence of the degree of tetrahedral titanium centres incorporated within the materials (Figure 6.10)

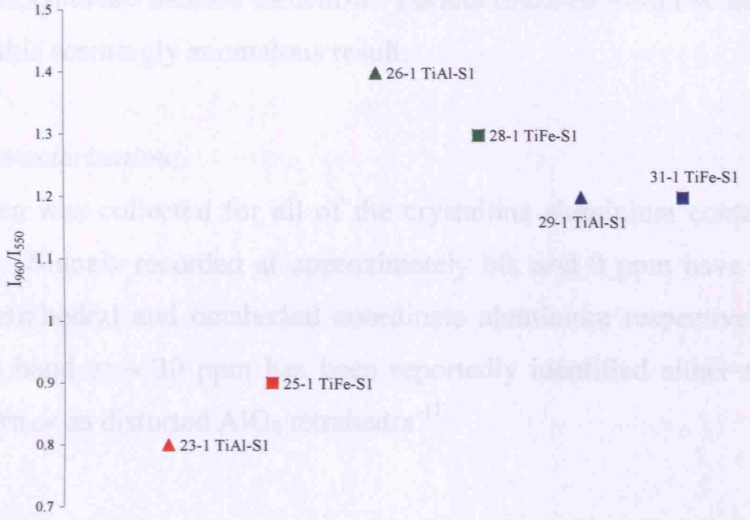

Figure 6.10: I_{960}/I_{550} values for different titanium containing MM'-S1 materials synthesised from cogel precursors prepared from mixing of powder (red), one solution (green) and two solution (blue) methods.

The ratio of intensities of the 960 cm^{-1} and 550 cm^{-1} bands (I_{960}/I_{550}) was highest for TiM-S1 materials prepared from cogel materials synthesised from the one solution method, and lowest for materials prepared from cogel materials formed from the mixing of powders method. It had been reported that materials with a higher I_{960}/I_{550} ratio have a higher degree of tetrahedral titanium incorporation.[8] Thus, materials TiAl-S1 26-1 and TiFe-S1 28-1 contained the most tetrahedral titanium centres of all the materials examined and hence were predicted to be the most catalytically active for oxidative catalysis. However, since the relationship between the titanium concentration and the intensity of the 960 cm^{-1} band has not been completely resolved in the literature, thus no quantitative conclusions are drawn. It was interesting that the materials prepared from the mixing of powders method exhibited the lowest tetrahedral titanium concentration, which was agreeable with the UV-vis data obtained. This also demonstrated materials prepared from these cogel materials to have the widest range of titanium coordinated environments. Yet this was not the case when the singular titanium cogel was used to make framework TS-1, this material was showed to exhibit a high concentration of tetrahedral coordination

environments (Chapter 3). Therefore, the coordination of the titanium centres must be effected by this synthesis method somehow. Further research would be needed in order to further probe this seemingly anomalous result.

^{27}Al NMR Characterisation:

^{27}Al NMR data was collected for all of the crystalline aluminium containing materials, (Figure 6.11). Signals recorded at approximately 60, and 0 ppm have reportedly been assigned to tetrahedral and octahedral coordinate aluminium respectively.[9,10] Whilst a third possible band at ~ 30 ppm has been reportedly identified either as aluminium in AlO_5 polyhedra or as distorted AlO_4 tetrahedra.[11]

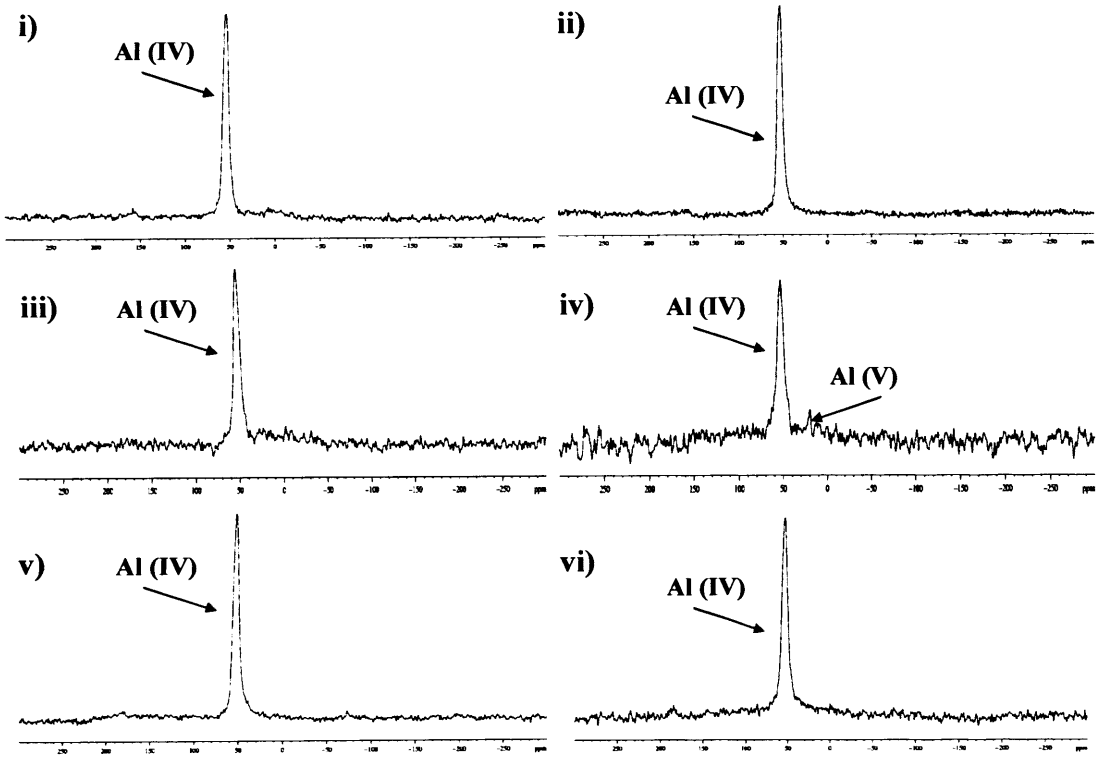

*Figure 6.11: ^{27}Al NMR spectra of MAl-S1 materials: **i)** TiAl-S1 23-1, **ii)** FeAl-S1 24-1, **iii)** TiAl-S1 26-1, **iv)** FeAl-S1 27-1, **v)** TiAl-S1 29-1, **vi)** FeAl-S1 30-1.*

The NMR data collected from the TiAl-S1 materials only exhibited one narrow signal, confirming the majority of the aluminium centres to exhibit tetrahedral coordination geometry and thus have potential catalytic ability. The FeAl-S1 materials all exhibited

the same narrow band at similar ppm values, but FeAl-S1 27-1 gave rise to an additional band. This second band positioned at 20 ppm and was caused by either five coordinated or distorted four coordinate aluminium heteroatoms. This additional band was much smaller than the main signal at 54 ppm, thus although the aluminium centres were in two clear coordination geometries, the majority were in a tetrahedral environment.

The aluminium centres in these bimetallosilicate materials appear to be predominantly tetrahedrally coordinated and thus catalytically active. Quantitative and comparative conclusions about the potential catalytic ability can not be made except that FeAl-S1 29-1 was likely to be the least active as not all of the aluminium centres were tetrahedrally bound.

Overall the materials with the most catalytic potential are those prepared from cogel materials synthesised via the two solution method. Materials prepared from cogel materials synthesised from the mixing of powders method exhibited the least ideal heteroatom coordination geometries. UV-vis data demonstrated the titanium centres to have the widest range of coordination geometries and IR results showed these materials to have the lowest I_{960}/I_{550} values. It should be reiterated that the reasons for this low catalytic potential are still not understood.

The framework materials prepared utilising cogel materials form via a one solution method, appeared to contain the highest concentration of tetrahedral titanium centres, from the I_{960}/I_{550} ratio. However, the NMR results for these materials demonstrated the aluminium centres to be the least well incorporated within the framework. Therefore, the MM'-S1 materials prepared from cogel materials formed from the two solution method appeared to contain heteroatoms in the most potentially reactive coordination geometries.

6.4.2 Ammonia Absorption

Ammonia absorption was used to identify the relative strength and concentration of acid sites of the bimetallosilicate materials (Chapter 2.2.6). TPD of ammonia allowed identification of strong Brønsted and Lewis acid sites, which have been shown to be utilised for acid catalysis.[12] The acid sites of the cogel materials, prepared from the two solution method (TiAl 29, FeAl 30, TiFe 31) , and the MM'-S1 materials (TiAl-S1 29-1, FeAl-S1 30-1, TiFe-S1 31-1) prepared from them were analysed as these materials exhibited the greatest catalytic potential. (All materials were pre-calcined prior to TPD evaluation).

The TPD spectra for the cogel materials appeared similar, exhibiting one predominate band at low temperature and a small band at a high temperature (Figure 6.12). The large low temperature band correlated with weak acid site concentration, hence all of the cogel materials contained more of the weak acid sites than the strong acid sites employed as acid catalysis sites. The temperature of ammonia desorption from these weak acid sites was approximately the same for all of the cogel materials, occurring at ~ 160 °C. The high temperature desorption band was particularly well defined for the TiAl cogel material, its band of desorption occurring at ~ 420 °C. Whilst the band relating to the strong acid sites was less well defined for the TiFe cogel, it was centred at a higher temperature of ~ 450 °C. Therefore, the TiFe cogel had a stronger acid site than the TiAl cogel material, hence the TiFe cogel was predicted to be a more active acid catalyst. The band relating to the strong acid sites was the least well defined for the FeAl cogel than for the other cogel materials evaluated. The band was so broad it was impossible to gauge the average temperature of desorption for the second band. It was hypothesised that this second band was actually two overlapping bands, one relating to the iron centres and another relating to the aluminium centres. Thus the FeAl cogel would contain two different types of strong acid site, which it was predicted, would catalyse acid reactions differently.

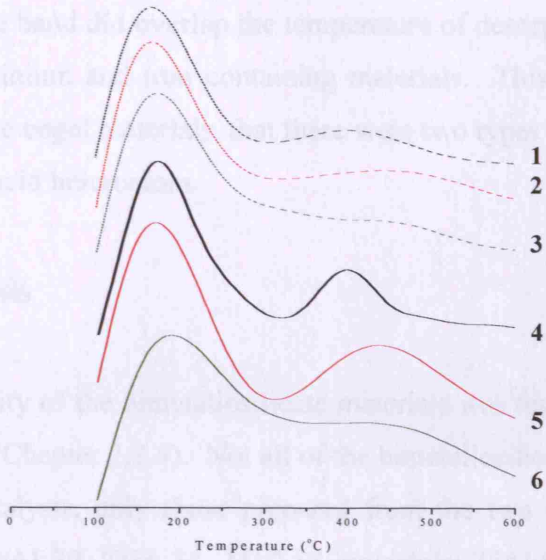

*Figure 6.12: TPD of ammonia for bimetallosilicate materials. **(1)** TiAl Cogel 29, **2)** TiFe Cogel 31, **3)** FeAl Cogel 30, **4)** TiAl-S1 29-1, **5)** TiFe-S1 31-1, **6)** FeAl-S1 30-1.)*

The TPD profiles of the framework materials appeared similar to those of the cogel materials (Figure 6.12). The all the framework profiles exhibit one band at ~ 160 °C and another band at a high temperature. Similarly to the cogel materials, all of the MM'-S1 materials contained a greater concentration of weak acid sites than the catalytically active strong acid sites. Once more the TiAl containing material had the most well resolved desorption bands compared to the other framework materials. The temperature of desorption from the strong acid sites being ~ 420 °C, which was the same temperature for the TiAl cogel, as well as for the materials which contained just the aluminium heteroatom (Chapter 4). The desorption of ammonia from TiFe-S1 produced well resolved bands, the strong acid sites desorbed ammonia at ~ 450 °C. Therefore, TiFe-S1 contained stronger acid sites than TiAl-S1 and hence it was predicted would be a more active acid catalyst.

The FeAl-S1 material gave rise to overlapped desorption bands in the TPD of ammonia, the low temperature band, corresponding to the weak acid sites, was broader than for any of the other materials tested. Additionally, the band relating to the strong acid sites could not be resolved and thus the temperature of desorption was not determined. Although this

broad high temperature band did overlap the temperature of desorption for the strong acid sites of both the aluminium and iron containing materials. This would corroborate the hypothesis made for the cogel materials, that there were two types of strong acid sites, one for each incorporated acid heteroatom.

6.4.3 Acid Catalysis

The acid catalytic ability of the bimetallosilicate materials was tested by the alkylation of benzene with ethanol (Chapter 2.3.4). Not all of the bimetallosilicate material synthesised were employed as catalysts, only those prepared from the two solution method (*cogel materials:* TiAl 29, FeAl 30, TiFe 31, *MM'-S1 materials:* TiAl-S1 29-1, FeAl-S1 30-1, TiFe-S1 31-1). (The acid catalyst results were not normalised for the number of potential acid sites)

The products formed from the reaction of benzene with ethanol were ethyl benzene (EB), diethyl benzene (DEB) and triethyl benzene (TEB). The reaction of ethanol molecules alone produced diethyl ether (DEE), ethene, propene, butene, hexene and pentene. All of these possible products from the reaction were sought regardless of their phase. The results presented herein are after two hours of reaction, the reproducibility of the was ensured and catalysts were re-calcined to verify reusability.

The percentage conversion for the TiAl cogel was 8.3 % for benzene and 22.6 % for ethanol (Figure 6.13). Whilst the conversion for the TiFe cogel was higher with benzene and ethanol conversion of 10.4 % and 30.2 % respectively. Thus, as the TPD results predicted, the TiFe cogel was more catalytically active than the TiAl cogel, the stronger acid sites on the TiFe material allowing a greater conversion of both reactants. However, the TPD results did not clearly predict that the FeAl cogel would have far higher conversions of 18.0 % and 49.7 % for benzene and ethanol respectively.

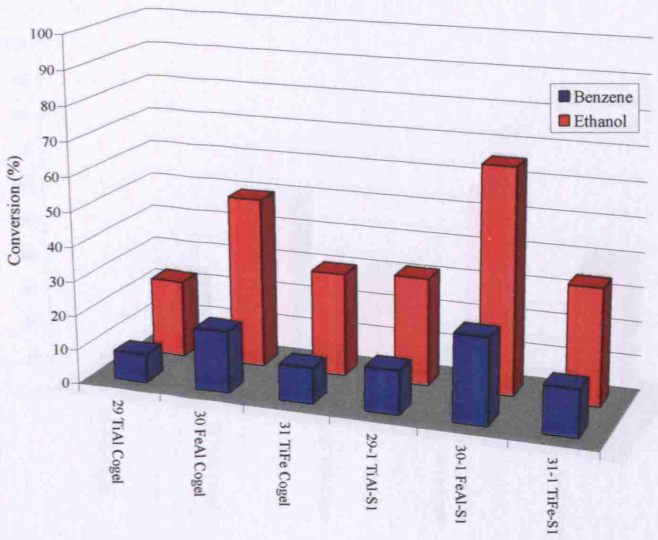

Figure 6.13: Benzene and ethanol conversions (%) after two hours reaction for cogel and framework bimetallosilicate materials.

Although the TPD results did not accurately predict the strength of the stronger acid sites within cogel FeAl, compared to either the TiAl or TiFe cogel materials, a qualitative prediction could have been made. It could have been assumed that as the FeAl cogel material contained twice the number of potentially catalytically active sites, it would have exhibited twice the catalytic reactivity as was the case (Figure 6.14). In agreement with this both the TiAl and TiFe cogel materials containing half the acid site concentration of their mono-heteroatom counterparts, demonstrated approximately half their catalytic reactivity. The catalytic results were deliberately not normalised with respect to potential acid site concentration to allow comparison between each of the types of catalytic reaction investigated.

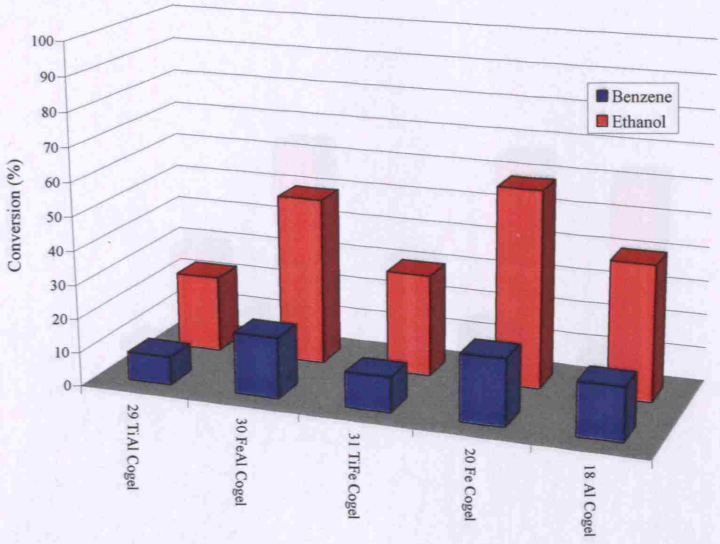

Figure 6.14: Benzene and ethanol conversions (%) after two hours reaction for mono- and bimetallosilicate cogel materials.

The framework bimetallosilicate materials demonstrated greater catalytic reactivity than the corresponding cogel materials (Figure 6.13 above). TiAl-S1 was the least active with benzene and ethanol conversion of 12.8 % and 31.5 % respectively. TiFe-S1 was slightly more active with benzene and ethanol conversions of 13.8 % and 34.1 % respectively. The activity was only slightly greater for the TiFe materials than TiAl materials and was attributed to the greater acid strength of the acid sites required for catalysis. Similarly to the cogel materials the activity of both TiAl-S1 and TiFe-S1 was approximately half that of the comparable mono-heteroatom catalysts, as they contained half the number of acid sites (Figure 6.15).

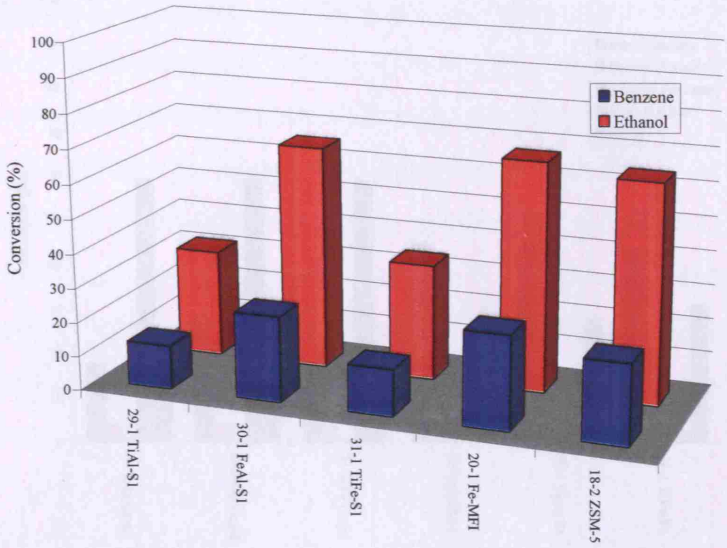

Figure 6.15: Benzene and ethanol conversions (%) after two hours reaction for mono- and bimetallosilicate MFI framework materials.

FeAl-S1 exhibited the greatest activity of the framework materials, with benzene and ethanol conversions of 25.2 % and 65.7 % respectively. This high activity was attributed to the greater concentration of acidic heteroatoms within FeAl-S1, than either TiFe-S1 or TiAl-S1. The activity of the FeAl-S1 was comparable to both the Fe-MFI and ZSM-5 materials, its actual values being between those reported for Fe-MFI (benzene: 27.5 %, ethanol: 67.2 %) and ZSM-5 (benzene: 23.4 %, ethanol: 64.2 %).

The product selectivity was similar for all of the bimetallosilicate cogel materials the majority product was always DEE (Figure 6.16). All of the cogel materials tested exhibited EB selectivity of ~ 17 %, compared with ~ 60 % for DEE. It was noteworthy that the chemical identity of the cogel did not alter the product selectivity, which demonstrated the similar acid catalytic behaviour of the aluminium and iron heteroatoms.

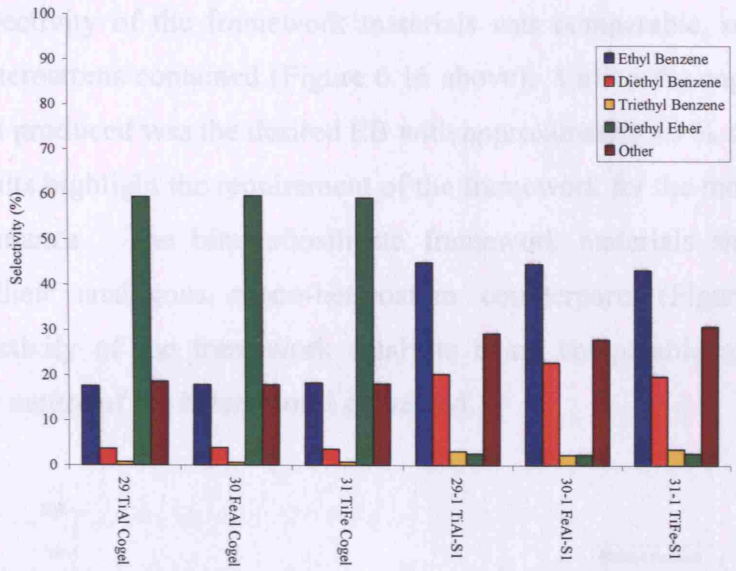

Figure 6.16: Product selectivity for bimetallosilicate catalysts after two hours reaction.

The preference of the bimetallosilicate cogel materials to form products which do not require the benzene reagent such as DEE, was analogous to the trend observed for the mono-heteroatom cogel materials prepared (Figure 6.17). It was hypothesised that amorphous structure of the cogel materials prevented the larger benzene molecules from interacting with the catalytically active sites.

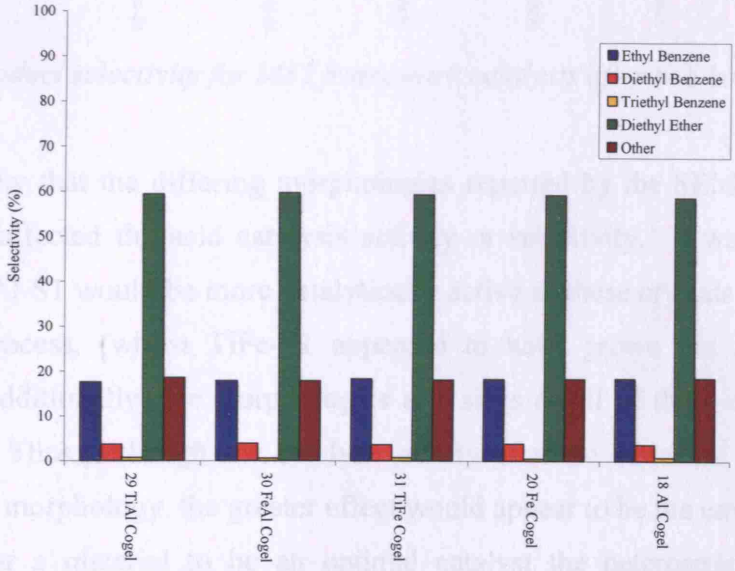

Figure 6.17: Product selectivity for cogel catalysts after two hours reaction.

The product selectivity of the framework materials was comparable, regardless of the nature of the heteroatoms contained (Figure 6.16 above). Unlike the cogel materials the majority product produced was the desired EB with approximately 40 % selectivity. Thus again, these results highlight the requirement of the framework for the most advantageous catalytic performance. The bimetallosilicate framework materials show comparable selectivity to their analogous mono-heteroatom counterparts (Figure 6.18). The percentage selectivity of the framework catalysts being comparable regardless of the concentration or nature of the heteroatoms contained.

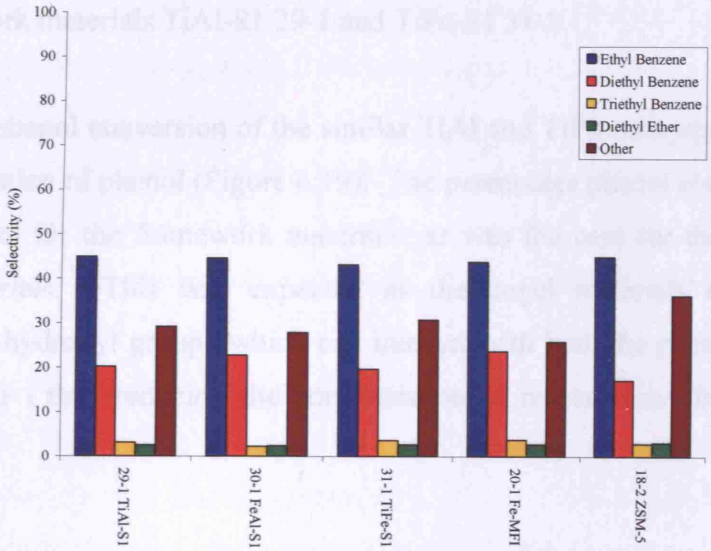

Figure 6.18: Product selectivity for MFI framework catalysts after two hours reaction.

It was noteworthy that the differing morphologies reported by the SEM images did not appear to have affected the acid catalysis activity or selectivity. It was predicted that TiAl-S1 and FeAl-S1 would be more catalytically active as these crystals were grown via an aggregate process, (whilst TiFe-S1 appeared to have grown via a single crystal mechanism). Additionally, the morphologies and sizes of all of these crystal materials were different. Thus, although the catalytic ability of these materials is known to be effected by their morphology, the greater effect would appear to be the environment of the heteroatom. For a material to be an optimal catalyst the heteroatom sites must be accessible by the reagents (regardless of bulk), the inner pores and cavities should be well

formed. Additionally, the heteroatom must be isolated and the coordination geometry tetrahedral. The overall morphology of the material may then have an effect upon the catalytic ability but it would appear to be a secondary consideration.

6.4.4 Oxidative Catalysis

The ability of titanium centres, within the bimetallosilicate materials, to catalyse oxidative catalysis was tested by the hydroxylation of phenol reaction (Chapter 2.3.2). The materials employed as catalysts for this reaction were cogel materials TiAl 29 and TiFe 31, and framework materials TiAl-S1 29-1 and TiFe-S1 31-1.

The percentage phenol conversion of the similar TiAl and TiFe catalysts was comparable for the hydroxylation of phenol (Figure 6.19). The percentage phenol conversion was less for the cogel than for the framework materials, as was the case for the solely titanium containing materials. This was expected as the cogel materials exhibit a higher concentration of hydroxyl groups which can interact with both the phenol and hydrogen peroxide reagents , thus reducing the concentration of reactants available for reaction. (Chapter 3.4.6).

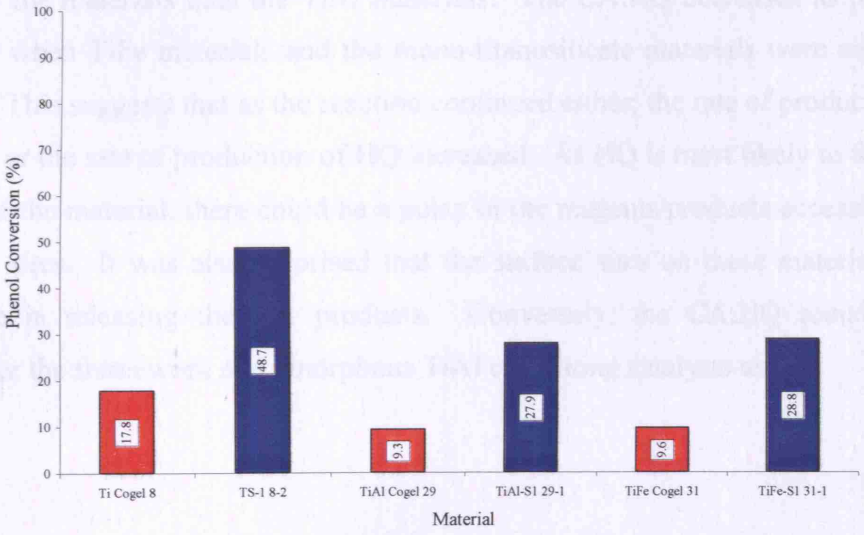

Figure 6.19: Phenol conversion (%) after six hours reaction for mono- and bimetallosilicate MFI framework materials (Red: Cogel, Blue: Framework).

The percentage phenol conversion for the bimetallosilicate materials was greater than double that of the corresponding mono-titanosilicate materials. It had been expected that the bimetallosilicate materials would exhibit approximately half the activity of the mono-titanosilicate materials, as the effective oxidative site concentration is halved. However, the inclusion of an acidic heteroatom within the silica matrix (within the bimetallosilicate materials) produces a charge imbalance within the matrix, which is frequently stabilised by a proton bound to a bridging oxygen atom. This bridging proton slightly reduces the silanol concentration of the material, as the silanols are converted into bridging oxygen atoms with a charge compensating proton. Hence, the reduction in silanol concentration reduces the interaction of the peroxide and phenol reagents with the surface of the catalyst, increasing the effective reagent concentration for catalysis.

The selectivity of the bimetallosilicate materials was different from the titanosilicate materials (Figure 6.20). For both the cogel and framework TiAl materials had lower CA selectivity than the corresponding TiFe materials. It has previously been reported that CA is mainly produced on the external surface of the TS-1 framework, whilst hydroquinone is produced within the pores (due to geometric constraints of the MFI pores).[13] Thus it was theorised that the TiFe materials had a greater concentration of oxidative sites on the surface of the materials than the TiAl materials. The CA:HQ decreased as the reaction continued when TiFe materials and the mono-titanosilicate materials were employed as catalysts. This suggests that as the reaction continued either; the rate of production of CA decreased or the rate of production of HQ increased. As HQ is most likely to form within the bulk of the material, there could be a delay in the reagents/products accessing/leaving the active sites. It was also theorised that the surface sites on these materials may be ineffective in releasing the CA products. Conversely, the CA:HQ remain roughly constant for the framework and amorphous TiAl containing catalysts tested.

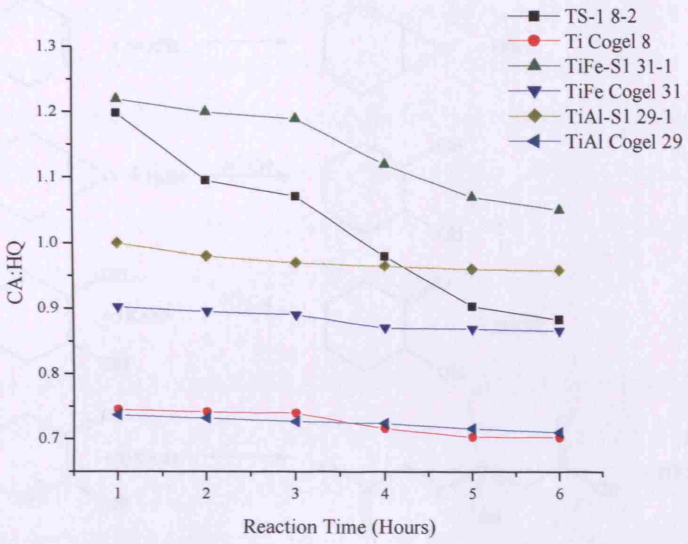

Figure 6.20: CA:HQ ratio for titanium containing catalysts during the hydroxylation of phenol reaction.

By utilising these bimetallosilicate materials as catalysts for the hydroxylation of phenol reaction, the titanium centres were shown to be active for oxidative catalysis. However, the catalytic properties of the titanium centres have been altered by the incorporation of acid centres, from those reported for the titanosilicate materials (Chapter 3).

6.4.5 Acidic and Oxidative Catalysis

The formation adipic acid from cyclohexene occurs via a multi-step pathway, this pathway involves both oxidative and acid catalysed steps (Chapter 2.3.3, Figure 6.21 below). The ability of the bimetallosilicate materials synthesised, to simultaneously catalyse both oxidative and acidic reactions was tested for the TiAl and TiFe materials. (The FeAl materials, which contained no oxidative centre, were not tested.)

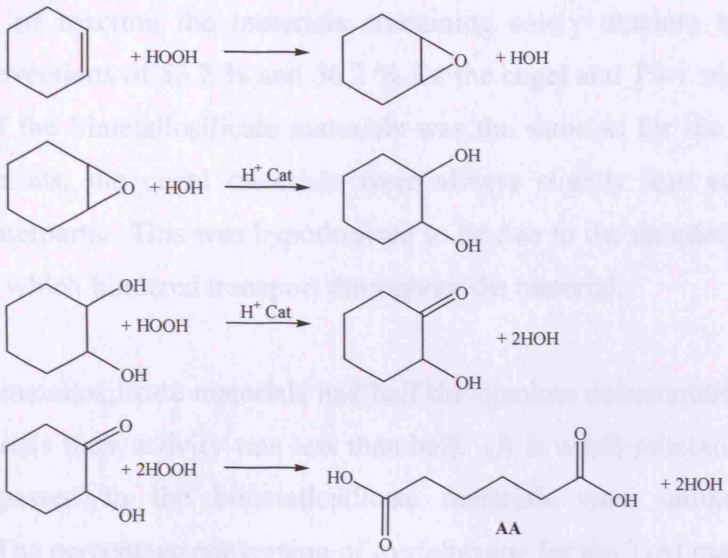

Figure 6.21: Reaction pathway for the oxidation of cyclohexene to AA.

The conversion of cyclohexene slowed dramatically after 24 hours of reaction, regardless of the catalyst employed (Figure 6.22). This decrease was observable for both the mono- and bimetallosilicate materials, as previously described (Chapter 3.4.7) this was attributed to both the limited amount of oxidant in the reaction and the number of ongoing competitive catalytic processes involved.

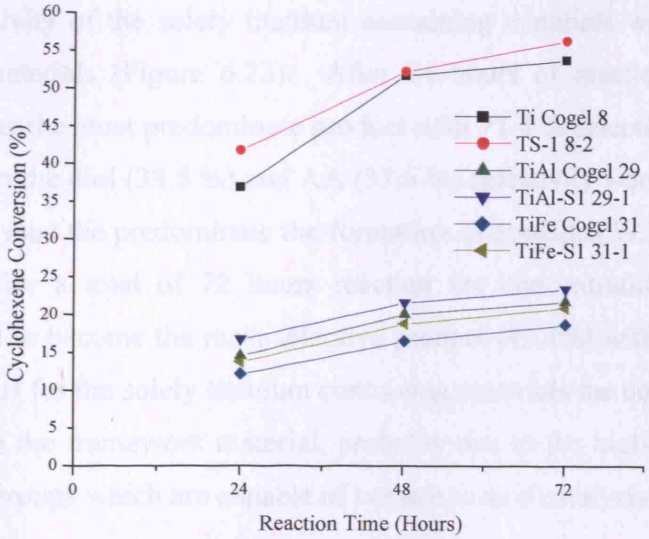

Figure 6.22: Cyclohexene conversion (%) for adipic acid formation utilising titanium containing catalysts over 72 hours. (Results were not normalised with respect to oxidative site concentration)

After 72 hours of reaction the materials containing solely titanium had the highest cyclohexene conversions of 53.7 % and 56.2 % for the cogel and TS-1 respectively. The activity trend of the bimetallosilicate materials was the same as for the solely titanium containing materials, the cogel materials were always slightly less active than their framework counterparts. This was hypothesised to be due to the unordered nature of the cogel materials, which hindered transport throughout the material.

Although the bimetallosilicate materials had half the titanium concentration of the mono-functional materials their activity was less than half. (It is worth reiterating that the acid centres encompassed in the bimetallosilicate materials were unlikely to convert cyclohexene.) The percentage conversion of cyclohexene for the TiAl materials was 21.7 % for the cogel and 23.4 % for TiAl-S1, similarly the cyclohexene conversions for the TiFe cogel was 18.7 % and 20.9 % for TiFe-S1. The bimetallosilicate materials contained acid centres which competed for reaction of the oxidant, leading to the formation of AA via another two oxidative steps. These two steps also required peroxide and the use of the active titanium sites. Thus, the conversion of cyclohexene was lower than would be expected if the reaction had not proceeded further.

The product selectivity of the solely titanium containing materials was different for the cogel and TS-1 materials (Figure 6.23). After 24 hours of reaction using the cogel catalyst the diol was the most predominate product with 71.4 % selectivity, however after 72 hours of reaction the diol (38.8 %) and AA (37.6 %) selectivity were comparable. The TS-1 material catalysed the predominate the formation of epoxide (59.3 %) after 24 hours of reaction, but after a total of 72 hours reaction the concentration of the diol had gradually increased to become the most selective product (43.4%) with an AA selectivity of just 15.3 %. Thus for the solely titanium containing materials the cogel showed greater AA selectivity than the framework material, probably due to the higher concentration of terminal hydroxyl groups which are capable of behave as acid catalysis sites.

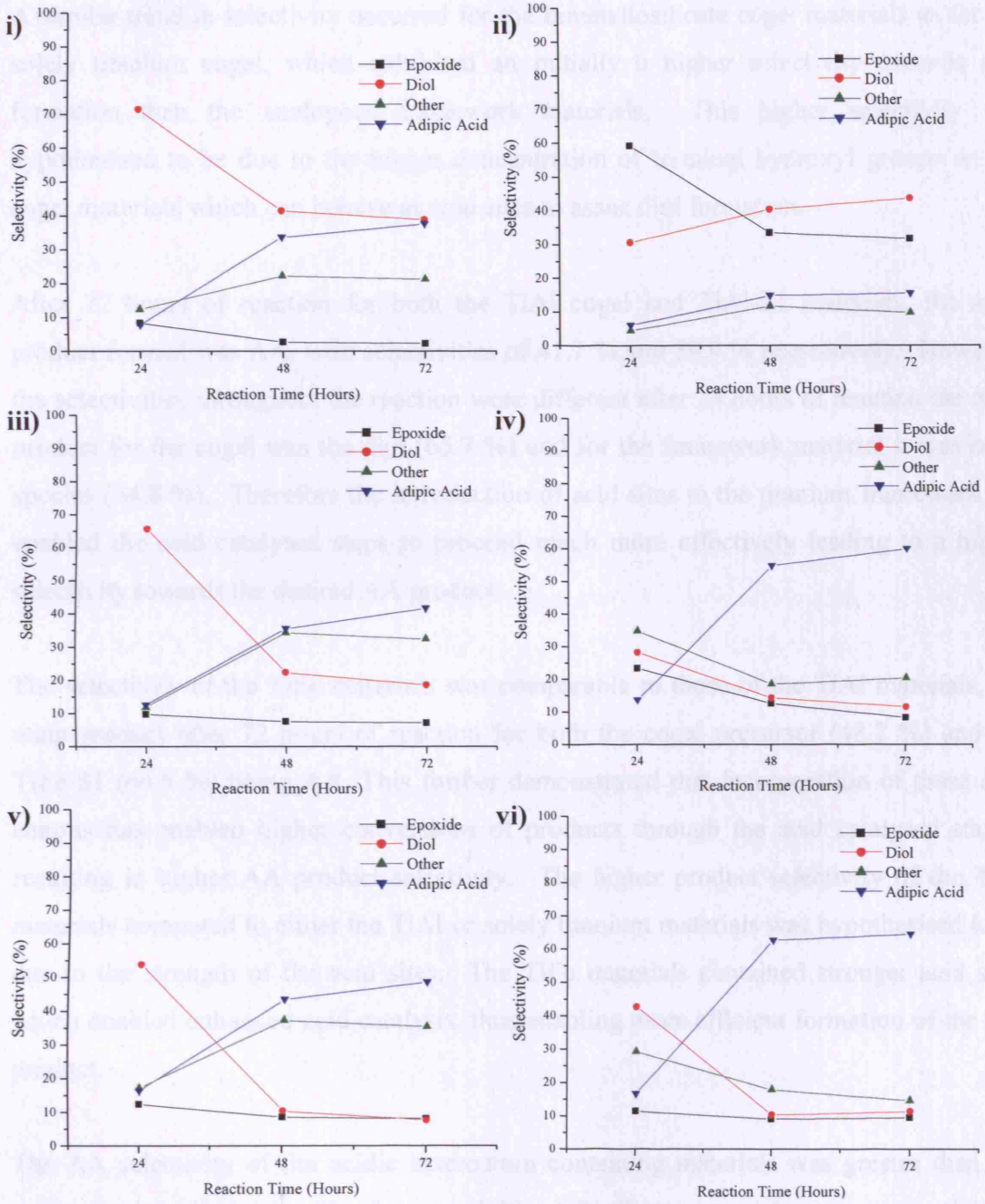

Figure 6.23: Selectivity (%) of adipic acid over 72 hours for titanium containing materials: ***i)*** *Ti Cogel 8,* ***ii)*** *TS-1 8-2,* ***iii)*** *TiAl Cogel 29,* ***iv)*** *TiAl-S1 29-1,* ***v)*** *TiFe Cogel 31,* ***vi)*** *TiFe-S1 31-1.*

A similar trend in selectivity occurred for the bimetallosilicate cogel materials as for the solely titanium cogel, which exhibited an initially a higher selectivity towards diol formation than the analogous framework materials. This higher selectivity was hypothesised to be due to the higher concentration of terminal hydroxyl groups on the cogel materials which can behave as acid sites to assist diol formation.

After 72 hours of reaction for both the TiAl cogel and TiAl-S1 materials, the main product formed was AA, with selectivities of 41.7 % and 59.9 % respectively. However, the selectivities throughout the reaction were different after 24 hours of reaction the main product for the cogel was the diol (65.7 %) and for the framework material it was other species (34.8 %). Therefore the introduction of acid sites to the titanium framework has enabled the acid catalysed steps to proceed much more effectively leading to a higher selectivity towards the desired AA product.

The selectivity of the TiFe materials was comparable to those of the TiAl materials, the main product after 72 hours of reaction for both the cogel precursor (48.7 %) and the TiFe-S1 (64.5 %) being AA. This further demonstrated that incorporation of these acid centres has enabled higher conversions of products through the acid catalysed stages, resulting in higher AA product selectivity. The higher product selectivity of the TiFe materials compared to either the TiAl or solely titanium materials was hypothesised to be due to the strength of the acid sites. The TiFe materials contained stronger acid sites which enabled enhanced acid catalysis, thus enabling more efficient formation of the AA product.

The AA selectivity of the acidic heteroatom containing materials was greater than the mono-titanium materials. The framework bimetallosilicate materials were more selective than their amorphous cogel counterparts. Therefore, whilst the cogel materials are catalytically active and do shown good selectivity towards the desired AA product the more ordered framework materials were more selective as well as more active.

6.5 Conclusions

Cogel precursors were prepared containing two different heteroatoms, using three different procedures: mixing of powders, one solution and two solution. From these precursors MFI framework materials were synthesised which contained the two heteroatoms on the lattice sites.

XRD results demonstrated the cogel materials to be amorphous as well as confirming the MFI framework of the crystalline materials produced. The bulk density results obtained confirmed the conclusion identified in other reported chapters, that the cogel materials were denser than the crystalline materials due to the open nature of the framework structure. Additionally, it was concluded that the heavier the metal incorporated within the material the more dense the material. There was no noticeable difference between either the cogel of resultant MFI materials prepared from different procedures.

The SEM images obtained highlighted the different morphologies of the crystalline materials produced, whilst the cogel materials appeared comparable, being amorphous with no ordered morphology. Not only were the crystalline materials shown to possess a range of morphologies, but the nature of formation of these crystals also appeared different. Some crystals had grown via an aggregate process whilst others had formed via a single growth mechanism, although these difference had little impact upon catalytic activity. The difference between the crystals was partially attributed to the method of the cogel preparation and also to the identity of the incorporated heteroatoms.

The nature of either the titanium or iron containing materials was characterised by UV-vis spectroscopy. The titanium containing materials did not exhibit any extra framework titanium species and the titanium centres appeared to be tetrahedrally bound. The titanium containing cogel with the most uniformly bound titanium centres was prepared from the mixing of powders method. Conversely, for the framework materials the widest range of titanium coordination was for those materials prepared from the mixing of powders method. The iron UV-vis data was unable to characterise the exact coordination

geometry of the iron centres, but was able to confirm that the materials tested contained isolated iron centres. The iron containing cogel prepared from the mixing of solution method exhibited the most overlapped spectra whilst the cogel prepared from the two solution method was the most resolved. The framework iron containing materials gave rise to slightly different spectra, exhibiting different band intensities. The crystalline material prepared utilising a cogel synthesised by the two solution method was different to the framework materials produced from cogel materials prepared by either of the other two methods.

The titanium containing framework materials were further characterised to evaluate the degree of titanium incorporation within the structure. The relative I_{960}/I_{550} ratios were compared, the highest value (therefore the greatest degree of titanium incorporation) was reported for materials synthesised from cogel materials prepared from the one solution procedure and the lowest from cogel materials prepared from the mixing of powders procedure.

^{27}Al NMR data demonstrated the all of the aluminium containing framework materials to have tetrahedral coordination geometry. Only the FeAl-S1 materials prepared from a cogel synthesised by the mixing of liquids procedure gave rise to an additional band, which related to different coordination geometry.

From these characterisation results the materials prepared utilising the two solution method were concluded to exhibit the greatest potential catalytic ability and were further evaluated by ammonia absorption and catalysis experiments.

Temperature programmed desorption of ammonia was undertaken to evaluate the relative strength and concentration of the acid sites of the materials. All of the materials tested desorbed ammonia at two temperatures relating to desorption from strong and weak acid sites. Those materials tested which contained iron desorbed ammonia at higher temperatures than the other materials. The spectra of the FeAl materials were severely overlapped so that the bands relating to the strong and weak acid sites could be even

partially separated. It was hypothesised that this was due to the materials containing two types of strong acid site, one for each incorporated acid heteroatom.

The catalytic ability of these bimetallosilicate materials was tested by separate acid and oxidation catalysis. The alkylation benzene reaction was employed to deduce the catalytic activity of the iron and aluminium centres. Similarly the hydroxylation of phenol was utilised to test the catalytic ability of the titanium heteroatoms. Both of these preliminary catalysis reactions demonstrated the heteroatoms within the cogel and framework materials to be catalytically active. The ability of the bimetallosilicate materials to behave as both acidic and oxidative catalysts was tested using the formation of AA reaction. Both the cogel and framework materials were demonstrated to be effective catalysts for this reaction. Although the results showed the framework materials to be both more catalytically active and selective than the cogel materials.

Therefore the cogel precursors have been utilised to produce materials capable of behaving as both oxidative and acidic catalysts. These catalysts are both active and selective towards the products formed. Further from this the synthesis procedure has been demonstrated to be both facile (compared to standard procedures) and reproducible.

6.6 References

(1) Neri, G.; Rizzo, G.; Galvagno, S.; Loiacono, G.; Donato, A.; Musolino, M. G.; Pietropaolo, R.; Rombi, E. *Applied Catalysis A: General* **2004**, *274*, 243.

(2) Bellussi, G.; Clerici, M. G.; Giusti, A.; Buonomo, F.; 226.258: European Patent, 1988.

(3) Bellussi, G.; Clerici, M. G.; Carati, A.; Esposito, A.; 266.825: European Patent, 1988.

(4) Camblor, M. A.; Corma, A.; Martinez, A.; Perez-Pariente, J. *Journal of the Chemical Society, Chemical Communications* **1992**, 589.

(5) Ovejero, G.; Grieken, R. V.; Uguina, M. A.; Serrano, D. P.; Melero, J. A. *Catalysis Letters* **1996**, *41*, 69.

(6) Treacy, M. M. J.; Higgins, J. B. *Collection of Simulated XRD Powder Patterns for Zeolites*; 4th ed.; Elsevier, 2001.

(7) Serrano, D. P.; Uguina, M. A.; Ovejero, G.; Grieken, R. V.; Camacho, M. *Microporous Materials* **1996**, *7*, 309.

(8) Serrano, D. P.; Uguina, M. A.; Ovejero, G.; Grieken, R. V.; Camacho, M. *Microporous Materials* **1995**, *4*, 273.

(9) Freude, D.; Ernst, H.; Wolf, I. *Solid State Nuclear Magnetic Resonance* **1994**, *3*, 271.

(10) Peeters, M. P. J.; Kentgens, A. P. M. *Solid State Nuclear Magnetic Resonance* **1997**, *9*, 203.

(11) Okada, K.; Tomita, T.; Kameshima, Y.; Yasumori, A.; MacKenzie, K. J. D. *Journal of Colloid and Interface Science* **1999**, *219*, 195.

(12) Lonyi, F.; Valyon, J. *Microporous and Mesoporous Materials* **2001**, *47*, 293.

(13) Perego, C.; Carati, A.; Ingallina, P.; Mantegazza, M. A.; Bellussi, G. *Applied Catalysis A: General* **2001**, *221*, 63.

Chapter 7: Conclusions and Further Work

7.0 Summary

The title of this thesis is multifunctional microporous metallosilicate catalysts, several types of these materials have been synthesised and characterised and the results reported herein. Heteroatom inserted microporous materials are by their nature multifunctional, the porous framework lends itself to shape selectivity whilst the heteroatom itself adds chemical reactivity to the material (Figure 7.1). The conventional synthesis of these materials commonly leads to products exhibiting non-ideal characteristics such as heteroatom clustering, and non-catalytically active coordination geometry. To overcome these problems, the materials produced in this work were synthesised from an amorphous cogel precursor. The cogel precursor already contained the isolated heteroatoms in the desired tetrahedral coordination geometry. Thus it was theorised that the materials produced would not suffer from the same problems commonly encountered with the conventional synthesis process.

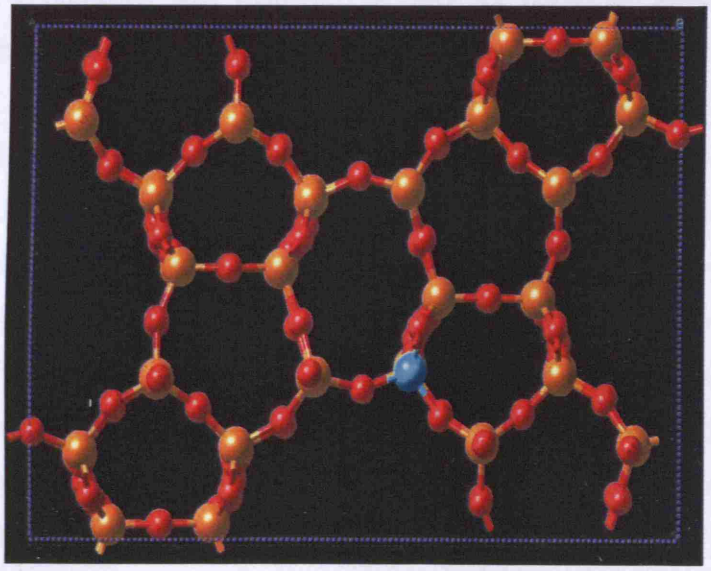

Figure 7.1: MFI framework with one inserted heteroatom (blue).

Titanosilicate, aluminosilicate and ferrisilicate materials were produced and characterised utilising a suite techniques. The catalytic ability of both the framework materials and the amorphous precursors used to form them, were tested. Further from this, the properties of the framework materials were in some case altered via silylation. A range of bimetallosilicate materials were also synthesised from cogel precursors, these were framework materials containing two of the heteroatoms previously employed. These materials were similarly characterised and their catalytic properties also evaluated. The differing chemical nature of the inserted heteroatoms allowing one catalyst to behave as both an oxidative and an acidic catalyst.

7.1 Titanosilicates (Chapter 3)

The synthesis parameters of the titanosilicate precursors were altered and the effect of these alterations upon the materials characteristics and catalytic abilities tested. When these amorphous materials were synthesised using either titanium butoxide or isopropoxide the predominate coordination geometry of the titanium species in the final framework materials was tetrahedral, but when titanium ethoxide was used a wider range of coordination geometries was evident. A broader range of titanium coordination geometries also became evident when the Si:Ti ratio was increased from 80 to 10.

The catalytic ability of the titanosilicate materials was also tested via the epoxidation of cyclohexene and hydroxylation of phenol. Alteration of the titanosilicate synthesis parameters was demonstrated to have little effect upon a materials catalytic ability for the epoxidation of cyclohexene reaction. The cogel and framework TS-1 materials had similar activity for this reaction but the TS-1 materials were more selective towards the epoxide products than the amorphous cogel materials. Upon alteration of the oxidant to a urea adduct the activity of the TS-1 materials increased whilst that of the cogel materials decreased. Yet the epoxide selectivity for both the framework and amorphous catalysts increased. Upon silylation of the catalysts, the activity of the TS-1 materials increased slightly, whilst that of the cogel materials decreased, whilst again the selectivity of both types of materials increased.

For the hydroxylation of phenol reaction the framework TS-1 materials were more active than the analogous cogel materials. Comparably to the epoxidation of cyclohexene reaction the cogel materials were less selective than their framework counterparts. Thus it was concluded that the framework was required for the most effective catalysis.

Further work based upon that undertaken for the titanosilicate materials so far, could include utilising the cogel precursors to produce other framework types. Preliminary work to this effect was undertaken and although the beta framework structure was successfully synthesised, the framework itself was not completely stable. Thus further work would be required to establish a reproducible synthesis procedure. Another branch of further work could be alteration of the titanium concentration to elucidate the optimum concentration of successful titanium incorporation within the framework.

7.2 Aluminosilicates (Chapter 4)

Several types of aluminium containing cogel materials were synthesised and from these precursors both ZSM-5 and Al SAPO-5 framework materials were produced. The catalytic ability of all of these materials was tested by the formation of ethyl benzene reaction. The cogel materials were less active and selective than the corresponding ZSM-5 materials, this difference in catalytic ability was in part, attributed to the instability of the aluminium centres within the cogel materials upon calcination. The Al SAPO-5 materials demonstrated the least catalytic activity and selectivity.

Further work which could be undertaken for the aluminosilicate materials may include further characterisation of the Al SAPO-5 materials to confirm the environment of all of the aluminium centres. Additionally the concentration and framework type of the materials produced could be varied.

7.3 Ferrisilicates (Chapter 5)

Several synthesis parameters were altered to produce the cogel and framework ferrisilicate materials. It was shown that once a material was calcined the range of iron coordination geometries widened. Whilst the materials of higher iron concentration Si:Fe 10 exhibited more oligomeric iron centres than the corresponding lower iron concentration materials. The ferrisilicate materials demonstrated stronger acid sites than those in analogous aluminosilicate materials. Both the framework and amorphous ferrisilicate materials were active catalysts for the reaction of benzene with ethanol, but again the framework materials were more catalytically active and selective.

Further research which could be undertaken for the ferrisilicate materials may include fully characterising the iron centres to establish their coordination geometry. Also further evaluation into the exact nature of the acid sites within these materials.

7.4 Bimetallosilicates (Chapter 6)

Three different synthesis procedures were employed to produce the bimetallosilicate cogel materials, these and the framework materials prepared from them, were characterised. The SEM images of the framework materials suggested that different crystal growth mechanisms were employed to form different materials, additionally a wider range of morphologies was also exhibited.

Catalytic reactions were also undertaken to confirm the activity of the oxidative heteroatom centres (epoxidation of cyclohexene) and the acidic centres (ethyl benzene formation). Further from this those materials which exhibited the greatest catalytic potential (and contained both oxidative and acidic heteroatoms) were used as catalysts for the formation of adipic acid reaction. As for all of the catalysis reactions tested, the amorphous cogel materials were less effective catalysts than their framework counterparts.

Further work which could be undertaken for these bimetallosilicate materials could be to study the formation process of these materials and hence to fully conclude why heteroatoms produce crystals of a specific morphology. Further from this the concentration of the heteroatoms could be altered so that they were not incorporated in equal amounts, and the effect upon the materials catalytic ability compared.

7.5 Overall Conclusions and Further Work

The overall results presented within this work demonstrate the synthesis of a range of heteroatoms inserted materials from amorphous cogel precursors. These MFI framework materials are catalytically active and selective, either to an equal or greater extent than analogous materials prepared from conventional means. The synthesis of both the cogel and framework materials was facile and reproducible. A continuation of this work could be to produce a wider range of framework types from the cogel materials (Figure 7.2).

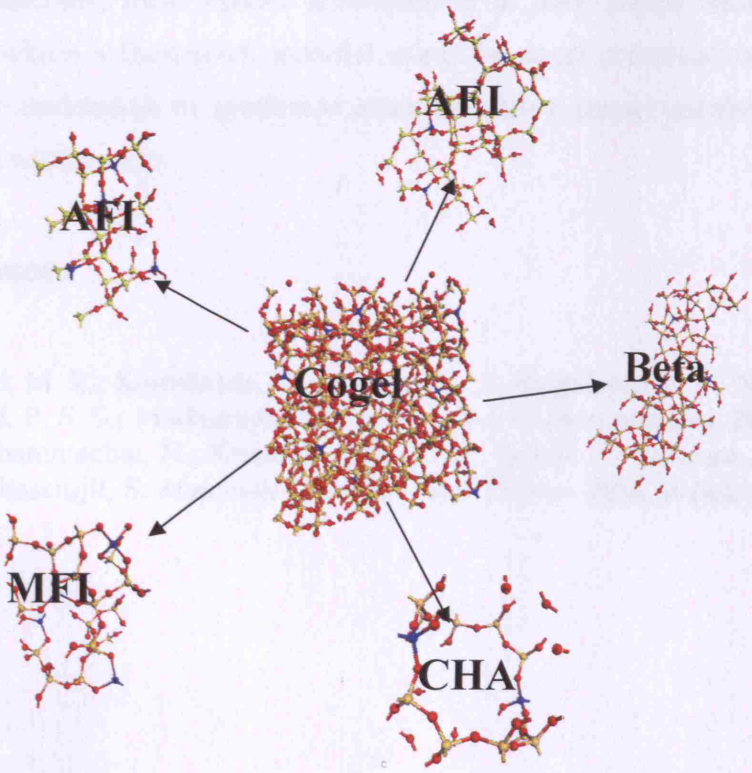

Figure 7.2: Further areas of possible research, demonstrating versatility of cogel precursors.

Further research could also include alteration of the crystallisation method of the cogel materials, so that instead of conventional hydrothermal conditions the gel was exposed to microwave radiation. Microwave radiation has been reportedly employed to produce TS-1 materials in a similar method to the conventional means.[1,2] The materials produced were comparable to standards in the literature but the synthesis time was greatly reduced, reportedly only taking approximately four hours.

Another extension to this work could be to utilise computational experimentation to fully evaluate the mechanism of crystal growth from the cogel precursors. Then from this computationally calculate the optimum synthesis procedures for both the cogel and framework materials.

Another possible pathway for further experimentation could be to alter the identity of the heteroatoms inserted. Preliminary results have been obtained for cobalt, nickel and tin containing materials, these results demonstrated at least partial incorporation of the heteroatoms within a framework material using the cogel precursor method. Research could also be undertaken to synthesise materials with a greater number of heteroatoms encompassed within them.

7.6 References

(1) Prasad, M. R.; Kamalakar, G.; Kulkarni, S. J.; Raghaven, K. V.; Narasimha, K.; Prasad, P. S. S.; Madhavendra, S. S. *Catalysis Communications* **2002**, *3*, 399.

(2) Phonthammachai, N.; Krissanasaeranee, M.; Gulari, E.; Jamieson, A. M.; Wongkasemjit, S. *Materials Chemistry and Physics* **2006**, *Article in Press.*